UNIVERSIDAD DE GRANADA

FACULTAD DE FARMACIA

DEPARTAMENTO DE FISIOLOGÍA

CENTRO DE GENÓMICA E INVESTIGACIÓN ONCOLÓGICA (GENYO)

Programa de Doctorado en Nutrición y Ciencias de los Alimentos

TESIS DOCTORAL INTERNACIONAL

GUT MICROBIOME-INTESTINAL BARRIER CROSSTALK DURING IRON DEFICIENCY ANAEMIA: USE OF NUTRITION-BASED STRATEGIES

Ana del Carmen Soriano Lerma

Directores

Dra. Mª Inmaculada López Aliaga

Dr. José Antonio García Salcedo

Editor: Universidad de Granada. Tesis Doctorales
Autor: Ana del Carmen Soriano Lerma
ISBN: 978-84-1117-798-6
URI: https://hdl.handle.net/10481/81260

UNIVERSIDAD DE GRANADA

FACULTAD DE FARMACIA

DEPARTAMENTO DE FISIOLOGÍA

Dª Mª INMACULADA LÓPEZ ALIAGA. CATEDRÁTICA DE UNIVERSIDAD ADSCRITA AL DEPARTAMENTO DE FISIOLOGÍA DE LA UNIVERSIDAD DE GRANADA

INFORMA:

Que los trabajos de investigación que se exponen en la Memoria de Tesis Doctoral titulada: **"GUT MICROBIOME-INTESTINAL BARRIER CROSSTALK DURING IRON DEFICIENCY ANAEMIA: USE OF NUTRITION-BASED STRATEGIES"**, que presenta la Licenciada Dª. Ana del Carmen Soriano Lerma al superior juicio del Tribunal que designe la Universidad de Granada, han sido realizados bajo mi dirección durante los años 2018-2023, siendo expresión de la capacidad técnica e interpretativa de su autor en condiciones tan aventajadas que la hacen merecedora al Título de Doctor, siempre y cuando así lo considere el citado Tribunal.

Fdo. Prof. Dra. Dª Mª Inmaculada López Aliaga

En Granada, a 10 de Febrero de 2023

UNIVERSIDAD DE GRANADA

FACULTAD DE FARMACIA

DEPARTAMENTO DE FISIOLOGÍA

D. JOSÉ ANTONIO GARCÍA SALCEDO, INVESTIGADOR DEL INSTITUTO DE INVESTIGACIÓN BIOSANITARIA ibs.GRANADA, ADSCRITO AL SERVICIO DE MICROBIOLOGÍA DEL HOSPITAL UNIVERSITARIO VIRGEN DE LAS NIEVES

INFORMA:

Que los trabajos de investigación que se exponen en la Memoria de Tesis Doctoral titulada: **"GUT MICROBIOME-INTESTINAL BARRIER CROSSTALK DURING IRON DEFICIENCY ANAEMIA: USE OF NUTRITION-BASED STRATEGIES"**, que presenta la Licenciada Dª. Ana del Carmen Soriano Lerma al superior juicio del Tribunal que designe la Universidad de Granada, han sido realizados bajo mi dirección durante los años 2018-2023, siendo expresión de la capacidad técnica e interpretativa de su autor en condiciones tan aventajadas que la hacen merecedora al Título de Doctor, siempre y cuando así lo considere el citado Tribunal.

Fdo. Dr. D. José Antonio García Salcedo

En Granada, a 10 de Febrero de 2023

UNIVERSIDAD DE GRANADA

FACULTAD DE FARMACIA

DEPARTAMENTO DE FISIOLOGÍA

La doctoranda Dª. ANA DEL CARMEN SORIANO LERMA y los directores de la Tesis Dª Mª INMACULADA LÓPEZ ALIAGA y D. JOSÉ ANTONIO GARCÍA SALCEDO, garantizamos, al firmar esta Tesis Doctoral, que el trabajo ha sido realizado por la doctoranda bajo la dirección de los directores de la Tesis y hasta donde nuestro conocimiento alcanza, en la realización del trabajo, se han respetado los derechos de otros autores a ser citados, cuando se han utilizados sus resultados o publicaciones.

En Granada a 10 de Febrero de 2023.

Directores de la Tesis Doctoral

Prof. Dra.
Dª Mª Inmaculada López Aliaga

Dr.
D. José Antonio García Salcedo

Doctoranda

Dª. Ana del Carmen Soriano Lerma

UNIVERSIDAD DE GRANADA
FACULTAD DE FARMACIA
DEPARTAMENTO DE FISIOLOGÍA

TESIS DOCTORAL INTERNACIONAL

La presente memoria de Tesis Doctoral se ha llevado a cabo bajo la concesión de un Contrato de Formación de Profesorado Universitario (FPU 17/05413) por parte del Ministerio de Educación, Cultura y Deporte. El trabajo experimental se ha realizado en el Departamento de Fisiología y en GENYO, Centro de Genómica e Investigación Oncológica: Pfizer/Universidad de Granada/Junta de Andalucía, así como en Teagasc Food and Agriculture Centre en Fermoy (Irlanda), gracias a la obtención de una beca para la movilidad internacional financiada por la Organización Europea de Biología Molecular (EMBO)

Trust the wait. Embrace the uncertainty. Enjoy the beauty of becoming. When nothing is certain, anything is possible.

Mandy Hale

Nothing in life is to be feared, it is only to be understood. Now is the time to understand more so that we may fear less.

Marie Curie

Agradecimientos

Esta tesis doctoral es resultado y mérito de muchas personas. Entre ellas y las más influyentes, sin duda, mis padres, Ana y Miguel. Siempre alimentaron mi curiosidad desde pequeña con historias del sistema solar y libros de adivinanzas. Me disteis la vida, pero también me enseñasteis a vivirla.

A mi madre, de quien heredé mi carácter, gracias a ella soy luchadora y constante. Siempre te agradeceré toda tu paciencia, tus constantes mimos y tu capacidad para ponerme los pies sobre la tierra. Tu fortaleza y tus ganas de seguir creciendo han sido y son una inspiración para mí.

A mi padre, de quién heredé la vocación científica y quien me engañó para que me metiera en este mundillo. Mi maestro en la sombra, del que he aprendido que el conocimiento es la mayor recompensa. Gracias por tu infinito tiempo y especialmente por tu calma, que apacigua todas mis tormentas.

A Pedro, mi persona favorita que me ha acompañado en esta y en todas mis aventuras. Qué fácil se vuelve todo lo difícil cuando estoy contigo; gracias por tu eterna sonrisa y tu corazón enorme. Sin duda este título de doctor también debería de ser para ti por todo lo que me has aguantado.

Al resto de mi familia: mis abuelos, mis titos y mis primos. A mi abuela, mi mayor fan y en la que más confío. A mi abuelo, que sigue cuidándome desde arriba. A mis titos y primos, por todo vuestro cariño y apoyo.

A mis directores, José Antonio e Inma, que también han aportado su gran cubo de arena a esta tesis. A José Antonio, que me anima siempre a pelear mis batallas; gracias por toda la confianza, incluso en mis etapas de novata, que me ha hecho ser una investigadora resolutiva y multidisciplinar. A Inma, que me arropó sin dudar en el

Departamento y en el grupo de investigación al llegar. Gracias por tu energía, tu optimismo y tu disposición siempre a ayudar. Tu bondad no conoce límites.

A María José, que siempre me saca una sonrisa, aunque las cosas se pongan feas.

A mi laboratorio 22, el mejor equipo que me podía tocar tanto profesional como personalmente. A mis alpacas Virginia, Mati, Viky, María e Inma, y a mi pastor Ángel. Sin vosotros esto, simplemente, no hubiera sido posible; imposible enumerar todas vuestras hazañas. Gracias por todos los momentos estos 5 años, los pasteles real fooder, las reuniones de los lunes hasta las 8 y las conversaciones de desdramatización. Esto no es el final, si no otro principio.

A todos mis amigos de Genyo: Amador, Alberto, Carlos, Juan, Dani, Marisol, Menci, Ana, Vivi, Juanro, Félix… Gracias por las tardes de tenis, vóley o cualquier deporte que encarte, las barbacoas con barreñito, las excursiones con la excusa de ir al chiringuito, bastantes charlas de ciencia y apoyo moral.

A mis amigos de Irlanda: Coral, Enriqueta, Mona, Yasmín, Fran, Orla, Amy, Talita, Renata, Reno, MarLuci y Gaetan. Esta isla me robó el corazón, entre otras cosas, por la gente tan especial que conocí.

A mis farmafriends, a quien echo de menos todos los días y quienes me recuerdan que la distancia no se mide en kilómetros si no en ganas.

A las de siempre, Inés S, Inés M, María, Carmen e Icíar. Lo que unió el balonmano y el instituto, nada lo puede romper.

A mi low maintenance bestie, Celia, que siempre presume de mí para subirme la moral. Hemos compartido literalmente toda nuestra vida, y lo que nos queda.

Gracias a la vida por haberme dado esta oportunidad. Me llevo todo lo aprendido, que es mucho, además de personas maravillosas.

INDEX

TABLE OF CONTENTS

ABBREVIATIONS

16S rRNA	16S ribosomal RNA
3'UTR	3' Untranslated region
5'UTR	5' Untranslated region
AEBP1	Adipocyte enhancer binding protein 1
AIDS	Acquired immunodeficiency syndrome
AG	Anaemic group fed with fermented goat's milk-based diet
AHR	Aryl hydrocarbon receptor
AMPs	Antimicrobial peptides
ARNT	Aryl hydrocarbon receptor nuclear translocator
ARNT1	Aryl hydrocarbon receptor nuclear translocator 1
ARNT2	Aryl hydrocarbon receptor nuclear translocator 2
ARNT3	Aryl hydrocarbon receptor nuclear translocator 3
AS	Anaemic group fed with standard diet
ATP	Adenosin triphosphate
BFU-Es	Burst forming units-erythroid
BMP6	Bone morphogenetic protein 6
BSA	Bovine serum albumin
BTF3	Basic transcription factor 3
CFU-Es	Colony forming units-erythroid
CG	Control group fed qith fermented goat's milk-based diet
CLD1	Claudin 1
CoA	Coenzyme A
COL6	Collagen VI
COL6A1	Collagen VI alpha 1 chain
CS	Control group fed with standard diet
D20	Day 20 along the induction of iron deficiency anaemia
D40	Day 40 along the induction of iron deficiency anaemia
Dcytb	Duodenal cytochrome b
DGC	Distance-based greedy clustering

DMT1	Divalent metal transporter 1
DNA	Desoxiribonucleic acid
ELISA	Enzyme-like immunosorvent assay
ENTPD1	Ectonucleoside triphosphate diphosphohydrolase 1
EPO	Erythropoietin
F	Forward
FAO	Food and Agriculture Organization
FFAR	Free fatty acid receptors
FGF13	Fibroblast growth factor 13
FGM	Fermented goat's milk
FMT	Faecal microbiome transplantation
FN1	Fibronectin 1
FOS	Fructooligosaccharides
FPN	Ferroportin
FTN	Ferritin
GMOS	Goat's milk oligosaccharides
GO	Gene onthology
GOS	Galactooligosaccharides
GSEA	Gene set enrichment analysis
HDAC	Hystone deacetylases
HEPH	Hephaestin
HFE	Homeostatic iron regulator (Hemochromatosis protein)
HIF	Hypoxia inducible factor
HIF-1α	Hypoxia inducible factor 1α subunit
HIF-2α	Hypoxia inducible factor 2α subunit
HIF-3α	Hypoxia inducible factor 3α subunit
HIF-1β	Hypoxia inducible factor 1β subunit
HIF-2β	Hypoxia inducible factor 2β subunit
HIF-3β	Hypoxia inducible factor 3β subunit
HIV-1	Human immunodeficiency virus 1
HMP	Human Microbiome Project
HRE	Hypoxia responsive element

HRP	Horseradish peroxidase
IDA	Iron deficiency anaemia
Ig	Immunoglobulins
IgA	Immunoglobulin A
IgG	Immunoglobulin G
IgM	Immunoglobulin M
IL-6	Interleukin 6
IL-10	Interleukin 10
IL-18	Interleukin 18
IREs	Iron responsive elements
IRP1	Iron responsive protein 1
IRP2	Iron responsive protein 2
IRPs	Iron responsive proteins
KEGG	Kyoto Encyclopedia of Genes and Genomes
KO	KEGG orthologs
LAL	Limulus amebocyte lysate
LDA	Linear discriminant analysis
LEfSe	Linear discriminant analysis Effect size
LOG_2FC	Log_2 fold change
LPS	Lipopolysaccharide
LUM	Lumican
MALDI-TOF MS	Matrix-assisted laser desorption ionization–time of flight mass spectrometry
MCH	Mean corpuscular haemoglobin
MCHC	Mean corpuscular haemoglobin concentration
MCV	Mean corpuscular volume
MDR1	Multidrug resistance 1 gene
MetaHIT	METAgenomics of the Human Intestinal Tract
mRNA	Messenger RNA
RNA-Seq	mRNA sequencing
MUC2	Mucin 2
NCOA4	Nuclear receptor coactivator 4

NES	Normalized enrichment score
NGS	Next generation sequencing techniques
NRF2	nuclear factor erythroid 2-related factor 2
NT5E	5'-nucleotidase ecto
OTUs	Operational Taxonomic Units
Padj	p-adjusted value
PCoA	Principal coordinate analysis
PCR	Polymerase chain reaction
PHDs	Prolyl hydroxylases
PICRUSt	Phylogenetic Investigation of Communities by Reconstruction of Unobserved States
PPIB	Anti-cyclophilin B
qPCR	quantitative polymerase chain reaction
R	Reverse
RBCs	Red blood cells
RIN	RNA Integrity Number
RNA	Ribonucleic acid
ROS	Reactive oxygen species
RT	Room temperature
SCFA	Short chain fatty acids
SHIME	Simulator of Human Intestinal Microbial Ecosystem
SOP	Standard operating procedure
Tf	Transferrin
TfR1	Transferrin receptor 1
TfR2	Transferrin receptor 2
Th1	Type 1 T helper cells
Th17	Type 17 T helper cells
TNF	Tumor necrosis factor

FIGURE INDEX

TABLE INDEX

RESUMEN & ABSTRACT

RESUMEN

La anemia es un síndrome plurietiológico caracterizado por un descenso en los niveles de hemoglobina por debajo de las concentraciones fisiológicas, que pueden variar de acuerdo a la edad, género o condición fisiológica. Se estima que afecta al menos a un tercio de la población mundial, con una prevalencia aumentada en países subdesarrollados, donde supone una carga económica considerable. La deficiencia de hierro es la causa más frecuente de anemia, produciendo aproximadamente el 50% de los casos, y considerándose la deficiencia de micronutrientes más prevalente a nivel mundial.

La escasa variedad de alternativas terapéuticas es uno de los mayores problemas de la anemia ferropénica (AF). Los suplementos de hierro orales constituyen la primera línea de tratamiento a pesar de sus numerosos efectos adversos. Dado que la absorción de hierro en el intestino es muy limitada, el hierro de los suplementos que no ha sido absorbido se acumula en el intestino, produciendo estrés oxidativo y deteriorando el epitelio intestinal. El exceso de hierro también produce alteraciones en el microbioma. Por tanto, las alteraciones gastrointestinales son efectos adversos muy comunes de los suplementos de hierro, en muchas ocasiones causando el abandono del tratamiento cuando los síntomas de la anemia desaparecen pero antes de que los depósitos de hierro se recuperen completamente, lo que suele provocar recidivas. Un porcentaje considerable de las anemias ferropénicas acaban volviéndose refractarias al tratamiento y se cronifican.

A pesar de que se conoce el efecto perjudicial de los suplementos de hierro para la salud intestinal, las cuestiones relacionadas con la alteración del microbioma y el estado del epitelio intestinal durante la AF todavía permanecen abiertas. El intestino humano alberga la comunidad de microorganismos más amplia de todo el organismo. Durante los últimos años, se han establecido multitud de relaciones causales entre alteraciones del microbioma intestinal y cambios en el estado de salud. Algunos de estos

estudios analizan las alteraciones microbiológicas a nivel intestinal durante la AF y sugieren que los microorganismos podrían estar contribuyendo a la génesis de la AF al competir por el hierro con las células del hospedador o alterar la homeostasis intestinal. La mayoría de los estudios se centran en el microbioma del intestino grueso y las heces y no utilizan las nuevas metodologías de secuenciación masiva.

El microbioma intestinal es un componente clave de la barrera intestinal, ya que la disbiosis intestinal suele asociarse con alteraciones de dicha barrera. En condiciones fisiológicas, existen una gran variedad de antígenos, toxinas y microorganismos en el lumen intestinal y la función de la barrera es prevenir su paso a la circulación sistémica. Existen evidencias en la bibliografía de que un paso incrementado del contenido del lumen a los tejidos puede desencadenar inflamación y agravar ciertas enfermedades. La barrera intestinal apenas ha sido estudiada en el contexto de la AF, a pesar de que se conoce que la falta de hierro puede dificultar la replicación del ADN y el ciclo celular.

Dado que abordar el deterioro del microbioma y de la barrera intestinal sería una de los objetivos a la hora de optimizar las terapias de la AF, la leche fermentada de cabra se ha estudiado como una estreategia nutricional para restaurar la salud intestinal en este contexto. El alto valor nutricional de la leche de cabra junto con su reducido riesgo de alergenicidad la sitúa en un lugar aventajado para su uso en determinadas situaciones patológicas. Los oligosacáridos son los nutrientes de mayor interés desde el punto de vista microbiológico debido a su alto potencial prebiótico. Estos oligosacáridos se encuentran en mayor concentración en la leche de cabra que en la leche de otros animales, además de ser estructuralmente más diversos y guardar una gran similitud con los oligosacáridos de la leche materna humana, que constituye el patrón de referencia en cuanto a efectos beneficiosos intestinales. Por otro lado, la fermentación mejora la digestibilidad de la leche, sus características organolépticas y la biodisponibilidad de los oligosacáridos, aumentando su potential prebiótico. Se ha demostrado que la leche de cabra aumenta la biodisponibilidad de hierro, pero se

desconoce si este efecto depende de sus propiedades moduladoras del microbioma intestinal. Se ha descrito que los oligosacáridos de la leche de cabra ejercen efectos beneficiosos sobre el microbioma intestinal y la integridad de la barrera, pero los estudios sobre la leche fermentada de cabra son escasos.

En la presente tesis se ha llevado a cabo una caracterización completa de las alteraciones del microbioma intestinal a lo largo del tracto digestivo durante la AF, así como un análisis en profundidad de la integridad de la barrera, para valorar el estado general de la salud intestinal. Además, se ha estudiado la capacidad de la leche fermentada de cabra para recuperar la AF, así como sus propiedades moduladoras sobre la composición del microbioma y la integridad de la barrera intestinal.

La AF se indujo experimentalmente en un modelo animal mediante el uso de una dieta carente de hierro (AIN-93G sin hierro) durante un periodo de 40 días. Al final del periodo de inducción, parte de los animales se sacrificaron, obteniéndose las siguientes muestras biológicas: sangre total, suero, contenido y mucosa intestinal de cada segmento del tracto digestivo (duodeno, yeyuno, íleo, ciego y colon) y heces. Los animales restantes se sometieron a un periodo de tratamiento con dieta basada en leche fermentada de cabra o dieta estándar durante 30 días adicionales. Al terminar este periodo, los animales fueron sacrificados y se obtuvieron muestras biológicas similares.

Para confirmar que la AF se había inducido correctamente en los animales de experimentación se realizó el estudio de parámetros hematológicos. El microbioma intestinal se analizó en el contenido de todos los segmentos intestinales (duodeno, yeyuno, íleon, ciego y colon) y en las heces. En una primera aproximación, se realizó la secuenciación de la subunidad 16S del ARN ribosómico (secuenciación de amplicones) para identificar la región intestinal con mayor disbiosis. La secuenciación de amplicones demostró que existía una disbiosis intestinal en respuesta a la AF, más intensa hacia el intestino grueso (ciego y colon). Se realizó un análisis predictivo funcional sobre los datos de secuenciación que reveló que las rutas metabólicas microbianas más

enriquecidas en el intestino grueso durante la AF estaban relacionadas con el metabolismo de los ácidos grasos de cadena corta (AGCC). La determinación de estos metabolitos (ácidos butírico, propiónico y acético) confirmó un incremento de su concentración durante la AF, especialmente en el colon. De igual manera, el análisis taxonómico mostró un aumento de los miembros del género *Clostridium* en el intestino grueso de los animales anémicos, que estaban positivamente correlacionados con los niveles de ácido butírico y propiónico en el colon. El colon fue, por tanto, identificado como la región intestinal con la mayor disbiosis para llevar a cabo un análisis detallado del microbioma intestinal mediante secuenciación de metagenoma completo (secuenciación shotgun). Se confirmó un aumento de especies del género *Clostridium*, positivamente correlacionadas con los niveles de ácido butírico y propiónico, así como un aumento de vías microbianas productoras de AGCC, nucleótidos y un aumento de la carga bacteriana durante la AF. Así, especies clave del género *Clostrdium* y metabolitos clave fueron identificados como los principales contribuyentes a la disbiosis producida en respuesta a la AF. Dadas sus funciones beneficiosas en el epitelio intestinal, es muy probable que los AGCC formen parte de mecanismos de compensación desencadenados como consecuencia de la AF para aliviar las alteraciones sistémicas o intestinales derivadas de la enfermedad.

El análisis de la barrera intestinal en la mucosa del colon mediante secuenciación de ARN mensajero mostró un epitelio intestinal infradesarrollado debido a la infraexpresión de términos Gene Onthology (GO) relacionados con el desarrollo y la señalización sináptica del sistema nervioso entérico, desarrollo del tracto digestivo, ensamblaje de las uniones celulares e integridad celulares y organización de la matriz extracelular. Dado que el metabolismo del colágeno, como componente mayoritario de la matriz extracelular, es dependiente de hierro, se analizaron específicamente genes y proteínas relacionados con el colágeno, encontrando niveles disminuídos durante la AF. Debido a la estrecha relación existente entre los AGCC y la estabilización de la hipoxia

intestinal y al papel de la hipoxia en el mantenimiento de la barrera intestinal, se analizaron específicamente genes diana de hipoxia mediante PCR cuantitativa. La ausencia de diferencias en la expresión entre los grupos experimentales control y anémico sugiere que la alteración observada en la barrera intestinal es independiente de hipoxia. Por último, el aumento en los marcadores de translocación microbiana (lipopolisacárido bacteriano e inmunoglobulinas específicas de bacterias) en los animales anémicos apoya la falta de integridad de la barrera intestinal durante la AF.

Durante el periodo de tratamiento con las dietas a ensayar, la determinación de parámetros hematológicos mostró que la AF se recuperó más eficientemente con la dieta basada en leche fermentada de cabra respecto a la estándar. Las propiedades moduladoras del microbioma intestinal de la leche fermentada de cabra se estudiaron en contenidos intestinales de todos los segmentos del tracto digestivo recolectados tras el periodo de tratamiento. La dieta basada en leche fermentada de cabra dio lugar a un microbioma más diverso en cuanto al número de especies en la comunidad microbiana, y funcionalmente más activo que la dieta estándar, tanto en el intestino delgado como en el grueso de animales controles, lo que está en línea con una recuperación más eficiente de la AF. En cuanto a sus propiedades restauradoras del microbioma intestinal, tanto la dieta basada en leche fermentada de cabra como la dieta estándar recuperaron la disbiosis asociada a la AF del intestino delgado. Sin embargo, la dieta basada en leche fermentada de cabra fue más eficiente al recuperar la disbiosis más intensa del colon, confirmando sus propiedades prebióticas. En ningún caso se recuperó completamente el microbioma en los animales anémicos en relación al grupo control en durante el periodo de tratamiento empleado.

Por último, la dieta basada en leche fermentada de cabra no mostró ningún efecto positivo adicional sobre la integridad de la barrera intestinal comparada con la dieta estándar. Ambas dietas recuperaron los genes infraexpresados afectados durante la AF, restaurando la función de la barrera intestinal. La ausencia de diferencias

significativas entre las concentraciones séricas de lipopolisacárido bacteriano entre el grupo control y el anémico alimentados con dieta basada en leche fermentada de cabra o dieta estándar sugiere un estado similar de integridad de la barrera intestinal tras el tratamiento con ambas dietas.

En esta tesis se han analizado las alteraciones del microbioma y la barrera intestinal en un modelo animal representativo de una anemia ferropénica nutricional. Con el descubrimiento de una disbiosis intestinal intensa en el intestino grueso con un aparente papel compensador y un estado detereriorado del epitelio intestinal que genera translocación de componentes bacterianos, adoptar nuevas aproximaciones de tratamiento para la AF enfocados a la restauración de la salud intestinal parece de gran importancia. La leche fermentada de cabra se ha estudiado en este sentido, recuperando la AF y restaurando la disbiosis colónica más eficientemente que una dieta estándar; a pesar de que la dieta basada en leche fermentada de cabra también recuperó la integridad de la barrera intestinal, no mostró ningún efecto positivo adicional frente a la dieta estándar. Por tanto, la leche fermentada de cabra podría ser una estrategia nutricional prometedora para aliviar las alteraciones intestinales durante la AF y para reducir el impacto negativo de los suplementos de hierro en la salud intestinal.

ABSTRACT

Anaemia is a multifactorial syndrome characterised by a reduction in haemoglobin levels below homeostatic ranges, which vary according to age, gender and physiological conditions. It is estimated to affect one third of the global population with an increased prevalence in underdeveloped countries, where it imposes a considerable economic burden. Iron deficiency is the top leading cause of anaemia, causing approximately 50% of cases, and the most prevalent micronutrient deficiency worldwide.

The lack of variety in therapeutic alternatives is one of the major problems when treating iron deficiency anaemia (IDA). Oral iron (iron supplements) is the first treatment option, with side effects outnumbering its beneficial aspects. Since iron absorption is fairly limited, non-absorbed iron from supplements is accumulated in the intestine, triggering oxidative stress and damaging the intestinal epithelium. Excess of iron also causes alterations in the gut microbiome. Not surprisingly, gastrointestinal alterations are common side effects produced by oral iron supplements, which in the end lead to the abandonment of treatment before iron deposits have been completely restored andto repetitive episodes of IDA. A considerable percentage of iron deficiency anaemias become chronic and refractory to treatment.

Although it is well known that iron supplements exert a detrimental effect on gut health, questions regarding the alterations in the gut microbiome and the state of the intestinal epithelium and the gut barrier during IDA remain unanswered. The human intestine harbours the greatest and most diverse microbial community in the entire organism and causal relationships have been repeatedly established between the gut microbiome and the state of health. Some studies have investigated the microbial alterations in the context of IDA using classical methods and suggest that microorganisms might contribute to IDA through competition for iron with the host or by

altering intestinal homeostasis. Most of these studies have focused on the microbial communities in the large intestine and faeces and did not use state-of-the-art sequencing methods.

The gut microbiome is a key component of the intestinal barrier and intestinal dysbiosis has often been associated with alterations in the gut barrier. In physiological conditions, there is a wide variety of antigens, toxins and microorganisms in the intestinal lumen, and the gut barrier aims to prevent their leakage into the bloodstream. There is a considerable body of evidence to suggest that an increased leakage to extraintestinal tissues can trigger inflammation and lead to the aggravation of certain disorders. Despite the fact that iron shortage can impair DNA replication and cell cycle progression, therefore impairing the gut barrier, this aspect has been barely studied during IDA.

Since addressing the deterioration of the gut microbiome and the intestinal barrier, if altered during IDA, would be one of the goals when optimising IDA therapies, fermented goat's milk (FGM) was studied in this thesis as a nutritional tool to restore gut health. The higher nutritional value of goat's milk along with its reduced risk of allergy compared to cow's milk make it suitable to be used in specific scenarios. One of the nutrients showing the highest prebiotic potential are oligosaccharides, whose concentration is higher in goat's milk compared to other animals. They are more structurally diverse and bear a close resemblance to breast milk oligosaccharides, the golden standard in relation to beneficial effects on intestinal health. On the other hand, fermentation improves digestibility as well as sensory properties and nutritional value of milk, increasing the availability of oligosaccharides and enhancing their prebiotic impact. Goat's milk has been shown to increase iron bioavailability, but whether this effect might be microbiome-dependent is not known. Goat's milk oligosaccharides have been reported to exert beneficial effects on the gut microbiome and the gut barrier integrity, but studies describing the effect of FGM are scarce.

Therefore, a full characterisation of the alterations occurring in the gut microbiome along the gastrointestinal tract during IDA together with an in-depth analysis of the intestinal barrier have been included as the two hallmarks of intestinal health to study in this thesis. Moreover, the IDA recovering capacity of FGM was studied, along with its gut microbiome-shaping properties and its effects on the intestinal barrier.

IDA was experimentally induced in an animal model through the use of an iron-free diet (iron free AIN-93G diet) over a period of 40 days. At the end of the induction period, part of the animals were sacrificed. Blood, serum, intestinal content and intestinal mucous layer samples and faeces were collected from each intestinal region (duodenum, jejunum, ileum, cecum and colon). The remaining animals underwent the treatment period using either a FGM-based diet or a standard diet along 30 additional days. At the end of the treatment period, animals were sacrificed and similar samples were collected.

After confirming IDA had been correctly induced through the determination of haematological parameters, the gut microbiome was analysed in intestinal contents belonging to all segments (duodenum, jejunum, ileum, cecum and colon) and in faeces. In a first approach, 16S rRNA sequencing (amplicon sequencing) was used to identify the region showing the greatest dysbiosis. Amplicon sequencing revealed an intestinal dysbiosis occurred in response to IDA, with intensity increasing towards the most distal segments of the digestive tract (large intestine: cecum and colon). Predictive microbial functional analysis on 16S rRNA sequencing data revealed that the most enriched microbial pathways in the large intestine during IDA were related to short chain fatty acid (SCFA) metabolism. Determination of SCFA (butyrate, propionate and acetate) confirmed an increase during IDA, especially in the colon. Taxonomic analysis revealed an enrichment in members of the genus *Clostridium* in the large intestine, one of the major SCFA producers, which showed high positive correlations to butyrate and propionate levels in the colon of anaemic animals. Therefore, the colon was identified as the region showing the greatest dysbiosis during IDA. To take an in-depth look at the gut

microbiome alterations, whole metagenome sequencing was applied on colonic contents, revealing an enrichment in *Clostridium* species during anaemia, positively correlated to butyrate and propionate levels. Beside SCFA-related pathways being more abundant during IDA, nucleotide-producing pathways and bacterial load were also higher in the anaemic animals. Hence, key microbial species belonging to the genus *Clostridium* and key metabolites were identified as the main drivers of changes in the gut microbiome occurring in response to IDA. Given their well documented positive role on the intestinal epithelium, SCFA are likely to be part of microbial trade-off mechanisms taking place during IDA to compensate for systemic or intestinal disease-derived alterations.

Analysis of the intestinal barrier on the colonic mucous layer through mRNA-sequencing revealed an underdeveloped intestinal epithelium during IDA due to the downregulation of Gene Onthology terms related to the development and synaptic signalling within the enteric nervous system, the development of the digestive tract, cell junction assembly and cell integrity and organization of the extracellular matrix. Since collagen metabolism, as the major component of the extracellular matrix, is iron dependent, the expression of collagen-related genes and proteins was specifically analysed, finding also decreased levels during IDA. Due to the well stablished role of SCFA on the stabilization of intestinal hypoxia and the impact of hypoxia on the maintenance of the intestinal barrier, hypoxia target genes were analysed by quantitative PCR, showing no differences in expression levels between the control and the anaemic group. Therefore, the observed alterations in the intestinal barrier were hypoxia-independent. Microbial translocation was studied in serum samples using two biomarkers: lipopolysaccharide (LPS) and bacteria-specific immunoglobulins. Increased LPS translocation along with an increased immune response against dysbiotic bacteria is in accordance with an impaired intestinal barrier during IDA.

During the treatment period, the determination of haematological parameters revealed IDA was more efficiently recovered using a FGM-based diet compared to a

standard one. The gut microbiome-modulating properties of FGM were studied in intestinal content samples belonging to all intestinal segments and faeces collected after the treatment period. FGM showed microbiome-modulating properties in the small and large intestine of control animals in line with this increased efficiency. The gut microbiome shaped by the FGM-based diet was slightly more diverse in terms of the number of species in the microbial community and more functionally active than that shaped by the standard diet, which is confirmed by a higher bacterial load in the colon of animals fed with FGM-based diet. As far as its microbiome-restoring properties are concerned, FGM-based diet and standard diet similarly restored gut dysbiosis in the small intestine, since alterations in this region were less noticeable. Gut dysbiosis in the colon was more efficiently restored by FGM-based diet compared to standard diet, confirming its prebiotic potential. None of the diets completely restored the microbiome in relation to the control group during the employed treatment period.

Lastly, FGM did not show any additional positive effect on the gut barrier compared to the standard diet. Both diets restored the altered expression levels of key downregulated genes during IDA involved in the maintenance of the intestinal barrier. Absence of differences in serum LPS concentrations between control and anaemic groups fed with FGM-based diet or standard diet suggest a similar state of the intestinal barrier after treatment with both diets.

This thesis analyses the alterations in the gut microbiome and intestinal barrier occurring in an animal model that represents a nutritional iron deficiency. With the discovery of an intense gut dysbiosis in the large intestine with an apparent compensatory role and an overall deteriorated intestinal barrier that leads to an increased leakage of microbial components, taking gut-protective approaches seems imperative when treating IDA. Fermented goat's milk was studied in this context, recovering IDA and restoring the colonic microbiome more efficiently. Despite the fact that fermented goat's milk also restored the integrity of the intestinal barrier, no additional

positive effects were shown in this regard in comparison with the standard diet. Fermented goat's milk is therefore a useful nutritional tool to ease intestinal alterations occurring during iron deficiency and to reduce the negative impact of iron supplements on the gut health.

1.INTRODUCTION

1.1 Iron metabolism

Although required in small amounts that vary according to age, gender and physiological status, iron is an essential micronutrient for all living organisms. The existence of two oxidation states for iron, ferric and ferrous iron, makes it suitable as an electron donor and acceptor, which justifies its implication in a wide variety of biological functions. Ferric iron is insoluble at neutral pH and reducing conditions favour the ferrous soluble form of iron. Iron is involved in oxygen transport since it is part of the oxygen transporting and storing proteins haemoglobin and myoglobin. Iron also acts as a cofactor in many proteins, allowing DNA replication, neurotransmitter synthesis, ATP production in the mitochondria and xenobiotic and pathogen clearance (1). More importantly, along with erythropoietin (EPO) iron is capable of regulating the formation of red blood cells (RBCs) in the bone marrow; iron is the limiting factor during the maturation of erythroblasts and its shortage can trigger their apoptosis and the consequent anaemia (2). Mitochondria are major cellular hubs of iron utilization and accumulation, where iron is part of Fe-S clusters that are involved in the electron transporting chain and ATP synthesis, among other processes (3).

Given its physico-chemical properties, iron metabolism is complex and needs to be tightly regulated as both iron excess and deficiency have a negative impact on human health (1). Iron metabolism is based on continuous iron circulation and recycling since the human organism displays limited capacity for its elimination. Actually, iron is only removed via cell skin desquamation, sweat, blood loss and sloughing of intestinal epithelial cells. As regulation mechanisms to control such losses do not exist, dietary intake, intestinal absorption, and iron recycling have to be finely regulated (4).

1.1.1 Iron absorption

Iron is absorbed in the small intestine (duodenum and proximal jejunum), regions with the lowest pH, both in heme and non-heme forms (5). Absorption is only meant to compensate for iron losses (1-2mg/day) and only reaches 5-10% of the total amount ingested; most of iron used in the organism will then derive from its constant recycling (1).

Iron from animal-derived food takes the form of heme complexes that are more easily absorbed through specific transporters (approximately 20-50% of the ingested amount). Once inside enterocytes, iron is released via heme-oxygenase enzymes and either stored in the iron storing protein ferritin (FTN) or exported across the basolateral membrane via ferroportin (FPN) prior oxidation to ferric iron by hephaestin (HEPH). However, most iron is present in nature as inorganic or non-heme iron, and it can be found in the ferric form in plant-derived food. Inorganic iron absorption is less efficient compared to heme iron (0.1-35% of the ingested amount), but it can be more easily adjusted to meet iron demands. Since 85–100% of dietary iron is in the non-heme form, this regulation allows a better control of iron absorption. Ferric iron needs to be converted to ferrous iron to be uptaken by enterocytes. This process is mediated by the ferrireductase duodenal cytochrome b (Dcytb), which generates the ferrous soluble form which will then be transferred across the brush border membrane into the enterocyte by divalent metal transporter 1 (DMT1). Ferrous iron can then be stored in FTN or be exported into the bloodstream via FPN prior oxidation to ferric iron. When exported, ferric iron is transferred to transferrin (Tf), the main iron binding protein that will distribute it in the organism (2, 3, 6) (Figure 1)

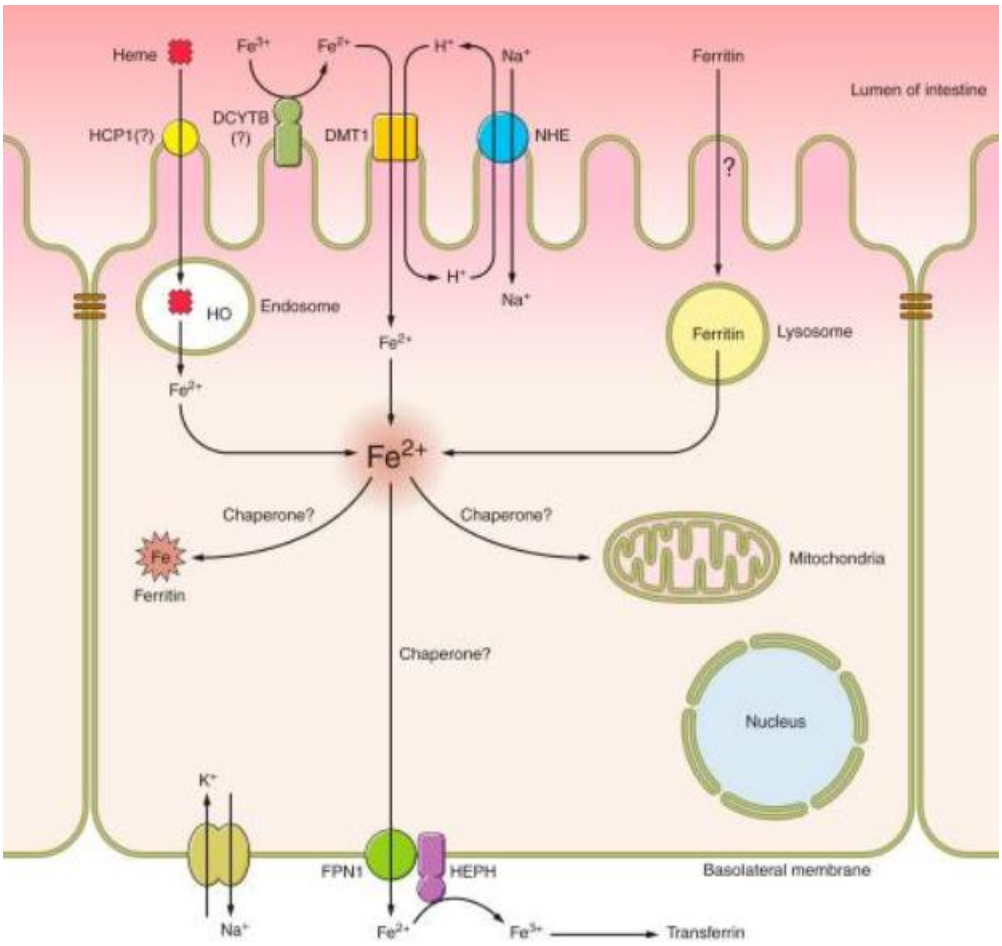

Figure 1. Intestinal iron absorption. Image from Gulec et al., (2014) (6).

Efficient iron absorption involves sequential steps and different proteins, thus being highly susceptible and easily disturbed. Iron absorption is influenced by endogenous and exogenous factors, including physiological and pathological states or the diet.

As a case in point, during pregnancy, iron requirements are increased due to the need to provide the mineral for the formation of new tissue both in the mother and the child. Furthermore, due to the lack of iron on breast milk, newborns will have their iron deposits repleted by the time they are delivered and such deposits will need to last until they are able to incorporate other types of food into their diets (approximately 6 months). The only way to cope with such high demands during pregnancy is through an increased

iron absorption and making use of deposits. Actually, the efficiency of iron absorption is enhanced especially in the middle of the second trimester (7).

Pathological states, such as iron deficiency, can also trigger an increase in iron absorption. Shortage of iron is characteristic of iron deficiency and one of its consequences is a reduced oxygen transport and local or systemic hypoxia. Hypoxic cellular conditions are known to stabilize the hypoxia inducible factor (HIF) subunit α, which is constitutively expressed in the cytosol but degraded in presence of oxygen. In such circumstances, prolyl hydroxylases (PHDs) label this subunit and it undergoes proteosomal degradation. However, when oxygen or iron levels are depleted, prolyl hydroxylases are inhibited and HIF-α subunit is able to bind its nuclear counterpart HIF-β subunit. Aryl hydrocarbon receptor nuclear translocator (ARNT), also known as HIF-β, is able to bind hypoxia responsive elements (HRE) in the DNA upon binding to HIF-α subunit. The expression of all genes containing hypoxia response elements in their promoters can therefore be modulated by HIFs (8).

Depending on the tissue, different isoforms of HIF-α and HIF-β can be expressed. Three isoforms exist for HIF-α and HIF-β subunits: HIF-1α, HIF-2α, HIF-3α and HIF-1β, HIF-2β and HIF-3β (also known as ARNT1, ARNT2 and ARNT3). The activity of HIF-1α and HIF-2α is critical to regulate gene expression in response to hypoxia via binding to HIF-1β, while the activity of HIF-3α has been less studied (9).

HIF-1α and HIF-2α are similar in structure, although their expression pattern varies from tissue to tissue. HIF-1α is constitutively expressed in all tissues while HIF-2α is only expressed in certain biological niches. They also display differences in relation regulation mechanisms, namely the presence of iron regulatory elements in the promotor of HIF-2α gene (9, 10).

It is in the small intestine where HIF-2α is known to have a pivotal role on iron absorption. During iron deficiency and due to the depletion of oxygen and iron levels,

prolyl hydroxylases are inhibited and HIF-2α is stabilized in the small intestine. Dcytb, DMT1 and FPN are known HIF-2α targets, whose expression increase upon HIF-2α stabilization. Therefore, during iron deficiency, an increase in iron absorption occurs as a trade off mechanism via HIF-2α stabilization (6, 11) (Figure 2).

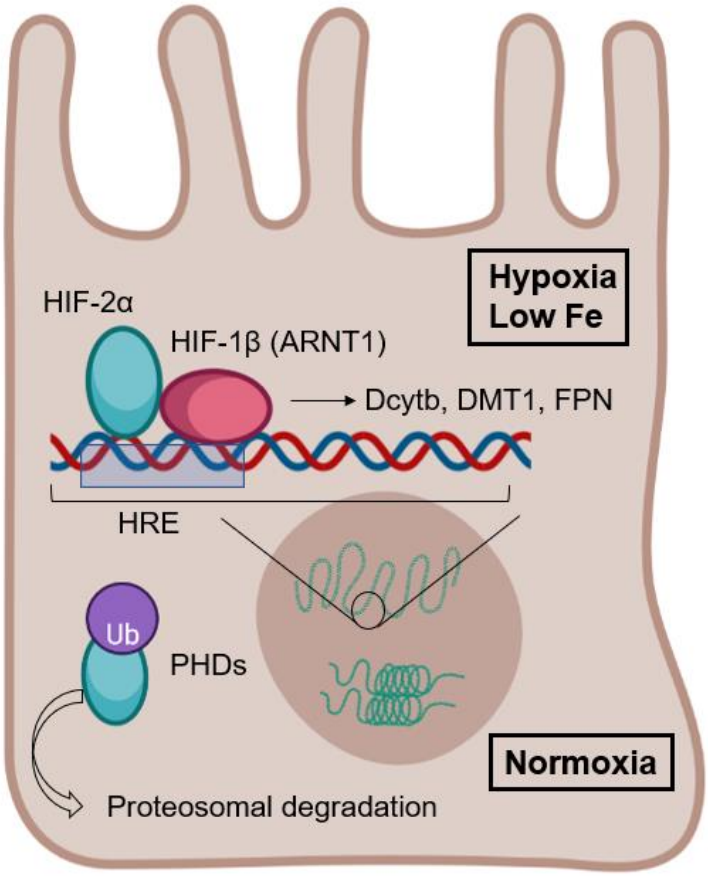

Figure 2. Influence of HIF-2α on intestinal iron absorption.

Among the exogenous aspects that might influence iron absorption, especially inorganic iron, it is worth highlighting dietary compounds. Iron needs to be present in its soluble ferrous state to be uptaken by enterocytes; exogenous factors can either promote or impair the reduction process from ferric to ferrous iron or form insoluble complexes in the intestinal lumen unable to be absorbed. Dietary compounds can also compete with

inorganic iron for transporting mechanisms in the enterocyte. When ingested in the same meal, heme iron (from meat or fish) and antioxidants such as ascorbic, citric, malic and tartaric acids can act as enhancers for iron absorption since the latter promote the ferrous state. On the contrary, iron absorption inhibitors include phytic acid in whole grain cereals, fiber, legumes, nuts, and iron-binding polyphenols from tea, coffee or wines, all of which bind iron forming non-absorbable complexes (1, 5).

Due to the importance of iron absorption in the regulation of systemic iron levels, and given the fact that the digestive tract harbours the greatest microbial community in the organism, the gut microbiome might be an influential factor affecting iron absorption and bioavailability. The ferric reducing capacity of some members of the microbiome, such as *Deferribacter* (12), or the wide variety of metabolites that are acting as signalling molecules to coordinate host-microbiome homeostasis (13) are likely to play a role in iron metabolism. The current state of knowledge as far as microbiome and iron metabolism is concerned is reviewed in section number 1.2.

1.1.2 Iron distribution

Transferrin (Tf) is the main iron carrying molecule, distributing iron from the absorption site (intestine), recycling and storing sites (spleen and liver) to cells and organs, mainly to the bone marrow for erythropoiesis and to cells with high turnover rate.

Transferrin can only bind 2 atoms of ferric iron (Holo-Tf), so a prior oxidation needs to take place outside cells via hephaestin. Import of cellular iron from transferrin takes place through transferrin receptors (TfR). Two types of TfR exist, TfR1 and TfR2, with TfR1 being the most abundandt and ubiquitously expressed across the organism. Upon binding, TfR1 is internilised in clathrin-coated vesicles, which are acidified to promote the dissociation of iron from Tf. Iron is then reduced and exported to the cytosol via DMT1. Tf-TfR1 complex is transported to the cell membrane, where apo-Tf (iron –

free Tf) is released and TfR1 remains in the membrane for another round of internalization (14).

Since two thirds of the total iron pool is invested in erythropoiesis, erythroblasts show the greatest TfR1 expression levels and these levels are correlated to the changing rates of haemoglobin production.

As far as TfR2 is concerned, it is mainly expressed in the liver and its major function is not related to iron distribution, although it can also recognize Holo-Tf. TfR2 is more likely to be a modulator of hepcidin transcription, the most important hormone regulating systemic iron metabolism. TfR2 binds the homeostatic iron regulator or hemochromatosis protein HFE, which along with its Holo-Tf recognizing properties, allow it to act as a sensor of circulating iron to activate hepcidin secretion in response to elevated transferrin saturation (15).

1.1.3 Iron recycling

Iron metabolism is based on constant recycling since absorption is meant to only compensate for iron loss. Most of iron in the organism is used in the bone marrow during erythropoiesis (16), where erythrocytes and haemoglobin are synthetized and released into the bloodstream. However, red blood cells (RBCs) show a short life span (around 120 days) and iron needs to be recovered after erythrocyte senescence. This recycled iron is the main contributor for subsequent rounds of erythropoiesis.

Iron recycling is carried out by macrophages in the spleen and the liver (Kupffer cells). After 120 days, erythrocytes naturally undergo a senescence process (eryptosis) triggered by a decrease in the pH and ATP levels, along with an increase in metabolic end products, cytokines, oxidative stress and free haemoglobin. These metabolic alterations contribute to lipid and protein oxidation in cell membranes and loss of

viscoelastic properties, which lead to erythrocyte lysis when entering the narrow network of blood vessels in the spleen (17). As a consequence of the aging process, erythrocytes also acquire specific membrane receptors that need to reach a specific threshold for macrophages to initiate erythrophagocytosis (18).

Senescent erythrocytes are then scavenged by macrophages in the liver and the spleen and digested in the phagolysosome, where heme is separated from haemoglobin molecules. Once in the cytosol, iron is separated from the protoporphyrin ring by heme oxygenase 1 (19), whose expression is regulated by HIF-1α (10).

Depending on the needs, iron can be locally stored inside macrophages via binding to FTN or can be exported and distributed through FPN and Tf. Iron flux from macrophages greatly exceeds inflows from dietary iron absorption and from iron deposits.

1.1.4 Iron storage

Unused iron can be stored inside cells, mainly macrophages, and organs, such as the liver or the spleen. Since free iron is involved in the production of reactive oxygen species (ROS), ferrous iron is stored through binding to FTN. FTN is the main iron storing protein composed of L and H subunits on variable ratios depending on cell type and physiological conditions (1). H-rich FTN display low iron binding capacity and they are more abundant in tissues with high ferroxidation activity and low storing potential, such as the heart or the brain. On the contrary, L-rich FTN show high iron binding capacity and they are more prevalent in tissues exerting iron storing functions, such as the liver or the spleen (20).

While being kept in a non-reactive form, iron stored in FTN deposits is soluble and easily accessible upon physiological demands. However, when cellular iron content

exceeds FTN loading capacity, excess of iron triggers the formation of non-soluble protein aggregates referred to as hemosiderine (21). Hemosiderine is thought to derive from the lysosomal degradation of FTN aggregates and has been associated with iron overload, tissue damage and ferroptosis (22, 23).

FTN expression is promoted by nuclear factor erythroid 2-related factor 2 (NRF2). However, iron is the main regulator of FTN at the translational level. FTN mRNA contains iron responsive elements (IREs), which are targeted by iron responsive proteins (IRPs). IREs and IRPs are cellular iron-dependent regulatory mechanisms that control gene expression and protein translation of genes involved in iron metabolism, such as FTN, FPN or TfR1. Their role is dependent on the gene in question and the iron balance; in the case of FTN, IRPs act as inhibitors of mRNA translation in the context of iron shortage, while iron overload prevent the activity of IRPs and promote the translation of FTN mRNA. Nuclear receptor coactivator 4 (NCOA4), whose expression is regulated by iron and HIFs, can also bind FTN and deliver it to the lysosomes during iron shortage (20).

Cellular and organ iron deposits represent quick and ready-to-use resources upon physiological or pathological demands, such as blood loss or pregnancy (7). When iron requirements outstretch the capacity of iron deposits, a state of iron deficiency is gradually established in the organism as discussed in following sections.

An overview of iron absorption, distribution, recycling and storage is provided in Figure 3.

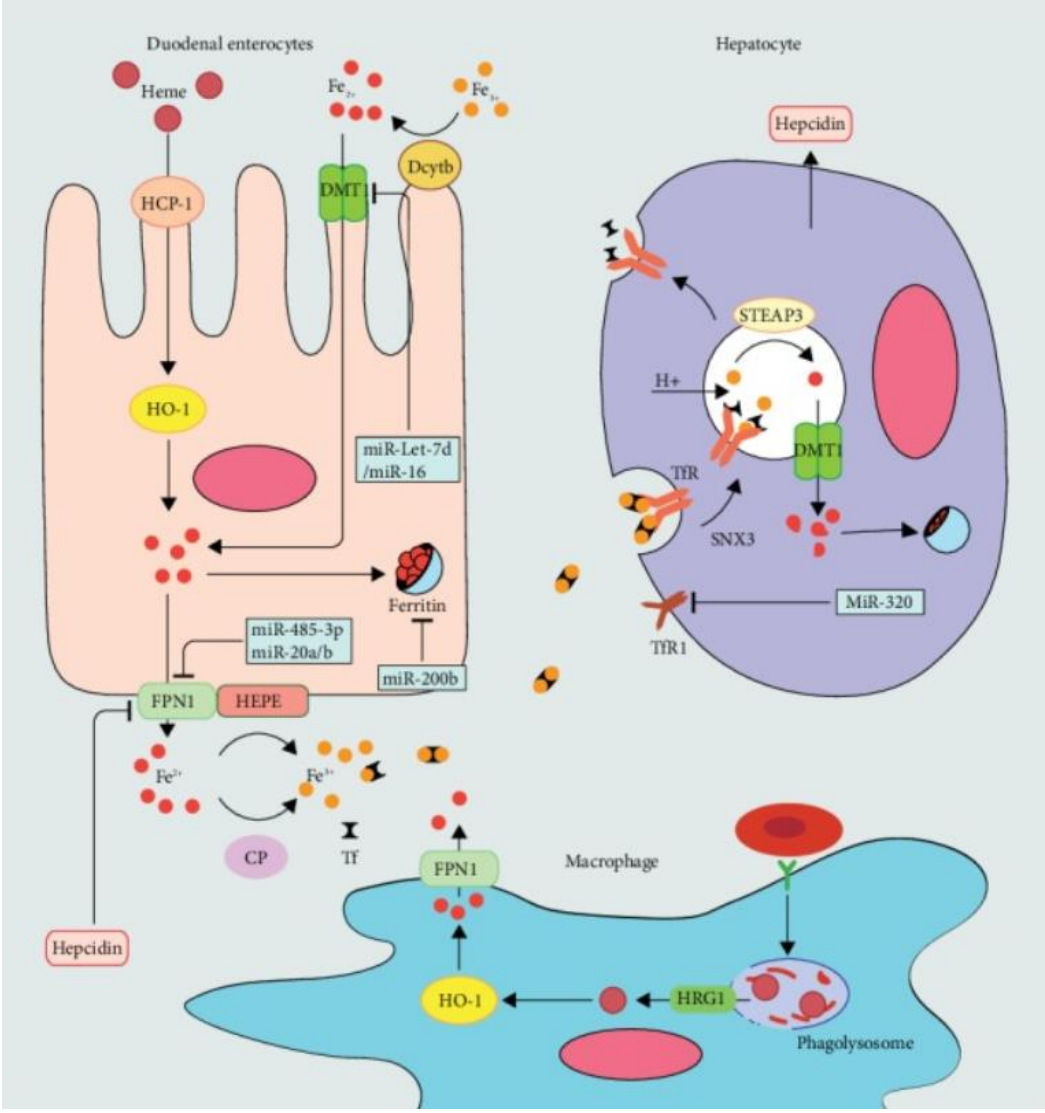

Figure 3. Overview of iron absorption, distribution, recycling and storage. Image from Li et al.,(2020) (24).

1.1.5 Cellular and systemic regulation of iron metabolism

A complex regulatory system operates to maintain iron levels within homeostatic ranges and to adjust iron metabolism to physiological needs.

At the cellular level, iron responsive proteins 1 (IRP1) and 2 (IRP2) are the master regulatory elements that control the translation of proteins related to iron uptake and distribution (DMT1, TfR1), storage (FTN) and export (FPN). They bind 5' and 3'

untranslated regions (UTR) of mRNAs, known as iron responsive elements (IREs), impairing or promoting their translation. Both L and H-FTN and FPN contain one single IRE in its 5'UTR, while TfR1 and DMT1 contain IREs in their 3'UTR. Binding of IRPs to 5'UTR IREs results in an impairment of mRNA translation while binding of IRPs to 3'UTRs results in stabilization of mRNAs and increased protein translation. The activity of IRPs depends on the cellular iron pool, whereby they target 5' and 3' UTR IREs during iron deficiency and remain inactive in iron-replete cells, with the ultimate goal of shifting iron metabolism towards an increased uptake and distribution during iron deficiency or an increased storage during iron repletion (25, 26).

A 5'UTR IRE is also present in HIF-2α mRNA. Hypoxic conditions resulting from iron deficiency and decreased oxygen transport contribute to the stabilization of HIF-2α, which along HIF-1α orchestrate a compensatory response consisting of an increased iron absorption and an increased production of EPO (10). However, a double regulatory mechanism exists as far as HIF-2α is concerned, since during iron shortage, IRPs targeting 5'UTR IRE in HIF-2α mRNA impair its expression (26).

An extra layer of complexity is added when considering the systemic regulation of iron metabolism. The hormone hepcidin is a key molecule in this regard. Being mainly produced in the liver, hepcidin levels are modified in response to systemic iron concentration, hepatic iron stores, inflammation, erythropoietic activity and hypoxia. High systemic iron levels, repleted iron deposits and inflammation (mainly IL-6) increase hepcidin synthesis and secretion. On the contrary, enhanced erythropoiesis rates and reduced systemic iron levels reduce hepcidin secretion (27).

The homeostatic iron regulator or hemochromatosis protein (HFE) and TfR2 (HFE/TfR2) system is involved in the regulation of hepcidin production. High iron levels are sensed in the liver through the interaction of Holo-Tf with TfR2, which triggers HFE-TfR2 binding and the consequent cellular signal for hepcidin synthesis. On the contrary, TfR1 binds to HFE protein when iron concentration is low, which leads to TfR2

degradation and the absence of such signal. Bone morphogenetic protein 6 (BMP6) – hemojuvelin system is involved in the regulation of hepcidin secretion according to liver iron deposits. Iron replete deposits lead to the formation of BMP6-hemojuvelin complex in the cell membrane and the cellular signal for hepcidin production. Iron depleted stores triggers furin secretion, which produces truncated forms of hemojuvelin and sequestration of BMP6 in the cytosol. The absence of BMP6-hemojuvelin complex prevents the production of hepcidin(27). Iron deficiency also decreases hepcidin secretion via increased erythropoiesis: decreased oxygen transport resulting from reduced haemoglobin levels triggers HIF-2α stabilization which in turn increases EPO secretion in the kidney; erythropoiesis is therefore enhanced with erythroblasts secreting erythroferrone, which sequesters BMP6 and impair hepcidin production. HIF can also regulate hepcidin levels in an EPO-independent manner; HIF stabilization in hepatocytes increases the expression of matriptase 2, which cleaves hemojuveline from the cell membrane impairing hepcidin production (10).

The main role of hepcidin is preventing iron release from iron storing and absorptive cells such as enterocytes and macrophages. To serve this purpose, hepcidin binds FPN and trigger its internalization and degradation, thus blocking iron export from cells (28). The FPN-hepcidin axis is known to be associated with some disorders such as hemochromatosis or anaemia of inflammation. Loss of function mutations in hepcidin regulatory genes (HFE, TfR2, hemojuvelin) or in the hepcidin gene itself cause hereditary hemochromatosis and lead to a non-regulated iron absorption and export; excess of iron is accumulated in tissues and organs disrupting homeostasis and sometimes leading to a premature death (28). On the other hand, anaemia of inflammation is characterised by an increased hepcidin secretion due to an inflammatory state, which prevents iron from being released into the bloodstream. Iron is therefore accumulated inside cells (mainly macrophages and enterocytes), not being available for erythropoiesis and causing the consequent anaemia (29).

A general overview of iron metabolism is provided in Figure 4, with filled arrows indicating the main pathways of iron circulation in the organism

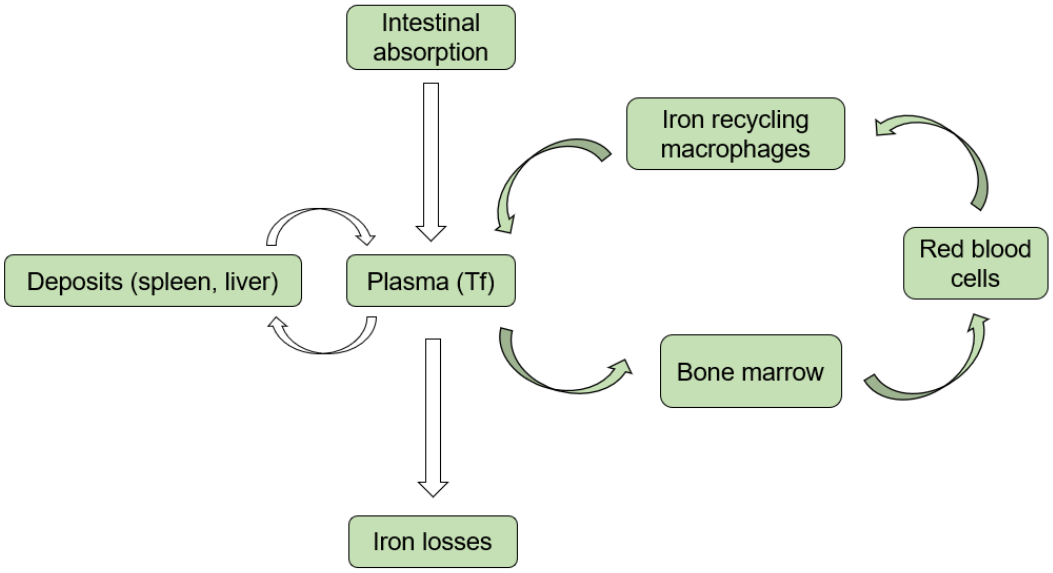

Figure 4. Overview of iron metabolism.

1.1.6 Alterations of iron metabolism: iron deficiency anaemia

Anaemia is a multifactorial syndrome characterised by a reduction in haemoglobin levels below homeostatic ranges, which vary according to age, gender and physiological conditions such as pregnancy. Anaemia is a common diagnosis for the majority of physicians (30), and it is estimated to affect one third of the global population with an increased prevalence in underdeveloped countries, where it imposes a considerable economic burden (31, 32).

Iron deficiency is the top leading cause of anaemia, causing 50% of cases (4), and the most prevalent micronutrient deficiency worldwide. In fact, iron deficiency along with vitamin A and iodide deficiency and protein-calorie malnutrition are the most serious

nutritional issues worldwide, according to the Food and Agriculture Organization (FAO). Due to their physiological state, growing children, adult and pregnant women and the elderly have been classically considered the at risk patients, although the increasing prevalence of malabsorption diseases also suggest an additional susceptible population in these subjects (33).

Iron deficiency anaemia (IDA) negatively affects school and work productivity (34). IDA has been associated with impaired motor and mental development in children and neuropsychiatric diseases, with alterations persisting even after 10 years of iron repletion (4). IDA has also been related to increase maternal and perinatal mortality in pregnant women (35) and to impaired cognitive function and dementia in the elderly (4).

Along with EPO, iron is the most important factor regulating erythropoiesis. Erythropoiesis consists of the formation of red blood cells (RBCs) from burst forming units-erythroid (BFU-Es) in the bone marrow. Colony forming units-erythroid (CFU-Es) are subsequently generated from BFU-Es; proerythroblasts, erythroblasts, intermediate normoblasts, late normoblasts and reticulocytes complete the whole sequence of RBCs formation. Erythropoiesis is specifically stimulated by the kidney-secreted hormone EPO. Hypoxia increases EPO secretion via HIF-2α-dependent mechanisms, representing a trade-off mechanism during iron deficiency whereby reduced oxygen transport derived from reduced haemoglobin levels triggers stimulating factors for erythropoiesis (36). The expression of EPO receptors is also increased by HIF-1α, with the greatest density being observed in CFU-Es and the lowest in more differentiated erythroid cells.

On the other hand, iron bioavailability also determines the rate of erythropoiesis. Although iron absorption contributes substantially to the iron pool in erythrocite precursors, the most important source of iron for daily heme and haemoglobin synthesis during erythropoiesis is the recycling from senescent erythrocytes, where macrophages in the spleen and the liver play a major role (37). Iron is taken up by precursor cells via TfR1, and after cytosolic and mitochondrial reactions, iron is incorporated into the

protoporphyrin IX ring to form the heme group (38). Globin chains are synthetized in the cytosol; incorporation of heme groups into globin chains results in haemoglobin.

Iron shortage can induce an insufficient erythropoiesis since it impairs heme and haemoglobin synthesis. Causes that can induce iron deficiency include decreased iron intake, more frequent in underdeveloped countries, decreased iron absorption, common in malabsorption diseases, increased iron requirements, such as pregnancy or growing children, and increased iron losses, such as bleeding (27).

Iron deficiency is often progressively induced, with three stages being differentiated. Latent iron deficiency is the first stage, where spleen and liver iron deposits are depleted and anaemia has not been established yet. The second stage is characterised by dysfunctional iron-containing enzymes, since iron in these proteins is also depleted to maintain erythropoiesis. Lastly, iron deficiency anaemia (IDA) is established, with decreased haemoglobin levels, number of RBCs and haematocrit. Due to lack of iron, erythrocytes are smaller (microcytic) and contained reduced amounts of haemoglobin (hypochromic), leading to reduced mean corpuscular volume, mean corpuscular haemoglobin and mean corpuscular haemoglobin concentration in the hemogram. Serum ferritin levels are also depleted, indicating the exhaustion of iron deposits (27, 37).

Common symptoms of IDA and other kind of anaemias include paleness in skin and mucous membranes due to decreased haemoglobin and redistribution of blood flow towards organs with vital functions such as the nervous system and muscles. As a consequence of a reduced oxygen transport, hypoxia produces the majority of symptoms in organs with high oxygen demand. Dizziness, blurry vision, neurological alterations such as impaired mental and motor capacity and muscle pain are common symptoms affecting the nervous system and muscles. Alterations at the cardiovascular and respiratory level, such as increased heart rate or increased respiratory frequency, also occur to compensate systemic hypoxia. Since iron is an essential micronutrient, cells

with high turnover rate are especially affected during IDA, including alterations in the skin and mucous membranes, hair or nails. Appetite and susceptibility to infection are also specific symptoms for IDA (27).

The identification and correction of the underlying cause of IDA is crucial to treat the disease. Even displaying limited efficacy, the first treatment option for patients suffering IDA consists of oral iron supplements taken three times a day. Standard dose is around 65 mg of elemental iron in the form of ferrous salts, although lower dosages have been shown to be also effective since iron absorption is a saturable mechanism. In fact, lower dosages might be beneficial to decrease the associated side effects reducing the non-absorbed iron fraction, without limiting the efficacy. Four forms of iron salts are available to treat IDA, ferrous sulphate, ferrous sulphate exsiccated, ferrous gluconate, and ferrous fumarate, with no clear differences between them. They should be taken between meals, avoiding the presence of inhibitors (tea, coffee, fibre) and including absorption promoters such as ascorbic acid (4, 33).

As a consequence of iron supplements, side effects occur in approximately 30%-50% of patients (33). Such effects derive from the accumulation of non-absorbed iron in the intestine, which generates ROS via Fenton and Haber-Weiss reaction, triggering oxidative stress. Lipid and protein oxidation in intestinal epithelial cells often lead to ferroptosis and an impairment in the intestinal barrier function (39, 40). Persistently high ROS levels can also increase mitochondrial permeability, causing swelling and even rupture. Therefore, energy supply in enterocytes is negatively affected during iron supplementation, which contributes to intestinal damage. Excess of iron in the intestine leads to intestinal dysbiosis, which triggers inflammation (41). As certain forms of iron supplements such as ferrous sulphate have been repetedly associated with gut dysbiosis, alternative iron salts are being currently developed to treat IDA, such as oral ferric maltol, with reduced gastrointestinal side effects (42). Lately, novel formulations of standard iron salts are also being designed, where ferric pyrophosphate is embedded

within a matrix of phospholipids and sucrose esters of fatty acids. This strategy aims to enhance intestinal absorption through para-cellular and trans-cellular routes and improve intestinal tolerance (43, 44).

Not surprisingly, gastrointestinal alterations are the most common side effects during iron supplementation (40). Overall, the limited intestinal absorption of iron supplements along with the high incidence of side effects hinder therapeutic compliance (33). As iron supplements should be taken during three months after the restoration of IDA, patients usually abandon the treatment when symptomatology disappears but before iron deposits have been completely restored, which leads to the reappearance of anaemia. A considerable percentage of iron deficiency anaemias become chronic and refractory to treatment.

Response to treatment is evaluated by reticulocyte count, which should rise as soon as four days after the treatment has started, and haemoglobin concentration, which start rising by the second week of therapy and should reach 20g/L to consider a positive response to oral therapy. Lastly, ferritin and serum iron levels should normalize, indicating a recovery of iron deposits (4). In the case of a reduced response, tolerability or adherence to oral therapy, intravenous iron, such as iron dextran, iron sucrose or ferric carboximaltose, is the second approach to treat IDA, although it increases the risk of systemic oxidative stress. Given the reduced availability of therapeutic options and the limited efficacy and considerable number of side effects, the optimisation of existing therapies and the development of new therapeutic tools would be of great scientific interest in the clinical management of IDA.

Although it is well known that iron supplements exert a detrimental effect on gut health, questions regarding the state of the intestinal epithelium and the gut barrier during IDA remain unanswered. Iron shortage impairs cell cycle progression and DNA replication (31). As a case in point, cells with a high division rate, such as skin or immune cells, are the most susceptible ones when it comes to iron deficiency. In this sense,

intestinal epithelial cells are characterised by a high turnover rate, being renewed every 3-5 days in the mammalian intestine (45). These digestive tract lining cells are part of the intestinal barrier, whose function is to provide an intact interface between the intestinal lumen and adjacent tissues. A wide variety of antigens, toxins and microorganisms are normally found in the intestinal lumen, with the intestinal barrier preventing their leaking into the bloodstream and the consequent disruption of tissue homeostasis.

The intestinal barrier is composed of three functional compartments: the physical, the biochemical and the immunological barrier. Intestinal epithelial cells are the mainstay of the physical barrier, with tight junctions allowing their sealing. Mucus integrity and a healthy microbiome also contribute to the functionality of the physical barrier. Lastly, the biochemical and immunological components provide antimicrobial peptides (AMPs) and immune cells, completing the whole spectrum of protective elements (Figure 5) (45).

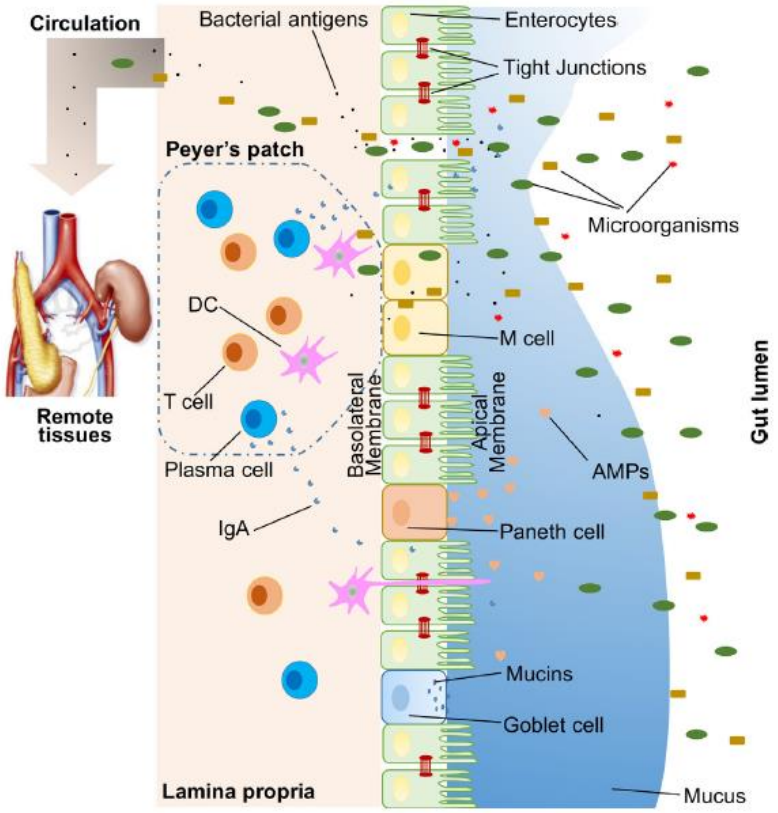

Figure 5. Components of the intestinal barrier. Mu et al., (2017)(45).

HIF-1α is a key regulator of the intestinal barrier, promoting the expression of genes involved in tight junction integrity, xenobiotic clearance, mucus synthesis and secretion, nucleotide signaling, energy metabolism and antimicrobial defense (8). HIF-1α levels are maintained via mitochondria-dependent mechanisms, involving the bacterial production of short chain fatty acids (SCFA) in the large intestine, as discussed in section number two (46).

Although microbial translocation can occur in a physiological setting (47), an impairment in the gut barrier functionality can also trigger microbial leaking. Major gaps in our knowledge exist with regards to microbial translocation in the context of IDA. Microbial translocation has been related to adverse cardiovascular outcomes and to the development of acute pancreatitis (48, 49). There is increasing evidence that seem to indicate that microbial translocation to extraintestinal sites might be involved in the pathogenesis of chronic, non-infectious diseases (50). Such is the case of *Enterococcus gallinarum*, which has been related to systemic lupus erythematosus due to its capacity to induce autoimmunity in prone hosts through translocation to the spleen, liver and mesenteric lymph nodes (51). Overall, and due to their resistance to harsh environmental conditions, enterococci are the main colonizers of extraintestinal tissues such as blood, lungs or pancreas; however, whether this translocation is the cause or the consequence of the associated diseases is largely unknown.

There are few studies that investigate the effect of iron deficiency on the gut epithelium and the intestinal barrier functionality. Li et al., (2016) (52) reported increased intestinal permeability and inflammation in iron deficient pigs. Others are mainly focused on the implications of iron overload (52, 53). Among them, Din et al., (2020)(53) noted a reduction of both villus height and the expression of tight junction proteins, along with an

increased production of ROS and fibrosis in the intestine of piglets fed with a high iron content diet.

Considering the detrimental effect of iron supplements on intestinal health, studying the intestinal barrier functionality and the biological processes occurring in the intestinal epithelium during IDA would be of great scientific interest to improve the clinical management of the disease. Finding tools to optimise current therapies by reducing their negative impact on the gastrointestinal tract seem imperative, as well as to take new therapeutic approaches to treat IDA. In this line, the use of prebiotics, probiotics and synbiotics (prebiotics and probiotics) have been recommended to prevent intestinal side effects during IDA therapy (40). The gut microbiome is also becoming a target to develop novel therapies against IDA; Das et al., (2020) (54) proposed the use of gut specific antibiotics to deplete intestinal bacteria competing for iron with the host, showing an improvement in iron deficient animals.

Since intestinal iron absorption is one of the most regulated aspects of iron metabolism, the study of the gut microbiome as a trigger or a facilitator of IDA could be of scientific interest to optimise existing therapies and to develop new therapeutic tools. Moreover, given the close relationship between gut health and gut microbial communities, studying the gut microbiome in the context of IDA would unveil key aspects to restore intestinal health during the recovery of the disease.

1.2 The human microbiome

The human organism co-habitates with trillions of symbiotic, body site-specific microbes that can be found in a wide varity of biological niches, such as the skin, the oral cavity or the gut (55). The whole spectrum of microorganisms (eukaryotes, archaea, bacteria and viruses) inhabiting the human body, along with their respective genes, is referred to as the human microbiome. Comprising a symbiotic community, the host

provides microorganisms with shelter and nutrients, while micoorganisms exert beneficial functions for the host in return (56). A complex interplay takes place between the host and its microbiome, with different cell events being orchestrated to maintain host homeostasis.

In the current -omic era, the human microbiome has become a valuable source of information that had previously been overlooked. The limitations in the solely culture-based procedures to study the microbiome led to the misconsideration of sterility in certain biological niches (57), the misrepresentation of certain microbial members in specific body sites (55), and a overall skewed study of microbial communities. However, the development of next generation sequencing (NGS) techniques has allowed a more comprehensive view of the human and environmental microbiome (58).

In an effort to elucidate the implications of microbial communities in health and disease, the Human Microbiome Project (HMP) was funded in 2007 (56). The HMP constitutes an extension of the Human Genome Project, an interdisciplinary consortium simultaneously launched in the United States, Europe and Asia. Making use of NGS techniques, the HMP also aims to pave the way for future research in this field describing the human microbiome in the state of health. One of its contributions include the broadest taxonomic and functional characterisation of the baseline Western microbiome in all the clinically relevant biological niches: 18 body habitats for women and 15 for men (excluding three vaginal sites), distributed among five major body areas (oral cavity, oropharynx, skin, faeces and vagina) (59). A great interindividual variability was found in all body areas when considering microbial taxa, while metabolic pathways were stable among individuals despite variation in community structure. A second wave of data was analysed to update those results (60).

In light of the above, and given the great difficulty in the definition of what a healthy microbiome would be because of its high interpersonal variability, the idea of a “functional core” is being implemented as an alternative approach. The functional core

includes microbial functions (not present in the host) that need to be provided in a specific niche during health but not necessarily by the same members of the microbiome in different individuals (55). Such core may be assessed at the genomic, transcriptomic or proteomic level.

1.2.1 How to study the human microbiome

The classic study of the human microbial communities has been entirely focused on culture-based methods, where samples were collected and grew on culture media. The analysis, and sometimes sequencing, of colonies allowed the identification of the microbial members present in that sample. The main issue arising from this approach is the loss of biodiversity due to the inability of certain taxa to grow in standard media (61). Therefore, the information obtained using these methods is often biased towards cultured microorganisms.

The current landscape to study the human microbiome is based on the use of NGS techniques and culturomics. NGS include a wide variety of techniques ranging from amplicon sequencing, whole genome sequencing and functional omics. The first two are referred to as metagenomics, consisting of either targeted sequencing of marker genes (ribosomal RNA 16S, rRNA 16S) or untargeted sequencing of whole genomes (shotgun) (62). Both of them can be used to gain insight into the structure and potential functioning of microbial communities. Amplicon sequencing targets marker genes such as 16S rRNA to study the bacterial structure of the human microbiome at the genus level. On the contrary, whole metagenome sequencing provides a more comprehensive and accurate functional and taxonomic characterisation of the microbiome at the species or strain level, including viruses, funguses and protozoa (63) (Figure 6). However, since changes in microbial functionality might occur with minimal changes in taxonomy and viceversa, functional assessment of the microbiome is necessary to have a complete perspective

of how microbial communities interact with the host. Functional omics serve this purpose and include metatranscriptomics, metaproteomics and metabolomics (64).

Culturomics has also gained traction in the last years as a complementary tool to NGS techniques to study the structure and functioning of the human microbiome. It consists of the diversification of culture conditions to allow more microorganisms to grow on culture media, along with their identification by matrix-assisted laser desorption ionization–time of flight mass spectrometry (MALDI-TOF MS). Culturomics allows scientists to overcome the inability of NGS techniques to detect non-abundant taxa, since they are limited by sequencing depth (65), and compositional limitations, inherent to NGS techniques (66).

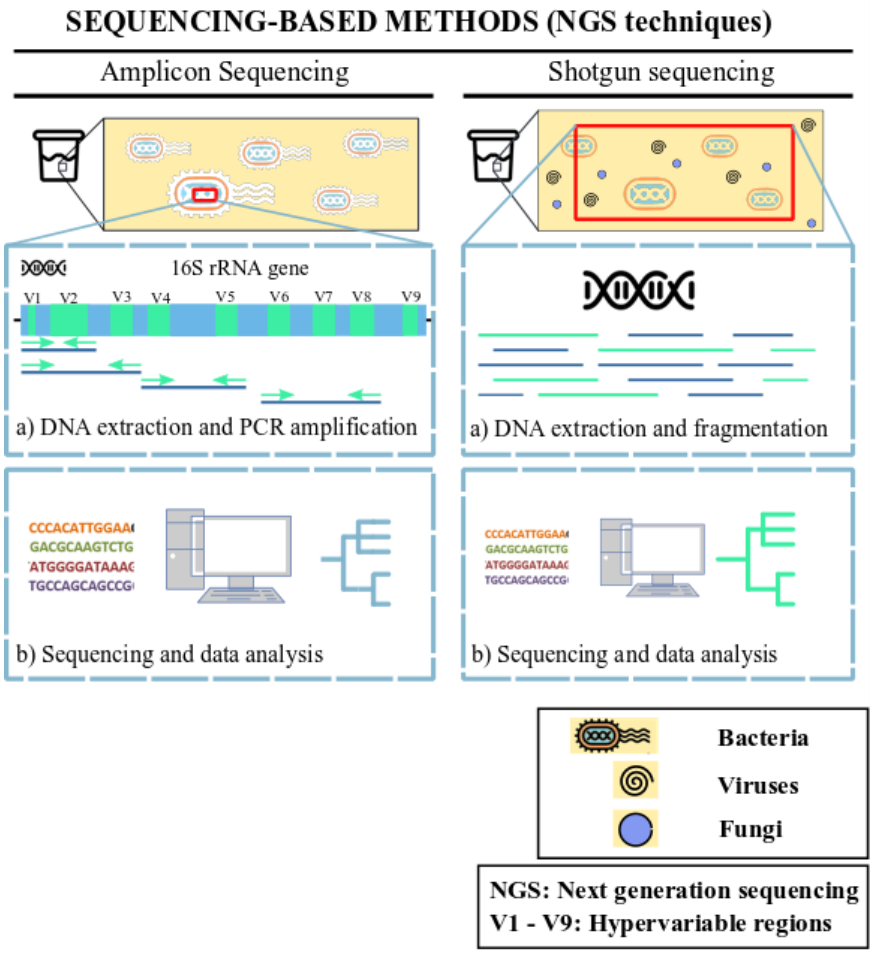

Figure 6. Methods to study the human microbiome. Adapted from Pérez Carrasco et al., (2021)(57).

1.2.1 The gut microbiome

The human intestine harbours the greatest and most diverse microbial community in the entire organism, including bacteria, viruses and some eukaryotes (56, 67). It is estimated that the number of bacteria in the gastrointestinal tract is 10-fold higher than the number of eukaryotic cells, and over 100 fold higher in the case of genomic content compared to the human genome (68).

In an attempt to characterise this microbial repertoire, the metagenomics of the Human Intestinal Tract (MetaHIT) project was funded to establish an extensive reference catalog of microbial genes and genomes present in the healthy human gut across three continents. It also aimed to develop bioinformatics tools to store and analyse the information gathered as well as to characterise the population based on the presence of microbial genes and taxa (69). Similarly, the HMP also characterised the structure of the intestinal microbiome in 242 western healthy subjects, among other biological niches (59). The latest estimation of the total genetic repertoire in the integrated catalogue of genes of the human microbiome from the MetaHIT and HMP projects was about 9×10^6 genes, 40 % of which with unknown function. In contrast, the latest version of human genome estimates around 20000 protein coding genes (70).

As discussed in previous sections, interindividual variability is high in relation to the structure of the microbiome but not in relation to its functionality, and that statement is also applicable to the gut microbiome. Therefore, characterising a “healthy” microbiome as an ideal set of specific microbes is no longer a practical definition. According to Hollister et al., (2014) (71), the healthy gut microbiome has been defined by high diversity, richness and evenness of its microbial communities, since in that case there would be an enhanced functional redundancy to cover for potential alterations. The presence of core functions in the gut provided by microorganisms, such as transcription, translation, energy production, synthesis of structural constituents, production of short

chain fatty acids (SCFA) or the production of vitamins and essential amino acids are also part of a healthy gut microbiome. The last hallmark of gut health is the microbial resistance and resilience, by which microbial communities tend to not alter its composition and return to their initial state after perturbations (55).

The colon is the most studied segment within the gastrointestinal tract (55), since faecal samples are the most easily accessible ones. In the stomach and small intestine, less diverse and populated communities can be found (67). However, up to 10^{12} bacterial cells are present per gram of colonic content, distributed between 300 and 1000 species. The most dominant phyla include *Bacteroidetes* and *Firmicutes*, while *Proteobacteria*, *Actinobacteria*, *Verrucomicrobia* and *Fusobacteria* are less abundant (71). Besides the longitudinal variation, the gut microbiome also differs axially from the mucous to the intestinal lumen. Biopsy or surgical specimens are required to evaluate the composition of the mucous-associated microbiome while colonic or faecal pellets are required to evaluate the microbiome of colonic content samples. Even though differences have been described between the mucous and the content-associated microbial communities, the accessibility of faecal samples makes the content-associated microbiome the most preferable choice.

1.2.1.1 Functions of the gut microbiome

Three specific core functions provided by the gut microbiome can be highlighted:

Microbial digestion

The gut microbiome relies on dietary indigestive compounds for their survival. Microorganisms are able to use different nutritional sources while providing the host with microbial enzymes for their digestion. Along the digestion process they obtain energy

and substances for their own metabolism as well as producing metabolites with an impact on the host (discussed below) (72).

Microbial synthesis

The gut microbiome provides the host with compounds with limited availability in the environment (diet, self-synthesis). Such is the case of SCFA, key bacterial metabolites obtained from the fermentation of dietary fibers or proteins and peptides (73). Fibers escape host digestion and are fermented in the large intestine by specific members of the microbiome, yielding three major end products: acetate, propionate and butyrate. In case of fiber shortage, branched chain fatty acids, such as isobutyrate, 2-methylbutyrate and isovalerate are obtained from the fermentation of aminoacids. There is extensive research on the beneficial role of SCFA on intestinal health. They exert their effects through binding to free fatty acid receptors (FFAR) or through the inhibition of histone deacetylases (HDAC), modifying the accessibility to chromatin structures and gene expression. Propionate and butyrate are known HDAC inhibitors, being also able to act as FFAR ligands depending on their concentration range (73). SCFA are synthesized in the large intestine; while butyrate is consumed by colonocytes, propionate shows mainly local effects and acetate may act locally or be absorbed into the bloodstream. They all contribute to the motility of the gastrointestinal tract and increase its secretory activity, although butyrate and propionate has more specific local functions. Butyrate acts as the main source of energy for colonocytes, shifting their glucose-based metabolism to β-oxidation through HDAC inhibition. The consequent increase in oxygen consumption through mitochondrial oxidative phosphorylation triggers cellular responses to hypoxia and the stabilization HIF-1α (Figure 7) (74).

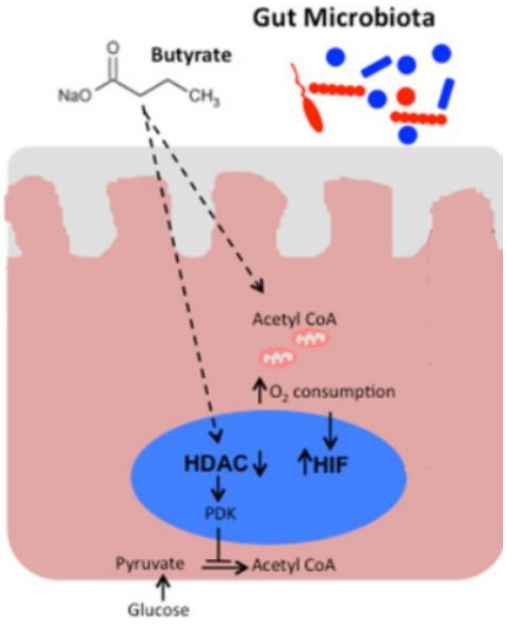

Figure 7. Stabilization of HIF-1α by butyrate. Adapted from Chun et al., (2017) (74).PDK: pyruvate dehydrogenase kinase

Compared to most tissues, the intestine is characterised by depleted oxygen levels to allow the survival of anaerobic microorganism (8). As described previously, hypoxia inducible factors (HIFs) consist of two constitutive subunits (α and β) that form a complex capable of binding hypoxia response elements in the DNA and modify the expression of HIF target genes. Under normoxia, the HIF-α oxygen dependent subunit is degraded by ubiquitination and HIF target genes are not expressed. Upon low oxygen levels, HIF-α subunit is stabilized, the HIFα-HIFβ complex formed and HIF target genes expressed. Two different isoforms of HIFα subunit are expressed in the intestine, HIF-1α and HIF-2α, differing mainly in their target genes. While glucose-dependent metabolism and intestinal barrier genes are dependent on HIF-1α, HIF-2α is involved in the transcription of genes related to oxygen carrying, vascularization and iron metabolism (74). There is a general consensus on the HIF-1α stabilizing properties of butyrate and propionate (73-75), while the role of SCFA on HIF-2α is still controversial (54). *In vitro* results suggest an inhibitory role of SCFA on aryl hydrocarbon receptor

nuclear translocator (ARNT) or HIF-1β subunit in the intestine, but no evidence was found *in vivo*.

Due to their role on HIF-1α stabilization in the large intestine, butyrate, and to a lesser extent propionate, are key metabolites in the maintenance of the intestinal barrier functionality (76). The gut barrier aims to provide an intact interface between the intestinal lumen and adjacent tissues to prevent the wide variety of antigens, toxins and microorganisms normally found in the intestinal lumen to leak into the bloodstream. Tight junction proteins, xenobiotic clearance, nucleotide signalling, energy metabolism and antimicrobial defense are the main pathways regulated by HIF-1α (8). As a case in point, administration of butyrate or dietetic interventions to increase SCFA production have been proven to recover intestinal barrier dysfunctionality (77) and to protect mice from infections (46).

Acting as HDAC inhibitors, other local functions of butyrate and propionate include antiinflamatory and immuno-modulatory properties on the enteric nervous system. Regulation of the immune response towards commensal bacteria is key to avoid the disruption of intestinal homeostasis. The hyporesponsive reaction of the intestinal epithelium is due to an increased production of IL-18 by intestinal epithelial cells, the formation of intestinal T regulatory cells and the formation of IL-10 producing T cells by butyrate and propionate (73, 78). In case of an infection, SCFA would also facilitate the differentiation of naive T cells into Th1 and Th17 cells to boost immunity (76).

Butyrate is also able to either exert antitumour effects or to facilitate natural turnover of colonocytes depending on its concentration within cells. Tumour cells are characterised by the use of glucose as a source of energy (Warburg effect); in these conditions, butyrate would be accumulated inside cells, where in high concentrations induce apoptosis. On the contrary, in physiological ranges, butyrate promotes the natural turnover of colonocytes and a healthy epithelium (73).

SCFA play a role in glucose homeostasis upon binding to FFAR2 and FFAR3 receptors in the intestine, promoting the secretion of glucagon-like peptide 1 and peptide YY, which increase insulin secretion (79). Furthermore, propionate is locally converted to glucose through intestinal gluconeogenesis; glucose is then absorbed and reaches the brain and liver, modulating appetite and alleviating the hepatic burden for gluconeogenesis (73). Lastly, SCFA have also been shown to stimulate the regeneration of neurons in the enteric nervous system (80).

Intestinal functions of SCFA have been summarised in Figure 8.

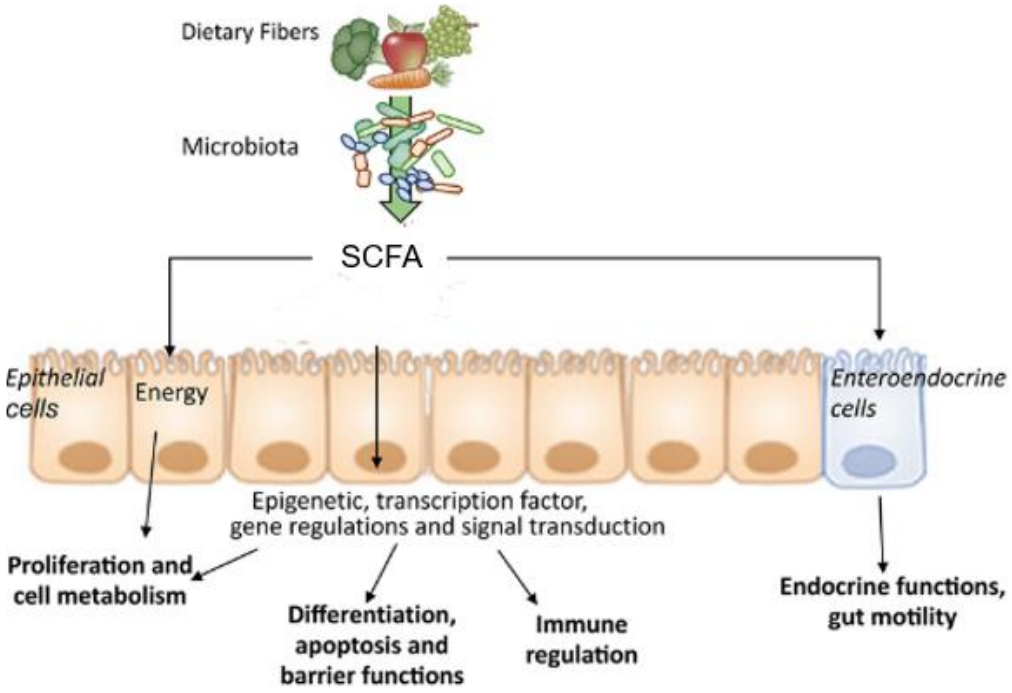

Figure 8. Overview on the intestinal functions of SCFA. Image adapted from Martin-Gallausiaux et al., (2021)(81).

When acetate accesses systemic circulation, it reaches the liver, brain and adipose tissue, where it promotes insulin sensitivity, appetite control and preadipocyte differentiation, presumably upon binding to FFAR2 (73).

Other metabolites produced by the gut microbiome include vitamins, essential and non-essential aminoacids, bile acids or neurotransmitters. Host synthesis is not sufficient to cover vitamin needs and they are also obtained from dietary resources and the gut microbiome (13). Vitamin K and vitamins belonging to the B group including biotin, cobalamin, folates, nicotinic acid, pantothenic acid, pyridoxine, riboflavin, and thiamine are known to be synthetized by the gut microbiome (72). Specifically, availability of folic acid, pyridoxin and cobalamin are crucial to allow the functioning of one-carbon metabolism, which spans all kingdoms including mammals and microorganisms. One-carbon intermediates facilitates a great number of biological processes such as epigenetics through methyl donor availability or redox balance, and represent one of the branches in the host-microbiome crosstalk.

The gut microbiome is also responsible for the diversity of the bile acid pool (72). When it reaches the distal small intestine, part of the bile acid pool is deconjugated while the rest is absorbed as part of the enterohepatic circulation. Once they are deconjugated, bile acids can be further transformed by the gut microbiome through epimerization, oxidation and dehydroxylation reactions. Secondary bile acids are formed, exerting their biological functions via interaction with G-protein-coupled bile acid receptor 1 or farnesoid X receptor, which are known to promote the secretion of glucagon-like peptide 1 and to regulate inflammation and immunity, respectively. Modifications in the bile acid pool by the gut microbiome might also account for variations in its biological functions, which has been related to some diseases such as hepatocellular carcinoma or colorectal carcinoma (13).

Lastly, as a result of its protein fermenting capacity, the gut microbiome is capable of metabolizing some aminoacids such as tryptophan, histidine, phenylalanine and tyrosine. Tryptophan metabolism by the gut microbiome yields a wide variety of biologically active molecules belonging to kynurenine family, serotonin family or indol family. The effect of kynurenine derivatives greatly depends on the target tissue and

active compound, while it is well known that the synthesis of serotonin can regulate important functions in relation to mood, sleep, appetite and behaviour, highlighting the importance of the gut microbiome – brain axis (82). Indol derivatives act as aryl hydrocarbon receptor (AHR) ligands; AHR are transcriptional factors activated by cytosolic ligands with immunomodulatory functions (13).

Although most of the synthetic activity of the gut microbiome provides benefits for the human health, toxic substances can also be produced from the metabolism of histidine, phenylalanine and tyrosine. Histamine and uraemic toxins (p-cresol sulfate, phenylacetylglutamine) contribute to allergies, neurological, kidney and cardiovascular diseases (13).

Protection against colonization

The gut microbiome is one of the main components of the gut barrier (45). Commensal microorganisms colonize the gastrointestinal tract and limit the availability of resources for other pathogens. As discussed above, microorganism-derived metabolites, such as SCFA, have the ability to regulate the immune response depending on the biological context. Antimicrobial mechanisms can also be triggered, as well as pathogen clearance in case of infection (73). SCFA are also able to stabilize HIF-1α pathways related to the maintenance of the intestinal barrier. Lastly, certain microorganisms are able to alter the expression of genes and proteins involved in the gut barrier functionality. Such is the case of tight junction complexes, major targets of certain species (*Lactobacillus rhamnosus*, *Streptococcus thermophilus*, *Lactobacillus reuteri* and *Bifidobacterium infantis*)(83).

Overall, a healthy microbiome contributes to the prevention of gastrointestinal infections and intestinal dysbiosis can be related to alterations in the gut barrier.

1.2.1.2 Gut microbiome and iron metabolism

Over the last decade, the gut microbiome is sparking the interest of the scientific community as one of the main factors to consider in the pathogenesis of diseases. The majority of research is based on association studies, but growing evidence is supporting causal relationships with regards to the gut microbiome contributing to disease.

Rodent animal models are the preferable choice in microbiome studies that involve human ethical implications. Li et al., (2019) (84, 85) analysed the structure and functionality of the gut microbiome in mice, rats and woodrats and the number of shared microbial taxa and genes with the human microbiome. The overlapping features were greater in the case of rats compared to mice and woodrats, suggesting a higher extrapolability of rat-derived microbiome data. Other mammals showing close proximity to the human microbiome have also been used in microbiome research (86), such as dogs or pigs, but their cost and ethical limitations force researchers to turn to more affordable options. Lately, the use of simpler models such as *Drosophila melanogaster*, *Caenorhabditis elegans* or the zebrafish *Danio rerio* is gaining popularity due to its low cost and labour-saving peculiarities, allowing an easier manipulation of the microbiome and the study of causal relationships (87).

The gut is the most studied biological niche in relation to the influence of its microbiome on the state of health. The gut microbiome has been extensively associated with intestinal and non-intestinal disorders such as metabolic syndrome, obesity, diabetes, cardiovascular diseases, inflammatory bowel disease, systemic lupus erythematosus, anxiety, depression, and so on (88-92). A general consensus exists as to its role in their physiopathology and the number of published articles is sufficient for reviews to be written on the topic. However, there is limited research as far as IDA and iron metabolism is concerned. No reviews have been published and only few studies

address the influence of IDA on the intestinal microbiome, with the rest being focused on the effects of iron supplements.

With regards to the effects of iron deficiency on microbiome structure, Coe et al., (2021) (93) found that certain Operational Taxonomic Units (OTUs) belonging to *Lachnospiraceae*, *Ruminococcaceae*, *Rikenellaceae, Prevotellaceae, Porphyromonadaceae* and *unclassified Bacteroidales* families were depleted as a consequence of iron deficiency, with the ones belonging to *Prevotellaceae, Porphyromonadaceae* and *unclassified Bacteroidales* not recovering after iron repletion. Other animal studies also revealed that microbiome structure is affected in response to iron deficiency (94), although NGS techniques were not applied, limiting the results to a few taxa analysed by temporal temperature gradient gel electroporesis and quantitative PCR (qPCR). Studies in patients show that the gut microbiome of patients suffering IDA differs from healthy controls (95, 96), with a predominance of *Proteobacteria* phyla and a decrease in SCFA-producing bacteria such as *Roseburia*, *Coprococcus* and *Butyricicoccus*. However, no changes in SCFA levels were observed in faecal samples.

It is also known that specific microorganisms can affect the expression and protein levels of genes related to iron metabolism, such as the increase in FTN produced by *Bacteroides thetaiotaomicron VPI-5482*, *Faecalibacterium prausnitzii A2-165* and *Streptococcus thermophilus LMD-9*. *Lactobacillus fermentum* has been shown to improve iron absorption due to its ferric-reducing activity (97). Few articles consider mechanistic approaches to study the relationship between the gut microbiome and IDA. Das et al., (2020) (54) demonstrated that specific microbial metabolites, namely 1,3-diaminopropane and reuterin, are able to impair iron absorption through the inhibition of aryl hydrocarbon receptor nuclear translocator (ARNT), also known as HIF-1β. In this same study, SCFA showed *in vitro* evidence for the inhibition of ARNT, but those results were not replicated *in vivo*. Lastly, Zhang et al., (2022) (98) revealed that the gut microbiome also regulates bone marrow macrophage functions via SCFA, influencing

local iron availability and controlling self-renewal and differentiation decisions of hematopoietic stem cells. SCFA seem to be key metabolites in the physiopathology of IDA, possibly through multiple roles, but there is a lack of consensus on their functions in this context. Gut bacteria are also able to make use of host iron compounds (heme, Tf), as well as to take up iron from the environment through the secretion of siderophores, competing for iron with the host and thus influencing the appearance and recovery of IDA (99).

There is a considerable number of studies that describe the detrimental effects of iron supplements on the gut microbiome. Given the fact that intestinal iron absorption ranges between 5 and 15% in the duodenum and jejunum, most of iron from supplements access the large intestine. Therefore, the use of iron supplements and iron fortification has been shown to trigger gut microbial alterations. The proportions of some genera were repeatedly higher upon treatment in several studies, such as *Dialister*, *Lachnospira*, *Clostridium cluster XIVa*, *Oscillibacter*, *Xylanibacter*, *Helicobacter*, *Shigella* and *Slackia* (100-102), while others were found in lower relative abundances, namely *Phascolartobacterium*, *Pediococcus*, *Sporacetigenium*, *Oscillospira*, *Acetanaerobacterium*, *Barnesiella*, *Asaccharobacter* and *Alloscandovia* (101, 103). Ippolito et al., (2022) (104) recently reported that iron-rich diets promote a more severe enteropathy by *Salmonella Typhimurium*. Such microbial alterations often lead to increased risk of diarrhoea and gut inflammation (41).

Overall, there is a lack of studies in this field and whether the gut microbiome contributes to the generation or the recovery of IDA remains largely unknown. Most studies are focused on how the gut microbiome responds to an externally induce anaemia, while none of them considers if the gut microbiome can actually be the cause of IDA.

1.2.1.3 The gut microbiome and the diet

Different strategies have been described to alleviate disease-associated microbial alterations, such as faecal microbiome transplantation (FMT) or dietary interventions. FMT has been shown to be more effective than probiotics to reconstitute the gut microbiome (105), but it takes second place in terms of practical use due to its high cost and difficult implementation. Diet can alter the microbiome structure and functioning in a reproducible and rapid manner. David et al., (2013) (106) reported changes in the gut microbiome structure of healthy subjects just one day after the food had reached the large intestine. However, subjects' gut microbiota reverted to their original state two days after the diet ended, which reflects its resilience even after long-term dietary interventions (107).

Among dietary interventions, fermented dairy products have been extensively studied due to their great impact on the gut microbiome (108). Overall, fermentation of dairy products increases the availability of nutrients, such as amino acids or oligosaccharides (109), increasing their prebiotic potential. In particular, goat's milk has attracted considerable attention due to its numerous health benefits, which will be reviewed in the next section, especially on the gut microbiome. However, limited research exists on its fermented counterpart.

A diet-shaped healthier gut microbiome in the context of IDA could be beneficial for the recovery of the disease. In fact, there is evidence reporting that the gut microbiome can actually contribute to mucosal healing via stimulation of dendritic cells to secrete hepcidin; enhanced iron pools inside intestinal phagocytes prevented microbial infiltrations and facilitated tissue repair (110). Some microbial metabolites have also been shown to positively contribute to the host mitochondrial iron pool, such as enterobactin (111).

Therefore, the following section will include an updated review of the existing literature supporting the use of fermented goat's milk as a nutritional tool to promote gut health and the recovery of IDA.

1.3 Fermented dairy products

Fermented products derive from either spontaneous fermentation of the raw product or the addition of a starter culture to the raw material and the consequent fermentation process. There is a wide variety of fermented dairy products, including yogurt, kefir, sour cream, cheese, yakult or nunu, among others (112, 113).However, yogurt leads the fermented food industry in most parts of the world as well as being the most studied fermented dairy product.

Yogurt is a type of fermented milk whose fermentation process is performed by lactic acid bacteria such as *Lactobacillus*, *Lactococcus*, *Streptococcus* and *Leuconostoc;* they are added to raw milk and carry out the conversion of lactose to lactic acid (113). Although the fermentation process was traditionally used to preserve milk, it includes additional advantages such as the improvement of food digestibility, nutritional value and sensory properties (112). Lactose-intolerant patients may benefit from this, since lactose levels are decreased in yogurt compared to milk as a consequence of fermentation. Fermentation also increases the availability of certain nutrients such as amino acids or oligosaccharides, increasing the prebiotic impact of fermented derivatives (109).

The health benefits of yogurt have been well documented and are known for decades. These effects may arise from a direct impact of nutrients or from its prebiotic and probiotic properties, since yogurt-contained bacteria are known to survive the gastrointestinal transit and reach the large intestine. Therefore, protection against infections and diarrhoea derive from the acidic environment, antibacterial compounds

and the healthy microbiome shaped after yogurt consumption. Yogurt also shows immunomodulatory, anticholesterol and anticancer properties (113).

Due to the well studied effect of fermented milk derivatives on the gut microbiome and intestinal health(108), and since they are the most accessible choices in the consumer market, this section will discuss the benefits of the use of fermented goat´s milk (FGM) in comparison to other fermented milks from domestic animals within the context of IDA.

1.3.1 Fermented goat's milk

Even though the consumption of cow´s milk and its derivatives remain predominant, there is an increasing demand for non-bovine milk and non-bovine milk-based products due to additional advantages such as a reduced risk of allergy or to its higher nutritional value (114).

In particular, the use of goat´s milk as a substitute for cow´s milk is on the rise in certain populations such as children and the elderly. Actually, Andalucía is the major producer of goat´s milk in Spain, reaching 212.3 tons of milk in 2020 (115).

Despite the larger production of cow´s milk and its higher affordability for consumers, the biomedical interest of goat´s milk deserves in-depth investigation. Its enhanced nutritional properties make it a promising nutritional tool to be used in specific scenarios, which will be reviewed in next section.

1.3.1.1 Composition of fermented goat´s milk

Composition of fermented goat´s milk resembles that of the raw milk, so they are similarly treated along the section unless otherwise indicated and compared to its most consumed counterpart, cow´s milk.

Proteins

Protein levels in fermented goat´s milk are higher compared to fermented cow´s milk. In relation to protein quality, all aminoacids except for alanine are higher in fermented goat´s milk (116).

As in cow´s milk, two kinds of protein fractions are present in goat´s milk, namely casein proteins (α-s1 casein, α-s2 casein, β-casein and κ-casein) and whey proteins (β-lactoglobulin, α-lactoalbumin, enzymes, immunoglobulins and so on) (117). However, their amino acid sequence and quantity varies between both dairy products. Casein, β-lactoglobulin and α-lactoalbumin are the major allergens of cow´s milk. It has been shown that consumption of goat´s milk resolved around 30-40% of these cases due to its extremely low levels of α-s1 casein as well as the structural differences in β-lactoglobulin and α-lactoalbumin (114). Moreover, casein forms small-sized micelles in goat´s milk, which enhance digestibility (118).

Milk proteins can be digested by enzymes during the fermentation process or through digestion in the gastrointestinal tract to release oligopeptides. The proteome from goat´s milk showed proteins not present in cow´s milk, such as dystroglycan or factor H, and often these parental proteins yield small fragments with additional functions, such as immunomodulation, opioid-like activity, antimicrobial, antihypertensive and antioxidant actions (118, 119).

Lipids

Fat levels are similar in fermented goat´s milk compared to its counterpart (116). However, fat globules are smaller in fermented goat´s milk, which leads to the formation of a softer curd during subsequent fermentations and an increased digestibility (120).

Monounsaturated fatty acids, polyunsaturated fatty acids and medium chain triglycerides are higher in goat´s milk compared to cow´s milk. To name but a few, butyric (C14:0), caproic (C6:0), caprylic (C8:0), capric (C10:0), lauric (C12:0), myristic (C14:0), palmitic (C16:0) and linoleic (C18:2) acids show higher levels in goat´s milk, while stearic (C18:0) and oleic acid (C18:1) show lower levels compared to cow´s milk (117). Enrichment in capric, caprylic and caproic fatty acids also contribute to a better digestibility of goat´s milk compared to cow´s milk (118).

Many of the beneficial effects of goat´s milk or its derivatives have been put down to the presence of medium chain triglycerides. As such, goat´s milk and fermented goat´s milk has been proven effective to treat malabsorption syndromes, streatorrhea or hyperlipoproteinemia since medium chain triglycerides provide cells with a direct source of energy instead of being deposited in the adipose tissue (117).

Carbohydrates

Carbohydrates are the main contributors to the prebiotic effect of dairy products. A prebiotic is defined as a specific component present in foods that modulates the composition and functioning of the gut microbiome producing beneficial effects for the host. Lactose is the main carbohydrate in both fermented cow´s and goat´s milk, showing similar levels in both cases (116). Other types of carbohydrates include oligosaccharides, glycopeptides, glucoproteins and nucleotide sugars.

From a microbiological point of view, oligosaccharides are the most interesting molecules due to its prebiotic properties. Goat’s milk contains the most structurally diverse and the highest amount of oligosaccharides compared to other domestic animals. Actually, oligosaccharides present in goat’s milk are the most structurally similar to the ones present in breast milk, the golden standard in relation to beneficial effects on intestinal health (Figure 9) (121). Besides showing a strong prebiotic potential, they possess anti-inflammatory, pathogen inhibitory properties and enhance the integrity of

the intestinal barrier (122). As case in point, one study reported that the microbiome shaped by goat´s and breast milk were more similar in structure than that shaped by cow´s milk (123).

Fermentation of goat´s milk increases the availability of certain nutrients such as oligosaccharides, enhancing their prebiotic impact and their beneficial properties on intestinal health (109).

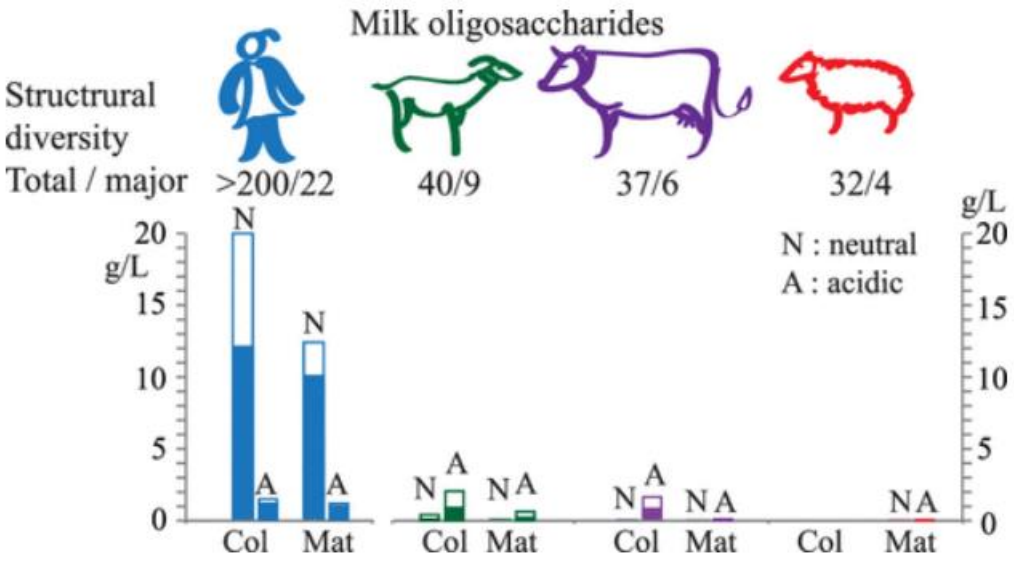

Figure 9. Overview of milk oligosaccharides in breast, goat´s, cow´s and sheep´s milk. Legend: Col (colostrum), Mat (mature milk). Image from van Leeuwen et al., (2020) (121)

Vitamins and minerals

As for the mineral content, fermented goat´s milk shows similar levels for potassium, phosphorus and iodide and higher levels for calcium, magnesium, zinc, iron, cupper and selenium compared to fermented cow´s milk.

In relation to vitamin composition, vitamin C, folic acid and vitamin E showed lower values in fermented goat´s milk, while vitamin B_6, vitamin A, vitamin B_{12} and vitamin D_3 showed higher levels compared to fermented cow´s milk (116).

Probiotics

Probiotics are living microorganisms that exert beneficial effecs to the host when administered in adequate doses. These microorganisms survive the transit through the gastrointestinal tract and exert their beneficial properties in the large intestine.

The microbial community present in milk is complex and it can contribute to different processes, including fermentation. Goat´s milk is often dominated by lactic acid bacteria including species of *Lactococcus, Lactobacillus* and *Leuconostoc*. *Enterococcus, Enterobacteriaceae, Micrococcaceae,* moulds and yeasts are also present (120).

1.3.1.2 Beneficial effects of fermented goat´s milk

As inferred from its composition, the consumption of FGM exerts both systemic and intestinal beneficial effects. As mentioned above, bioactive peptides in goat´s milk show hypotensive, immunomodulatory, anti-atherogenic, antioxidant and antiinflamatory properties. Bioavailability of magnesium, iron, calcium, copper and phosphorus is higher upon goat´s milk consumption in comparison to cow´s milk, and its fatty acid composition, especially regarding linoleic acid, exert anticarcinogenic effects (118). Recently, small fragments obtained from casein hydrolyzation have been described as antiviral compounds, preventing the replication of certain viruses such as SARS-CoV-2 or the human immunodeficiency virus 1 (HIV-1). Similarly, hydrolysed casein exerts antidiabetic effects, enhancing insulin sensitivity (124).

Goat´s milk has been shown to enhance iron availability and deposition in target organs (125). This effect might derive from the microbiome shaping properties of goat´s milk, although it was originally put down to its nutritional composition, mainly to goat´s milk proteins and medium chain triglycerides, which enhance iron solubility and the expression of absorptive iron transporters in the small intestine. Therefore, goat´s milk and FGM have been used as nutritional tools to promote systemic beneficial effects during the recovery of iron deficiency anaemia (IDA).

In this sense, it has been shown that the consumption of FGM reduces risk factors of cardiovascular disease, diminishing tumour necrosis factor (TNF) α and IL-6, which are involved in the pathogenesis of atherosclerosis (126). Similarly, FGM was shown to decrease adiposity and increase energy expenditure, lipolysis and satiety during the recovery of IDA (127). The total antioxidant capacity and biomarkers of oxidative damage were improved after consumption of FGM (128).

However, intestinal beneficial effects have not been studied in this context. There is evidence to suggest that oligosaccharides from goat´s milk have a positive impact on the gut barrier integrity. A oligosaccharide-enriched fraction from goat´s milk was used in an *in vitro* model of the small and large intestine to assess trans-epithelial electric resistance and mucus secretion, all parameters showing an increase upon treatment (122). If combined with probiotics, oligosaccharides showed a synergistic effect on mucin gene expression and protein abundance, tight junction proteins and trans-epithelial electric resistance (129).

As far as the effect of FGM on the gut microbiome, most studies are focused on the microbiome-shaping properties of goat´s milk. A strong emphasis is made about oligosaccharides being the main prebiotic compounds, with *in vitro* and *in vivo* studies supporting this finding. 17 strains of bifidobacterial strains isolated from infant faeces grew more efficiently when cultured on goat´s milk oligosaccharides (GMOS) compared

to other prebiotics such as galactooligosaccharides (GOS), fructooligosaccharides (FOS) or inulin (130), and so did *Lactobacillus* strains (131). Thum et al., (2016) (132) noticed the development and gut microbiome of offsprings is affected if their mothers have been fed with GMOS, showing increased bifidobacteria and butyrate in the colon.

However, it should be noted that those studies only address the effect of oligosaccharides on specific monocultured strains, and more comprehensive approaches are still needed to fully understand the microbiome-shaping properties of goat's milk. Li et al., (2020) (133) described *Bacteroidetes, Firmicutes* and *Actinobacteria* as the main phylum colonizing the gut microbiome in mice undergoing faecal microbiome transplant with human faeces and goat´s milk administration. *Enterobacteriaceae, Atopobiaceae* and *Eggerthellaceae* were the dominant families.

Studies analysing the effect of FGM on the gut microbiome are scarce. Only one study investigates the impact of FGM on the gut microbiome in mice and another two evaluate the effect of FGM-based beverages on the gut microbiome using an *in vitro* model. The starter culture used in the production of FGM has been shown to influence its impact on the gut microbiome, since consumption of FGM inoculated with *Streptococcus thermophilus* and *Lactobacillus bulgaricus* increased the relative abundance of *Acetatifactor*, *Alistipes*, *Coprococcus*, *Parabacteroides* and *Streptococus* genera, among others. Nevertheless, certain genera such as *Butyricicoccus*, *Desulfovibrio*, *Oscillibacter*, *Ruminiclostridium* and *Streptococcus* were enriched after consumption of FGM inoculated with *Streptococcus thermophilus, Bifidobacerium lactis* and *Lactobacillus bulgaricus* (134). With regards to FGM-based beverages, all formulated products were tested via Simulator of Human Intestinal Microbial Ecosystem (SHIME), showing modulatory properties of the gut microbiome and the production of SCFA both in samples belonging to obese and healthy subjects (135).

An overview of the beneficial effects of FGM is provided in Figure 10.

Given its strong prebiotic and probiotic impact, high availability of oligosaccharides due to fermentation, low allergenicity, high digestibility and high acceptance by consumers, FGM shows high potential to be used as a nutritional tool to promote intestinal health. As such, FGM will be studied in the context of iron deficiency anaemia to show its impact on the intestinal microbial communities, gut barrier and microbial translocation, paving the way for the development of FGM-based nutraceutics or functional foods.

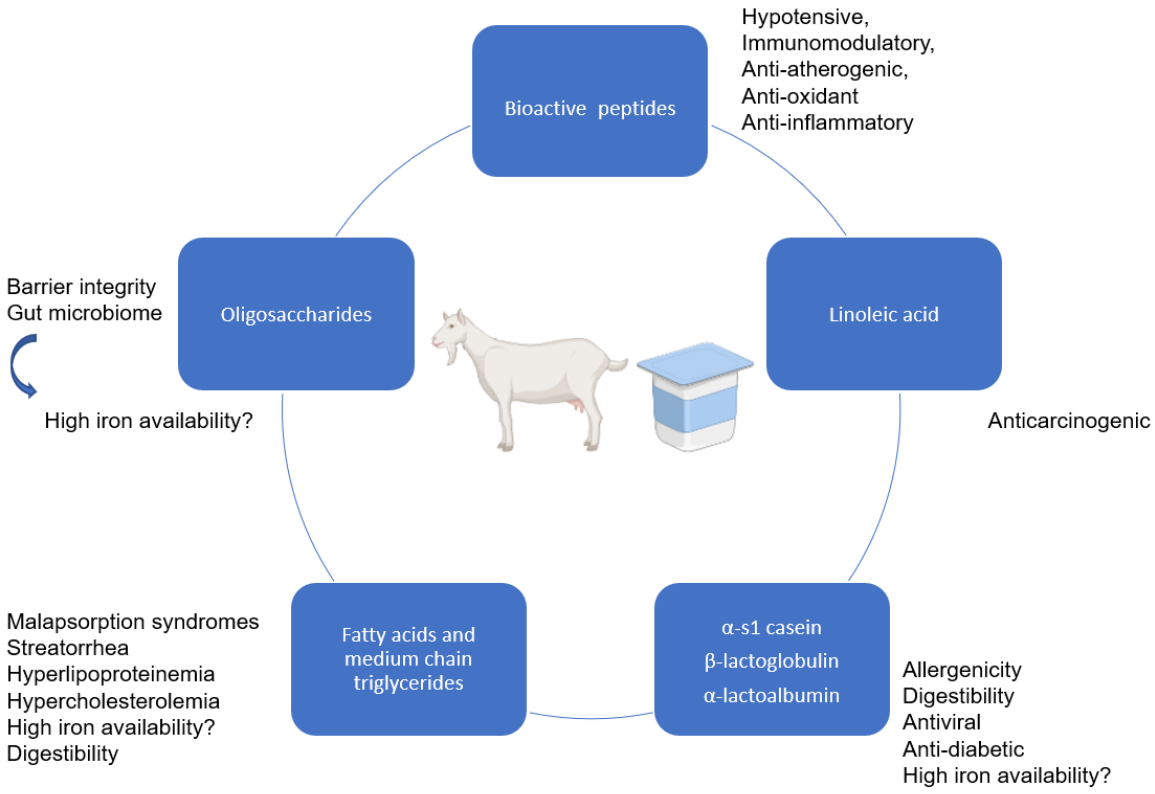

Figure 10. Composition and functions of fermented goat's milk

2. HYPOTHESIS & OBJECTIVES

Consequences of IDA on intestinal health are largely unknown. In particular, this thesis will be focused on the study of such consequences on the gut microbiome and the intestinal barrier. Considering microorganisms need iron to survive, alterations in the intestinal microbial communities are expected to occur in response to IDA.

On the other hand, iron is an essential micronutrient involved in DNA replication and cell cycle progression. Cells showing a high turnover rate are especially affected during IDA. Gastrointestinal tract lining cells, the mainstay of the intestinal barrier, are renewed every 3-5 days. Furthermore, a healthy microbiome also contributes to the gut barrier integrity. Iron deficiency and intestinal dysbiosis are expected to have a detrimental effect on the intestinal barrier, which will lead to an increase in paracellular permeability.

FGM has been shown to increase iron availability and absorption, although it is not known whether these effects are microbiome-dependent or whether they derive from a direct impact of FGM nutrients on the epithelium. Since intestinal health will presumably be affected during IDA, FGM will be used to ease the negative consequences of the disease on the intestine. FGM will shape a healthy microbiome characterised by an increased iron absorption and will recover IDA more efficiently than the conventional diet, restoring IDA-derived intestinal dysbiosis. Considering its high nutritional value and its potential as a promoter of the gut barrier integrity, FGM will recover the fuctionality of the intestinal barrier and will alleviate microbial translocation.

General objective

To understand the interplay between the gut microbiome and the intestinal barrier during the development and recovery of iron deficiency anaemia with fermented goat's milk-based diet, aiming to show its beneficial properties.

Specific objectives

1. Structural and functional characterisation of the gut microbiome along the gastrointestinal tract during the development of iron deficiency anaemia and identification of key microbial metabolites
2. Study the integrity of the intestinal barrier during the development of iron deficiency anaemia and the extent of microbial translocation
3. Evaluate the capacity of fermented goat´s milk to shape a healthy gut microbiome that contributes to a more efficient recovery of iron deficiency anaemia
4. Assess the impact of fermented goat's milk on the intestinal barrier function and paracellular permeability

3. MATERIAL AND METHODS

3.1 Experimental animals

Animal housing, care, handling procedures, and experimental protocols were approved by the Ethics Committee of the University of Granada and the local government Junta de Andalucía (ref 06/06/2019/100) in accordance with European guidelines (Declaration of Helsinki; Directive 2010/63/EU). Animal experiments were performed in the Animal Service of the University of Granada, with controlled sanitary and environmental parameters.

Weaned male Wistar rats (*Rattus Norvegicus albinus*), purchased from Charles River Laboratories (France), were used for the study. Animals were housed in groups or individually, using ventilated, thermoregulated cages with controlled temperature (23 ± 2 °C), humidity (60 ± 5%), and a twelve-hour circadian rhythm.

3.2 Experimental design

This study consists of two experimental periods (Figure 11); the first one includes the induction of IDA and the last one includes the treatment with experimental diets.

Induction of iron deficiency anaemia

During the induction period, diets and deionized water were available *ad libitum*. Animals were housed in groups and were randomly divided into the control (n=25) or anaemic (n=30) group, receiving the first one the AIN-93G diet (136) and the last one, the iron deficient counterpart for 40 days (137) (Figure 11). The iron deficient AIN-93G diet was elaborated through the elimination of the iron component from the mineral supplement (136).

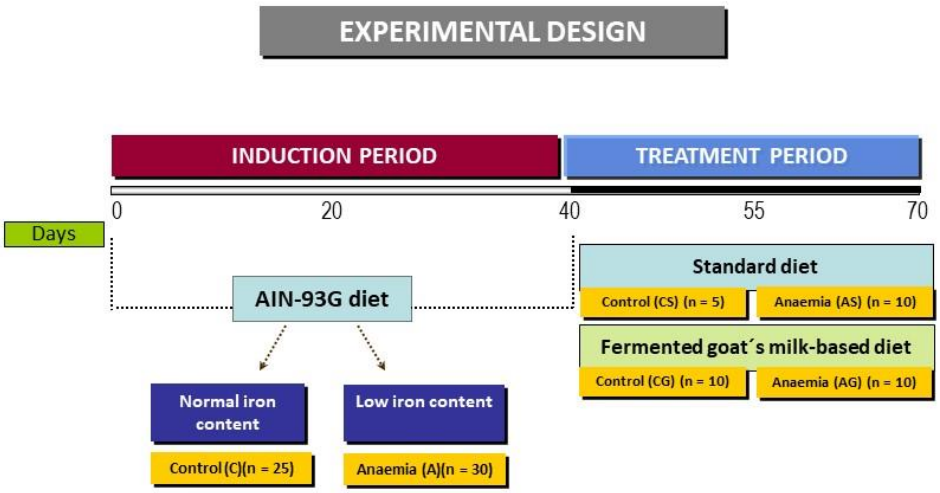

Day 0: collection of faeces
Day 20: collection of blood and faeces
Day 40: sacrifice of 10 control and 10 anaemic rats. Collection of blood, serum, faeces, intestinal contents and colonic mucous samples
Day 55: collection of faeces
Day 70: sacrifice of 20 anaemic rats (fed with standard diet or fermented goat's milk-based diet) and 15 control rats (fed with standard diet or fermented goat's milk-based diet). Collection of blood, serum, intestinal contents, and colonic mucous samples

Figure 11. Experimental design.

Along the induction of IDA, faeces samples were collected at day 0 (Baseline), 20 (d20) and 40 (d40) using metabolic chambers. Blood samples from the caudal vein were collected at day 20 and at the end of the induction period, using EDTA as anticoagulant to control haematological parameters. At the end of the induction period, 10 animals from each experimental group were intraperitoneally anesthetized using sodium pentobarbital (Exagon®, Richter Pharma AG, Austria) and bled out by cardiac puncture. Serum samples were obtained from total clotted blood via centrifugation (3000g, 10 min, 4ºC). The small and large intestine were then isolated, being divided into its respective segments: duodenum, jejunum and ileum, and cecum and colon respectively. Intestinal contents from the small intestine were obtained after washing each segment with sterile saline solution (0.9% sodium chloride, 59888 Sigma-Aldrich, USA). As for the large intestine, solid contents were directly squeezed out. After rinsing with sterile saline solution, colon segments underwent fixation for immunostaining

analysis or snap freezing in liquid nitrogen for gene expression analysis. All samples except for total blood, which was analysed immediately after collection, were frozen at -80ºC until analysis.

Treatment of iron deficiency anaemia with FGM-based diet

The rest of animals underwent the treatment period where IDA was treated with fermented goat's milk (FGM)-based diet or standard diet, resulting in four experimental groups (Figure 11): control animals fed with either fermented goat's milk (CG) or standard diet (CS) and anaemic animals fed with either fermented goat's milk (AG) or standard diet (AS). In this case, animals were placed in individual cages and diet intake was controlled (pair feeding with 80% of the average intake); deionized water was available *ad libitum*.

Along the treatment period, faecal samples were collected using metabolic chambers at day 55 (d55) and day 70 (d70). At the end of the treatment period (d70), haematological parameters were controlled in total blood. Animals were sacrificed as described previously. Serum samples, intestinal contents belonging to the small (duodenum, jejunum and ileum) and large intestine (cecum and colon) and colonic mucous samples were collected as previously described and immediately frozen until analysis.

3.3 Experimental diets

All diets used in this study were elaborated in the Diet Facility of the University of Granada.

AIN-93G diet and its iron deficient counterpart were elaborated as described by Reeves et al., (1993) (136), with iron being eliminated from the mineral supplement in the case of the iron deficient diet.

FGM was kindly provided by the dairy company Cantero de Letur (Albacete, Spain) and lyophilized as follows: -25ºC for 5 hours, 15ºC at 0.1mbar for 5 hours, 24ºC 0.45mbar for 37 hours and 25ºC 0.02 mbar for 2h. The experimental diet was elaborated with FGM powder to provide the total amount of fat in the diet (10%) as previously described (126) (Table 1). The remaining macronutrients were adequately adjusted to meet the rat nutritional requirements described by Reeves et al., (1993) (136) considering what had already been provided by the FGM component (Table 2). In the case of minerals and vitamins, only calcium, phosphorus, magnesium, zinc and sodium were adjusted; the rest of minerals and vitamins were not adjusted in the experimental diet and supplied as recommended by Reeves et al. (1993) (136).

Table 1. Composition of experimental FGM-based diet.

Component	**g/kg**
Protein	200
Fat	100
Sucrose	100
Micronized cellulose (fiber)	50
Choline	2.5
L-cystine	2.5
Mineral mix*	35
Vitamin mix*	10
Wheat starch	csp 1kg

*Specific vitamin and mineral supplements for FGM - based diet were formulated considering minerals and vitamins supplied by the FGM powder in order to meet the recommendations described by Reeves et al., (1993) (136)

Table 2. Nutritional analysis of fermented goat's milk performed by LAB laboratories (Almeria, Spain).

Component	Quantity
Water (g/100g)	2.7
Fat (g/100g)	39
Fibre (g/100g)	< 0.10
Protein (g/100g)	26
Lactose (g/100g)	20
Vitamin B1 (mg/100g)	0.37
Vitamin B2 (mg/100g)	0.48
Vitamin B3 (mg/100g)	0.2
Vitamin B5 (mg/100g)	1.4
Vitamin B6 (mg/100g)	0.058
Vitamin B8 (ug/ 100g)	17
Vitamin B9 (ug/ 100g)	54
Vitamin B12 (ug/ 100g)	< 2
Vitamin C (mg/100g)	< 1
Vitamin A (mg/100g)	0.35
Vitamin D (ug/ 100g)	< 50
Vitamin D2 (ug/ 100g)	< 50
Vitamin D3 (ug/ 100g)	< 1
Vitamin E (mg/100g)	0.28
Vitamin K (ug/ 100g)	5.4
Calcium (mg/100g)	914
Phosphorus (mg/100g)	658
Magnesium (mg/100g)	97
Iron (mg/100g)	0.273
Zinc (mg/100g)	2.65
Copper (mg/100g)	0.11
Selenium (ug/ 100g)	15.3
Sodium (mg/100g)	268

Standard diet used as a control to show the beneficial effect of FGM during the recovery of IDA was elaborated according to the recommentations provided by Reeves et al., (1993) (136).

All diets were microbiologically analysed ensuring the absence of pathogens, and pelletized for a better administration to the animals.

3.2 Haematological tests

Red blood cells, haemoglobin, haematocrit, mean corpuscular volume (MCV), mean corpuscular haemoglobin (MCH), mean corpuscular haemoglobin concentration (MCHC), leukocytes and platelets were measured using an automated haematology analyser Mythic 22CT (C2 Diagnostics, France).

3.3 Sample preparation

Intestinal content samples were prepared differently according to their liquid or solid nature: liquid intestinal contents from each segment in the small intestine were centrifuged (6000 rcf, 10 min, 4ºC), the supernatants recovered and the pellets frozen for subsequent DNA isolation procedures; obtained supernatants were centrifuged again at maximum speed (10 min, 4ºC), filtered (0.22um) to eliminate suspended particles and transferred to a vial for SCFA analysis through high-performance liquid chromatography (HPLC). As for solid samples belonging to the large intestine, 200 mg of intestinal content from each segment were weighted and homogenized in 1.8 mL of saline solution. Suspensions were subsequently centrifuged (6000 rcf, 10 min, 4ºC), the bacterial pellet frozen until DNA isolation and the supernatant centrifugued again at maximum speed (10 min, 4ºC), filtered (0.22um) and transferred to a vial for the determination of SCFA through HPLC.

3.4 DNA isolation, high-throughput sequencing and bioinformatic analysis

Intestinal content samples and faeces underwent DNA extraction procedures, sequencing and bioinformatic analysis to study the gut microbiome. DNA isolation was performed using QIAamp DNA Stool Mini Kit (19590, QIAGEN, Germany) according to the manufacturer's instructions using approximately 200mg of faeces or intestinal

content previously isolated as described in section 3.3. DNA quality and amount were determined using a spectrophotometer NanoDrop 2000 UV–Vis (ThermoFisher Scientific, USA).

16S amplification and sequencing was performed as follows: PCR amplification products of the V1-V3 variable regions of the 16S rRNA gene (138) were obtained using fusion universal primers 27F (Illumina adaptors + 5'AGAGTTTGATCMTGGCTCAG3') and 533R (Illumina adaptors + 5'TTACCGCGGCKGCTGGCACG3'), as described by Soriano-Lerma et al, (2020) (139). Amplicon multiplexing and sequencing was carried out with a dual indexing tag-tailed design using 8nt indexes from the Nextera XT Index Kit v2 (Illumina, USA). Paired-end sequencing of 16S PCR amplicon libraries was performed using the Illumina MiSeq instrument with v3 kit chemistry (300 + 300bp). Demultiplexing was performed by Illumina BaseSpace software with default settings. Bioinformatics analysis and quality-filtering were carried out using Mothur software v 1.43.0 (University of Michigan Medical School, USA), following the standard Miseq standard operating procedure (SOP). Chimeric reads were identified and excluded using Chimera UCHIME. Diversity was examined by operational taxonomic units (OTUs) at 3% dissimilarity and the distance-based greedy clustering (DGC) algorithm, calculating the coverage, number of observed species (sobs), richness index Chao1, specific diversity indexes (InvSimpson, Shannon), and evenness index Pielou. Redundant, non-chimeric FASTA files were taxonomically classified using Silva v132 database. Abundance was expressed as a percentage with respect to the total number of sequences in each sample. Genera with total abundance higher than 0.01% were considered for statistical analysis.

Predictive microbial functional analysis to analyse microbial functionality was carried out using Phylogenetic Investigation of Communities by Reconstruction of Unobserved States (PICRUSt) on high-throughput 16S rRNA gene sequencing data(140). Kyoto Encyclopedia of Genes and Genomes (KEGG) microbial pathways

classified at level 3 were statistically analysed as described by Díaz-Faes et al. (2021) (141).

Shotgun sequencing was performed as follows: libraries were prepared using the DNA prep protocol (20060060, Illumina, USA) with 25-500ng of input DNA, according to manufacturer´s instructions. All samples were quantified using Qubit system 2.0 (Thermo Fisher Scientific, USA) and pooled according to the lowest concentration. The final pool was sequenced using the 2x151 bp P1 reagent (20050264, Illumina, USA) and NextSeq2000 sequencer, obtaining 150M raw reads.

Quality processing of fastq files was performed using KneadData pipeline, based on Trimmomatic for quality trimming and Bowtie2 to remove host contaminating sequences belonging to human and rat genomes. Resulting fastq files were converted to fasta using IDBA-UD and processed using HUMAnN 3.0 pipeline (142). Taxonomy at the species level was assigned via alignment against ChocoPhlAn v30 database and MetaPhlAn classifier. Translated search and functional profiling was performed using DIAMOND aligner and the UNIPROT database, clustering sequences at 90% of homology to ensure good representation of gene families in the UniRef clusters; gene families were then regrouped using the Kyoto Encyclopedia of Genes and Genomes (KEGG) orthologs database.

Statistically significant KEGG orthologs (KO) were mapped to KEGG pathways and pathways of interest were coloured according to log2 fold change (log_2FC) values using KEGG Search & Colour pathway tool.

3.5 SCFA analysis

SCFA analysis (acetic, propionic and butyric acids) was carried out at the technical facility of the University of Granada by high-performance liquid chromatography (HPLC) using the Acquity UPLC-I Class System (Waters Corporation, USA) with an UV–vis detector set at 210 nm (TUV Detector). Dilutions of SCFA standards (Acetic acid:

A6283, Sigma-Aldrich, USA; Propionic acid: 81910, Sigma-Aldrich, USA; Butyric acid:108111000, Acros Organics, USA) were prepared in saline solution at concentrations ranging from 87 to 0.087mM for acetic acid, 67 to 0.067mM for propionic acid and 54.5 to 0.0545mM in the case of butyric acid.

A Waters CORTECS™ C18 column (2.1 x 100 mm, 1.6 µm) was used at room temperature, at a flow rate of 0.2 mL/min; water buffer (solvent A) /acetonitrile (solvent B) gradient elution was performed as follows: from 1% to 100% B and down to 1% B, 0–7.5 min. The injected sample volume was 10µL.

3.6 16S quantitative PCR (qPCR)

To quantify the total bacterial load, 16S rRNA gene-targeted quantitative PCR (qPCR) was performed. Power SYBR green PCR (4309155, Thermo Fisher Scientific, USA) was used in a total reaction mixture volume of 10 µL. The universal bacterial primers were forward (F): 5'-AAACTCAAAKGAATTGACGGGG-3' and reverse (R): 5'-GGGTTGCGCTCGTTRYGG-3' (143). Primers in a final concentration of 0.5 µM each and DNA volume of 1 µl (<50ng) were added to the PCR master mix in MicroAmp Fast 96-Well reaction plates (4346907, Thermo Fisher Scientific, USA). qPCRs were performed using QuantStudio 6 system (Thermo Fisher Scientific) and cycling conditions included 95°C for 10 min and 40 cycles consisting of denaturalization at 95°C for 15 seconds and annealing-extension at 60°C for 1 min. Negative controls containing no template DNA were subjected to the same procedures. The specificity of the amplified products was determined by analysis of melting curves. The number of 16S copies per sample were obtained via interpolation in the standard curve, for which known concentrations of *Escherichia coli* 16S gene were used.

3.7 RNA isolation and gene expression qPCR

Total cellular RNA was isolated from colonic mucous samples with Trizol Reagent (15596, Invitrogen, USA). Reverse transcription was performed using RevertAid First Strand cDNA Synthesis Kit (K1622, Thermo Fisher Scientific, USA) with Oligo(dT) primers according to the manufacturer's protocol. qPCR was conducted on QuantStudio 6 system (Thermo Fisher Scientific, USA) with SYBR Green (4309155, Thermo Fisher Scientific, USA), a final concentration of primers of 0.5 µM and using 2µL of previously diluted cDNA (1:10). Cycling conditions included 95°C for 10 min and 40 cycles consisting of denaturalization at 95°C for 15 seconds and annealing-extension at 60°C for 1 min. For NT5E, ENTPD1 and CLD1 genes, the annealing-extension temperature was adjusted to 50°C to optimise performance. Target mRNA levels were normalized in relation to basic transcription factor 3 (BTF3) or anti-cyclophilin B (PPIB). Primers used in this study are listed in Annex 1.

3.8 mRNA sequencing (RNA-Seq)

RNA quality from colonic mucous samples was assessed through the determination of the RNA Integrity Number (RIN) via 2100 Bioanalyser Instrument (Agilent Technologies, USA). mRNA libraries were prepared using 500-1000 ng of total RNA as an input and the polyA selection protocol (TruSeq stranded mRNA Library Prep, ref. 20020595 / 20020594, Illumina, USA) at the Centre for Genomic Regulation (Spain). Libraries were then sequenced using the Hiseq2500 platform (Illumina, USA) and the paired-end 50bp format.

A total of 40 million raw reads per sample were obtained and mapped using "Rsubread" package. Reads were aligned and annotated using the rat genome rn6 as a reference, downloaded from http://hgdownload.soe.ucsc.edu/downloads.html#rat. Further analyses in R software were performed using "edgeR" package. Gene set enrichment analysis (GSEA) was performed using "fgsea" package and $\log_2$FC as the ranking parameter. Gene Ontology (GO) was used as reference database (including

Biological process, Cellular component and Molecular function categories). Differentially expressed GO terms during IDA were selected using p-adjusted (padj) values below 0.05; upregulation or downregulation of each pathway was assessed with positive and negative values of the Normalized Enrichment Score (NES), respectively. Visualization of parental terms was performed using REVIGO tool (144); results derived from GSEA were plotted using GOplot package (145).

3.9 Immunofluorescence

Colon fragments were harvested, washed and fixed 8 hours (RT) in 4% paraformaldehyde (P6148, Sigma Aldrich, USA). Tissues were embedded in Tissue-Tek OCT Compound (127217, Sakura Finetek, USA), frozen using isopentane and dry ice and stored at -80ºC. Sections were cut (4 µm) using a cryostat and labelled overnight at 4ºC with COL6 antibody (1:500) (MA5-32412, Thermo Fisher Scientific, USA) after blocking nonspecific binding sites with 10% bovine serum albumin (BSA) (A7906, Sigma Aldrich, USA), 0.5% (v/v) Triton-X100 (T8787, Sigma-Aldrich, USA) for 30 min. A secondary antibody conjugated with AlexaFluor-555 (A-31572, Thermo Fisher Scientific, USA) was used for detection (1:1000). Counterstaining was performed using DAPI (0.5ug/mL) (D1306, Invitrogen, USA). Sections were mounted in Vectashield medium (H-1000-10, Vector Laboratories, USA). Images were acquired through a Confocal Zeiss LSM 710 inverted microscope. Immunofluorescence images were quantified measuring the area positive for both DAPI and antibody signal using ImageJ (National Institute of Health, USA). To allow comparability, instrument settings were equally adjusted across samples.

3.10 ELISA

Bacteria-specific IgG, IgM and IgA detection

The determination of faecal bacteria-specific Ig was as previously described (146). Faecal bacteria were obtained using 200mg of faecal pellets. After homogenization in sterile PBS, filtration through a 100 µm strainer, bacteria were separated from debris/rat cells by removing the pellet after centrifugation at 400g for 10 min (4ºC). Faecal bacteria were washed, heat-killed at 85°C for 1 h, and resuspended in 20 mL PBS, and 100 µL of this suspension was added to each well of a 96-well ELISA plate (M5785-1CS, Sigma-Aldrich, USA) for overnight coating at 4°C. Number of bacteria in each suspension was determined by spectrophotometry at 600nm and adjusted across experimental groups. Wells were then blocked with 1% (w/v) BSA in PBS for 2 hours at room temperature. Rat sera were diluted at 1:100 and incubated overnight at 4°C for detection of IgG, IgM, and IgA. Incubation with secondary Anti-rat IgG, IgM and IgA (A110-143P, BioNova científica S.L., Spain) (1:10000) for 1.5 hours in darkness was followed by the addition of horseradish peroxidase (HRP) substrate (11112422001, Roche Applied Science, Germany). Absorbance was measured using NanoQuant Infinite M200 Pro multi-plate reader (Tecan).

3. 11 Lipopolysaccharide (LPS) detection

LPS determination was performed via chromogenic enzymatic reactions using Limulus amebocyte lysate (LAL) chromogenic assay (A39552, Thermo Fisher Scientific, USA), according to manufacturer's instructions. Serum samples were diluted 1:20 and heat inactivated at 70ºC for 15 min.

3. 12 Statistical analyses

Principal coordinate analysis (PCoA) based on Bray Curtis distances were implemented in PRIMERe Permanova + (PRIMER-E Ltd, Plymouth, UK). Heatmaps, bubble plots for relative abundance, pearson correlations and statistical analysis of

shotgun and RNA-Seq data were performed using R software (R Foundation for Statistical Computing, Vienna). In particular, statistically significant KEGG orthologs (KO) from shotgun data were selected using “edgeR” package and padj values below 0.05, while statistically significant species were determined using ALDEx2 package.

Clustering procedures based on Bray Curtis distances were performed in Past 4.02 (147); dendrograms were drawn using MEGA7 (148). Linear discriminant analysis Effect size (LEfSe) was carried out using Galaxy with default parameters (149). Correlation network diagrams were represented using Gephi 0.9.2 and Fruchterman Reingold algorithm. Multivariant correlation analysis were implemented via Statgraphics Centurion XVII (Statpoint Technologies, USA).

Statistical significance was assessed through GraphPad Prism software (Dotmatics, UK) using Student’s two-tailed t test or a non-parametric alternative in case data were not normally distributed.

For all tests, p values below 0.05 were considered significant (unless otherwise indicated) and expressed as follows: *$p < 0.05$, **$p < 0.01$, ***$p < 0.001$ and ****$p<0.0001$.

4. RESULTS

4.1 Study of the gut microbiome and the integrity of the intestinal barrier during IDA

4.1.1 Study of haematological parameters during the development of iron deficiency anaemia

A decrease in the number of red blood cells, haemoglobin concentration, haematocrit and mean corpuscular volume (MCV) by day 20 (d20) and day 40 (d40) confirmed that IDA had been correctly induced (Table 3). Mean corpuscular haemoglobin showed a significant decrease at day 40 while mean corpuscular haemoglobin concentration was diminished at day 20 and day 40.

Table 3. Haematological parameters during the development of iron deficiency anaemia (day 20 and day 40). Means and standard deviations are shown for each group, time and parameter. (*) represents statistical differences ($p<0.05$) between control and anaemic group at each respective time (d20 and d40).

	Control		**Anaemia**	
	d20	**d40**	**d20**	**d40**
Red blood cells (10^6/µL) (RBC)	6.56 ± 0.56	8.12±0.45	3.07±0.65*	2.15±0.51*
Haemoglobin (g/dL)	13.27±3.06	16.05±0.89	6.55±1.17*	4.16±0.52*
Haematocrit (%)	43.32±4.65	47.89±2.75	17.98±2.71*	21.34±9.27*
Mean corpuscular volume (fL) (MCV)	65.97±2.29	59.14±1.54	59.15±4.95*	40.22±0.65*
Mean corpuscular haemoglobin (pg) (MCH)	20.32±4.84	19.82±0.67	22.14±5.22	16.17±1.4*
Mean corpuscular haemoglobin concentration(g/dL) (MCHC)	30.87±7.58	33.49±0.75	36.99±6.73*	16.17±4.11*
Leukocytes (10^3/µl)	10.47±3.06	13.23±2.25	13.61±3.03*	10.51±1.48*
Platelets (10^3/µL)	901.27±407.42	889.64±445.55	Over range	Over range

4.1.2 Structural and functional characterisation of the gut microbiome during IDA. Identification of key microbial metabolites

4.1.2.1 IDA is associated with dysbiosis along the gastrointestinal tract, especially in the large intestine

To provide a comprehensive view of the gut microbiome along the gastrointestinal tract during IDA, all intestinal content and faeces were sequenced using amplicon methods. Sequencing of 16S rRNA gene amplicons resulted in a total of 1.860.784

sequences after bioinformatic processing. Multivariant analysis methods were first applied to assess differences in the microbial composition considering the whole microbial community. Among them, Principal Coordinate Analysis (PCoA) evaluates microbial similarity between samples, and segregates them in a two-dimension plot whereby samples that are microbially similar cluster together while those that are not cluster separately. The two axes (coordinates) in the plot explain most of the variability between samples and often acquires a biological significance, as it will be discussed (150, 151).

First, PCoA considering bacterial relative abundances at the genus level was applied on faeces samples collected at baseline, d20 and d40, showing differences between control and anaemic animals over time. PCoA accounted for 57.2% of bacterial variation considering the first two principal coordinates (Figure 12). Samples were separated along the Y axis according to the duration of the deficiency (Figure 12A) and along the X axis according to their iron status (Figure 12B). Specifically, control and anaemic baseline samples grouped together, while d20 and d40 samples were segregated into anaemic and control groups. D20 and d40 samples clustered separately from baseline samples (Figure 12A and 12B).

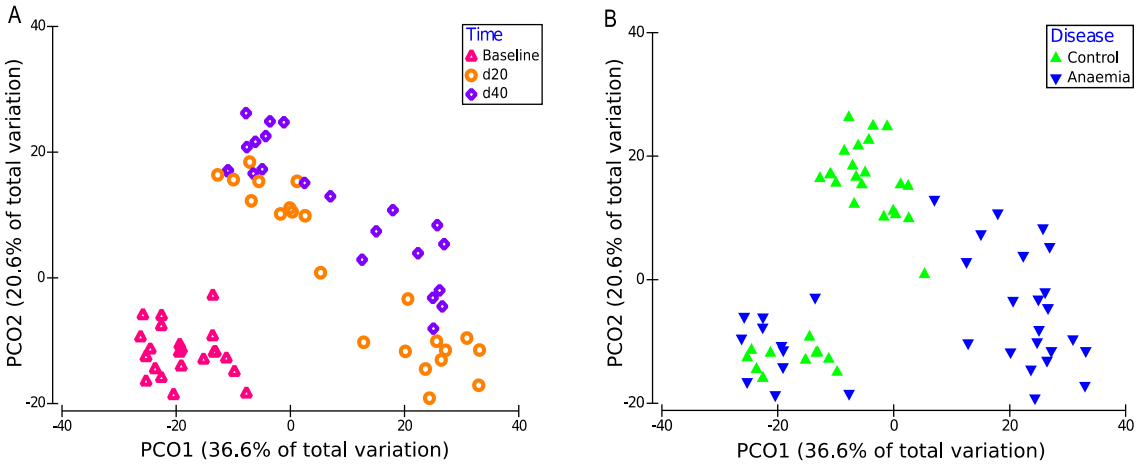

Figure 12. Principal coordinate analysis (PCoA) based on Bray-Curtis distances. Plots for faecal samples collected during the development of iron deficiency anaemia (baseline, d20 and d40) considering bacteria with a relative abundance higher than 0.01%. Samples are represented by coloured symbols according to the legend. (A) Different time points are considered regardless of iron status (B) Control and anaemic groups are considered regardless of time points.

When analysing intestinal contents (day 40), PCoA showed a clear distinction between samples belonging to the small and large intestine along the X axis (Figure 13A), regardless of their iron status (Figure 13B) and explaining 50.8% of bacterial variation. These results were further confirmed by Bray Curtis distance-based clustering methods (Figure 14) (152), where samples were also divided into two clusters according to the major anatomical region.

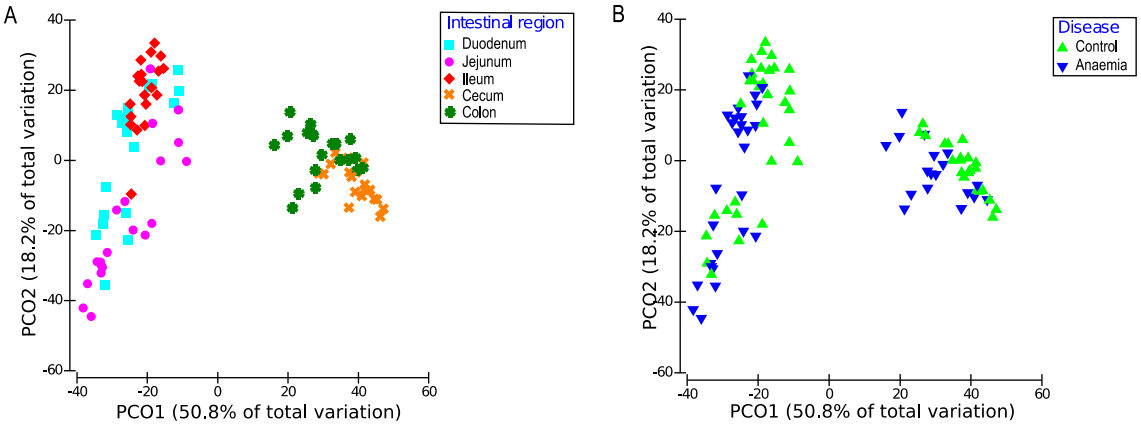

Figure 13. Principal coordinate analysis (PCoA) based on Bray-Curtis distances. Plots for intestinal content samples along the gastrointestinal tract, considering bacterial genera with a relative abundance higher than 0.01%. Samples are represented by coloured symbols according to the legend. (A) Anatomic regions are considered regardless of iron status (B) Experimental groups are considered regardless of the intestinal segment.

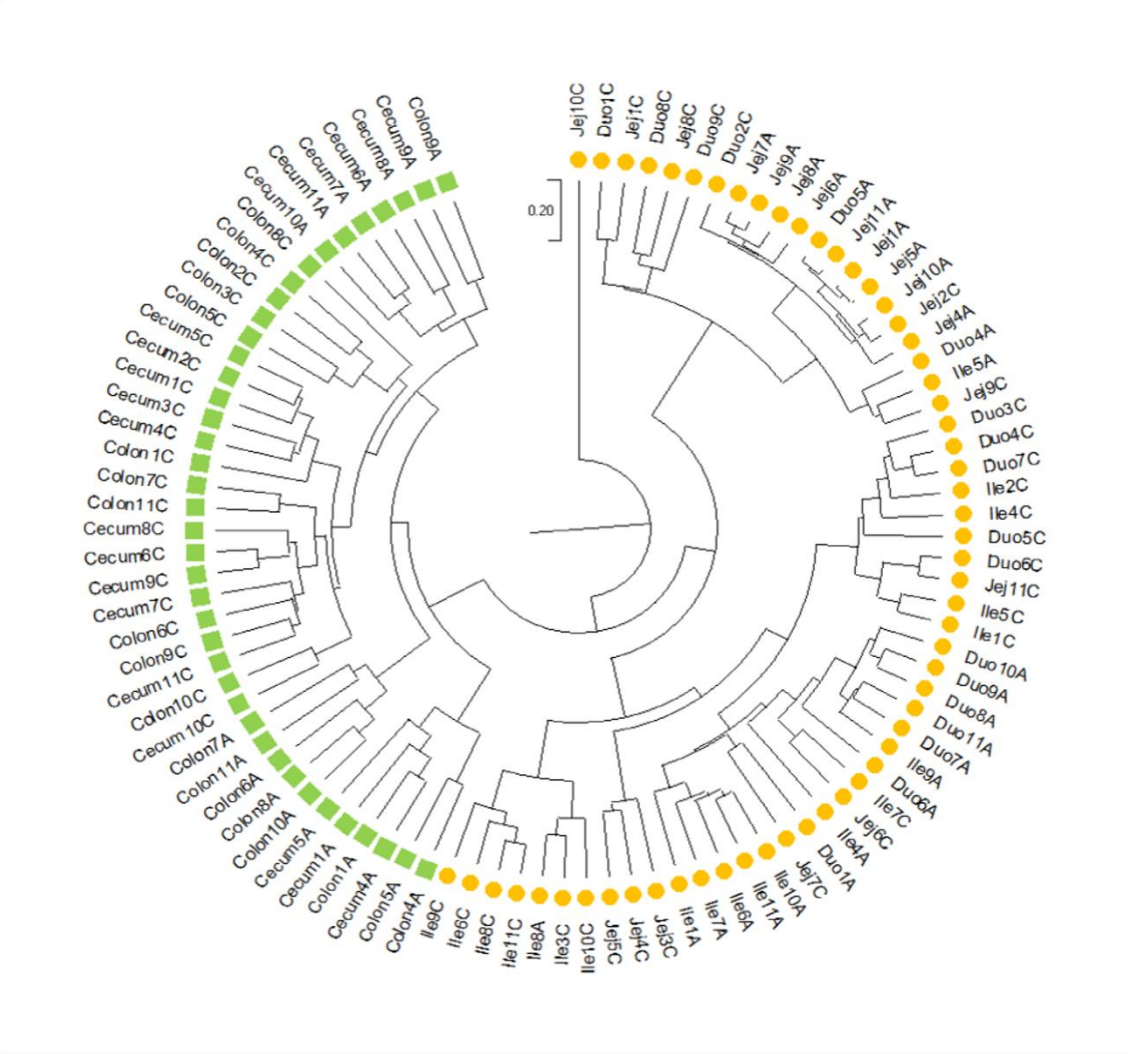

Figure 14. Bray Curtis-based hierarchical clustering of 100 samples, based on global bacterial profiles (genus level) along the upper and lower GI tract. Major anatomic sites are denoted by unique symbols: green squares for the large intestine and orange circles for the small intestine. Each sample is identified by its major anatomic site, being Duo: duodenum, Jej: jejunum and Ile: ileum, followed by one number indicating the animal identification, plus either C or A, which indicates whether that sample belongs to either the control or the anaemic group.

As microbial differences might be overlooked when analysing samples with great dissimilarity, genera-based PCoA was performed separately in the small and large intestine to analyse disease-driven dysbiosis. In the small intestine, duodenum, jejunum and ileum were separated along the X axis, explaining 47.3% of bacterial variation (Figure 15A). Duodenum showed an intermediate microbial composition while jejunum

and ileum samples clustered separately (Figure 15A). Anaemic and control samples also showed different microbial composition, as they were separated along the Y axis (17.5% of bacterial variation) (Figure 15B).

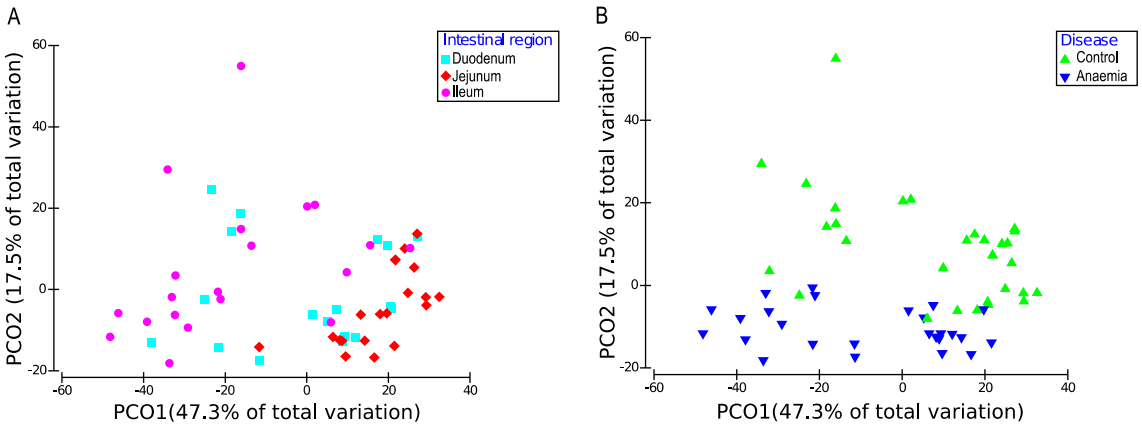

Figure 15. Principal coordinate analysis (PCoA) based on Bray-Curtis distances. Plots for intestinal contents in the small intestine considering bacterial genera with a relative abundance higher than 0.01%. Samples are represented by coloured symbols according to the legend. (A) Intestinal segments are considered regardless of iron status (B) Experimental groups are considered regardless of intestinal subsites.

Same results were obtained for the large intestine, with cecum and colon samples being separated along the Y axis (17.3% of bacterial variation) (Figure 16A), and anaemic and control animals along de X axis (37.5% of bacterial variation) (Figure 16B). It is worth highlighting that a higher percentage of microbial variation was explained by the segregation of intestinal content samples into anaemic and control groups in the large intestine compared to the small intestine (37.5 vs 17.5%, see above). However, the anatomical region is the main factor explaining bacterial variation in the small intestine (47.3% vs 17.3%).

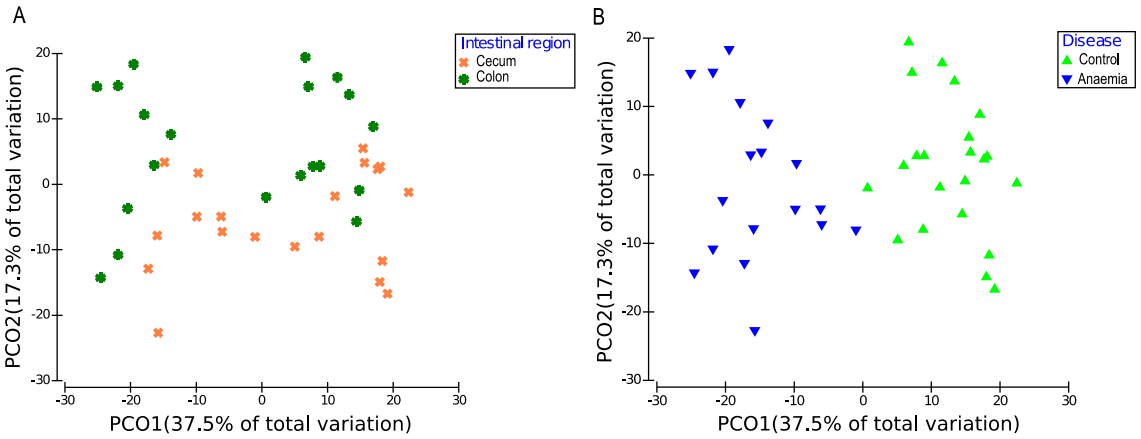

Figure 16. Principal coordinate analysis (PCoA) based on Bray-Curtis distances. Plots for intestinal contents in the large intestine considering bacterial genera with a relative abundance higher than 0.01%. Samples are represented by coloured symbols according to the legend. (A) Intestinal segments are considered regardless of iron status (B) Experimental groups are considered regardless of intestinal subsite.

Relative abundances considering the fifty most abundant genera were represented in a heatmap in each experimental group and intestinal segment (Figure 17). Again, a clear distinction of samples belonging to the small and large intestine was shown. Differences between control and anaemic animals were less apparent in the small intestine considering the majority of microbial genera, with dysbiosis being greater in the distal part of the gastrointestinal tract. Particularly, the colon showed more drastic changes in the relative abundance of certain genera (Figure 17, highlighted in green, see legend).

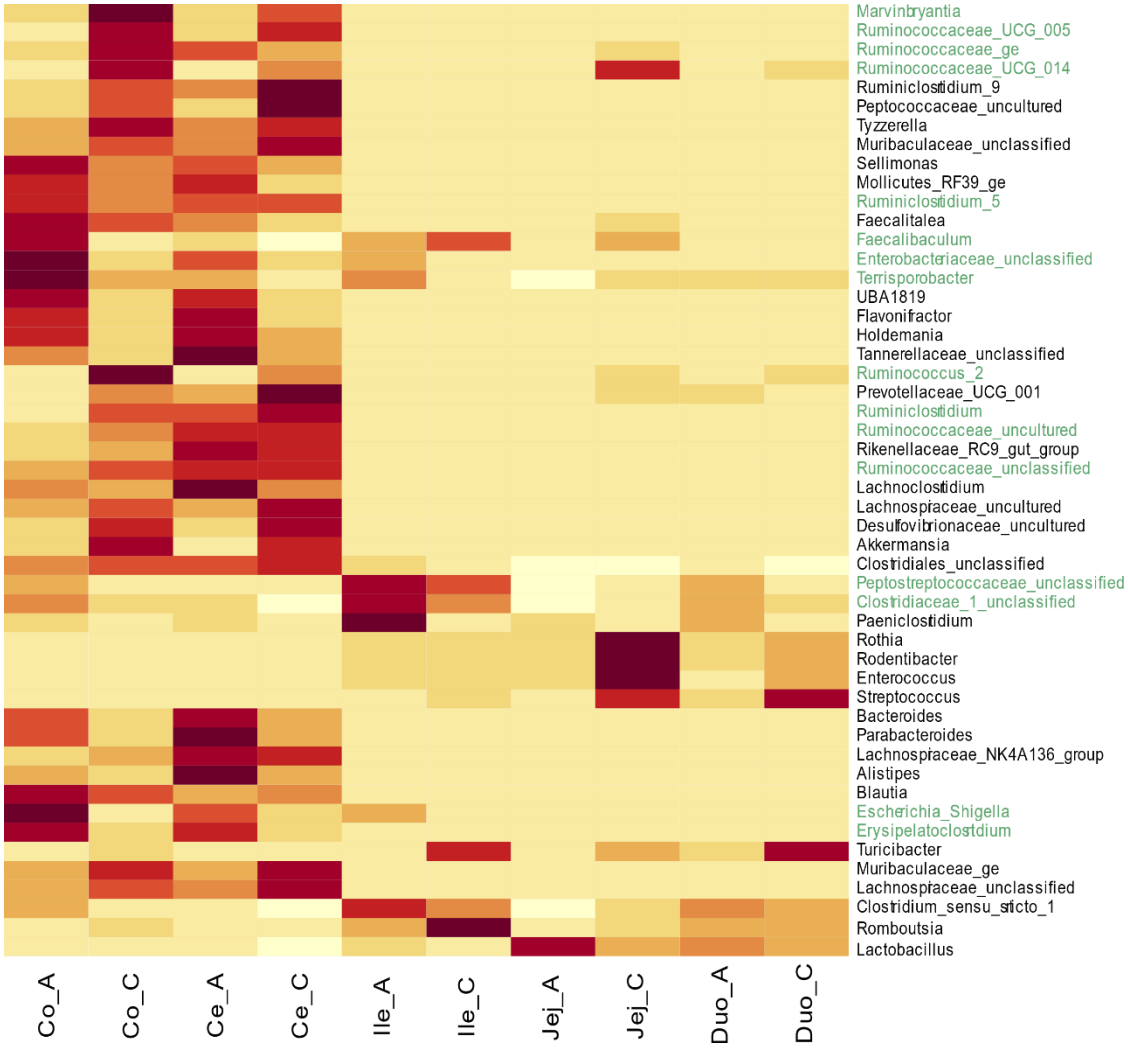

Figure 17. Heatmap representing mean relative abundance of the fifty most abundant genera in each intestinal segment and experimental group. A yellow-to-red scale has been used to score abundances, with red colours corresponding to greater values. Values have been scaled in the row direction to illustrate differences in microbial genera between experimental groups. Highlighted in green are bacterial taxa with clear differences between colon and cecum, therefore emphasizing a greater dysbiosis in the colon. Co: Colon, Ce: Cecum, Ile: Ileum, Jej: jejunum, Duo: duodenum; _A and _C stand for anaemic and control group.

4.1.2.2 During IDA, an enrichment in SCFA-related metabolic pathways and certain SCFA-producing genera is noticed towards the distal part of the gastrointestinal tract

Linear discriminant analysis Effect size (LEfSe) was next applied to identify differentially distributed bacteria for control and anaemic animals in the small and large

intestine (149). As stated before, a lower number of bacterial genera with statistical differences between experimental groups was found in the small intestine (Figure 18) compared to the large intestine, showing a greater dysbiosis in the latter (Figure 19).

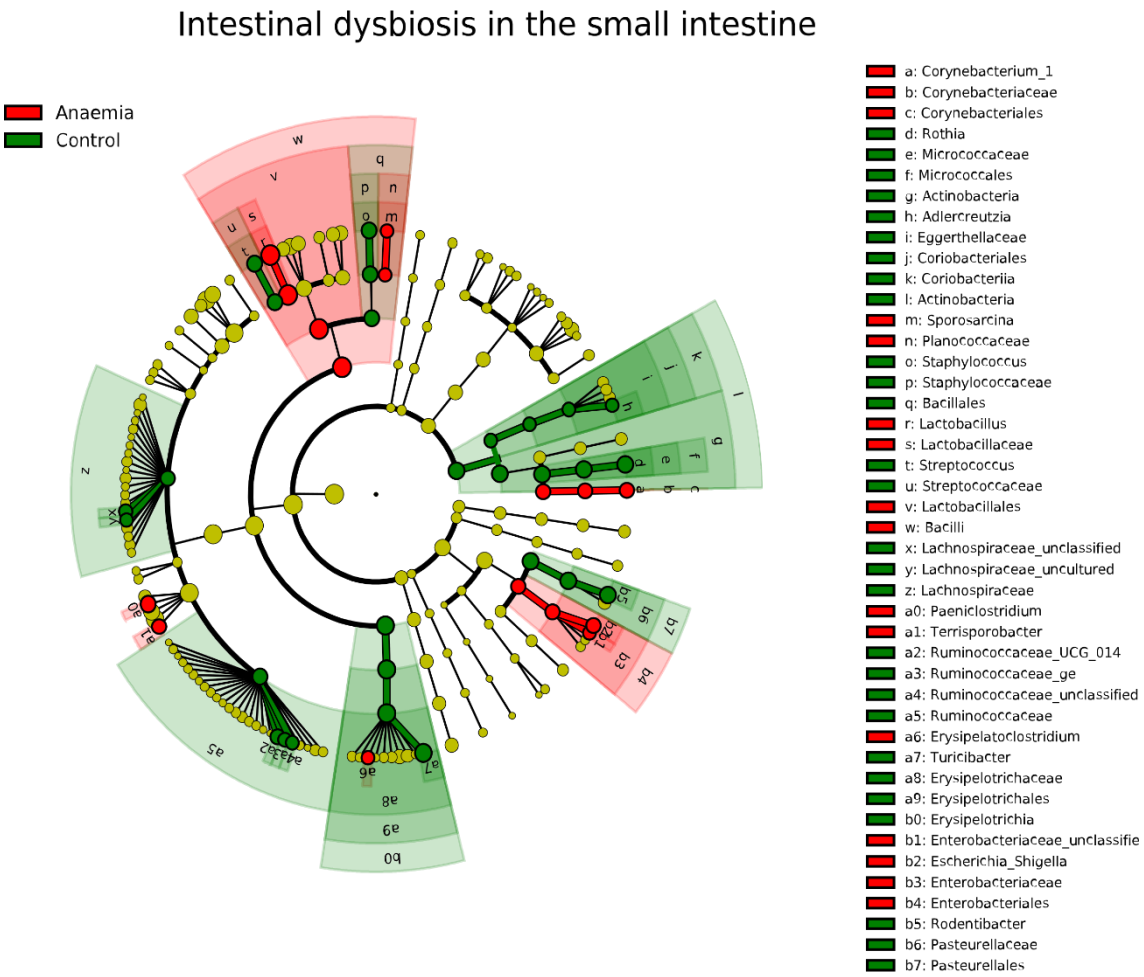

Figure 18. Linear discriminant analysis Effect size (LEfSe): cladogram for differentially distributed taxa ($p<0.05$, linear discriminant analysis (LDA) >2) between control and anaemic groups in the small intestine. Taxonomic features are represented in a hierarchical structure, with higher phylotypes oriented towards the inner part of the plot: domain, phylum, class, order, family and genera. Taxa showing significant differences are coloured according to their greatest abundance in either the control or anaemic group (red for anaemia, green for control, yellow for non-significant).

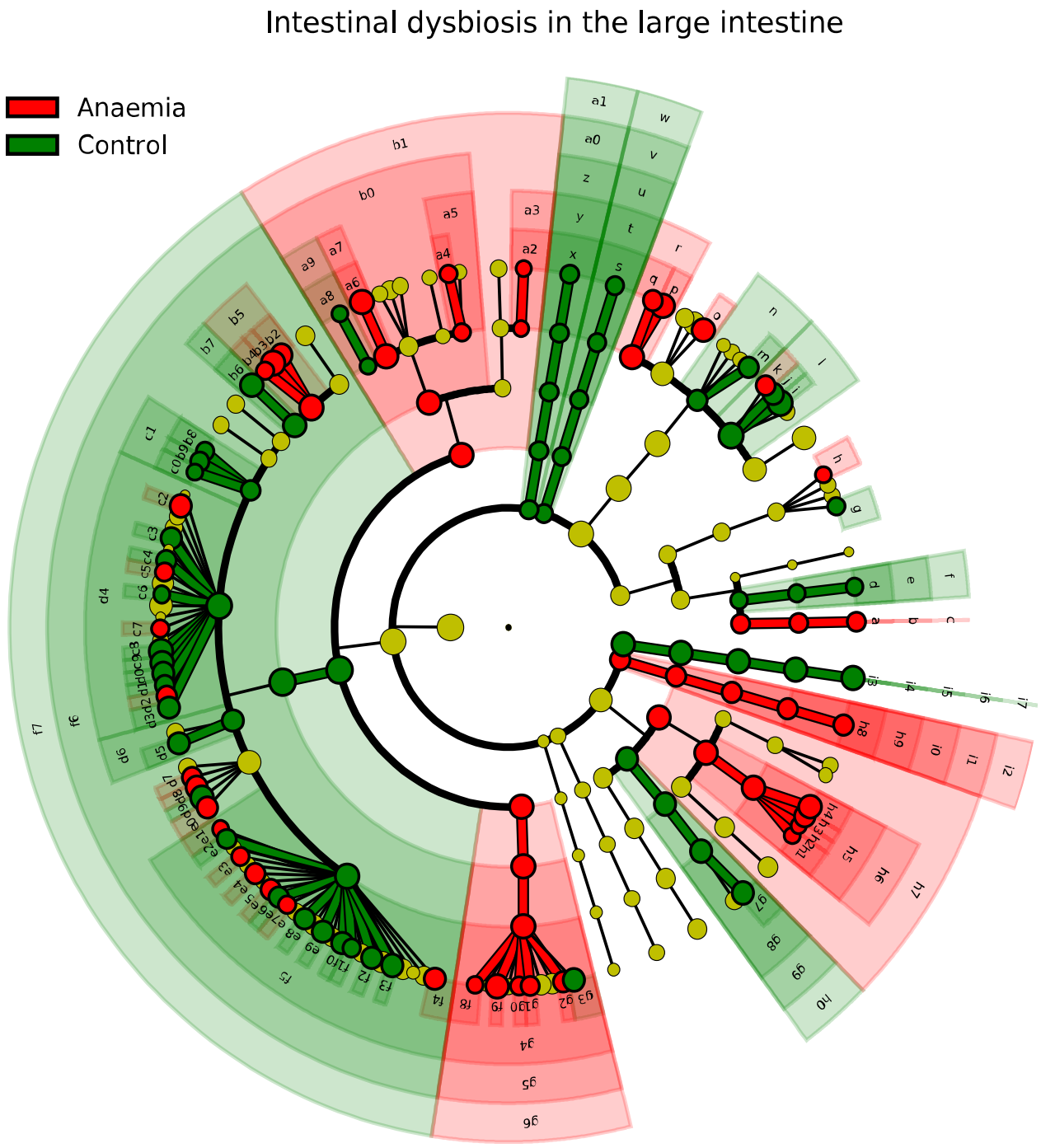
Intestinal dysbiosis in the large intestine
Anaemia
Control

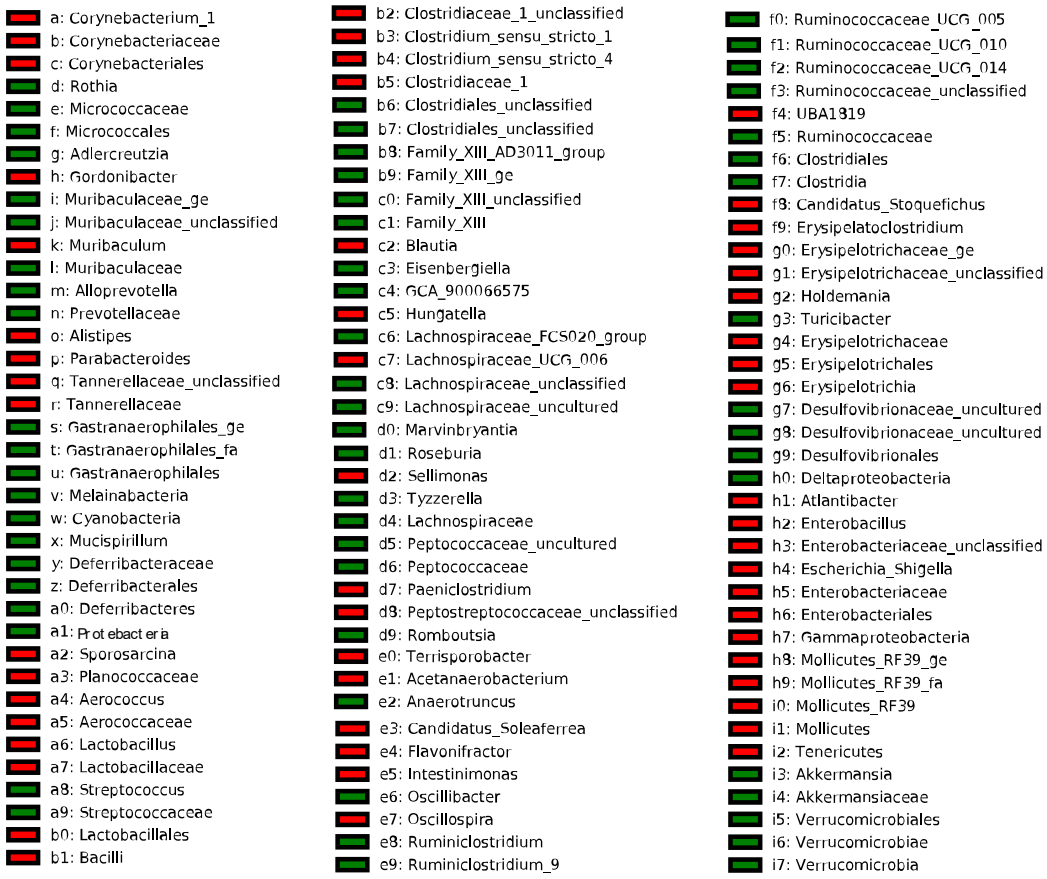

Figure 19. Linear discriminant analysis Effect size (LEfSe): cladogram for differentially distributed taxa ($p<0.05$, LDA>2) -between control and anaemic groups in the large intestine. Taxonomic features are represented in a hierarchical structure, with higher phylotypes oriented towards the inner part of the plot. Taxa showing significant differences are coloured according to their greatest abundance in either the control or anaemic group (red for anaemia, green for control, yellow for non-significant).

The majority of microbial genera with statistical differences between the control and anaemic groups in the small intestine matched those altered in the large intestine (Figures 18 and 19). However, new enriched genera appeared in the large intestine for anaemic animals, such as *Clostridium_sensu_stricto_1* and *Clostridium_sensu_stricto_4*, *Flavonifractor*, *Intestinimonas* or *UBA1819* (Figure 19). Members from the *Lachnospiraceae* and *Ruminococcaceae* families were especially abundant in control animals both in the small and large intestine, with specific genera

differing between both sites (Figures 18 and 19). *Romboutsia* and *Roseburia* were, however, only enriched in the large intestine in control animals.

Phylogenetic Investigation of Communities by Reconstruction of Unobserved States (PICRUSt) was employed to infer microbial functional traits(140). LEfSe was implemented on microbial functional data to identify which metabolic pathways were more prevalent during IDA along the gastrointestinal tract. In agreement with a less intense dysbiosis, no metabolic pathways were enriched in the small intestine of anaemic animals, while 15 pathways did in the case of the large intestine (Table 4). The top five (phosphotransferase system, butyrate metabolism, fatty acid metabolism, carbon fixation pathways and propionate metabolism), which showed the highest enrichment, were related to acetic, propionic, and butyric acid metabolism.

Table 4. KEGG microbial pathways differentially enriched in IDA. Effect size-related parameter LDA and p-values are included in subsequent columns for each pathway.

KEGG microbial pathways at level 3	**LDA (log10)**	**P-value**
Bacterial phosphotransferase system	2.6403	0.0002
Butyrate metabolism	2.4731	0.0063
Fatty acid metabolism	2.4437	0.0021
Carbon fixation pathways	2.4308	0.0260
Propanoate metabolism	2.4257	0.0007
Valine, leucine and isoleucine degradation	2.4242	0.0088
Replication, recombination and repair proteins	2.3643	0.0001
Benzoate degradation	2.3106	0.0008
Geraniol degradation	2.2296	0.0074
Lysine degradation	2.1943	0.0037
Beta-alanine metabolism	2.1381	0.0023
Tryptophan metabolism	2.1130	0.0194
Limonene and pinene degradation	2.0609	0.0048
Aminobenzoate degradation	2.0199	0.0209
Fatty acid biosynthesis	2.0039	0.0001

4.1.2.3 An increase in SCFA concentration parallels changes in the gut microbiome during IDA

SCFA were determined in intestinal contents from each segment along the gastrointestinal tract, showing an increase in anaemic animals in relation to control ones, especially in distal segments (Figure 20). Specifically, propionic acid significantly increased in the jejunum of anaemic rats compared to control ones, while the colon showed significant differences in all three fatty acids (Figure 20).

An increase in butyric, propionic and acetic acids was also noticed towards the distal parts of the gastrointestinal tract compared to proximal ones, both in control and anaemic animals (Figure 20). In control rats, the highest levels of butyric acid were found in the cecum; propionic acid significantly increased along the jejunum, ileum and cecum, whereas acetic acid showed its greatest concentration in the cecum, with a significant decrease in the jejunum and colon (Figure 20). In anaemic rats, butyric acid progressively increased from the jejunum to the colon where it reaches the highest levels. Propionic acid showed the lowest levels in the jejunum and the highest in the colon, while acetic acid showed its greatest concentration in the cecum (Figure 20).

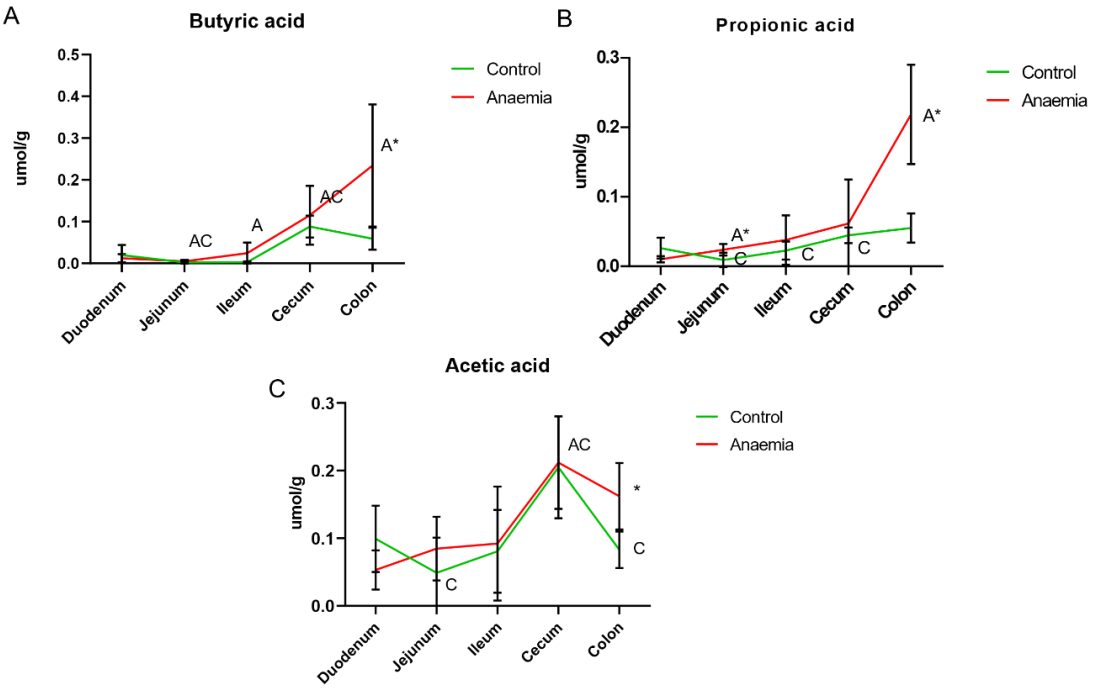

Figure 20. Changes in butyric, propionic and acetic acids concentrations (µmol/g) in intestinal contents along the digestive tract. Means are shown for each experimental group (control and anaemic), and standard deviation are illustrated by error bars. (*) represents statistical differences ($p<0.05$) between control and anaemic group in that intestinal region. C and A represents statistical differences ($p<0.05$) between the intestinal region in question and the one immediately before in control and anaemic groups respectively.

4.1.2.4 Specific bacterial genera are correlated to SCFA concentrations in the colon of control and anaemic animals

Network diagrams illustrating positive and negative correlations between SCFA and bacterial genera were elaborated, considering the colonic region of anaemic and control animals (Figures 21 and 22). Correlations were drawn as edges, using cutoff values of –0.5 and 0.5 and a red-blue scale according to their weight; positive and negative values were represented in red and blue respectively. SCFA and bacterial genera were represented as nodes, which were also coloured according to the number of connections in a similar scale, with red colours corresponding to greater connectivity. Node and label size were adjusted so that highly connected nodes showed bigger size and labels. A greater number of nodes and edges was found in the colon of anaemic animals, with 61 nodes and 77 edges (Figure 21), as opposed to 33 and 41 found in control rats (Figure 22). Both in the case of anaemic and control animals, parallel correlations could be observed between butyric and propionic acids, with acetic acid showing the opposite tendency. Such is the case of *Ruminococcaceae_ge* in the colon of anaemic animals, which showed negative correlations with butyric and propionic acids while being positively correlated to acetic acid (Figure 21). *Lachnospiraceae_NK4A136_group* and *Romboutsia* also followed the same pattern in the colon of control animals (Figure 22).

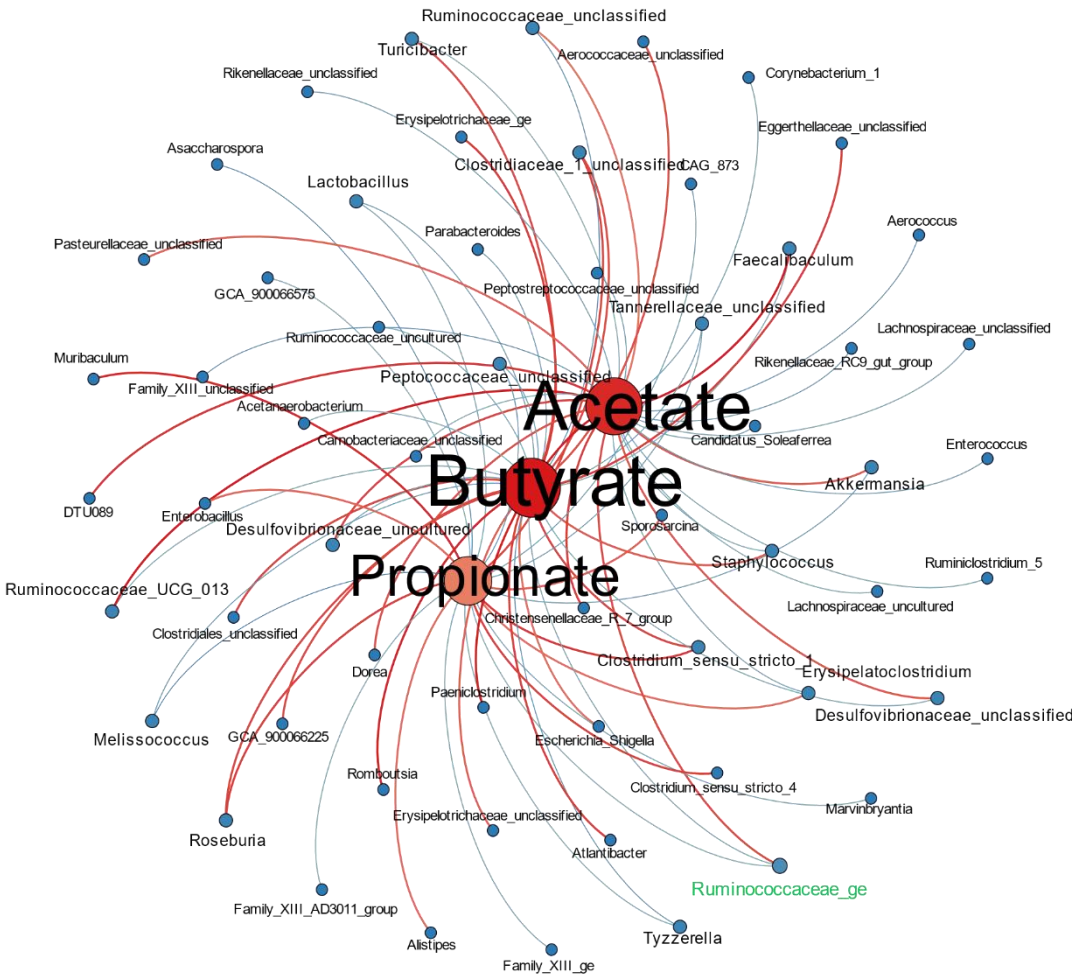

Figure 21. Correlation network between short chain fatty acids (SCFA) and microbial community members at the genus level in the colon of the anaemic group. Correlations were drawn as edges, using cutoff values of –0.5 and 0.5 and a red-to-blue scale according to their weight; positive and negative values are represented in red and blue respectively. SCFA and bacterial genera are represented as nodes, using a similar colour scale according to their connectivity. Node and label size were adjusted so that highly connected nodes showed bigger size and labels. Highlighted in green are microbial genera mentioned in the text.

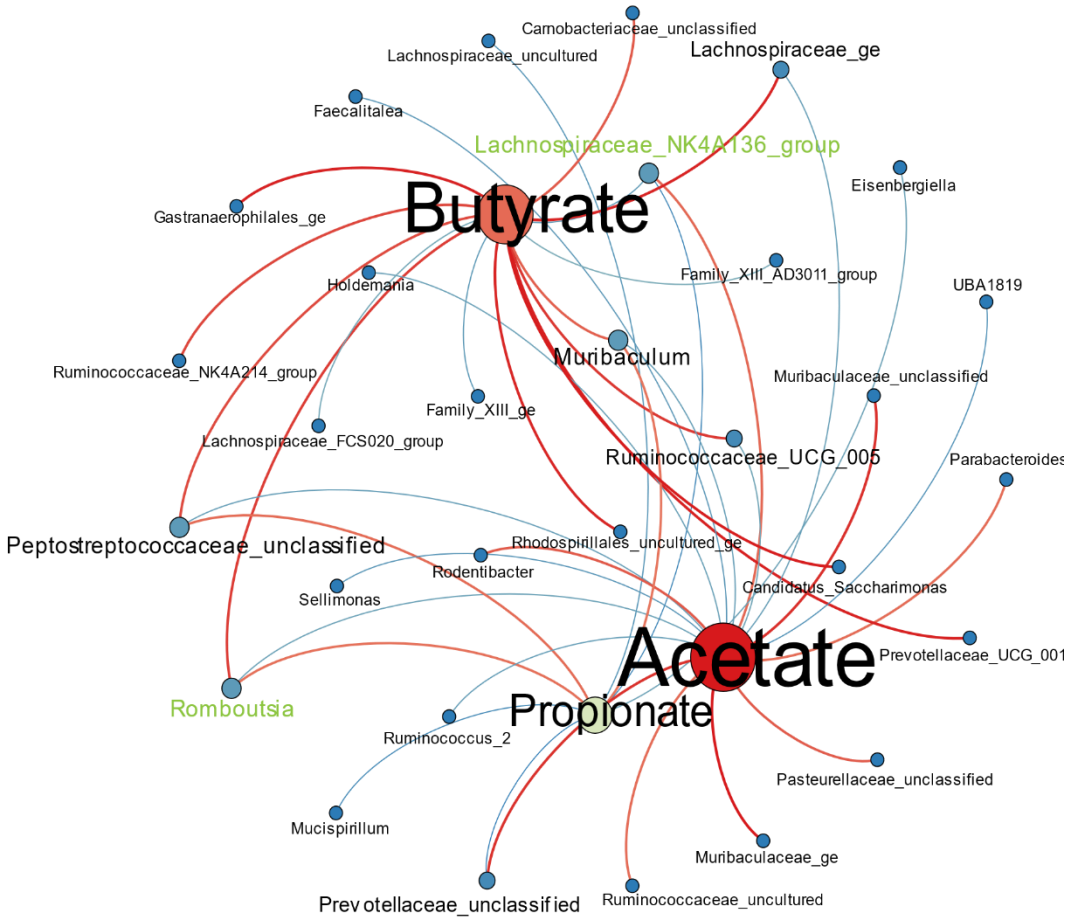

Figure 22. Correlation network between short chain fatty acids (SCFA) and microbial community members at the genus level in the colon of the control group. Correlations were drawn as edges, using cutoff values of –0.5 and 0.5 and a red-to-blue scale according to their weight; positive and negative values are represented in red and blue respectively. SCFA and bacterial genera are represented as nodes, using a similar colour scale according to their connectivity. Node and label size were adjusted so that highly connected nodes showed bigger size and labels. Highlighted in green are microbial genera mentioned in the text.

Aiming to identify which bacterial genera mainly contributed to variations in butyric, propionic and acetic acids, multivariant regression analysis was next performed for each SCFA in the colon of both experimental groups. *Clostridium_sensu_stricto_1* and *Clostridium_sensu_stricto_4* explained 83.77% of butyric acid variation in anaemic animals, while *Clostridium_sensu_stricto_1* was responsible for 54.6% of changes in

propionic acid. Lastly, contribution of *Akkermansia* and *Christensenellaceae_R-7_group* to acetic acid variation was worth 83.68% (Figure 23A). Different microbial genera were identified as main contributors to SCFA variation in the colonic region of control animals. Specifically, *Rhodospirillales_uncultured_ge*, *Paeniclostridium*, *Romboutsia*, *Ruminococcaceae_UCG_005* and *Pasteurellaceae_unclassified* explained 98.14% of butyric acid variation. Lastly, *Lachnospiraceae_NK4A136_group* and *Muribaculaceae_ge* represented 59.37% and 73.42% of changes in propionic and acetic acid respectively (Figure 23B).

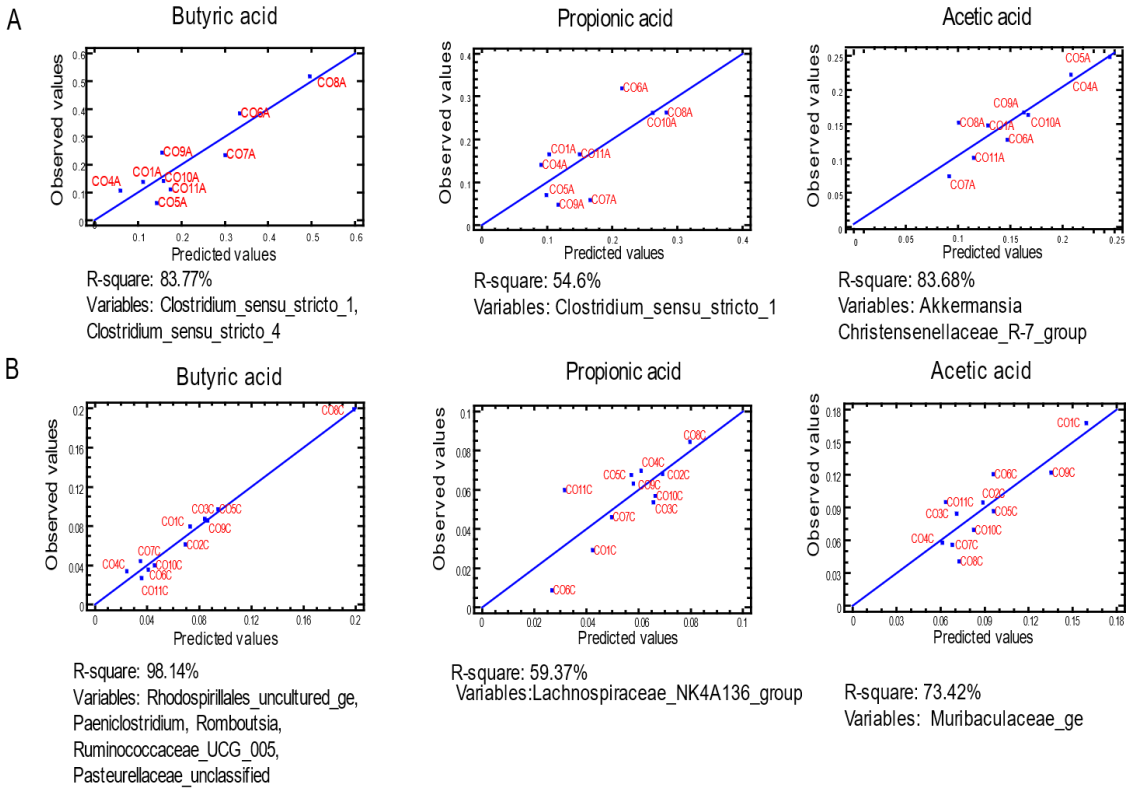

Figure 23. Multivariant correlation analysis considering short chain fatty acids and the colonic region of both experimental groups. Microbial genera showing significant Pearson correlations were introduced in the analysis, using the backward selection settings. (A) Multivariant correlation analysis considering butyric, propionic and acetic acid and the colonic region of the anaemic group. (B) Multivariant correlation analysis considering butyric, propionic and acetic acid and the colonic region of the control group.

4.1.2.5 Validation through shotgun sequencing confirms an enrichment in SCFA-related pathways and *Clostridium* species during IDA

Shotgun sequencing was applied on colonic content samples to fully characterise alterations in the gut microbiome at the species level and microbial functional traits. A total of 142M reads were obtained after bioinformatic processing.

To analyse the microbial functional traits, differentially abundand KEGG orthologs (KO) between the anaemic and control groups were determined (Annex 2). These bacterial KO genes were then mapped onto KEGG pathways to assess whether they clustered in specific KEGG pathways (Table 5). Additional information on KOs mapped to KEGG pathways is shown in Annex 3.

Table 5. Statistically significant KOs mapped to KEGG pathways; KOs with higher and lower abundance during IDA are shown. Pathways are shown in decreasing order of mapped KOs. Only pathways containing between 50-20 KOs were considered for subsequent analysis to exclude the most general and the least abundant ones.

KEGG pathways	Number of mapped KOs	KOs with higher abundance in IDA	KOs with lower abundance in IDA
Biosynthesis of aminoacids	47	30	17
Pyruvate metabolism	35	29	6
Purine metabolism	29	27	2
Quorum sensing	27	24	3
Butanoate metabolism	24	22	2
Amino sugar and nucleotide metabolism	24	18	6
Nucleotide metabolism	23	23	0
Propanoate metabolism	23	21	2
Glyoxylate and dicarboxylate metabolism	22	19	3
Glycolysis / gluconeogenesis	22	17	5
Pyrimidine metabolism	21	20	1
Ribosome	21	1	20
Carbon fixation pathways in prokaryotes	21	15	6
Sulphur metabolism	21	17	4
Oxidative phosphorylation	21	15	6

Pathways of interest were then coloured according to log_2FC values of differentially abundant KO genes, revealing a general increased abundance of genes related to biosynthesis of amino acids (Figure 24), amino sugar and nucleotide metabolism (Figure 25), glycolysis and gluconeogenesis (Figure 26), pyruvate metabolism (Figure 27), butanoate metabolism (Figure 28), propanoate metabolism (Figure 29), purine metabolism (Figure 30) and pyrimidine metabolism (Figure 31) during IDA.

KO genes involved in the synthesis of certain amino acids were more abundant during IDA, such as tyrosine, phenylalanine, cysteine, methionine or alanine (Figure 24, highlighted in green squares), while KOs involved in the synthesis of valine, leucine, or isoleucine were decreased (Figure 24, highlighted in orange squares).

Analysis of amino sugar and nucleotide metabolism revealed a higher abundance of genes associated with peptidoglycan production (Figure 25, highlighted in green) and with the synthesis of metabolic sugar intermediates (Figure 25, highlighted in blue). As far as glycolysis and gluconeogenesis is concerned, KO genes related to the transformation of monosaccharides and sugar intermediates into pyruvate and acetyl-CoA were enriched in anaemic animals (Figure 26, highlighted in blue). KO genes involved in the metabolism of pyruvate showed also increased abundances during IDA, leading to the formation of formate, succinate (Figure 27, highlighted in blue) and acetate (Figure 27, highlighted in green). Most KO genes belonging to the acetyl-CoA and 4-aminobutanoate/succinate pathway were increased within the butanoate metabolism during IDA (Figure 28, highlighted in green and blue respectively). Similarly, part of the glutarate pathway also showed higher abundance (Figure 28, highlighted in purple), as well as last steps involving the transformation of butanoyl-CoA into butanoate (Figure 28, highlighted in orange), all of them leading to an increased production of butanoate (Figure 20A). In the case of propanoate metabolism, most pathways involved in the transformation of propanoyl-CoA into propanoate were more abundant in the anaemic group (Figure 29, highlighted in orange), along with the 1,2-propanediol pathway (Figure

29, highlighted in green) and the methylisocitrate pathway (Figure 29, highlighted in green), which would result in an increased production of propanoate (Figure 20B).

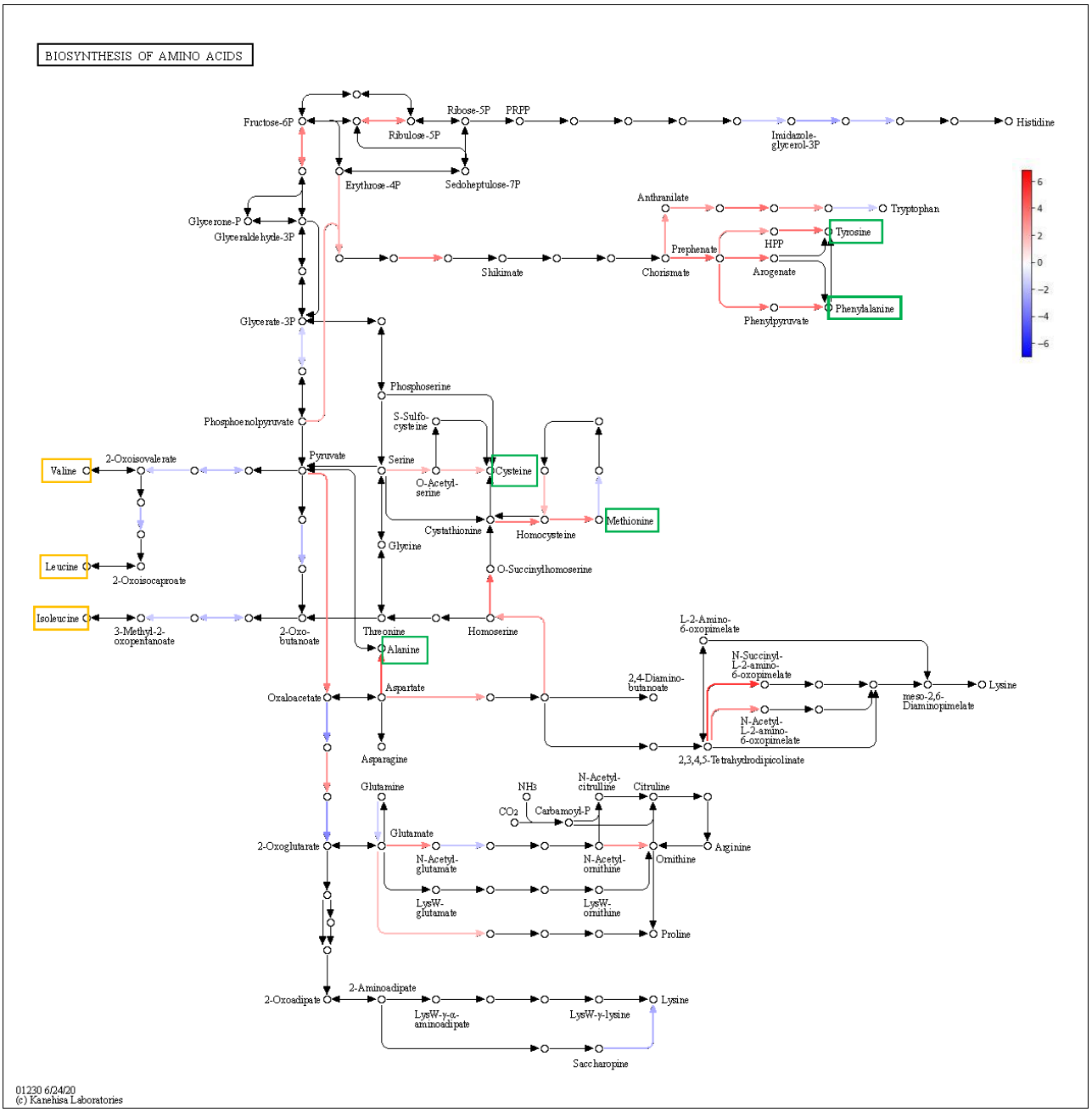

Figure 24. Biosynthesis of amino acids pathway (KEGG) coloured according to log_2FC values of statistically significant KO genes. Colour legend: amino acids – producing pathways with increased relative abundance during IDA (green squares); amino acids – producing pathways with decreased relative abundance during IDA (orange squares).

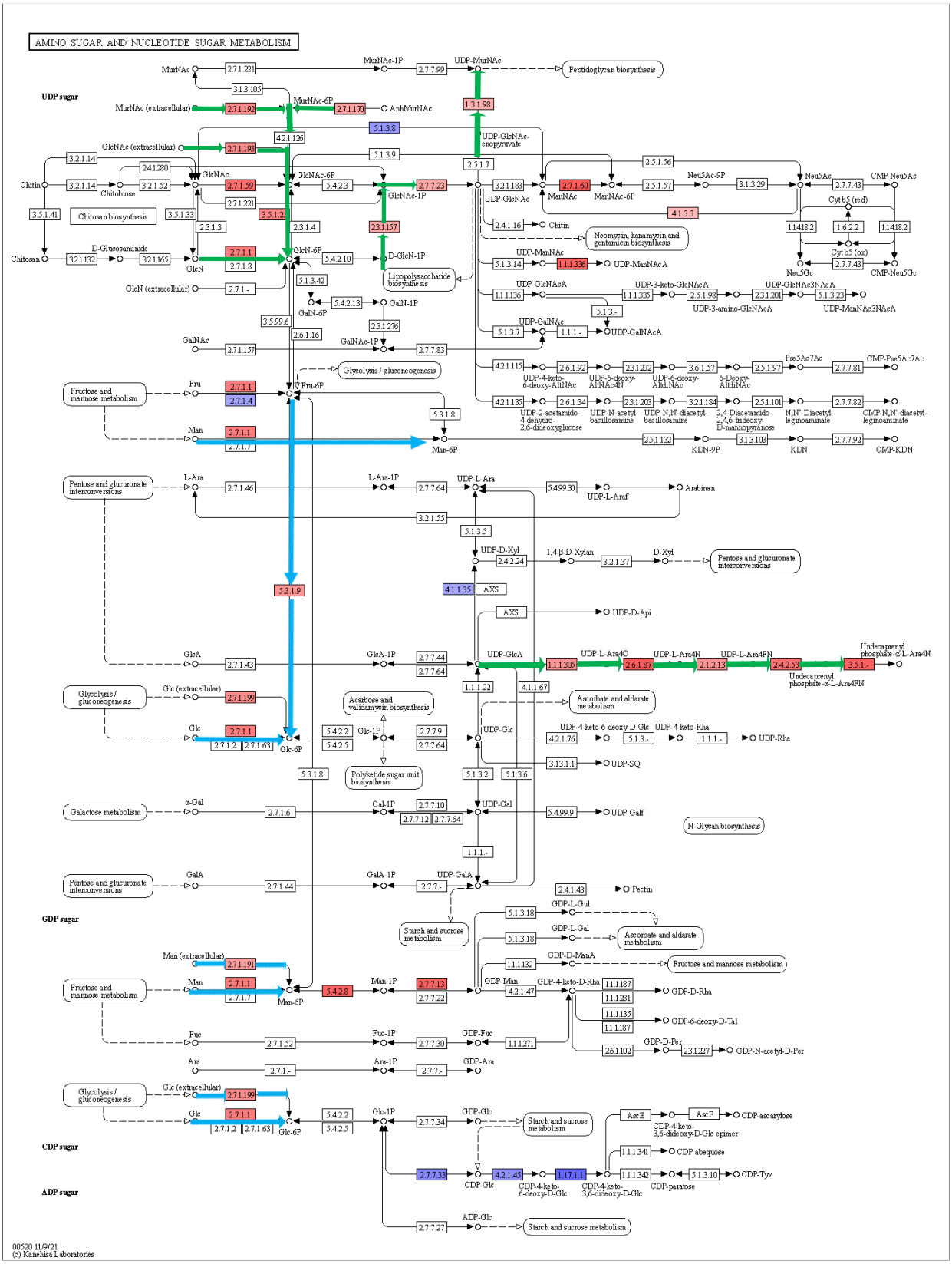

Figure 25. Amino sugar and nucleotide metabolism pathway (KEGG) coloured according to log2FC values of statistically significant KO genes. Colour legend: synthesis of cell wall components (green), metabolism of sugar intermediates (blue).

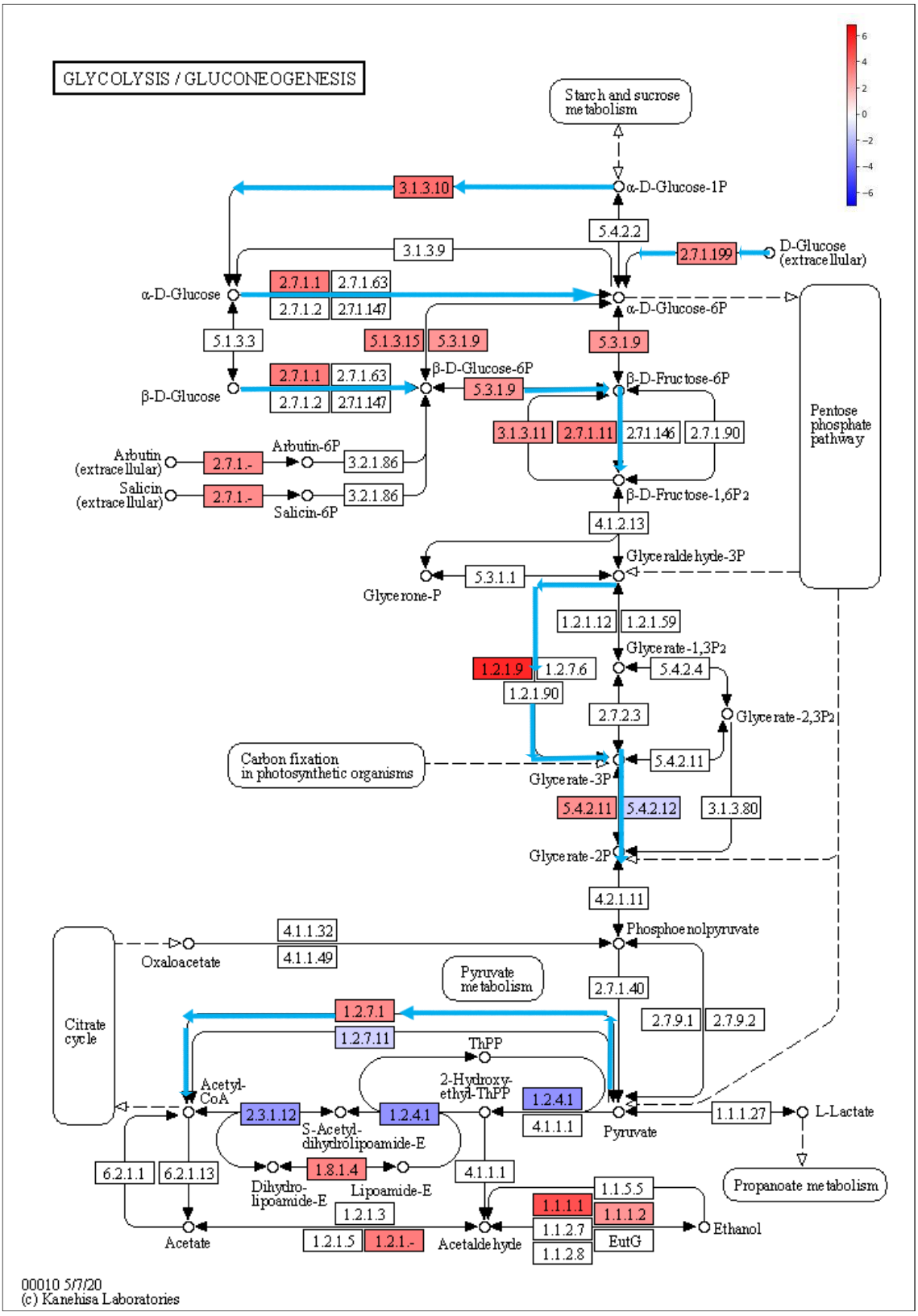

Figure 26. Glycolysis and gluconeogenesis pathway (KEGG) coloured according to log2FC values of statistically significant KO genes. Colour legend: metabolism of carbohydrates and sugar intermediates towards the formation of pyruvate and acetyl-CoA (blue).

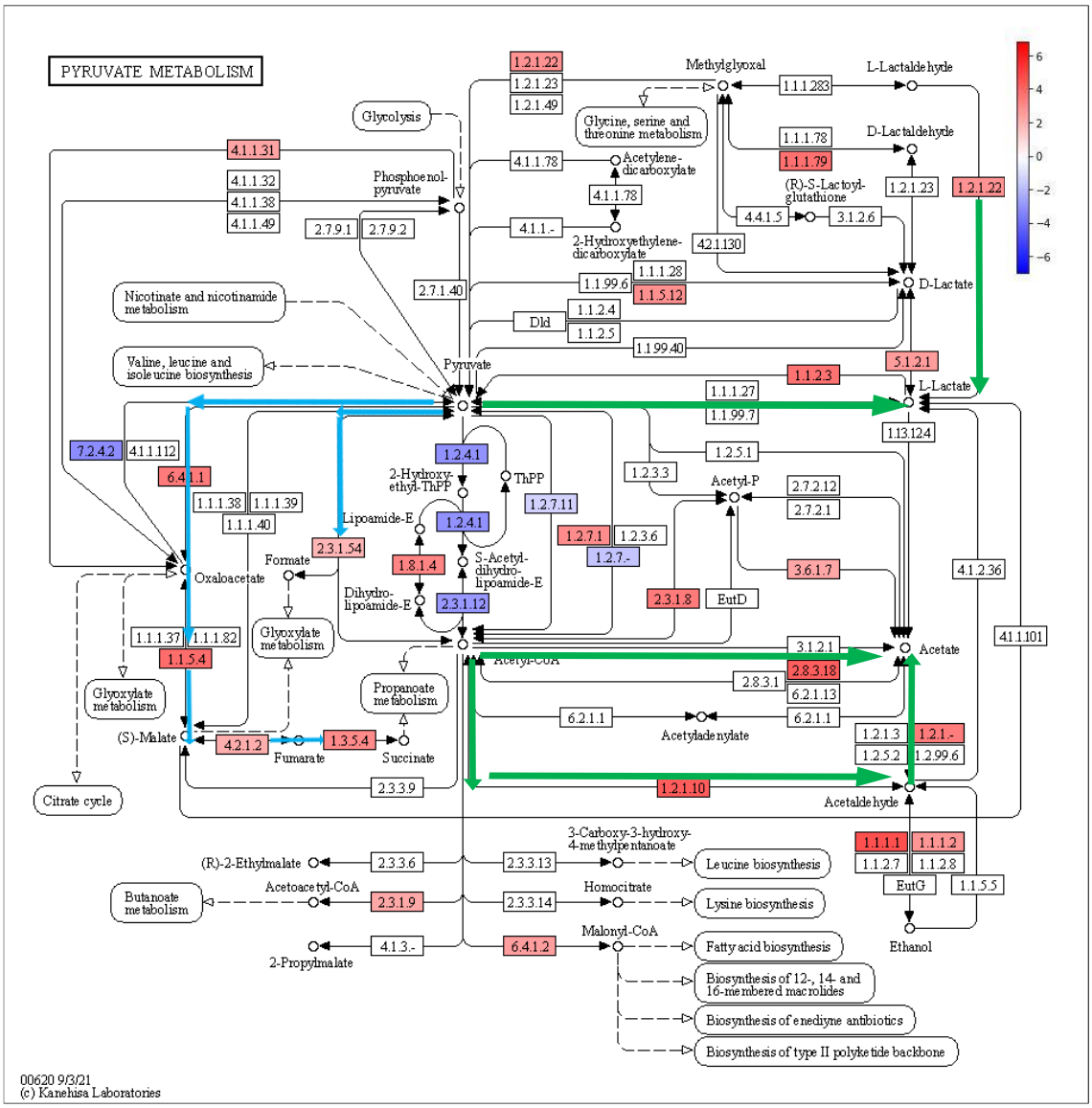

Figure 27. Pyruvate metabolism pathway (KEGG) coloured according to log2FC values of statistically significant KO genes. Colour legend: metabolism of pyruvate towards the formation for formate and succinate (blue), lactate and acetate (green)

Lastly, purine and pyrimidine pathways were characterised by an increased abundance of genes related to the production of guanine, xanthine, hypoxanthine and adenine in the case of purine metabolism (Figure 30, highlighted in green), and uracil, cytosine and thymine in the case of pyrimidine metabolism (Figure 31, highlighted in green), KO genes involved in the production cyclic AMP and GMP, along with

hyperphosphorylated guanine derivates (pppGpp), were also more abundant during IDA (Figure 30, highlighted in purple).

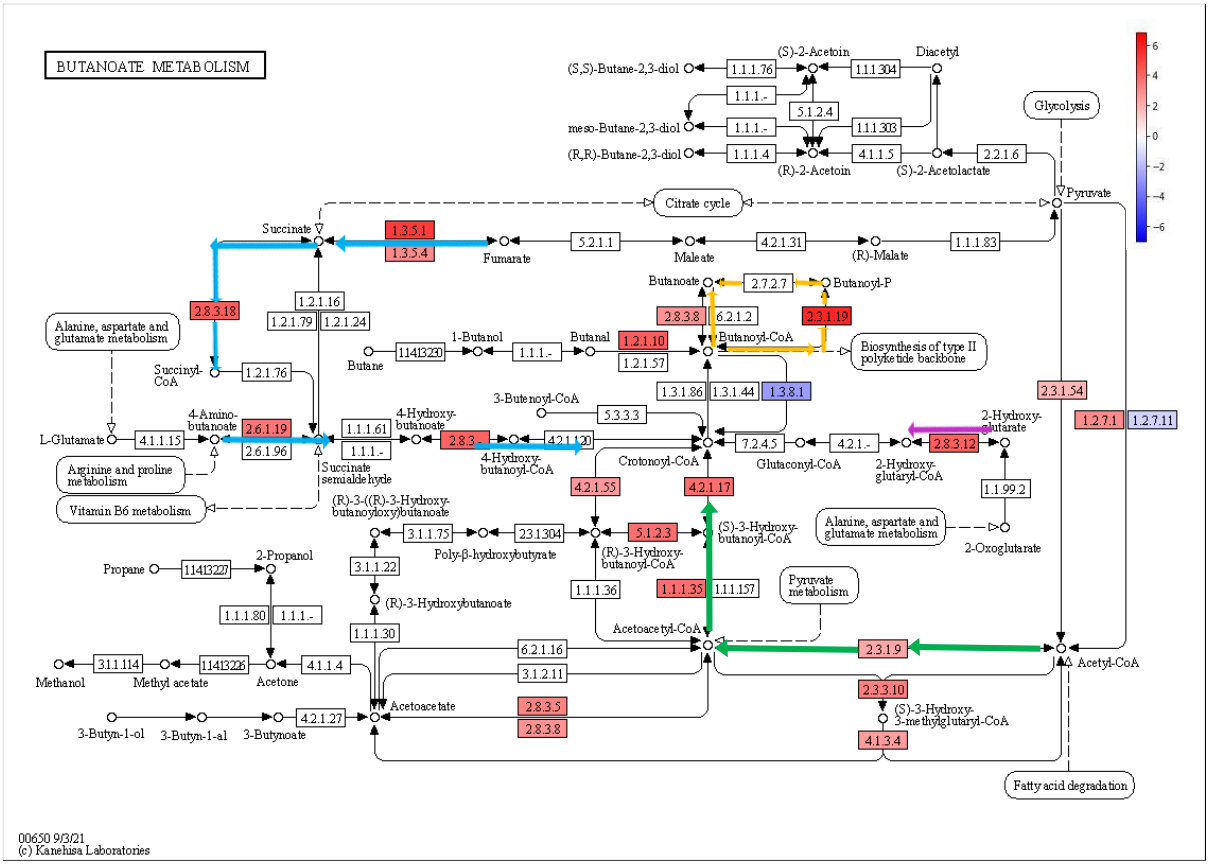

Figure 28. Butanoate metabolism pathway (KEGG) coloured according to log2FC values of statistically significant KO genes. Colour legend: 4-aminobutanoate/succinate pathway (blue), Acetyl-CoA pathway (green), glutarate pathway (purple), Butanoyl-CoA – Butanoate conversion (orange).

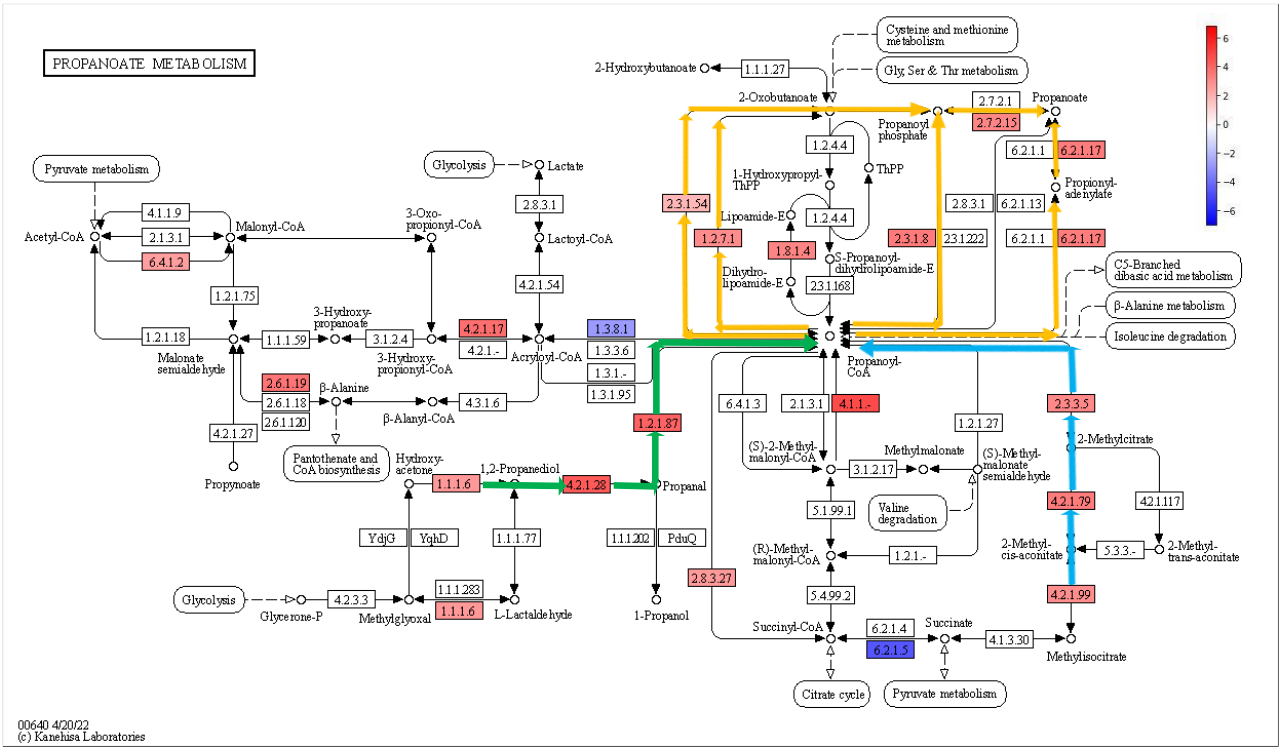

Figure 29. Propanoate metabolism pathway (KEGG) coloured according to log_2FC values of statistically significant KO genes. Colour legend: 1,2-propanediol pathway (green), methylisocitrate pathway (blue), Propanoyl-CoA – Propanoate conversion (orange).

Since high synthesis of nucleotides suggest a high division rate, bacterial load was also quantified by qPCR in colonic content samples belonging to anaemic and control animals. A higher number of 16S copies was found during IDA (Figure 32).

Similar to taxonomic analysis at the genus level, analysis of the differentially abundant bacterial taxa showed that *Clostridium* species, among others, were more abundant during IDA (Figure 33A).

Since members of the genus *Clostridium* are among the major producers of SCFA in the large intestine (153), Pearson correlations were calculated between SCFA and differentially abundant species and plotted in a heatmap (Figure 33B). A brown-to-purple scale was used, with negative and positive correlations drawn as brown and purple respectively. Overall, acetic acid correlations tended to oppose those of propionic and butyric acid in all bacteria. All *Clostridium* species (*Clostridium simbiosum*,

Clostridium disporicum, *Clostridium perfringens, Clostridium innocuum)* except *Clostridium bolteae* showed positive correlations to butyric and/or propionic acid, and negative correlations to acetic acid.

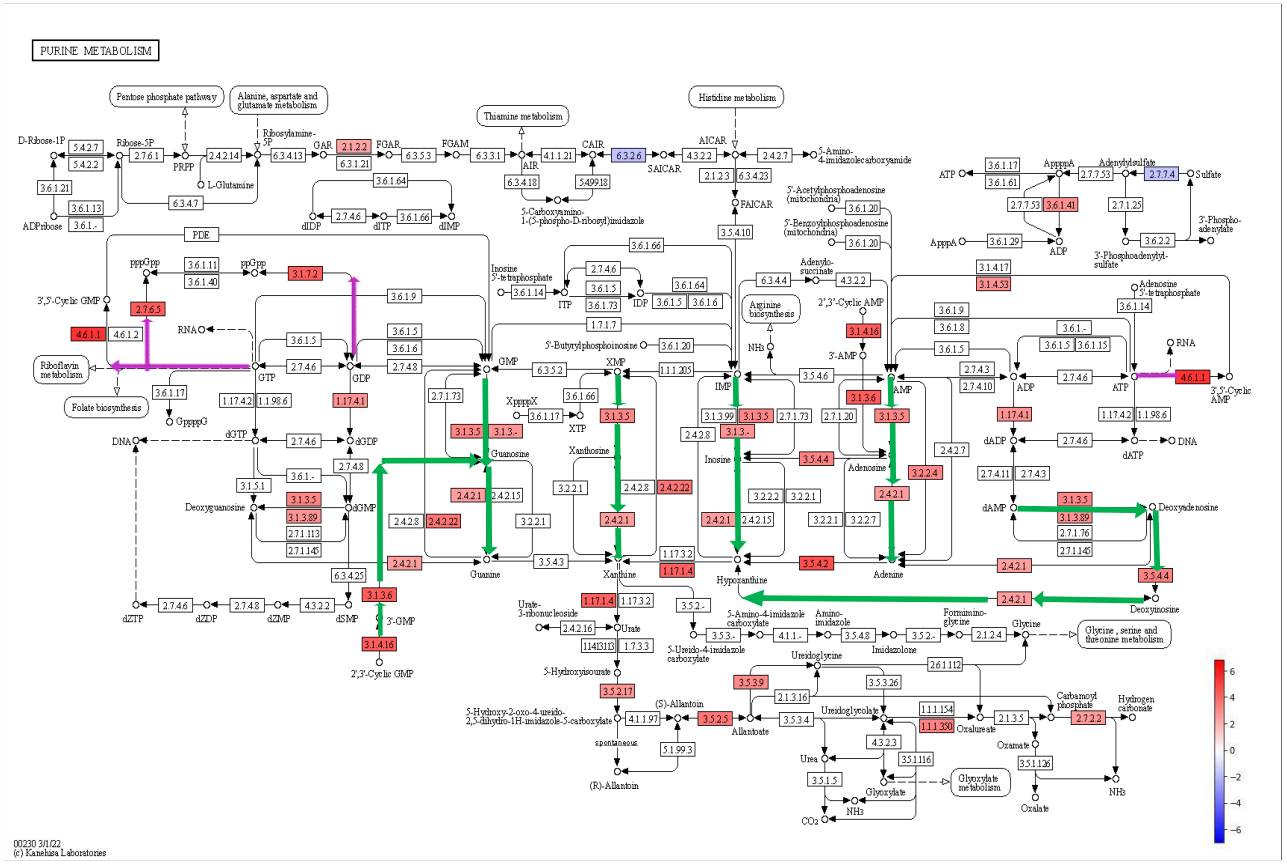

Figure 30. Purine metabolism pathway (KEGG) coloured according to log_2FC values of statistically significant KO genes. Colour legend: formation of purine-derived nucleotides (green) and nucleotides derivatives (purple).

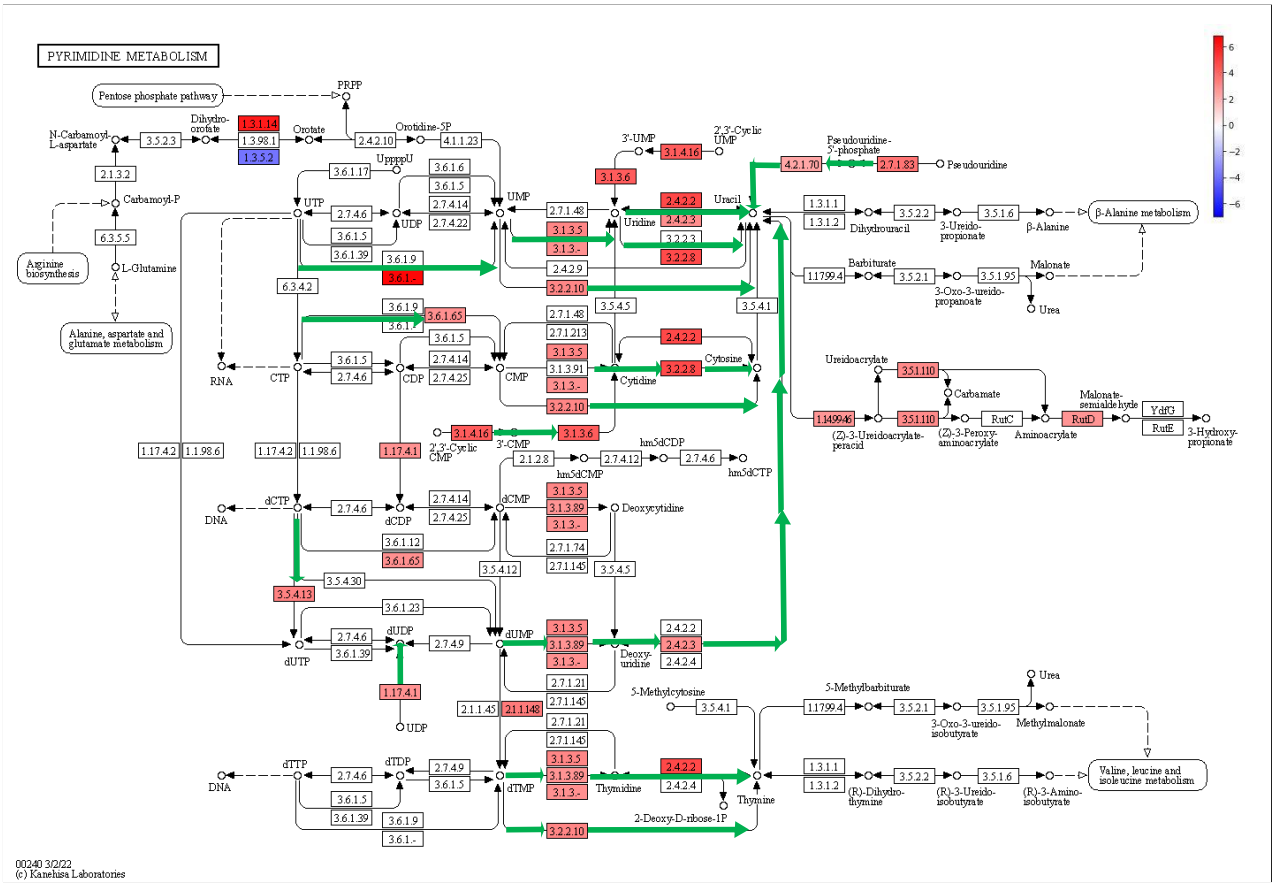

Figure 31. Pyrimidine metabolism (KEGG) coloured according to log_2FC values of statistically significant KO genes. Colour legend: formation of pyrimidine-derived nucleotides (green).

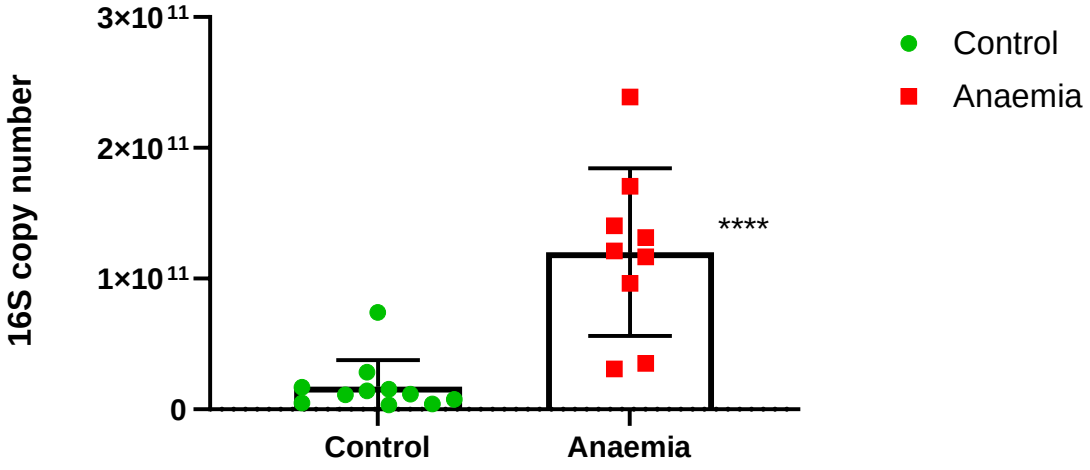

Figure 32. Bacterial load in colonic contents of control and anaemic animals quantified by qPCR.

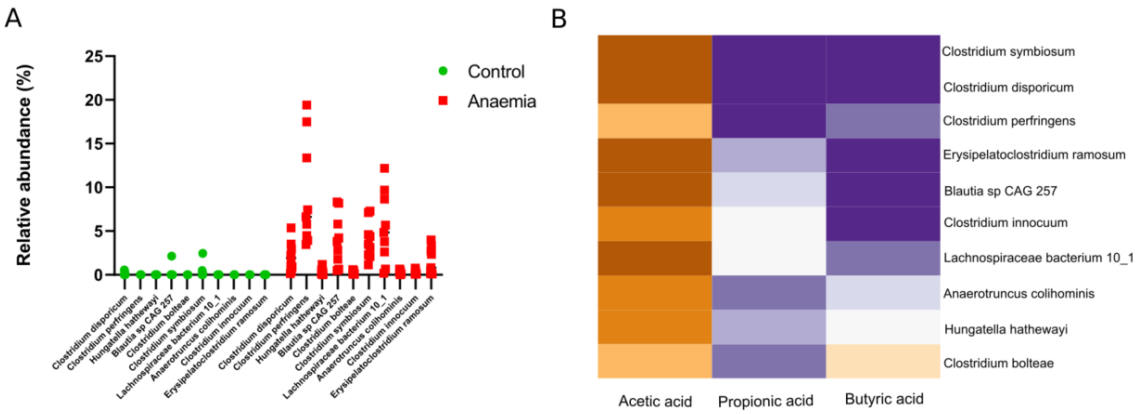

Figure 33. Taxonomic analysis at the species level and Pearson correlations between statistically significant species and SCFA levels. (A) Scatter plot of differentially abundant species ($p<0.05$) in the control and anaemic group determined by ALDEx2 (B) Heatmap illustrating Pearson correlations between species in A and SCFA levels. A blue-to-purple scale was used, with brown and purple indicating negative and positive correlations respectively.

4.1.3 Study the integrity of the intestinal barrier during the development of iron deficiency anaemia and the extent of microbial translocation

4.1.3.1 Changes in colonic metabolism during IDA reveals hypoxia-independent alterations in the intestinal barrier

RNA-Seq was performed to gain insight into alterations in gene expression taking place during IDA in the colonic epithelium.

Gene set enrichment analysis (GSEA) was next applied to assess whether deregulated genes during anaemia clustered in specific Gene Ontology (GO) terms. GO database was used including all categories (Biological process, Cellular component and Molecular function). Significant parental terms resulting from GSEA were divided into upregulated (Normalized Enrichment Score, NES > 0) (Figure 34A, 34C, 34E) or downregulated pathways (NES < 0) (Figure 34B, 34D, 34F) for each category, and represented in a bubble plot. Each bubble represents a significantly deregulated parental GO term, grouped by semantic similarity. The colour of the bubbles is indicative of the NES value; the darker the blue, the higher value of NES, which indicates that particular

GO term is strongly deregulated. Only the most representative GO terms (larger sizes, see legend) were displayed to facilitate visualization.

Downregulated GO terms outnumbered upregulated ones. It is notable the fact that upregulated GO terms include those involved in lipid metabolism (highlighted in dark blue) and metabolic pathways in response to microorganisms (highlighted in red) and mitochondria-related pathways (highlighted in yellow). On the contrary, GO terms related to the development of the enteric nervous system and the digestive tract (highlighted in black) were downregulated, along with those involved in the neural signalling within the enteric nervous system (highlighted in green). Cell junction assembly and cell integrity GO terms (highlighted in brown), along with extracellular matrix-associated ones (highlighted in pink) were also downregulated.

GO terms directly related to colonic intestinal dysbiosis and SCFA metabolism during IDA, as well as to the intestinal barrier, along with their genes, were represented in a circle plot to show individual gene deregulation (Figure 35). Downregulated genes belonged to extracellular matrix-associated pathways while upregulated ones belonged to GO terms involved in host-microbial interactions and lipid metabolism.

Lastly, a chord diagram was plotted to identify key deregulated genes during IDA in relation to the intestinal barrier (Figure 36). On the left part, genes and their corresponding log_2FC are associated to one or more selected GO terms, shown on the right. Interestingly, a considerable number of genes relating to the collagen family of proteins were downregulated. *Adipocyte enhancer binding protein 1* (*AEBP1*), *collagen VI alpha 1 chain* (*COL6A1*), *fibronectin 1* (*FN1*), *lumican* (*LUM*) and *fibroblast growth factor 13* (*FGF13*) (highlighted in green) were selected along the whole spectrum of downregulation to be validated by quantitative PCR (qPCR) (Figure 37A). *COL6A1* was the most significantly downregulated gene during IDA (Figure 37A), and its protein levels were assessed via immunofluorescence (Figure 37B), finding also a significant decrease (Figure 37C).

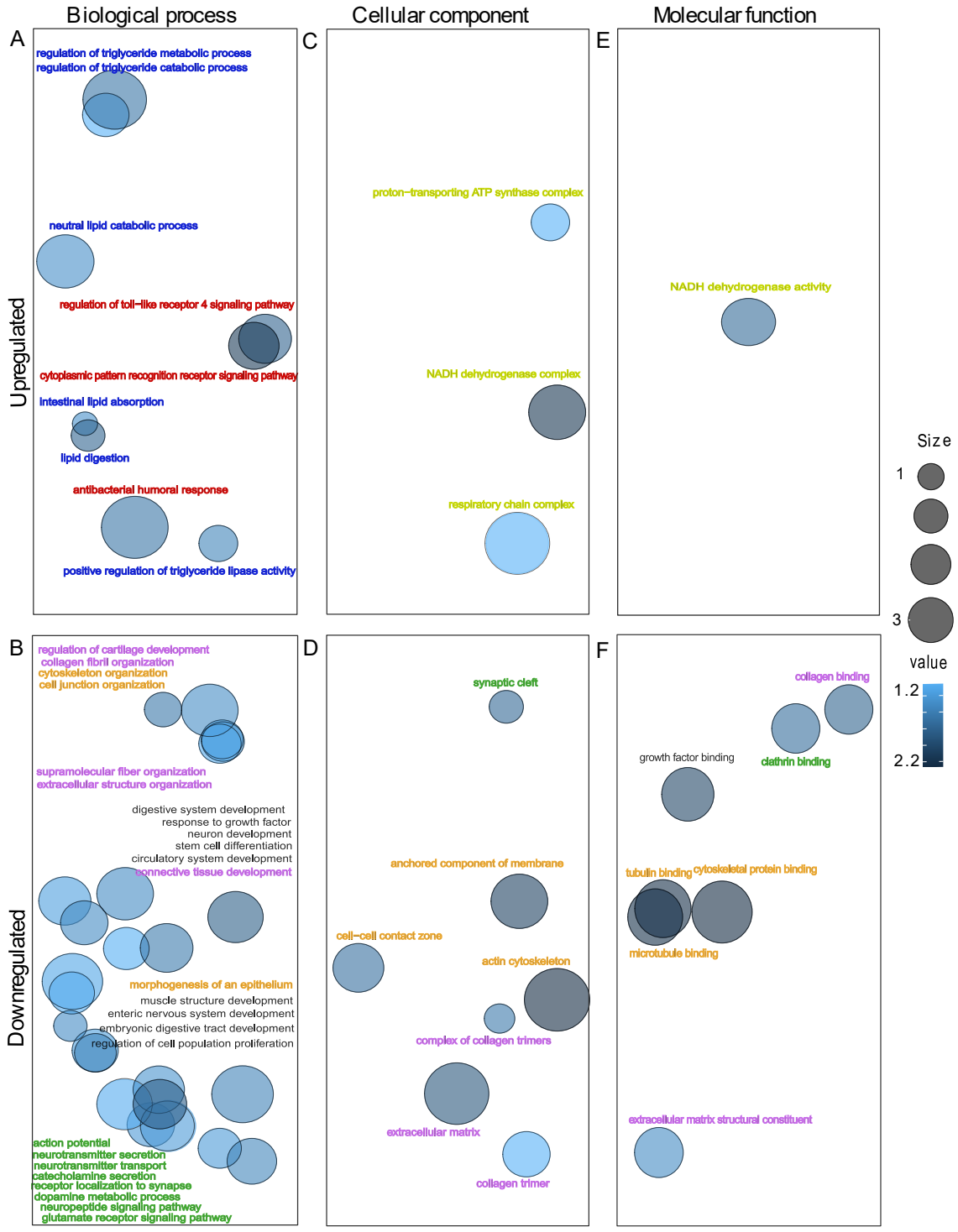

Figure 34. Bubble plots representing parental upregulated (Normalized Enriched Score, NES>0) or downregulated (NES<0) GO terms grouped by semantic similarity. Bubble colours have been adjusted according to NES values: the darker the blue, the higher absolute value of NES. Bubble size is indicative of how general the GO term is in the Gene Ontology Annotation database; larger sizes indicate more general terms. Only the most representative GO terms were displayed to facilitate visualization. A and B represents Biological process category, C and D Cellular

component category and E and F Molecular Function category. (A) Upregulated parental GO terms during IDA (Biological process category). (B) Downregulated parental GO terms during IDA (Biological process category). (C) Upregulated parental GO terms during IDA (Cellular component category). (D) Downregulated parental GO terms during IDA (Cellular component category). (E) Upregulated parental GO terms during IDA (Molecular function category). (F) Downregulated parental GO terms during IDA (Molecular function category). Colour legend: dark blue (lipid metabolism); red (host-microbe interactions); yellow (mitochondrial related pathways); brown (cell junction, integrity, cytoskeletal organization); dark green (synaptic signalling); black (development of enteric nervous system and digestive tract); pink (extracellular matrix).

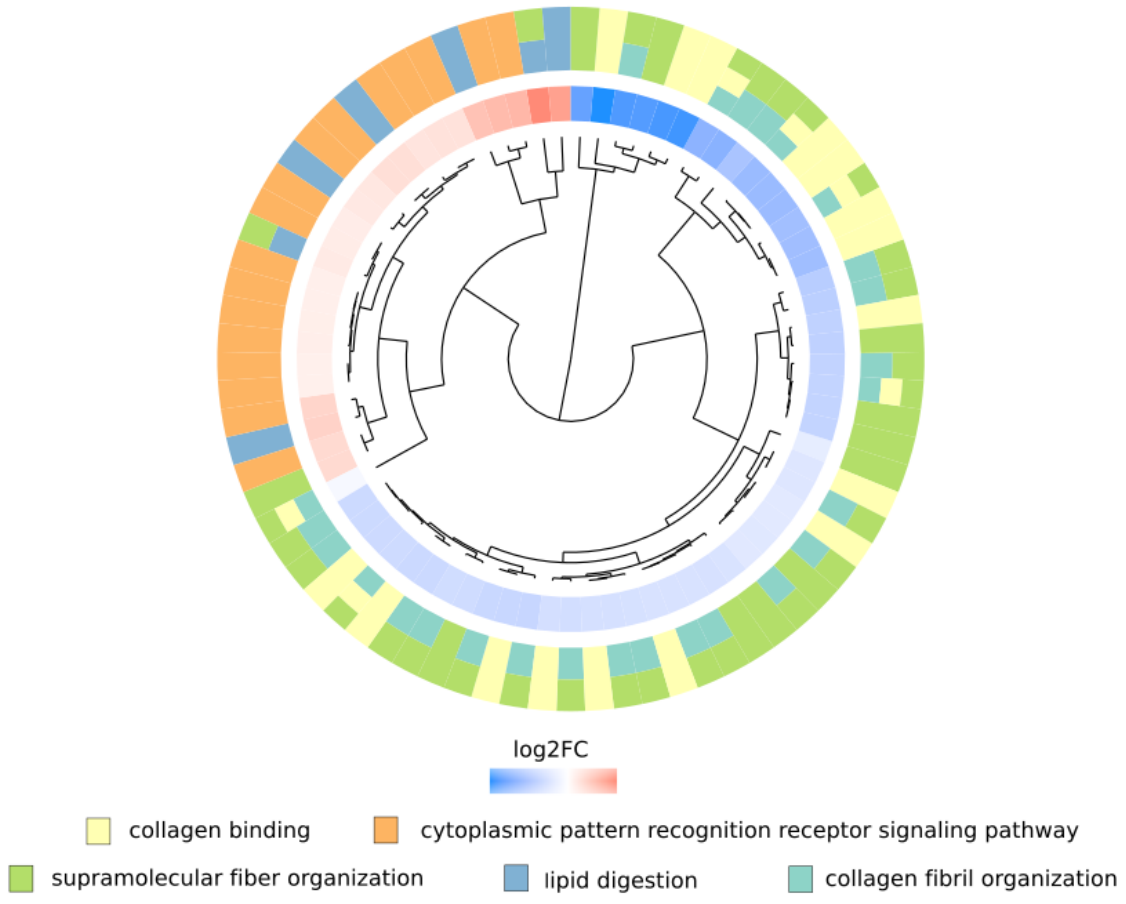

Figure 35. Hierarchical clustering of genes belonging to GO terms of interest derived from GSEA results. Genes are grouped by their expression level (log_2FC) in the inner circle and assigned to functional pathways in the outer circle. A blue-to-red scale was used for log_2FC, with blue values indicating downregulation and red values indicating upregulation.

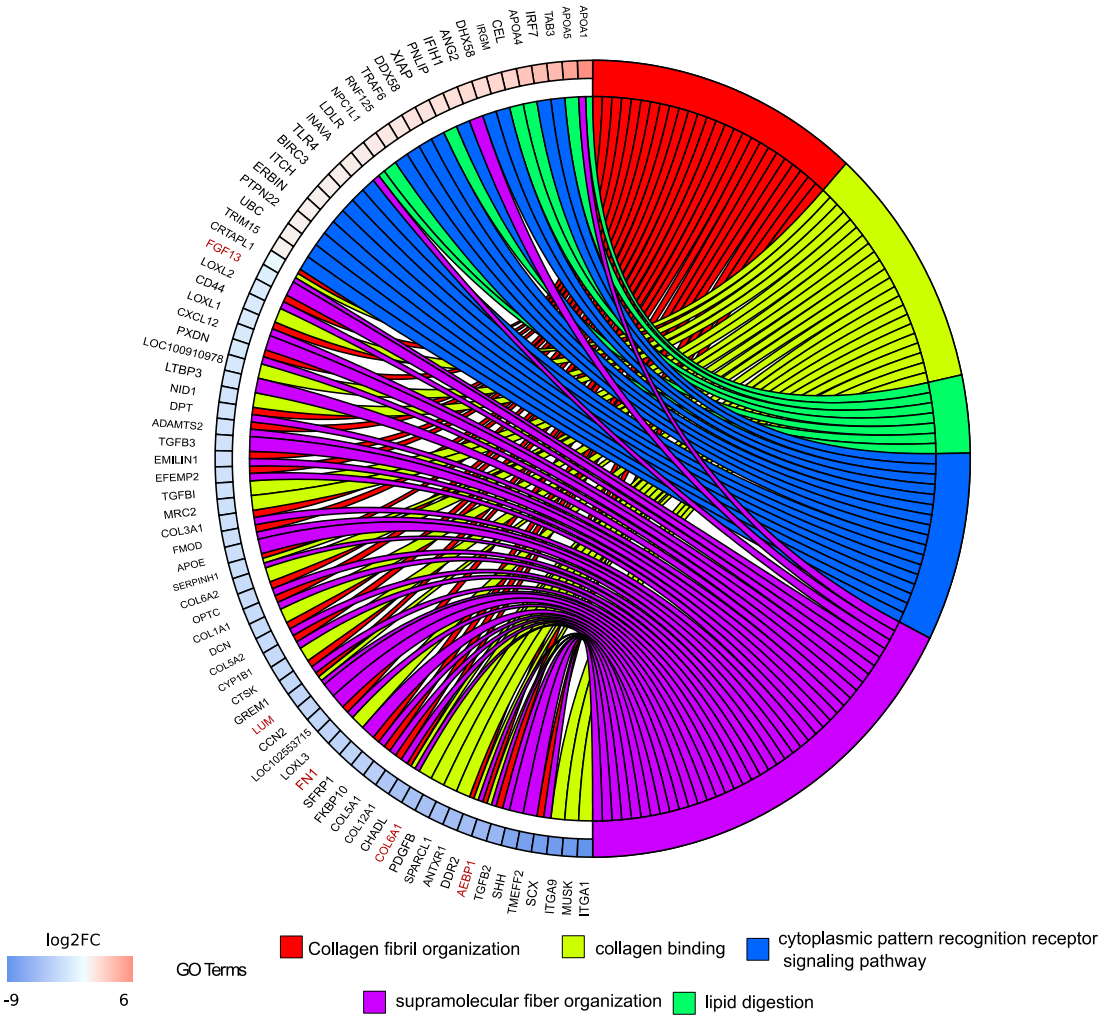

Figure 36. Identification of key altered genes in the colonic mucous during IDA. Chord diagram illustrating the relationships between the list of selected GO terms and their leading-edge subset of genes obtained from GSEA, including log_2FC values. Left half of chord diagram displays whether genes are up- or downregulated during IDA; genes are linked to one or several GO terms (right half) by coloured bands, according to the legend. Highlighted in red are the selected genes for qPCR validation.

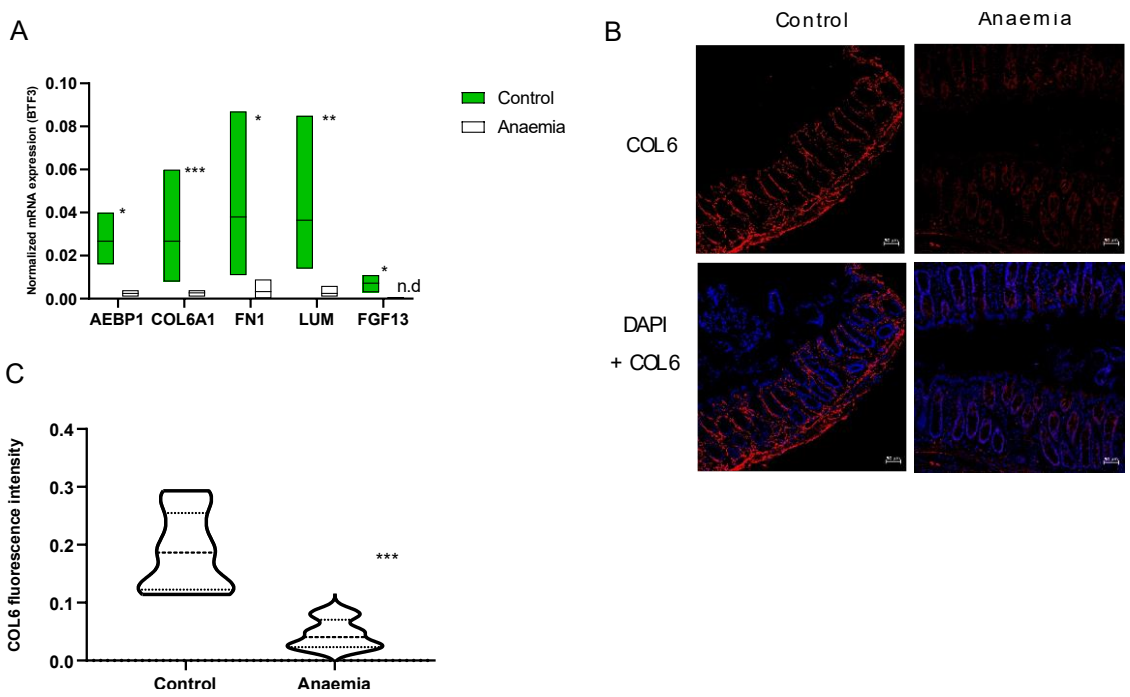

Figure 37. Validation of genes selected in Figure 36. (A) qPCR validation: normalized mRNA expression was calculated using BTF3 as housekeeping gene. n.d.: not detected (B) Immunofluorescence showing COL6 staining (red) in colonic mucous slides belonging to anaemic and control animals; counterstaining was performed using DAPI (blue); scale bar = 50µm (C) COL6 fluorescence level quantification from sections in (B) by Image J (n = 10 images per experimental group).

Given the importance of HIF-1α in the maintenance of the intestinal barrier and its dependence on SCFA levels and mitochondrial iron containing complexes, HIF-1α targets were also studied by qPCR during IDA in the colonic epithelium.

Specific HIF1α targets related to the intestinal barrier were selected, namely *5'-nucleotidase ecto* (*NT5E*), *ectonucleoside triphosphate diphosphohydrolase 1* (*ENTPD1*), *claudin 1* (*CLD1*), *multidrug resistance 1 gene* (*MDR1*) and *mucin 2* (*MUC2*) (8, 154, 155), and their expression measured in the colonic mucous of anaemic and control animals. Surprisingly, no significant changes were observed in any gene between experimental groups (Figure 38).

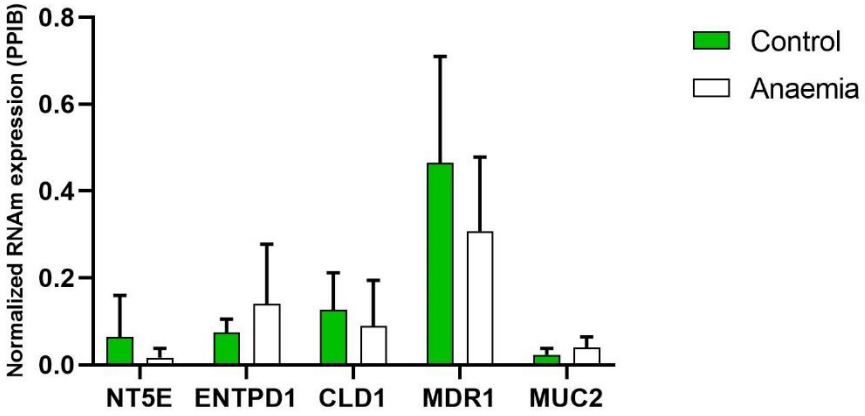

Figure 38. Study of HIF-1α target genes by qPCR. Normalized mRNA expression was calculated using PPIB as housekeeping gene. Mean and standard deviations are shown for biological replicates. NT5E: 5'-nucleotidase ecto, ENTPD1: ectonucleoside triphosphate diphosphohydrolase 1, CLD1: claudin 1, MDR1: multidrug resistance 1 gene, MUC2: mucin 2.

4.1.3.2 Increased LPS translocation and immune response towards dysbiotic bacteria are observed during IDA as a consequence of impaired gut barrier

LPS translocation was analysed in serum samples via ELISA, along with bacteria-specific immunoglobulins (Ig), to assess the consequences of an impair gut barrier.

LPS detection in serum samples was significantly higher for anaemic rats compared to control ones (Figure 39A). When assessing immune response, Ig detection against autologous faecal bacteria was greater for anaemic animals compared to control (Figure 39B, "Paired faeces"). However, no significant differences were found in the heterologous immune response of the control and anaemic animals against bacteria obtained from faeces belonging to the control group (Figure 39B, "Control faeces").

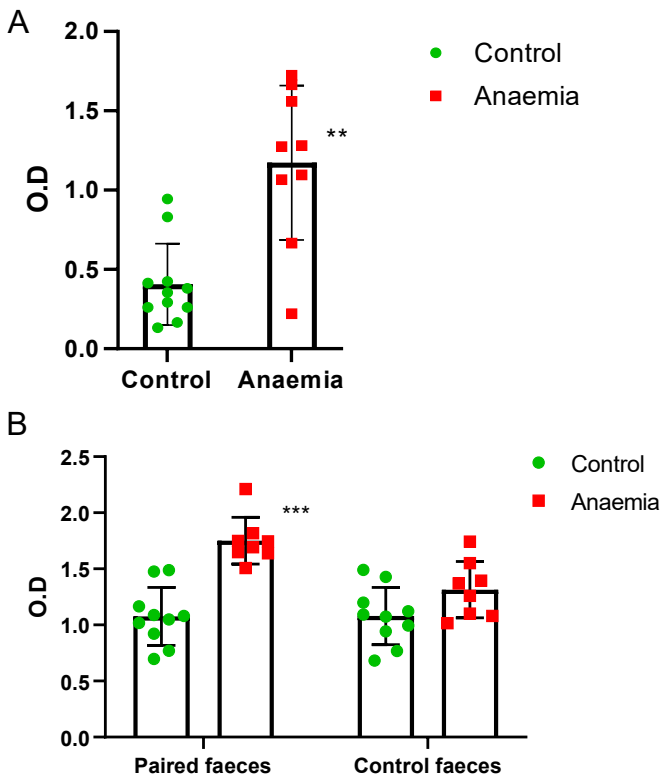

Figure 39. Study of microbial translocation biomarkers in serum samples belonging to anaemic and control animals. Mean and standard deviations are shown for biological replicates. (A) LPS levels in both experimental groups. (B) Bacteria-specific IgG, IgA and IgM in serum samples of both experimental groups. Left bar diagram shows the autologous immune response of control and anaemic animals against bacteria obtained from faecal pellets belonging to their own experimental group (*Paired faeces*). Right bar diagram represents the heterologous immune response of control and anaemic animals against bacteria obtained from faecal pellets belonging to the control group (*Control faeces*)**.**

4.2 Study of the gut microbiome and the integrity of the intestinal barrier during the recovery of IDA with fermented goat's milk-based diet

4.2.1 Study of haematological parameters during the recovery of iron deficiency anaemia with fermented goat's milk-based diet or standard diet

Comparisons of anaemic animals fed with FGM-based diet (AG) and anaemic animals fed with standard diet (AS) with their control counterparts (control animals fed with FGM-based diet, CG, or standard diet, CS) revealed that IDA was recovered after

treatment with FGM-based diet and standard diet (Table 6). No parameters, showed statistical significance between anaemic and control animals fed with FGM-based diet (AG-CG). However, mean corpuscular volume, mean corpuscular haemoglobin and platelets differed between anaemic and control animals fed with standard diet (AS-CS), with AS group showing the lowest levels for mean corpuscular volume and mean corpuscular haemoglobin and the highest levels for platelets.

Table 6. Haematological parameters during the recovery of iron deficiency anaemia (day 70). Means and standard deviations are shown for each group and parameter. (*) represents statistical differences ($p<0.05$) between control and anaemic groups.

	FGM-based diet		**Standard diet**	
	AG	**CG**	**AS**	**CS**
Red blood cells (10^6/µL) (RBC)	7.597±0.41	7.59±0.18	8.007±0.5	7.44±0.39
Haemoglobin (g/dL)	13.3±0.71	13.79±0.47	13.69±0.84	13.92±0.54
Haematocrit (%)	37.5±3.02	38.32±1.38	38.2±2.3	39.1±1.55
Mean corpuscular volume (fL) (MCV)	49.35±2.55	50.48±1.2	47.73*±1.67	52.58±1.13
Mean corpuscular haemoglobin (pg) (MCH)	17.53±0.81	18.17±0.41	17.12*±0.57	18.72±0.37
Mean corpuscular haemoglobin concentration (g/dL) (MCHC)	35.56±1.11	35.99±0.79	35.85±0.8	35.6±0.28
Leukocytes (10^3/µL)	5.67±1.58	5.26±1.52	5.85±1.62	7.16±1.99
Platelets (10^3/µL)	1120.6±120.87	1063.25±865.15	1114.25*±93.99	828.8±55.67

4.2.2 Evaluate the capacity of fermented goat´s milk to shape the gut microbiome towards an enhanced iron absorption. Evaluate the dysbiosis restoring properties of fermented goat´s milk during the recovery of iron deficiency anaemia

4.2.2.1 Fermented goat's milk-based diet shapes a diverse and metabolically active microbiome in the small and large intestine compared to standard diet

Since FGM facilitated recovery of IDA compared to standard diet, the microbiome modulating capacity of FGM was evaluated in control animals at the structural and functional level.

Sequencing of 16S rRNA gene amplicons from intestinal content samples and faeces (d55 and d70) resulted in a total of 4.066.451 sequences after bioinformatic processing.

First of all, Principal Coordinate Analysis (PCoA) at the genus level was performed on faecal samples and intestinal contents from the small and large intestine and all experimental groups to discern which was the most influential factor conditioning gut microbiome structure

As observed in Figure 40, samples clustered according to the major intestinal region (small intestine SI, and large intestine LI and faeces). Therefore, subsequent analyses were performed on each anatomical major region separately (small intestine, and large intestine and faeces).

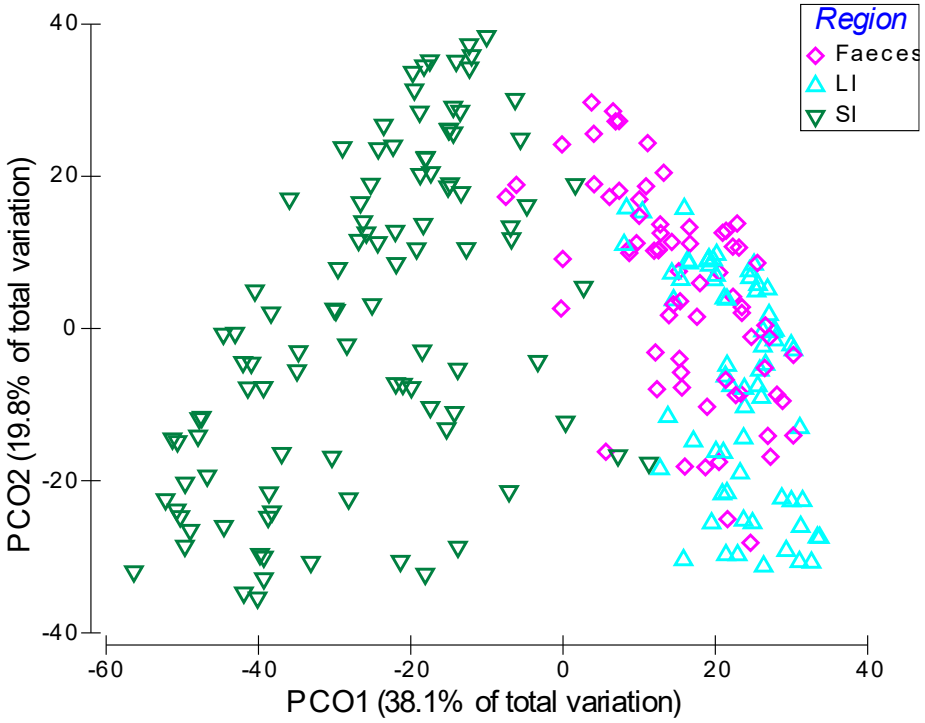

Figure 40. Principal coordinate analysis (PCoA) based on Bray-Curtis distances. Plots for all samples (faecal and intestinal contents) collected during the recovery of iron deficiency anaemia (d55 and d70 for faeces, d70 for intestinal contents) considering bacteria with a relative abundance higher than 0.01%. Samples are represented by coloured symbols according to the legend (SI, small intestine, LI, large intestine). PRIMER e Permanova + was used in the implementation of the statistical analysis.

Both genera-based PCoA in small (Figure 41A) and large intestinal contents (Figure 41B), revealed that samples separated according to the type of diet (FGM-based diet or standard diet). Hence, after the anatomic region, diet was the most influential factor on microbiome structure both in the small and large intestine.

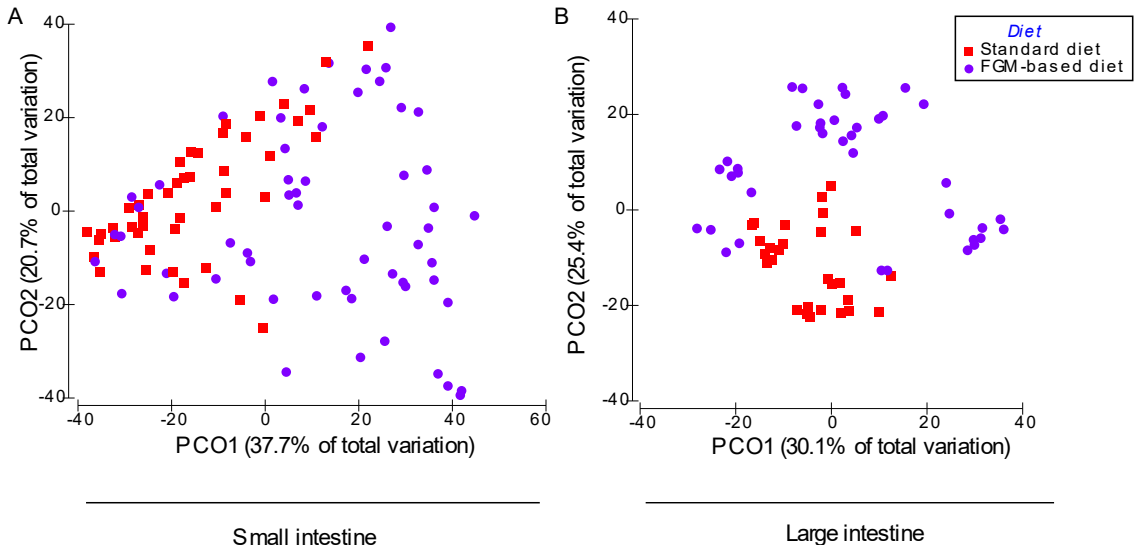

Figure 41. Principal coordinate analysis (PCoA) based on Bray-Curtis distances. Plots for small and large intestine content samples collected after the recovery of iron deficiency anaemia (d70). Bacteria with a relative abundance higher than 0.01% were considered. Samples are represented by coloured symbols according to the type of diet and correspond to control and anaemic animals fed with FGM-based diet or standard diet (see legend). (A) Small intestine content samples from control and anaemic animals fed with FGM-based diet or standard diet according to legend (B) Large intestine content samples from control and anaemic animals fed with FGM-based diet or standard diet according to legend.

The structural and functional traits of the resulting microbiome were then characterised in the small and large intestine of control animals fed with FGM-based diet (CG) or standard diet (CS).

The number of observed species (sobs) and alpha diversity parameters Chao1, InvSimpson, Shannon and Pielou indexes were calculated for both experimental groups in the small and large intestine. Sobs and Chao1 index were significantly higher in the

small intestine of control animals fed with FGM-based diet (CG) compared to standard diet (CS) (Figure 42A), while an increasing tendency in both parameters was shown in the large intestine (Figure 42B). InvSimpson, Shannon and Pielou indexes did not differ between groups neither in the small nor in the large intestine (Figure 43).

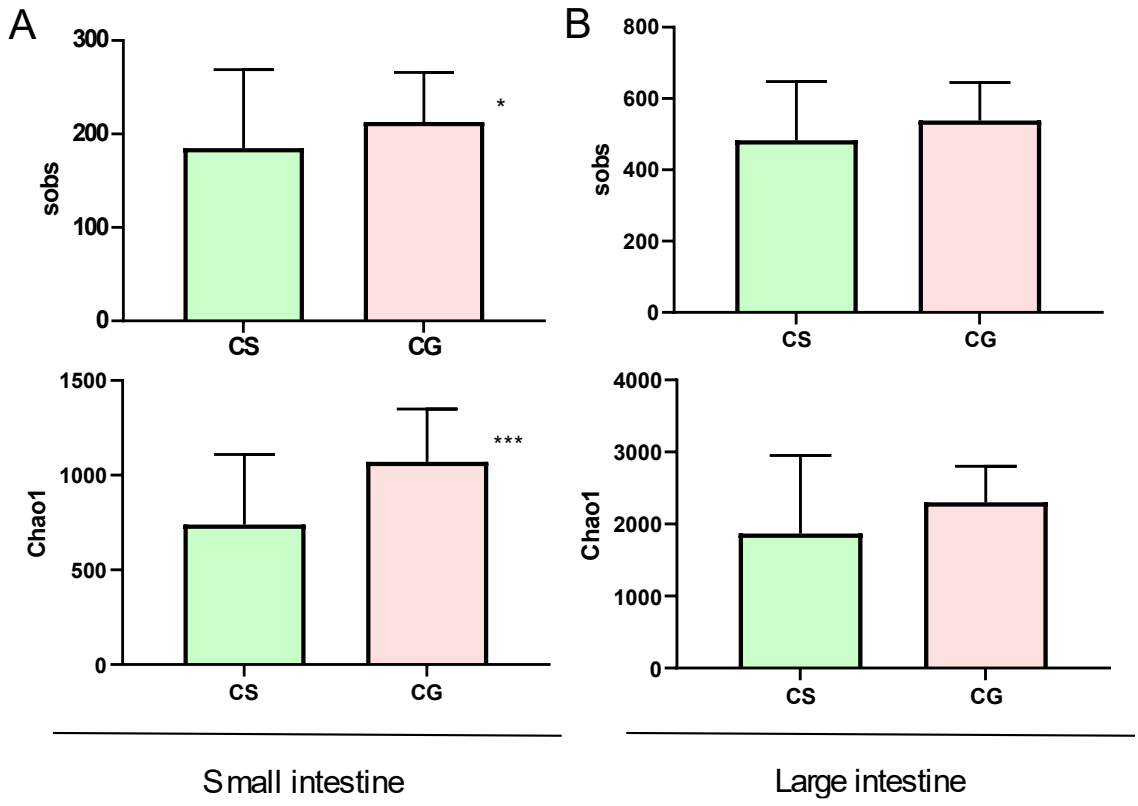

Figure 42. Number of observed species (sobs) and alpha diversity index Chao1 in the small and large intestine of control animals fed with standard diet (CS) or FGM-based diet (CG). OTUs were defined at 3% of dissimilarity. (A) Sobs and Chao1 index in the small intestine of CS and CG animals. (B) Sobs and Chao1 index in the large intestine of CS and CG animals.

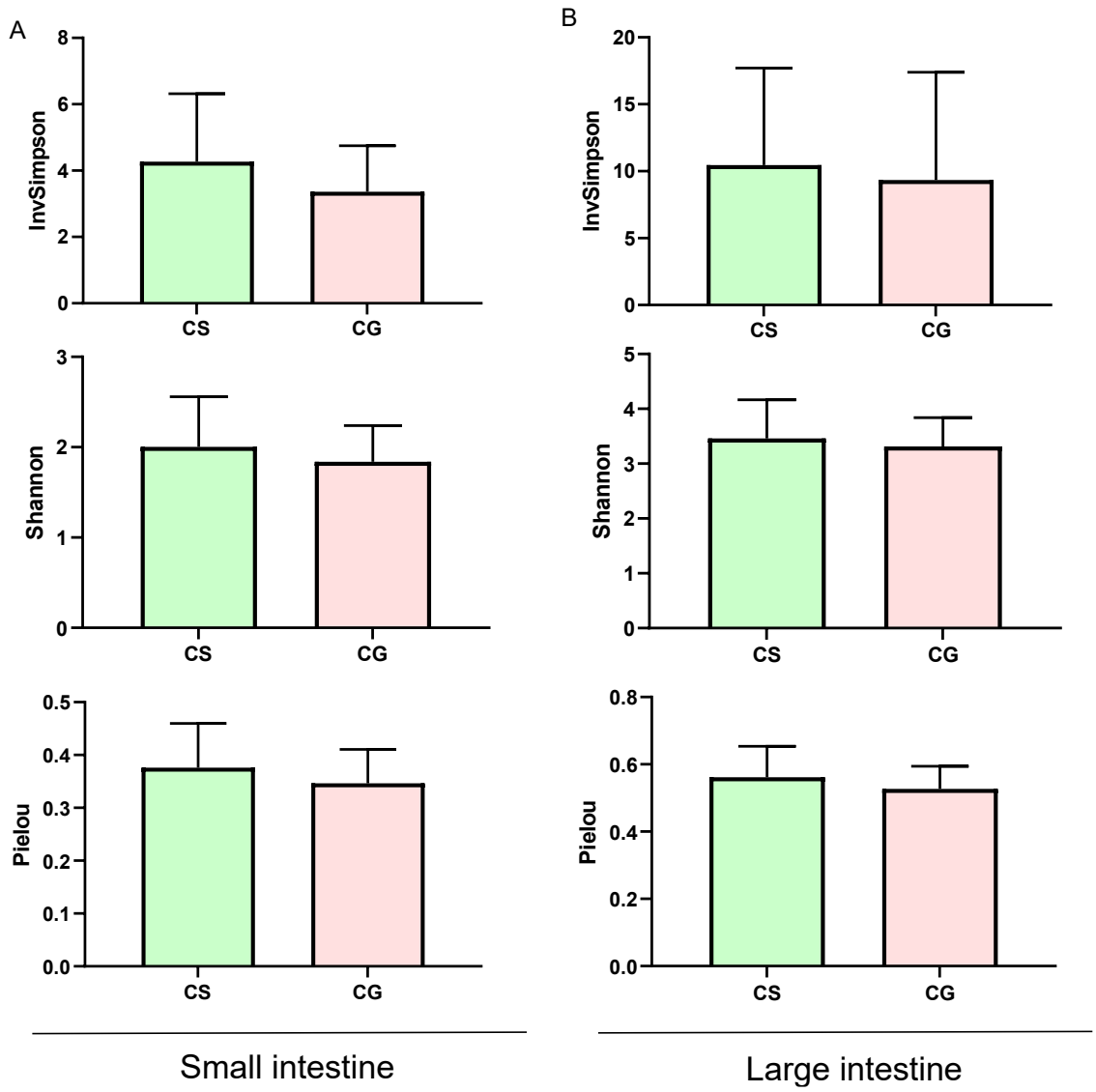

Figure 43. Alpha diversity indexes InvSimpson, Shannon and Pielou in the small and large intestine of control animals fed with FGM-based diet (CG) or standard diet (CS). (A) Alpha diversity indexes in the small intestine of CG and CS groups (B) Alpha diversity indexes in the large intestine of CG and CS groups.

Bubble plots representing the bacterial abundance of the 50 most variable genera were drawn for the small and large intestine, including CG and CS groups. A different microbiome structure could be observed, with some genera being more abundant in the small intestine of control animals fed with FGM-based diet (CG) (Figure 44A), such as *Lactobacillus* and *Streptococcus*, and others in the large intestine (Figure 44B), namely *Blautia*, *Faecalibaculum*, *Lachnospiraceae_unclassified*, *Streptococcus* and

Turicibacter, compared to animals fed with standard diet (CS). However, *Clostridium_sensu_stricto_1* or *Romboutsia* were enriched in the small and large intestine of control animals fed with standard diet (CS) (Figure 44A and 44B), while *Ruminococcaceae_ge*, *Ruminococcaceae_unclassified* or *Akkermansia* were only increased in the large intestine (Figure 44B).

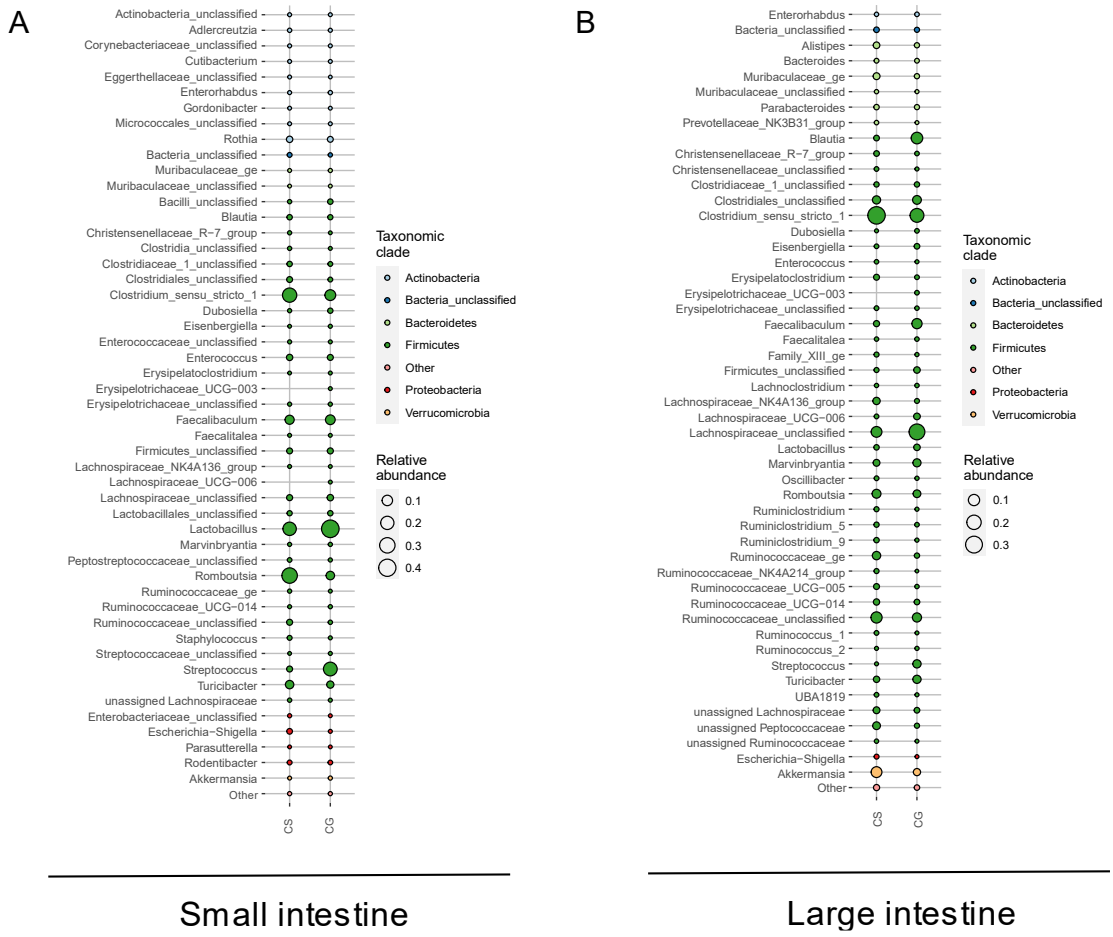

Figure 44. Bubble plots showing bacterial abundance for the 50 most variable genera across samples. Control animals fed with FGM-based diet (CG) and standard diet (CS) were compared in the small and large intestine. Bacterial genera have been coloured according to the phylum they belong to. (A) Bubble plot showing bacterial abundance in small intestine content samples from control animals fed with FGM-based diet or standard diet. (B) Bubble plot showing bacterial abundance in large intestine content samples from control animals fed with FGM-based diet or standard diet.

To analyse the functional profile of the intestinal microbiome in control animals fed with FGM-based diet (CG) or standard diet (CS), PICRUSt was applied on 16S data. Statistical analysis was performed with Kyoto Encyclopedia of Genes and Genomes (KEGG) pathways classified at level 3 using LEfSe with default parameters in the small and large intestine. Microbial pathways significantly enriched in the small and large intestinal contents from control animals fed with standard diet (CS) or FGM-based diet (CG) were represented in a barplot (Figures 45 and 46). The enriched microbial pathways in the small intestine of control animals fed with standard diet (CS) included those involved in bacterial mobility and secretion and synthesis of secondary metabolites (Figure 45, highlighted in red). However, FGM-based diet shaped a metabolically active microbiome, characterised by pathways involved in DNA replication, RNA synthesis, protein translation and export, vitamin synthesis and xenobiotic clearance (Figure 45, highlighted in green). Similar results were obtained in the large intestine; microbial pathways involved in bacterial mobility and secretion, synthesis of fatty acids, synthesis of secondary metabolites and degradation pathways were enriched in control animals fed with standard diet (CS) (Figure 46, highlighted in red). Synthesis of nucleic acids, amino acid metabolism and carbohydrate metabolism were the main microbial functional traits in the large intestine of control animals fed with FGM-based diet (CG) (Figure 46, highlighted in green).

To show the enhanced metabolic rate of the gut microbiome in control animals fed with FGM-based diet, bacterial load was quantified by 16S qPCR, with 16S copy number being higher in the colon of control animals fed with FGM-based diet (CG) compared to standard diet (CS) (Figure 47).

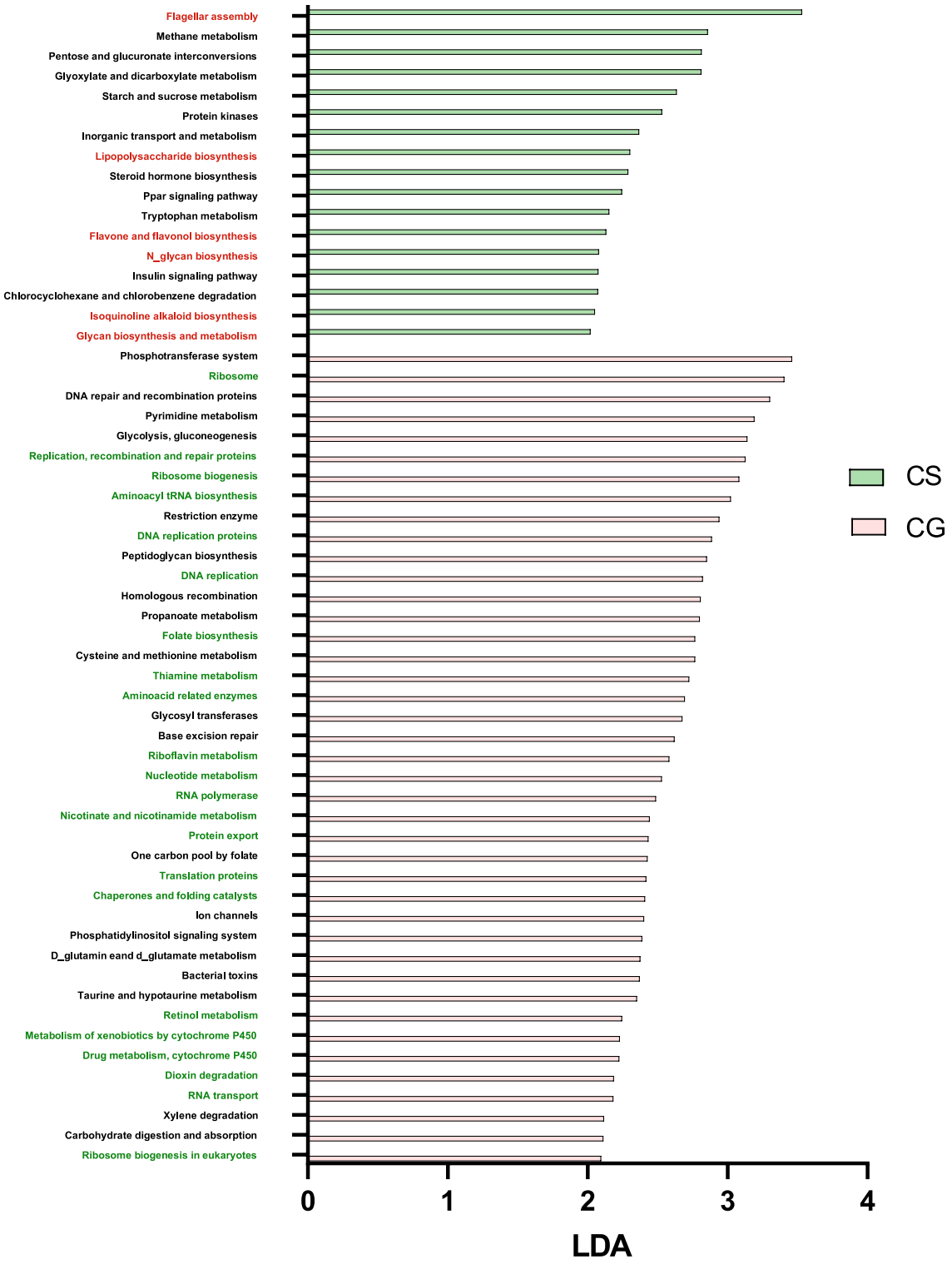

Figure 45. Barplot showing significantly enriched KEGG microbial pathways in control animals fed with standard diet (CS) or FGM-based diet (CG) in small intestine content samples. Only KEGG pathways with LDA > 2 were displayed. Highlighted in red and green are microbial pathways of interest in CS and CG groups respectively.

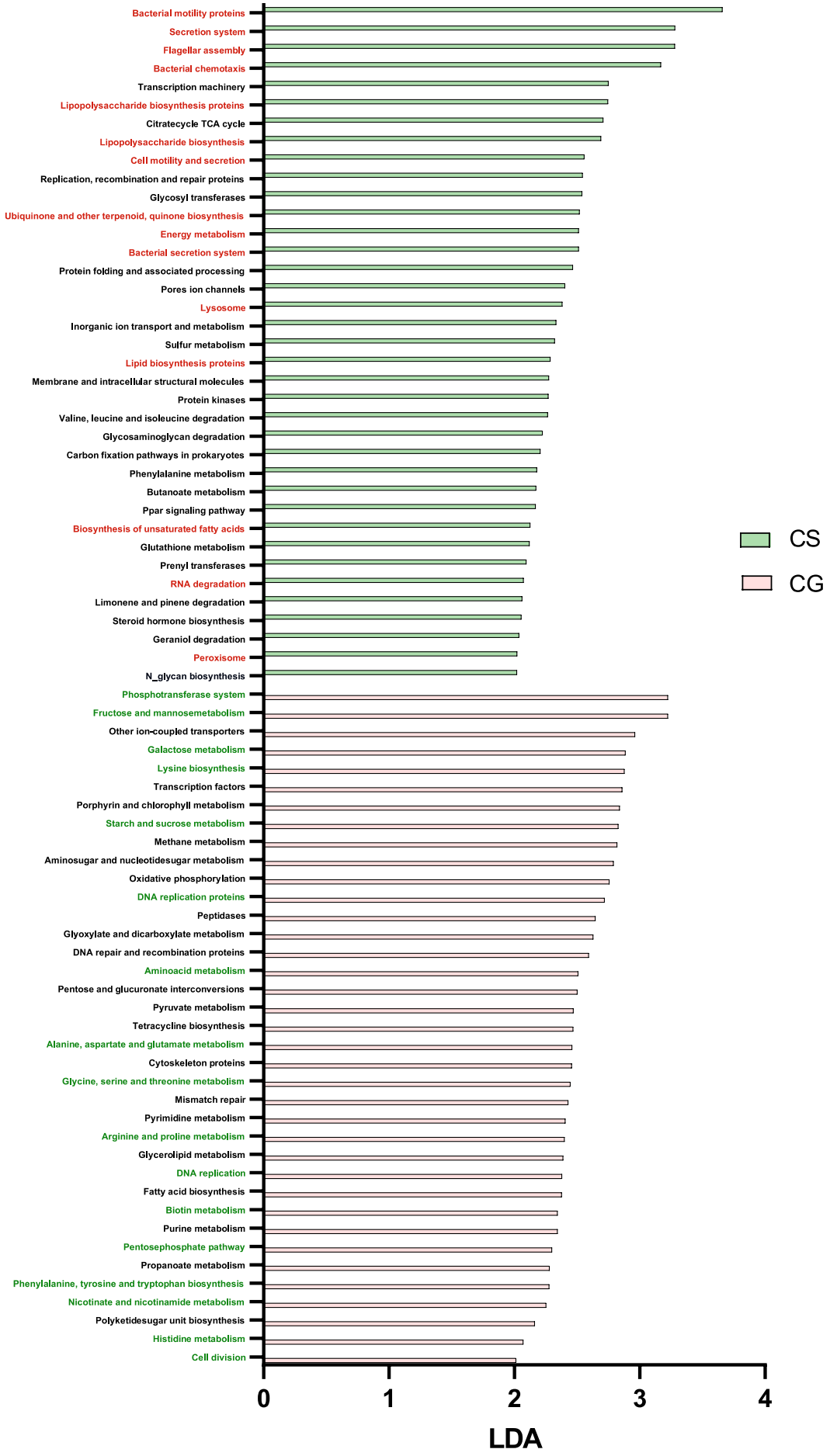
Bacterial motility proteins
Secretion system
Flagellar assembly
Bacterial chemotaxis
Transcription machinery
Lipopolysaccharide biosynthesis proteins
Citratecycle TCA cycle
Lipopolysaccharide biosynthesis
Cell motility and secretion
Replication, recombination and repair proteins
Glycosyl transferases
Ubiquinone and other terpenoid, quinone biosynthesis
Energy metabolism
Bacterial secretion system
Protein folding and associated processing
Pores ion channels
Lysosome
Inorganic ion transport and metabolism
Sulfur metabolism
Lipid biosynthesis proteins
Membrane and intracellular structural molecules
Protein kinases
Valine, leucine and isoleucine degradation
Glycosaminoglycan degradation
Carbon fixation pathways in prokaryotes
Phenylalanine metabolism
Butanoate metabolism
Ppar signaling pathway
Biosynthesis of unsaturated fatty acids
Glutathione metabolism
Prenyl transferases
RNA degradation
Limonene and pinene degradation
Steroid hormone biosynthesis
Geraniol degradation
Peroxisome
N_glycan biosynthesis
Phosphotransferase system
Fructose and mannosemetabolism
Other ion-coupled transporters
Galactose metabolism
Lysine biosynthesis
Transcription factors
Porphyrin and chlorophyll metabolism
Starch and sucrose metabolism
Methane metabolism
Aminosugar and nucleotidesugar metabolism
Oxidative phosphorylation
DNA replication proteins
Peptidases
Glyoxylate and dicarboxylate metabolism
DNA repair and recombination proteins
Aminoacid metabolism
Pentose and glucuronate interconversions
Pyruvate metabolism
Tetracycline biosynthesis
Alanine, aspartate and glutamate metabolism
Cytoskeleton proteins
Glycine, serine and threonine metabolism
Mismatch repair
Pyrimidine metabolism
Arginine and proline metabolism
Glycerolipid metabolism
DNA replication
Fatty acid biosynthesis
Biotin metabolism
Purine metabolism
Pentosephosphate pathway
Propanoate metabolism
Phenylalanine, tyrosine and tryptophan biosynthesis
Nicotinate and nicotinamide metabolism
Polyketidesugar unit biosynthesis
Histidine metabolism
Cell division
CS
CG
0
1
2
3
4
LDA

Figure 46. Barplot showing significantly enriched KEGG microbial pathways in control animals fed with standard diet (CS) or FGM-based diet (CG) in large intestine content. Only KEGG pathways with LDA > 2 were displayed. Highlighted in red and green are microbial pathways of interest in CS and CG groups respectively.

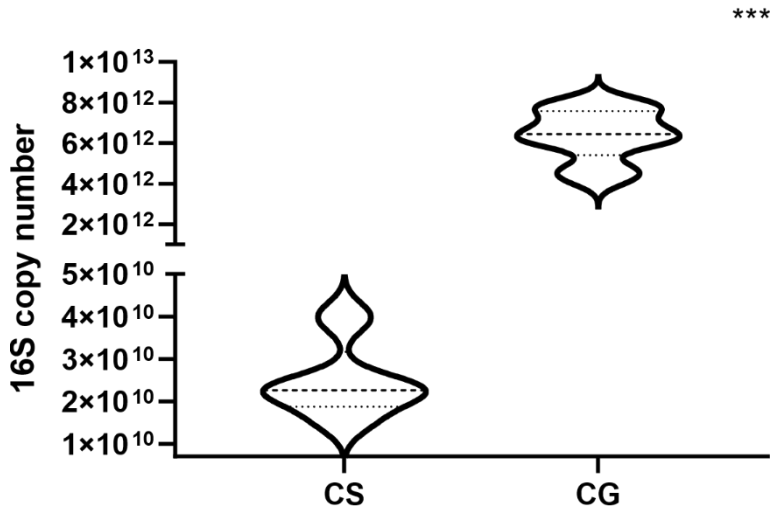

Figure 47. Violin plots for 16S copy number determined by qPCR in the colonic content of control animals fed with standard diet (CS) or FGM-based diet (CG).

4.2.2.2 Unlike standard diet, fermented goat's milk-based diet restores colonic dysbiosis during the recovery of iron deficiency anaemia

To analyse whether FGM-based diet and standard diet could restore IDA dysbiosis, PCoA was performed on small and large intestinal content samples at the genus level. In the case of the small intestine, no clustering could be observed neither between anaemic and control animals fed with FGM-based diet (AG-CG) (Figure 48A) nor between anaemic and control animals fed with standard diet (AS-CS) (Figure 48B), suggesting dysbiosis had been restored by both diets in the small intestine.

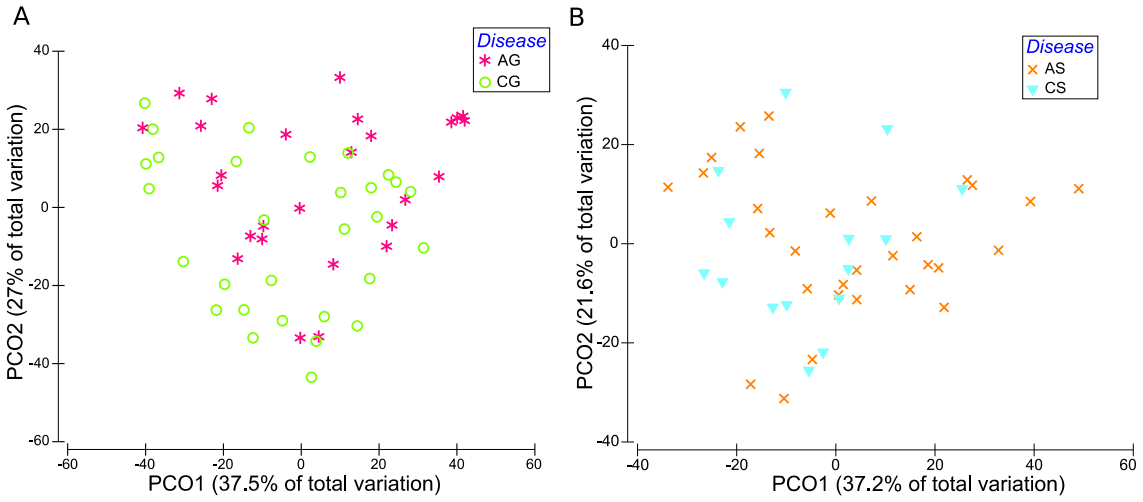

Figure 48. Principal coordinate analysis (PCoA) based on Bray-Curtis distances. Plots for small intestine content samples collected after the recovery of iron deficiency anaemia (d70). Bacteria with a relative abundance higher than 0.01% were considered. Samples are represented by coloured symbols and correspond to control and anaemic animals fed with FGM-based diet (A) or standard diet (B) (see legend). (A) Small intestine content samples from control and anaemic animals fed with FGM-based diet (B) Small intestine content samples from control and anaemic animals fed with standard diet.

Since the colon was the region showing the greatest dysbiosis during IDA, PCoA was performed on colonic content samples, revealing almost no clustering between anaemic and control animals fed with FGM-based diet (AG-CG) (Figure 49A). However, samples belonging to anaemic and control animals fed with the standard diet (AS-CS) did cluster separately (Figure 49B). Therefore, FGM-based diet restored IDA colonic dysbiosis more efficiently than standard diet.

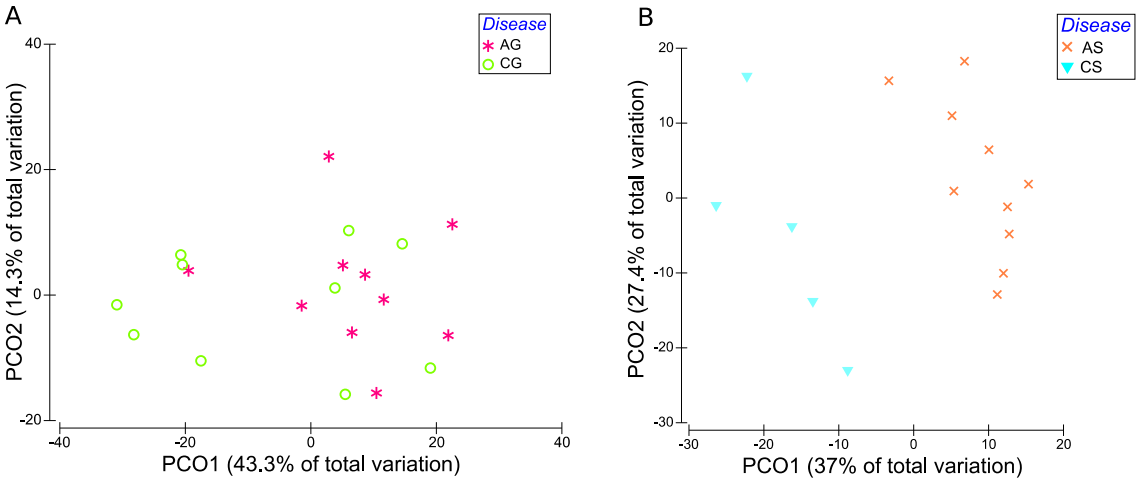

Figure 49. Principal coordinate analysis (PCoA) based on Bray-Curtis distances. Plots for colonic content samples collected after the recovery of iron deficiency anaemia (d70). Bacteria with a relative abundance higher than 0.01% were considered. Samples are represented by coloured symbols and correspond to control and anaemic animals fed with FGM-based diet (A) or standard diet (B) (see legend). (A) Colonic content samples from control and anaemic animals fed with FGM-based diet (B) Colonic content samples from control and anaemic animals fed with standard diet.

Given the fact that colonic dysbiosis was recovered by d70 in the case of FGM-based diet, faecal samples collected at d55 and d70 were also analysed for both diets to check how long the diet took to restore the microbiome. PCoA at the genus level for anaemic and control animals fed with FGM-based diet (AG-CG) or standard diet (AS-CS) showed a differentiation of samples according to time (Figure 50A and 51A). In the first case (AG-CG), d55 and d70 samples were separated along the X axis (Figure 50A); at d55, samples belonging to anaemic (AG) and control animals (CG) clustered separately, but not at d70 (Figure 50B).

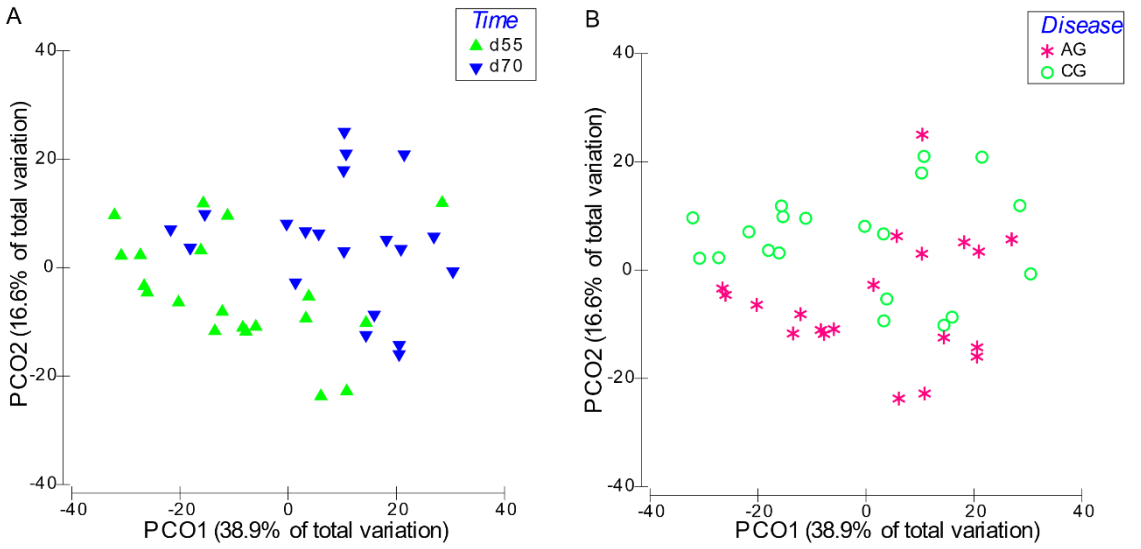

Figure 50. Principal coordinate analysis (PCoA) based on Bray-Curtis distances. Plots for faecal samples collected during the recovery of iron deficiency anaemia (d55 and d70) considering bacteria with a relative abundance higher than 0.01%. Samples are represented by coloured symbols according to the legend and correspond to control and anaemic animals fed with FGM-based diet (A) Different time points are considered regardless of anaemic or control condition (B) Control and anaemic groups are considered regardless of timing.

However, in the case of anaemic and control animals fed with standard diet (AS-CS), d55 and d70 samples were separated along the Y axis (Figure 51A), and in both cases, the anaemic group (AS) clustered separately from the control one (CS) along the X axis (Figure 51B). These findings suggest that FGM-based diet, unlike standard diet, was able to restore the colonic dysbiosis at d70 but not at d55.

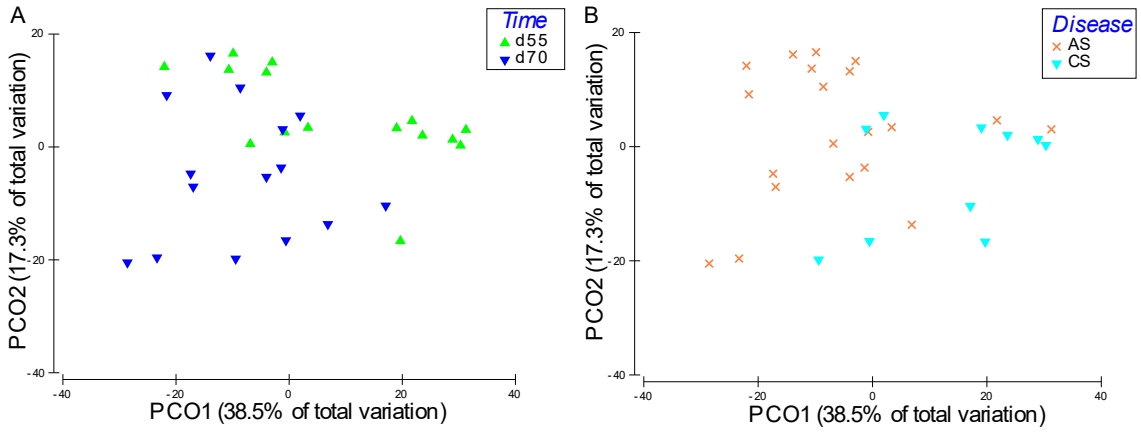

Figure 51. Principal coordinate analysis (PCoA) based on Bray-Curtis distances. Plots for faecal samples collected during the recovery of iron deficiency anaemia (d55 and d70) considering bacteria with a relative abundance higher than 0.01%. Samples are represented by coloured symbols according to the legend and correspond to control and anaemic animals fed with standard diet. (A) Different time points are considered regardless of anaemic or control condition (B) Control and anaemic groups are considered regardless of timing.

To individually identify which microbial taxa were recovered with FGM-based diet and standard diet, LEfSe analysis was performed on colon content samples belonging to anaemic and control animals fed with FGM-based diet (AG-CG) or standard diet (AS-CS). Fewer microbial taxa differed between AG and CG groups (Figure 52A) compared to AS and CS groups (Figure 52B), again showing the greater capacity of FGM-based diet to restore colonic dysbiosis.

Next, a Venn Diagram was plotted to analyse if the majority of colonic dysbiotic bacteria during IDA were recovered with FGM-based diet. Microbial taxa showing differences between the anaemic and their respective control group during the generation of IDA and after the recovery with each diet were considered dysbiotic for this analysis. Out of 84 colonic dysbiotic taxa during IDA, only 5 remained dysbiotic after treatment with FGM-based diet while 16 did after treatment with standard diet. 7 taxa were not recovered with any diet (Figure 53), namely *Lachnospiraceae_NK4A136_group*, *Ruminococcaceae_uncultured*, *Lachnospiraceae_UCG_006*, *Ruminococcaceae_UCG_005*, *Erysipelotrichaceae_ge*, *Marvinbryantia* and *Sellimonas*.

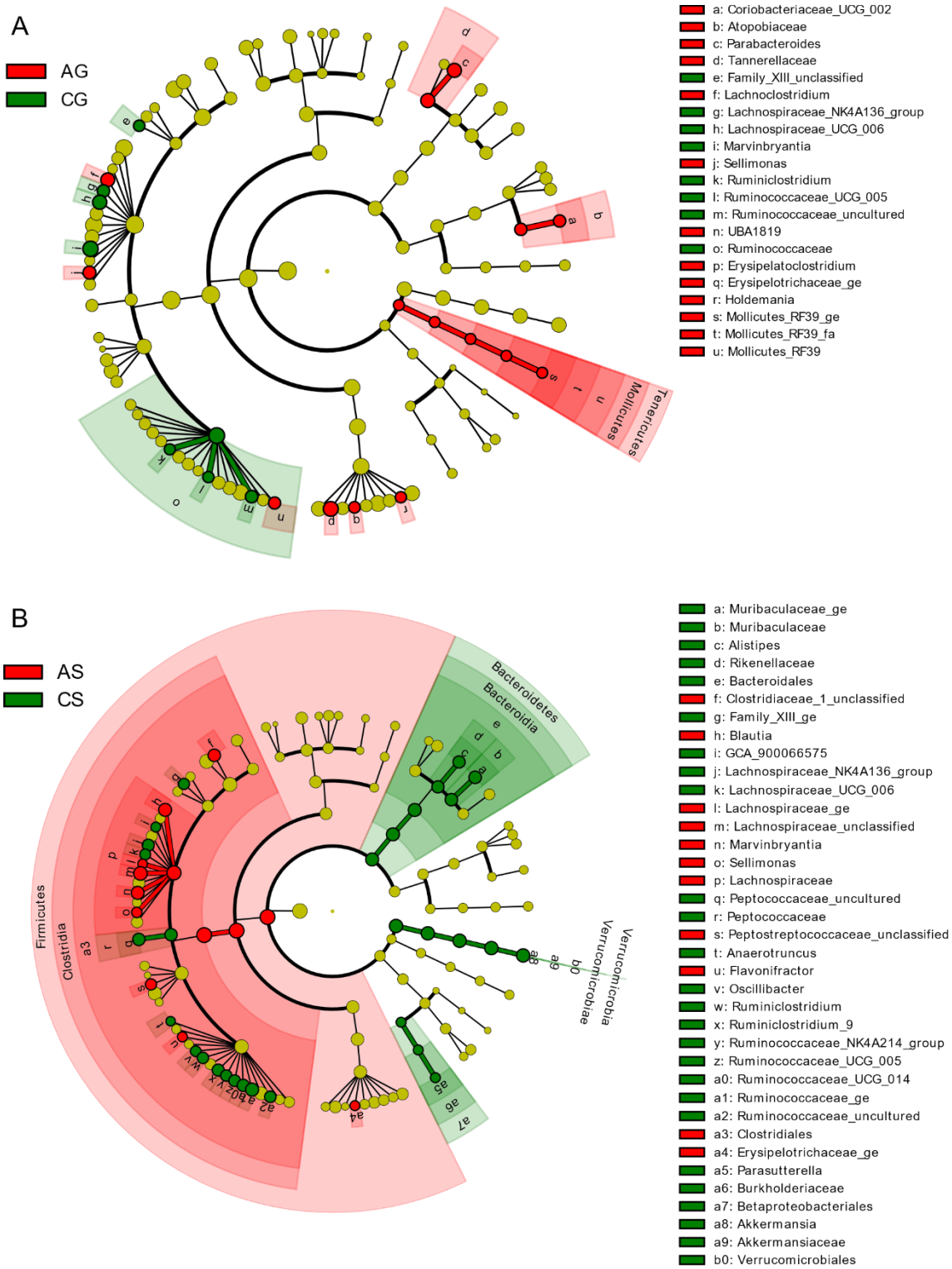

Figure 52. Linear discriminant analysis Effect size (LEfSe): cladogram for differentially distributed taxa ($p<0.05$, LDA>2) between control and anaemic groups fed with FGM-based diet (A) or standard diet (B) in colonic content samples. Taxonomic features are represented in a hierarchical structure, with higher phylotypes oriented towards the inner part of the plot. Taxa

showing significant differences are coloured according to their greatest abundance in each experimental group (red for anaemic animals fed with FGM-based diet or standard diet, green for control animals fed with FGM-based diet or standard diet, yellow for non-significant). (A) LEfSe analysis showing differentially abundant taxa between anaemic and control animals fed with FGM-based diet. (B) LEfSe analysis showing differentially abundant taxa between anaemic and control animals fed with standard diet.

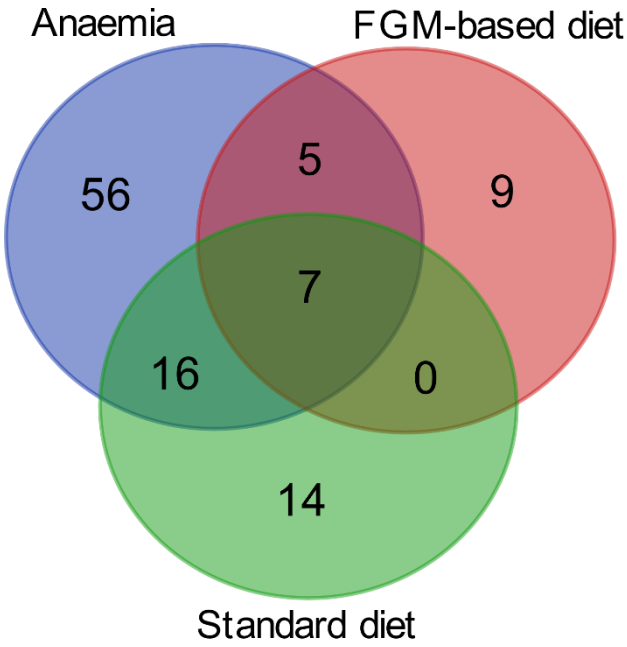

Figure 53. Venn diagram representing dysbiotic microbial taxa during IDA (purple) and after de recovery with standard diet (green) and FGM-based diet (pink). Overlapping areas show shared dysbiotic taxa.

4.2.3 Assess the impact of fermented goat's milk on the intestinal barrier and paracellular permeability

4.2.3.1 Fermented goat's milk-based diet and standard diet restore the intestinal barrier biomarkers and ease LPS translocation associated with IDA

The gut barrier function is impaired during IDA, leading to an increased LPS translocation. Among others, extracellular matrix associated pathways and genes were downregulated due to iron deficiency. Genes that showed statistical differences during

IDA were checked after treatment with FGM-based diet and standard diet, namely *lumican* (*LUM*), *collagen VI alpha 1 chain* (*COL6A1*) and *adipocyte enhancer-binding protein 1* (*AEBP1*), *fibronectin 1 (FN1)* and *fibroblast growth factor 13* (*FGF13*). To check whether reduced expression levels were restored after treatment, AG-CG and AS-CS groups were compared; no statistical differences were found between anaemic and control animals fed with FGM-based diet (AG-CG) or standard diet (AS-CS) for any gene (Figure 54).

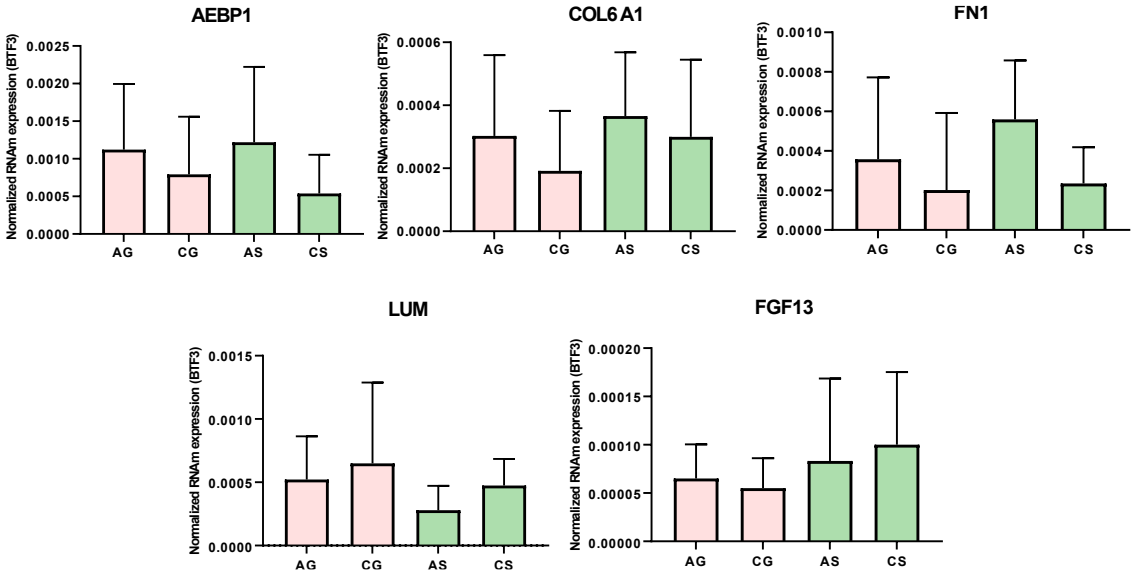

Figure 54. qPCR analysis of the intestinal barrier genes affected during IDA and after the recovery with FGM-based diet or standard diet. Target mRNA levels were normalized in relation to basic transcription factor 3 (BTF3).

Having evaluated the expression level of key downregulated genes during IDA involved in the maintenance of the intestinal barrier, microbial translocation biomarkers were next studied to discern whether the intestinal barrier was affected to some extent after treatment with FGM-based diet and standard diet. For that purpose, bacteria specific IgG, IgM and IgA were detected in serum samples belonging to all experimental groups. First, the autologous immune response was studied through the determination of immunoglobulins (Ig) in sera belonging to all experimental groups via ELISA; each

serum was tested against bacteria obtained from faecal pellets belonging to their own experimental group. Differences in the immune response between anaemic and control animals fed with FGM-based diet (AG-CG) and standard diet (AS-CS) were evaluated, finding an increased response in both anaemic groups (AG, AS) compared to their control counterpart (CG, CS) (Figure 55A). To determine whether the immune response was being produced against dysbiotic bacteria from IDA, still present after the treatment in AG and AS groups, bacteria from pellets belonging to control groups (CG, CS) were tested against Ig from anaemic groups (AG, AS) and control groups (CG, CS) to check the heterologous immune response. In this case, no statistical differences were found neither between AG-CG groups nor AS-CS groups (Figure 55B), suggesting that the previously detected Ig in treated anaemic animals targeted IDA dysbiotic bacteria (Figure 55A). Lastly, detected Ig in both anaemic groups (AG, AS) could derive from ongoing translocation after IDA recovery or previous exposure during IDA (Figure 39). To investigate that aspect, LPS translocation and the immune response against bacteria obtained from faecal pellets belonging to anaemic animals were evaluated in both treated anaemic groups (AG, AS) and in the non-treated anaemic and control animals, prior to IDA recovery (A, C respectively). All treated (AG, AS) and non-treated anaemic (A) groups showed a similarly increased immune response compared to control animals (C) (Figure 55C), suggesting that bacteria-specific Ig detected in treated anaemic animals (AG, AS) might stemmed from the increased microbial leaking occurring during IDA prior to the recovery. LPS determination in serum samples from all experimental groups yielded no differences between anaemic and control animals fed with FGM-based diet (AG-CG) or standard diet (AS-CS) (Figure 55D). Since ongoing LPS translocation after IDA recovery was similar in all experimental groups, differences in Ig levels in treated anaemic animals must derive from previous exposure during IDA microbial translocation.

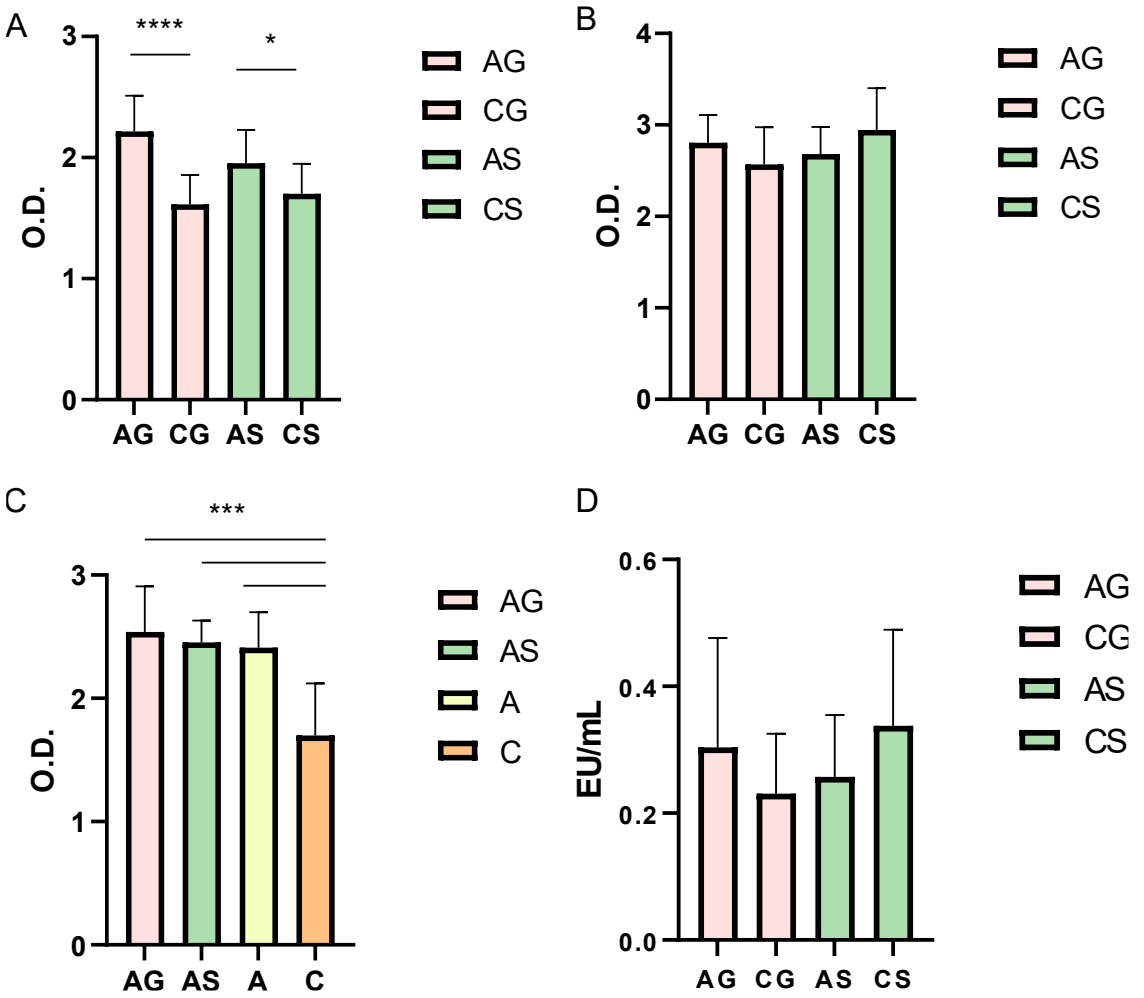

Figure 55. Analysis of microbial translocation after the recovery of IDA with FGM-based diet or standard diet. Sections A, B and C represent immunoglobulin levels against bacteria obtained from faecal samples, while section D represent LPS levels. (A) IgA, IgM and IgG levels in each experimental group against bacteria obtained from faecal pellets from that same group (autologous immune response). (B) IgA, IgM and IgG levels in each experimental group against bacteria obtained from faecal pellets from the respective control group, CG for AG-CG groups and CS for AS-CS groups. (C) IgA, IgM and IgG levels in each experimental group against bacteria obtained from faecal pellets belonging to the non-treated anaemic animals. (D) LPS levels in each experimental group. Abbreviations: anaemic and control animals fed with FGM-based diet (AG, CG respectively), anaemic and control animals fed with standard diet (AS, CS respectively), non-treated anaemic (A) and control animals (C). Data represent mean and standard deviations for each experimental group.

5. DISCUSSION

This study aimed to shed light on the gut microbiome-intestinal barrier interplay during the development of IDA and its recovery with FGM-based diet. Gut health has not been studied in detail in the context of IDA, although it is known that existing therapies exert additional damage to the intestine (39, 40). Therefore, FGM is studied as a nutritional tool to ease intestinal alterations during IDA.

In this study, the gut microbiome was analysed as one of the hallmarks of intestinal health. In this sense, alterations in the gut microbiome along the gastrointestinal tract were analysed in response to IDA.

Firstly, genera-based PCoA of faeces collected along the generation of IDA (baseline, d20 and d40) showed a differentiation of anaemic and control animals at d20 and d40, but not at baseline (Figure 12). Therefore, intestinal dysbiosis at the genus level appeared at d20 and was maintained until d40. This is in accordance with the findings described by Coe et al., (2021)(93), where a low-iron challenge induced gut dysbiosis in mice after 7 days, not progressing afterwards.

The most influential factor conditioning gut microbiome structure was the major anatomic region (Figures 13 and 14), as reported by Vasapolli et al., (2019) (156). Therefore, to better assess differences between the anaemic and the control groups, contents from the small and large intestine were analysed separately.

Differences in the composition of gut microbial communities within segments of the small intestine became more evident towards the most distal parts; duodenum showed an intermediate microbial composition while jejunum and ileum clustered differentially (Figure 15A). A greater percentage of bacterial variation is explained by segregation of samples into intestinal segments belonging to the small intestine (47.3%) (Figure 15A) compared to the separation observed by iron status (17.5%) (Figure 15B). In contrast, a sectional division could also be observed in the large intestine but contributed to a lesser extent to bacterial variation (17.3%) when compared to disease-

mediated effects (37.5%) (Figure 16A and 16B). Therefore, changes in microbiome structure in the large intestine are mainly attributed to the influence of iron deficiency. Particularly, a greater dysbiosis was noticed in the colon (Figure 17), where intestinal bacteria are more diverse and resilient (85).

Specific bacterial genera showed differences in their relative abundance in response to iron deficiency, both in the small (Figure 18) and large intestine (Figure 19). Gut dysbiosis in the upper gastrointestinal tract resembled that of the lower tract, although a higher number of microbial genera was altered in the latter. In accordance with Dostal et al. (2012) (94) and Mcclorry et al., (2018) (95), *Roseburia* genus, a classic butyrate producer, was depleted in the large intestine of anaemic animals, while other SCFA producing bacteria, such as members of the genus *Clostridium* (153), were increased (Figure 19). *Roseburia* genus heavily depends on iron as a cofactor or substrate for its metabolic reactions (94), which suggest the possible cause of depletion during IDA.

Functional analysis of 16S rRNA sequencing data revealed that, during IDA, the five most enriched metabolic pathways in the large intestine were related to SCFA metabolism (Table 4). Bacterial phosphotransferase systems contribute to carbohydrate uptake (157), the main source for SCFA production (73). Similarly, carbon fixation pathways are also related to acetate, propionate and butyrate synthesis (158, 159).

An enrichment in SCFA metabolic pathways in the colon of anaemic animals was validated through shotgun sequencing. During iron deficiency, shotgun sequencing revelaed that the metabolism of carbohydrates leaned towards an increased processing of monosaccharides through the amino sugar and nucleotide pathway (Figure 25, highlighted in green and blue), glycolysis and gluconeogenesis (Figure 26, highlighted in blue) and pyruvate metabolism (Figure 27, highlighted in green and blue). End products from these pathways included acetyl-CoA, formate or succinate. In this sense, crossfeeding mechanisms might contribute to SCFA production since the acetyl-CoA

and 4-aminobutanoate/succinate pathways within butanoate metabolism were increased during IDA (Figure 28, highlighted in green and blue respectively). Similarly, certain amino acids, such as cysteine, methionine and alanine whose synthesis pathways were increased during IDA (Figure 24, highlighted in green squares), can also be utilized in the production of SCFA (160).

Variations in SCFA concentrations paralleled changes in the intestinal microbial community. SCFA concentration was higher in anaemic compared to control animals, especially towards the most distal segments of the digestive tract such as the colon, while no changes were observed in the upper gastrointestinal tract (Figure 20). This is the first study showing an increase in SCFA in anaemia, as opposed to what had been previously reported (54, 94, 95). No changes or a decrease in SCFA had been shown in similar studies, although iron deficiency had been induced for a shorter period of time and faecal samples were used instead. Volatility of this type of metabolites could belie slight changes if biological samples are not rapidly gathered and processed, which is normally the case with faeces.

Correlations between bacterial genera and SCFA in the colonic region of control and anaemic animals were illustrated using network diagrams. Considering the same cutoff values, a higher number of nodes and edges was found in the iron deficient group (Figures 21 and 22). Therefore, variations in SCFA could be explained to a greater extent by variation in bacterial genera during IDA.

Statistically significant correlations were subsequently analysed by multivariant correlation analysis to discern which bacterial genera mostly contributed to variations in SCFA concentrations. Interestingly, in the colon of anaemic animals, *Clostridium_sensu_stricto_1* and *Clostridium_sensu_stricto_4* explained over 80% of changes in butyric acid, while the former represented over 50% of variations in propionic acid (Figure 23A). Shotgun sequencing also revealed a higher abundance of *Clostridium* species during IDA along with high positive correlations of *Clostridium* species to butyrate and propionate (Figure 33).

Considering the multiple roles of SCFA on the intestinal epithelium and their implication on the maintenance of the gut barrier, mRNA isolated from colonic mucous samples was sequenced in an attempt to identify the most important changes at the transcriptional level, with a special focus on the intestinal barrier. Gut health is considerably affected during IDA, and our results suggest the gut microbiome might be exerting trade-off effects at several levels through the production of SCFA. In fact, GO terms related to lipid metabolism and host-microbial interactions are upregulated in the colonic epithelium, suggesting a crosstalk occurring between the host and the microbiome (Figure 34A, 34C, 34E and Figure 35).

GSEA revealed a general downregulation during IDA (Figure 34B, 34D, 34F), with a decrease in GO terms involved in the development of the enteric nervous system and the digestive tract as well as in cell integrity related ones. Iron is an essential micronutrient involved in ATP synthesis through the mitochondrial respiratory chain (3); lack or shortage of iron triggers a sharp decrease in ATP levels and a general disruption of cell functioning. GO terms related to synaptic transmission signalling were also decreased during IDA, as previously reviewed by Capellini et al., (2019) (31). In this sense, SCFA might be involved in increasing enteric neuronal survival and neurogenesis (80) as well as in promoting natural turnover of colonocytes to make up for an underdeveloped epithelium (73).

Downregulation of certain GO terms might be indicative of an impairment in the gut barrier. As mentioned earlier, the development of the enteric nervous system was negatively affected during IDA and some authors have proposed glial cells as modulators of barrier permeability (50). More importantly, extracellular matrix-associated pathways and genes were also diminished during IDA (Figure 34B, 34D, 34F, Figure 35, Figure 36 and Figure 37A). Extracellular matrices are three-dimensional networks mainly composed of collagens and other macromolecules. Not only do they provide a physical scaffold for the development of tissues and organs but they also supply cells with

chemicals to regulate proliferation, survival and differentiation (161). Disruption of the extracellular matrix has been related to damage in the intestinal barrier, while its recovery has been associated with the restoration of the intestinal epithelium (162, 163). Iron containing proteins are required for collagen metabolism (164), which supports the downregulation of collagen genes during IDA (Figure 36). In particular, *COL6A1* mRNA and COL6 protein levels were validated by qPCR and immunofluorescence, confirming a decrease in the colonic mucous of anaemic animals (Figure 37B, 37C, 37D).

One of the main functions of SCFA in the colonic epithelium is the maintenance of the intestinal barrier through HIF-1α stabilization. Despite the increase in SCFA during IDA and the upregulation of GO terms related to the electron transport chain and ATP synthesis (Figure 34C and 34E), no differences in HIF-1α targets were found between the anaemic and control groups (Figure 38). HIF-1α stabilization by SCFA is mediated by iron-containing proteins in the mitochondria (75), and iron deficiency might therefore impair mitochondria-dependent hypoxic responses. Altogether, these results suggest that the observed damage in the intestinal barrier is dependent on iron deficiency, regardless of HIF-1α levels; further investigation would be needed to assess whether SCFA are involved in the maintenance of hypoxia-dependent components of the intestinal barrier during IDA.

LPS and bacteria-recognizing Ig were measured in serum samples to assess whether the impaired barrier functionality was responsible for an increased LPS translocation during IDA. LPS levels were increased in serum samples belonging to anaemic animals compared to control ones (Figure 39A). Immunoglobulin (Ig) detection of autologous faecal bacteria was also higher for the anaemic group, while no differences between anaemic and control animals were found when assessing immune response towards bacteria obtained from faecal control samples (Figure 39B). These results suggest an increased immune response is occurring against dysbiotic gut bacteria during IDA.

Both the gut microbiome and the intestinal barrier, the two hallmarks of intestinal health analysed in this study, were affected during IDA. These findings emphasize the need for minimising the negative impact of existing IDA therapies on the intestine (104).

Paganini et al., (2017) (100) demonstrated a positive effect of galactooligosaccharides mitigating the adverse effects of iron fortification. In our study, FGM-based diet was used to recover IDA and compared to a standard diet, showing a more efficient recovery of IDA along with positive effects on the gut microbiome.

No haematological parameters showed statistical differences between anaemic and control animals fed with FGM-based diet (AG-CG), while MCV, MCH and platelets differed between anaemic and control animals fed with standard diet (AS-CS), with AS group showing the lowest values for MCV and MCH (Table 6). MCV and MCH are quite sensitive and reliable parameters to diagnose IDA in the absence of vitamin B12 and folate deficiency (165). Considering both diets contain the same amount of iron, the higher efficiency of FGM in the recovery of IDA might derive from an increased bioavailability of the mineral (125). A direct impact of its nutrients on the intestinal epithelium and/or its microbiome-modulating properties may contribute to this observed effect.

After the major anatomic site (small or large intestine/faeces) (Figure 40), diet was identified as the most influential factor conditioning microbiome structure in the small and large intestine (Figure 41). Therefore, the microbiome-shaping properties of FGM were investigated in control animals and both intestinal segments.

FGM shaped a diverse and metabolically active microbiome in the small and large intestine (Figure 42, Figure 45, Figure 46). A diverse gut microbiome has generally been associated with health since it provides an enhanced functional redundancy to cover for potential alterations (55). As observed in Figure 44A, control FGM fed animals were characterised by an increased abundance of *Lactobacillus* and *Streptococcus* in the small intestine, while the large intestine was especially enriched in *Blautia*, *Faecalibaculum*, *Streptococcus* and *Turicibacter* (Figure 44B). Consumption of

Lactobacillus-based probiotics has been related to an enhanced iron status in female athletes (166). Since SCFA reduce intestinal pH favouring the presence of ferrous and soluble iron forms, SCFA producers, such as *Faecalibacterium*, can also contribute to a higher iron availability (44). Altogether, FGM shows potential microbiome-modulating properties that might be explotable in the context of IDA, although more in-depth analyses are still needed.

At the functional level, control FGM-fed animals showed enhanced DNA replication, RNA and protein synthesis (Figures 45 and 46, highlighted in green). A high division rate and an increased bacterial load was also shown in the colon of control FGM fed animals (CG) compared to standard diet fed animals (CS) (Figure 47). Another hallmark of intestinal health in relation to the gut microbiome is the presence of the "functional core" (55). Gut core functions include those involved in cell survival (energy production, transcription and translation) along with those involved in host-microbial interactions such as synthesis of vitamins, immunomodulatory compounds and essential aminoacids. Such functions are enriched in control animals fed with FGM-based diet (Figures 45 and 46, highlighted in green). This healthy microbiome shaped by FGM may also contribute to a healthy gut epithelium and a more efficient recovery of IDA (Table 6), although validation through shotgun sequencing would be needed.

Not only does FGM shape the gut microbiome in control animals but it also restores intestinal dysbiosis associated with IDA. Both FGM-based diet and standard diet were capable of restoring IDA microbial dysbiosis in the small intestine (Figure 48). However, only FGM-based diet restored colonic dysbiosis (Figure 49). IDA dysbiosis in the small intestine was shown to be less intense compared to the large intestine and the specifically to the colon (Figures 17, 18 and 19), and even diets with low prebiotic capacity may be able to restore it.

FGM-based diet took at least 30 days to restore IDA dysbiosis, as shown in Figure 50. Other methods have been used to restore intestinal dysbiosis, such as fecal microbiome transplantation (167), probiotics (168) and food with probiotic and prebiotic

potential such as milk (169). In the case of probiotics the majority of intervention studies schedule the administration during at least 6 months in newborns (168), while beneficial effects were shown after a 28 day administration period for goat's and cow's milk in an animal model (169), in accordance with our results. However, the gut microbiome is characterised by its resilience to external or internal factors and thus, consumption of any food that intends to modify intestinal microbial communities is advised to be consumed on a regular basis (107).

The microbiome-restoring properties of FGM-based diet are in line with its higher efficiency in the recovery of IDA. Given that gut dysbiosis appears as a consequence of IDA, when IDA is cured, intestinal dysbiosis will be as well. Some microbial taxa still showed statistical differences between anaemic and control animals fed with FGM-based diet (AG-CG) (Figure 52A), but fewer than in the case of anaemic and control animals fed with standard diet (AS-CS) (Figure 52B). Actually, out of 84 colonic dysbiotic taxa during IDA, only 5 remained dysbiotic after treatment with FGM-based diet while 16 did after treatment with standard diet; 7 genera were not recovered with any diet (Figure 53). Coe et al., (2021) showed that the relative abundance of specific OTUs decreased during iron deficiency and was not restored after iron repletion(93). Persistent dysbiosis might be related to the refractory traits of IDA, where the disease could reappear in patients with intestinal alterations. Since non-restored taxa in out study did not match the ones described by Coe et al., (2021)(93), treatment with FGM-based diet for a longer period of time would be of interest to completely restore colonic dysbiosis.

Some genera were not restored after IDA recovery, and those are likely to trigger an immune response during IDA due to the observed Ig levels in treated anaemic animals (AG, AS) towards IDA dysbiotic bacteria still present in the faeces of anaemic animals but not in the faeces from control animals (Figure 55A and 55B). Such immunoglobulin (Ig) levels did not differ between the anaemic and the control group (AG-CG, AS-CS) when serum samples were tested against faecal bacteria obtained from control animals fed with FGM-based diet or standard diet (Figure 55B), and were similar

to the ones observed in serum samples belonging to anaemic animals when tested against bacteria obtained from their own faecal pellets (Figure 55C). Among them, members of the *Erysipelotrichaceae* family have been described as SCFA producing, immunogenic bacteria and as promoters of inflammation in patients suffering AIDS, multiple sclerosis and Chron disease (170, 171).

To study the intestinal barrier, key affected genes during IDA (Figure 37) were studied by qPCR after treatment with FGM-based diet or standard diet. No significant differences were found between anaemic and control animals fed with FGM-based diet (AG-CG) or standard diet (AS-CS) (Figure 54). Impairment in the intestinal barrier during IDA seems to depend on iron deficiency regardless of hypoxia, which justifies the lack of differences in gene expression since both diets are meeting the animal iron requirements. The observed damage in the intestinal barrier seems to be also independent of gut dysbiosis, since both diet recovers intestinal barrier affected genes but only FGM-based restores intestinal dysbiosis.

Furthermore, to globally check the integrity of the intestinal barrier, LPS determination was performed in serum samples belonging to all experimental groups, yielding no differences between anaemic and control animals fed with FGM-based diet (AG-CG) or standard diet (AS-CS) (Figure 55D). These results suggest a similar state of the intestinal barrier after treatment with both diets.

6. CONCLUSIONS

First conclusion

In the proposed model, gut dysbiosis is triggered as a consequence of iron deficiency anaemia at the structural and functional level, especially towards the colon. Predictive functional analysis on 16S rRNA sequencing data and validation through shotgun sequencing reveals an enrichment in short chain fatty acid-producing pathways and short chain fatty acid-producing bacteria in the large intestine, especially in the colon, in response to iron deficiency anaemia, such as *Clostridium* taxa. Concentrations of short chain fatty acids tend to increase during iron deficiency anaemia from the most proximal to the most distal intestinal segments, with the colon showing the greatest difference.

Second conclusion

A higher number of correlations is found between the concentration of short chain fatty acids and bacterial genera in the colon during iron deficiency anaemia, suggesting that bacterial variation contributes to a greater extent to short chain fatty acids viability during iron deficiency anaemia. *Clostridium sensu stricto 1* and *4* genera, as well as *Clostridium* species, are positively correlated to colonic propionic and butyric acid concentration and negatively correlated to colonic acetic acid concentration. Given its positive role on gut health, short chain fatty acids are likely to be part of trade-off mechanisms taking place during iron deficiency anaemia.

Third conclusion

An underdeveloped epithelium and an impaired gut barrier are inferred from transcriptionally downregulated processes in the colonic mucous layer during iron deficiency anaemia. In particular, the development and synaptic signalling within the enteric nervous system, the development of the digestive tract, cell junction assembly and cell integrity and the organization of the extracellular matrix are decreased.

Alterations observed in the intestinal barrier are hypoxia-independent. An increased lipopolysaccharide translocation and an increased immune response against dysbiotic bacteria support an impairment in the intestinal barrier during iron deficiency anaemia.

Fourth conclusion

Fermented goat's milk-based diet recovers iron deficiency anaemia more efficiently than the standard diet and shows microbiome-modulating properties in the small and large intestine of control animals in line with this increased efficiency. The gut microbiome shaped by fermented goat's milk-based diet is more functionally active than that shaped by the standard diet. Fermented goat's milk-based diet and standard diet similarly restores gut dysbiosis in the small intestine. Gut dysbiosis in the colon is more efficiently restored by fermented goat's milk-based diet, although neither diet completely recovers the intestinal dysbiosis during the employed treatment period. Fermented goat's milk is therefore a useful nutritional tool to ease intestinal alterations occurring during iron deficiency.

Fifth conclusion

Both fermented goat's milk-based diet and standard diet restore the expression levels of key downregulated genes involved in the maintenance of the intestinal barrier during iron deficiency anaemia. Absence of differences in serum concentrations of lipopolysaccharide between control and anaemic groups fed with fermented goat's milk-based diet or standard diet suggest a similar state of the intestinal barrier after treatment with both diets.

Primera conclusión

En el modelo estudiado, se desencadena una disbiosis intestinal a nivel estructural y funcional como consecuencia de la anemia ferropénica, especialmente en el colon. El análisis predictivo functional en los datos de secuenciación de ARN ribosómico 16S y la validación por shotgun revela un enriquecimiento en vías y microorganismos productores de ácidos grasos de cadena corta en el intestino grueso, especialmente en el colon, en respuesta a la anemia ferropénica, como los géneros *Clostridum* y sus especies. Las concentraciones de ácidos grasos de cadena corta tienden a aumentar en la anemia desde las regiones intestinales proximales hacia las distales, siendo el colon el segmento con mayor aumento.

Segunda conclusión

Existe una mayor correlación entre los niveles de ácidos grasos de cadena corta y los géneros bacterianos en el colon de animales anémicos, sugiriendo que las variaciones de la abundancia bacteriana contribuyen en mayor medida a la variabilidad en la concentración de ácidos grasos de cadena corta durante la anemia. Los géneros *Clostridium sensu stricto 1* y *Clostridium sensu stricto 4,* así como las especies del género *Clostridium*, están positivamente correlacionadas con las concentraciones colónicas de ácidos propiónico y butírico y negativamente correlacionadas con la concentración colónica de ácido acético. Dado su papel positivo en la salud intestinal, es probable que los ácidos grasos de cadena corta formen parte de mecanismos de compensación llevados a cabo por el microbioma durante la anemia.

Tercera conclusión

La infraexpresión de vías metabólicas relacionadas con el desarrollo y transmisión sináptica del sistema nervioso entérico, el desarrollo del sistema digestivo, ensamblaje de las uniones celulares, integridad celular y organización de la matriz extracelular

sugieren un epitelio intestinal infradesarrollado y un deterioro de la barrera intestinal. Las alteraciones observadas en la barrera son independientes de la hipoxia intestinal. El aumento en la translocación de lipopolisacárido y la respuesta inmune incrementada en animales anémicos frente a las bacterias disbióticas confirma un daño en la barrera intestinal durante la anemia ferropénica.

Cuarta conclusión

La dieta basada en leche fermentada de cabra recupera la anemia ferropénica más eficientemente que la dieta estándar y muestra propiedades moduladoras del microbioma tanto en el intestino delgado como en el grueso de animales controles, en línea con esta eficiencia aumentada. La dieta basada en leche de cabra desarrolla un microbioma intestinal funcionalmente más activo que la dieta estándar. La dieta basada en leche fermentada de cabra y la dieta estándar recuperan de manera similar la disbiosis en el intestino delgado de los animales anémicos. La disbiosis colónica es recuperada con mayor eficiencia por la dieta basada en leche fermentada de cabra, aunque ninguna de las dietas recupera completamente la disbiosis intestinal en el periodo de tratamiento estudiado. La leche fermentada de cabra es, por tanto, una herramienta nutricional útil para aliviar el deterioro de la salud intestinal durante la anemia ferropénica.

Quinta conclusión

Tanto la dieta basada en leche fermentada de cabra como la dieta estándar recuperan los niveles de expresión de genes relacionados con el mantenimiento de la barrera intestinal y que se encuentran infraexpresados durante la anemia ferropénica. La ausencia de diferencias en la concentración de lipopolisacárido sérico entre los grupos anémico y control tratados con dieta basada en leche fermentada de cabra o dieta estándar sugiere un estado similar de la barrera intestinal después del tratamiento con ambas dietas.

7. ANNEXES

Annex 1. qPCR primers

Name	Gene	Pair	Sequence (5' → 3')
BTF3	basic transcription factor 3	F	TGGCAGCAAACACCTTCACC
		R	AGCTTCAGCCAGTCTCCTCAAAC
PPIB	anti-cyclophilin B	F	TCAAGCTGAAGCACTATGGG
		R	GCAATGGCAAAGGGTTTCTC
AEBP1	adipocyte enhancer binding protein 1	F	GGGTCCAGTGGAGAAAATCA
		R	GTTGTCCTCAATGCGGTGT
COL6A1	collagen VI	F	GCGATTGCCTTCCAAGACT
		R	CCTCAAGGCCACACTCTCC
FN1	fibronectin 1	F	GATGCCGATCAGAAGTTTGG
		R	GGTCGTGCAGATCTCCTCAT
LUM	lumican	F	CCTTCAACACAACCAGCTCA
		R	GTGACTTAAGGCCTTTCAGAGAA
FGF13	fibroblast growth factor 13	F	AGGCAGATGGAACCATTGAT
		R	CCCACAGGGATGAGGTTAAA
NT5E	5'-nucleotidase ecto	F	CTTCTGAACAGCACCATTCG
		R	CCTCCACTGGTTAATGTCTGC
ENTPD1	ectonucleoside triphosphate diphosphohydrolase 1	F	GTCGTCTCACACCAACCTGT
		R	GGTGTCTGGTGCTGTTTGGA
CLD1	claudin 1	F	TGTGTCCACCATTGGCATGA
		R	ACAGGGGTCATGGGGTCATA
MUC2	Mucin 2	F	GCCAGATCCCGAAACCA
		R	TATAGGAGTCTCGGCAGTCA
MDR1	multidrug resistance 1 gene	F	GCTTCTTCCAAAGTGTACATCTTG
		R	TGCCCATCTTTGAGAAGTTCTTG

Annex 2. Statistically significant KOs between the control and anaemic group (padj < 0.05).

	log_2FC	padj
K00005	2.67712	0.01349
K00009	4.44472	0.00586
K00010	5.79709	0.00293
K00030	-3.3807	0.01392
K00042	5.48833	0.00232
K00053	-1.9317	0.00927
K00060	-3.3695	0.00656
K00073	3.274	0.0184
K00075	2.07828	0.00906
K00077	3.99261	0.00379
K00087	4.20071	0.00634
K00094	3.27801	0.01583
K00098	3.21621	0.02066
K00101	3.69023	0.01685
K00104	2.07979	0.03595
K00108	4.22927	0.00581
K00111	2.51573	0.01574
K00113	3.39666	0.02154
K00116	3.83559	0.00779
K00117	2.7305	0.04625
K00121	3.98637	0.01132
K00123	3.70825	0.00543
K00124	3.56133	0.00671
K00127	2.99892	0.0146
K00131	5.72998	0.00232
K00138	3.44351	0.01345
K00146	2.66321	0.03739
K00161	-3.0295	0.03084
K00164	2.67376	0.03916
K00170	3.0141	0.0184
K00175	-1.3124	0.03806
K00180	-3.0101	0.01746
K00198	-2.3292	0.03653
K00208	2.93512	0.01971
K00219	3.21495	0.01582
K00230	4.91251	0.00467
K00242	5.15947	0.00293
K00244	3.04272	0.01735
K00245	4.57035	0.00467
K00247	4.35268	0.00797
K00248	-2.8156	0.03114
K00254	-3.8568	0.00615
K00259	3.15414	0.04649

K00261	-3.3701	0.02459
K00262	-1.6158	0.00686
K00265	-1.4807	0.0487
K00266	1.97983	0.02356
K00275	4.71166	0.00586
K00278	3.70383	0.00762
K00281	-2.8205	0.01473
K00282	3.89121	0.01186
K00285	3.83113	0.00762
K00290	-2.4153	0.00854
K00294	-5.1054	0.00371
K00313	4.55261	0.00586
K00324	3.7821	0.00972
K00325	4.38503	0.0061
K00331	-2.4466	0.01301
K00333	-5.9112	0.00334
K00334	2.39415	0.03028
K00338	4.73317	0.00467
K00340	-3.4713	0.01409
K00362	2.91404	0.02604
K00370	2.51992	0.02303
K00371	2.82547	0.02178
K00372	5.47175	0.00263
K00373	3.16514	0.01131
K00374	2.70051	0.01711
K00380	3.48101	0.01934
K00381	3.22596	0.01734
K00382	3.20707	0.00953
K00385	6.00628	0.00232
K00389	5.44555	0.0033
K00394	-4.3082	0.00666
K00425	2.67167	0.01163
K00427	4.39455	0.00586
K00432	4.95543	0.00531
K00526	2.84991	0.0309
K00548	3.4059	0.00805
K00558	-2.723	0.00372
K00563	2.74058	0.02459
K00564	3.31008	0.01426
K00568	3.5143	0.01334
K00573	3.18121	0.01727
K00574	3.00524	0.0084
K00595	3.79624	0.00762
K00598	3.14672	0.0246
K00620	2.92012	0.01483
K00625	1.58718	0.0474
K00626	2.24334	0.0184
K00627	-2.8798	0.01454

K00631	3.97114	0.00775
K00632	3.58561	0.00636
K00633	-2.313	0.04136
K00634	5.7631	0.00232
K00640	1.8668	0.04066
K00641	4.2292	0.0061
K00645	2.65337	0.01073
K00656	1.85073	0.03891
K00674	5.47157	0.00232
K00675	3.74952	0.01359
K00677	-1.8707	0.03106
K00681	3.51187	0.0125
K00684	-2.3666	0.04302
K00688	3.12851	0.00684
K00700	1.88662	0.02059
K00754	2.6843	0.04427
K00757	2.95907	0.01964
K00769	3.61578	0.01868
K00789	-1.5001	0.00854
K00795	4.64255	0.00379
K00799	2.26581	0.04177
K00806	2.17493	0.01923
K00817	-1.9459	0.01432
K00823	3.63908	0.02154
K00832	3.85378	0.00592
K00844	3.45559	0.01265
K00847	-2.5376	0.01161
K00848	3.87993	0.00702
K00852	3.07002	0.00586
K00855	3.76677	0.00775
K00858	2.0647	0.01737
K00865	3.85457	0.00451
K00867	3.96538	0.00454
K00878	-1.6871	0.0454
K00879	2.50563	0.04382
K00880	4.19771	0.00656
K00882	2.11349	0.02816
K00883	3.40197	0.03474
K00884	3.8766	0.01392
K00885	4.40903	0.00845
K00926	2.5516	0.01301
K00930	-1.6701	0.01706
K00931	1.6916	0.02578
K00932	3.13582	0.01845
K00937	2.69735	0.01583
K00950	2.62936	0.0302
K00957	-1.7052	0.04221
K00962	-1.2368	0.03595

K00970	-5.2516	0.00376
K00974	2.55694	0.02245
K00978	-3.3581	0.01022
K00986	-4.2251	0.00751
K00989	2.84585	0.00762
K00990	2.75636	0.0312
K00997	2.38699	0.0146
K00998	3.44101	0.01839
K01002	3.3357	0.01369
K01008	4.51858	0.00359
K01012	-1.7386	0.01345
K01028	3.20768	0.02709
K01034	2.85612	0.02175
K01035	3.08852	0.00851
K01040	4.1662	0.01261
K01042	5.49185	0.00237
K01048	5.12893	0.00376
K01055	3.32789	0.03099
K01058	3.98195	0.00608
K01060	3.83827	0.00847
K01066	3.46934	0.00992
K01070	3.60763	0.01334
K01082	2.65551	0.0278
K01085	3.80718	0.00994
K01087	3.91185	0.00824
K01092	-2.9137	0.01369
K01104	2.11006	0.01349
K01118	6.84331	0.00232
K01119	4.28107	0.00762
K01130	-5.6458	0.00372
K01138	5.0102	0.00451
K01139	4.26026	0.005
K01141	3.78173	0.00775
K01142	1.82163	0.01374
K01146	3.14667	0.02439
K01147	3.72856	0.00855
K01150	3.26883	0.02303
K01151	-2.1072	0.00974
K01155	-4.9747	0.00232
K01159	-1.7311	0.01297
K01163	2.04588	0.02157
K01169	3.6826	0.01369
K01193	2.03255	0.0246
K01195	6.66106	0.00232
K01197	6.79414	0.00232
K01205	3.58559	0.01972
K01220	3.94582	0.00868
K01226	6.62142	0.00232

K01235	3.57336	0.01328
K01246	-2.311	0.00586
K01250	4.77077	0.00586
K01252	3.74892	0.00762
K01255	4.49438	0.00272
K01273	3.6778	0.01217
K01297	1.60227	0.02782
K01304	2.14054	0.03036
K01305	3.26457	0.01022
K01355	4.20933	0.00783
K01356	2.07319	0.0154
K01358	-1.1425	0.02996
K01387	5.32833	0.00263
K01414	3.35092	0.01226
K01420	-3.3911	0.00447
K01421	6.03005	0.00232
K01423	3.58934	0.00762
K01442	1.57448	0.02714
K01443	3.04252	0.00673
K01447	-7.1538	0.00232
K01448	1.97929	0.02892
K01462	1.53443	0.02482
K01466	3.57161	0.01514
K01467	4.24315	0.0061
K01478	3.04613	0.00854
K01480	3.59952	0.00531
K01484	3.96761	0.00854
K01486	4.6259	0.00371
K01488	3.27173	0.0063
K01491	-1.0308	0.0494
K01494	3.26171	0.01733
K01497	3.40484	0.01979
K01512	2.31431	0.01903
K01521	3.83365	0.00992
K01525	2.86712	0.04603
K01531	5.33144	0.0027
K01537	2.02898	0.01556
K01571	-3.1742	0.00636
K01577	2.8781	0.02264
K01581	2.72506	0.03474
K01582	3.61496	0.00986
K01590	5.64314	0.00232
K01595	2.34487	0.02281
K01599	3.33171	0.01128
K01609	2.5866	0.04397
K01611	4.80846	0.00379
K01639	1.81084	0.03151
K01640	2.55079	0.03438

K01641	3.32381	0.03956
K01643	2.86398	0.00845
K01644	3.62543	0.00531
K01646	1.77109	0.04846
K01659	3.13198	0.04032
K01664	4.42583	0.00775
K01665	3.81364	0.00839
K01666	3.70455	0.00984
K01673	3.12856	0.00862
K01679	2.07329	0.04425
K01682	2.93992	0.03606
K01684	3.74695	0.00934
K01687	-1.4815	0.01262
K01693	-2.7358	0.01392
K01695	-1.4391	0.04372
K01698	2.09412	0.03898
K01703	-2.1253	0.00735
K01709	-3.1248	0.03838
K01715	3.12062	0.01216
K01716	3.29062	0.02752
K01720	3.45632	0.01363
K01725	4.15073	0.00801
K01738	1.77143	0.02933
K01740	-2.5797	0.00845
K01744	3.411	0.01036
K01749	4.51816	0.00272
K01753	2.99566	0.03173
K01760	3.63819	0.00624
K01766	3.50427	0.01703
K01770	-1.4077	0.01073
K01775	2.81442	0.00586
K01776	2.57206	0.00851
K01782	3.79144	0.0087
K01783	3.28556	0.00447
K01787	-2.9261	0.01923
K01792	3.15314	0.02459
K01816	3.29478	0.01466
K01818	-2.2135	0.00688
K01823	3.18015	0.01542
K01838	3.62666	0.01553
K01858	2.67959	0.04081
K01890	2.06961	0.01653
K01897	2.15291	0.02578
K01903	-4.6492	0.00543
K01908	3.40547	0.01931
K01910	2.33777	0.02398
K01911	2.53249	0.02235
K01918	-1.9367	0.00947

K01919	2.7966	0.01137
K01921	1.59934	0.03093
K01923	-1.7332	0.01667
K01929	3.03618	0.00543
K01958	3.50715	0.01682
K01962	2.49652	0.01304
K01963	2.95937	0.00797
K01974	4.86047	0.0033
K01975	4.0074	0.00666
K01994	-4.047	0.02384
K01999	4.08213	0.00586
K02000	2.93629	0.03182
K02003	-1.0938	0.03263
K02006	3.01694	0.00951
K02007	-3.4668	0.01037
K02008	5.12835	0.00263
K02009	4.05651	0.00454
K02010	2.95166	0.04483
K02017	3.69527	0.00608
K02018	2.24697	0.04305
K02019	3.15521	0.01493
K02020	3.68686	0.00845
K02022	-5.3913	0.00471
K02024	2.99758	0.03525
K02026	-1.6384	0.03316
K02032	-3.9671	0.0061
K02034	1.6066	0.0277
K02035	2.11307	0.01949
K02042	3.58985	0.00916
K02044	2.23098	0.0302
K02045	3.08156	0.03637
K02046	3.97819	0.00854
K02047	4.99111	0.00447
K02049	2.17853	0.02966
K02051	3.5463	0.00451
K02055	2.8432	0.02297
K02056	2.02732	0.02526
K02058	2.77876	0.02702
K02062	2.91048	0.02303
K02066	-3.0511	0.01054
K02068	3.64902	0.00854
K02072	2.57763	0.0125
K02078	-1.5019	0.01284
K02079	3.94556	0.00796
K02081	4.5276	0.00451
K02083	3.05266	0.02154
K02099	2.70705	0.04565
K02100	3.76824	0.0087

K02106	3.65282	0.0084
K02107	2.96054	0.04754
K02110	-1.5556	0.01254
K02116	5.46929	0.00232
K02122	3.2934	0.00762
K02160	1.882	0.04263
K02167	4.92959	0.00488
K02170	4.03852	0.00585
K02172	-3.8958	0.00488
K02189	5.53262	0.00232
K02192	4.18703	0.01124
K02193	3.72964	0.0061
K02194	3.05516	0.0242
K02195	4.30328	0.00586
K02196	3.95598	0.00992
K02198	2.93169	0.03093
K02199	2.52412	0.02306
K02200	2.57296	0.03599
K02221	2.9897	0.01743
K02227	4.2829	0.00376
K02237	2.42208	0.0137
K02245	2.47703	0.04287
K02255	3.15125	0.02878
K02257	3.56859	0.01224
K02283	-4.4428	0.0082
K02297	3.32122	0.01342
K02299	4.80732	0.0047
K02300	3.14466	0.02475
K02315	-1.6231	0.02775
K02317	3.78339	0.00929
K02337	-1.7722	0.02142
K02339	4.68896	0.00531
K02344	2.99354	0.04736
K02358	-1.0149	0.01816
K02361	3.89538	0.01311
K02363	4.46387	0.00586
K02379	4.12396	0.00636
K02380	4.68304	0.00475
K02386	3.68676	0.01149
K02389	3.34792	0.01864
K02392	2.5318	0.02535
K02395	2.73388	0.03954
K02396	2.68525	0.02356
K02398	3.00394	0.02284
K02399	3.28985	0.02303
K02402	3.89958	0.01265
K02406	-1.7754	0.04765
K02408	2.07715	0.04115

K02409	3.05422	0.03634
K02411	3.63278	0.01627
K02414	4.92848	0.00356
K02424	2.83352	0.01863
K02426	2.70941	0.0292
K02427	3.43309	0.0078
K02428	-1.319	0.02039
K02431	2.87618	0.02411
K02435	-2.2471	0.03471
K02438	2.86152	0.0282
K02439	3.77596	0.00671
K02440	2.00834	0.02913
K02441	3.87927	0.00751
K02446	2.81663	0.03254
K02459	4.20111	0.00809
K02466	2.6756	0.04397
K02471	2.59754	0.04758
K02472	4.14123	0.00725
K02477	2.96725	0.02475
K02483	4.41277	0.00657
K02485	3.17011	0.01784
K02494	3.8354	0.00702
K02495	4.10666	0.00552
K02499	2.84485	0.01542
K02500	-1.6843	0.0242
K02507	2.63744	0.04846
K02510	3.12406	0.01219
K02518	-1.0819	0.0256
K02521	3.44009	0.0179
K02523	4.16972	0.00542
K02526	2.83739	0.02439
K02527	2.85402	0.02042
K02532	3.11005	0.01675
K02533	2.78877	0.01755
K02535	3.18658	0.0159
K02549	2.68673	0.03582
K02551	-2.3559	0.01824
K02557	3.02907	0.01404
K02558	3.83071	0.00586
K02560	3.10619	0.02474
K02565	2.81425	0.03447
K02566	5.03422	0.00531
K02567	3.40291	0.00987
K02570	4.41102	0.00759
K02572	2.56166	0.02851
K02573	2.95902	0.01618
K02574	3.69211	0.00673
K02575	2.47568	0.02435

K02588	3.95879	0.00809
K02598	2.77707	0.03882
K02610	4.50336	0.00901
K02611	3.89146	0.00854
K02617	3.40826	0.02356
K02650	4.75272	0.00423
K02654	2.92015	0.03379
K02664	5.41299	0.00254
K02669	2.04689	0.04425
K02679	5.28796	0.00379
K02681	5.04795	0.00586
K02682	3.57563	0.01026
K02686	6.04059	0.00232
K02742	3.36805	0.02205
K02745	3.05309	0.01301
K02750	2.99883	0.02396
K02768	3.46851	0.00436
K02769	2.48204	0.01555
K02770	3.35	0.00543
K02775	2.81014	0.02663
K02777	3.00411	0.01115
K02784	3.65096	0.01426
K02796	2.43888	0.01966
K02798	3.61826	0.00644
K02799	5.10706	0.0033
K02800	5.10706	0.0033
K02803	3.10697	0.03287
K02806	3.39848	0.00868
K02818	5.03129	0.00526
K02819	4.91306	0.00543
K02821	5.05973	0.00272
K02823	6.05331	0.00232
K02835	-1.052	0.03891
K02836	1.41185	0.04772
K02838	-1.35	0.01809
K02841	2.30125	0.04115
K02846	3.83955	0.0111
K02851	2.23404	0.03563
K02856	4.58361	0.00531
K02858	4.37707	0.00531
K02867	-1.1965	0.02039
K02874	-1.4673	0.00916
K02876	-1.2177	0.01483
K02878	-1.1169	0.02143
K02879	-1.1436	0.02417
K02887	-1.0353	0.02296
K02890	-0.9964	0.04469
K02892	-1.038	0.0494

K02897	-1.2904	0.03263
K02899	-1.2949	0.01369
K02919	-2.4707	0.03547
K02933	-1.2465	0.02062
K02946	-1.3313	0.01159
K02948	-1.1996	0.0246
K02952	-1.0803	0.03076
K02959	-1.2975	0.02122
K02965	-1.5713	0.0063
K02970	-1.1296	0.03379
K02982	-1.3295	0.01028
K02992	-1.4399	0.00906
K03046	-1.1305	0.03673
K03060	2.62037	0.00586
K03071	4.20748	0.00537
K03072	5.28869	0.00232
K03076	-1.1245	0.04682
K03079	4.76474	0.00522
K03098	3.93731	0.00797
K03100	2.596	0.0063
K03101	2.59832	0.00776
K03116	-2.341	0.0158
K03117	3.33407	0.00917
K03118	-1.9423	0.01353
K03119	5.35878	0.00488
K03148	3.97625	0.00753
K03151	2.52522	0.00673
K03169	-1.5179	0.03547
K03181	4.77739	0.00509
K03182	3.37536	0.01438
K03186	2.48563	0.04454
K03190	3.72994	0.0277
K03205	-4.1641	0.00232
K03215	1.40033	0.03654
K03271	-3.2733	0.00934
K03273	3.80585	0.00754
K03286	3.27845	0.011
K03289	3.87221	0.00986
K03290	3.03012	0.03067
K03291	3.92952	0.00865
K03297	4.09484	0.00971
K03299	2.60163	0.03438
K03305	2.15145	0.04591
K03311	2.07899	0.04911
K03314	2.81368	0.04121
K03319	3.84209	0.00748
K03326	3.2838	0.03916
K03327	3.38842	0.01763

K03329	3.06043	0.02641
K03335	3.33162	0.00636
K03336	2.56688	0.01428
K03337	4.5191	0.00462
K03338	5.6559	0.00232
K03385	3.02242	0.01764
K03386	3.53584	0.00644
K03387	2.84645	0.03234
K03399	5.38582	0.00318
K03406	-4.5091	0.00779
K03414	3.85483	0.01106
K03415	-2.606	0.02578
K03427	-1.1803	0.02822
K03429	2.52992	0.02841
K03439	1.38082	0.03766
K03446	2.90715	0.03424
K03449	2.45958	0.03197
K03458	5.81152	0.00232
K03459	3.77044	0.01643
K03465	3.50986	0.00726
K03474	-2.0529	0.01629
K03477	2.56938	0.03891
K03478	4.21197	0.00586
K03480	6.4135	0.00232
K03481	5.65222	0.00232
K03485	4.22675	0.00759
K03487	2.84641	0.03424
K03488	2.73842	0.02435
K03497	-1.52	0.01115
K03500	4.45108	0.00293
K03501	1.54388	0.04554
K03516	2.41253	0.03823
K03521	-2.5374	0.0037
K03522	1.85744	0.03525
K03523	3.45378	0.00853
K03526	-1.3282	0.03813
K03529	4.64639	0.0033
K03531	2.27234	0.01344
K03533	4.06444	0.01353
K03543	2.85034	0.02933
K03546	2.34734	0.04804
K03547	2.24589	0.01359
K03548	3.23255	0.02543
K03549	1.80919	0.0385
K03551	-1.1257	0.02878
K03557	3.50605	0.01514
K03558	2.51824	0.03884
K03560	3.54564	0.01311

K03562	3.69507	0.00868
K03564	-1.5323	0.04461
K03566	4.20566	0.00775
K03568	4.3444	0.0034
K03569	-1.2016	0.03739
K03571	1.87399	0.03323
K03573	2.77694	0.03682
K03575	3.38698	0.0083
K03576	3.7324	0.00883
K03578	2.64177	0.04159
K03579	3.96886	0.00984
K03582	3.02646	0.02183
K03583	2.91964	0.01922
K03586	2.90744	0.01767
K03587	3.6536	0.00794
K03592	3.90042	0.005
K03593	2.35603	0.02878
K03597	3.06188	0.01839
K03598	2.8916	0.0312
K03599	2.77212	0.01661
K03603	2.4676	0.03959
K03605	3.51226	0.01039
K03607	4.05991	0.00775
K03608	3.59602	0.00543
K03610	5.04567	0.00286
K03612	1.83868	0.03653
K03618	3.77976	0.00829
K03619	4.13769	0.00702
K03623	2.72299	0.0268
K03628	-3.5642	0.00629
K03630	1.7187	0.03708
K03632	2.78364	0.04372
K03633	3.42013	0.01504
K03634	3.67843	0.00992
K03635	2.58828	0.03133
K03637	3.79627	0.00531
K03639	5.03971	0.00235
K03640	2.60974	0.03011
K03641	4.4206	0.00522
K03642	-5.2644	0.00325
K03643	4.04977	0.00986
K03645	4.05718	0.00586
K03646	2.61279	0.04631
K03651	2.85199	0.02108
K03652	2.48419	0.01538
K03656	4.47712	0.00551
K03657	2.00915	0.01113
K03658	2.9833	0.0385

K03660	-2.3721	0.04603
K03665	-1.5991	0.03028
K03666	4.89553	0.00232
K03669	3.10035	0.02332
K03674	4.45989	0.0063
K03683	3.3231	0.01814
K03684	4.19233	0.0061
K03687	2.55304	0.01193
K03690	2.49408	0.03151
K03696	2.71885	0.01363
K03716	5.14874	0.00293
K03719	3.42262	0.01596
K03720	5.41739	0.00272
K03722	2.47804	0.01769
K03732	3.25063	0.01755
K03733	-2.891	0.01253
K03735	2.40401	0.01675
K03737	-1.7128	0.02853
K03745	5.76564	0.00263
K03746	3.7858	0.01022
K03748	-1.7848	0.04911
K03749	4.02773	0.00681
K03752	3.51349	0.00531
K03753	4.48882	0.00371
K03755	3.48457	0.01755
K03756	3.14498	0.00987
K03758	5.53183	0.00232
K03759	3.39071	0.01733
K03760	2.55373	0.0278
K03761	4.09746	0.00673
K03762	4.46043	0.0068
K03764	3.05314	0.02387
K03767	4.06557	0.00824
K03772	2.78125	0.02062
K03776	4.04813	0.00854
K03777	2.90759	0.03263
K03779	4.02231	0.00827
K03781	-4.1035	0.00531
K03783	2.4969	0.01418
K03784	2.62955	0.01028
K03785	3.46648	0.00597
K03786	3.92714	0.00579
K03789	3.0075	0.01404
K03796	3.40362	0.01774
K03800	2.95552	0.01178
K03803	2.61683	0.01665
K03807	2.48461	0.0331
K03808	3.68609	0.01219

K03814	4.93222	0.00358
K03818	-4.0472	0.00586
K03820	2.85433	0.02475
K03824	2.66633	0.04122
K03826	2.06349	0.03592
K03831	4.33738	0.00531
K03833	5.58207	0.00232
K03840	5.27531	0.00376
K03841	2.7947	0.02062
K03852	-4.8995	0.006
K03855	3.7685	0.01016
K03856	2.12065	0.04682
K03892	2.19274	0.0242
K03923	4.44584	0.00358
K03969	3.61871	0.00531
K03970	5.03812	0.00491
K03971	5.00641	0.00467
K03973	4.55046	0.006
K04014	3.40823	0.00608
K04021	3.20081	0.02122
K04025	4.69374	0.00542
K04028	2.48472	0.01345
K04030	3.49051	0.00845
K04031	2.82753	0.0137
K04034	5.49742	0.00272
K04042	2.24796	0.01242
K04043	-0.8859	0.04682
K04062	2.90305	0.04758
K04070	3.85608	0.006
K04073	4.31138	0.00484
K04075	3.38036	0.00531
K04076	5.66058	0.00232
K04077	-0.986	0.0357
K04080	2.96462	0.02412
K04081	3.12773	0.01301
K04082	3.19388	0.01374
K04083	1.87983	0.02966
K04088	3.47867	0.01073
K04335	4.03394	0.01161
K04337	2.65708	0.03288
K04485	2.26938	0.02221
K04516	-1.6567	0.04136
K04517	2.51875	0.02601
K04565	3.61346	0.00929
K04651	3.66605	0.006
K04653	4.39318	0.00484
K04654	3.16869	0.01514
K04691	3.99597	0.00762

K04744	2.73571	0.02317
K04750	3.14727	0.01037
K04752	4.29509	0.00783
K04754	4.74305	0.00531
K04755	2.72904	0.02556
K04759	2.3341	0.01054
K04770	2.83015	0.0302
K04771	2.93145	0.00762
K04774	3.29524	0.01997
K04775	2.7629	0.04985
K04835	-3.1849	0.01979
K05245	3.35918	0.01538
K05337	3.10577	0.00868
K05341	-3.2682	0.01902
K05365	2.55321	0.0487
K05396	2.9273	0.02999
K05499	3.01404	0.02803
K05501	3.29888	0.0091
K05516	2.82498	0.02645
K05526	4.22866	0.00762
K05527	4.23572	0.00712
K05539	2.80681	0.02191
K05540	2.71487	0.01315
K05591	3.73294	0.01095
K05594	3.83276	0.0152
K05595	2.51584	0.02853
K05596	4.26716	0.00644
K05709	4.34722	0.00724
K05710	4.18652	0.00992
K05713	2.59538	0.04919
K05714	3.56485	0.01476
K05775	4.10907	0.00586
K05776	2.82396	0.03601
K05777	2.49793	0.03959
K05779	5.01316	0.00531
K05782	3.56328	0.0141
K05785	3.82222	0.00854
K05786	3.95481	0.0058
K05787	4.30053	0.00697
K05788	4.6656	0.00531
K05798	2.75929	0.04574
K05799	4.16854	0.00382
K05803	2.70069	0.03117
K05804	4.1874	0.00671
K05805	2.66865	0.02259
K05807	2.56153	0.03399
K05809	2.92943	0.04291
K05810	2.58098	0.01419

K05812	4.49263	0.0061
K05813	2.51417	0.02816
K05814	4.32603	0.00613
K05815	3.7307	0.00865
K05816	3.73385	0.01045
K05818	3.11604	0.0188
K05822	3.13746	0.03045
K05845	2.41923	0.03438
K05846	3.80291	0.00751
K05873	5.43797	0.00263
K05878	3.5541	0.01251
K05887	3.27338	0.03941
K05895	5.74103	0.00232
K05896	2.3626	0.01997
K05916	3.70086	0.008
K05919	2.61106	0.04305
K05939	3.4292	0.01764
K05942	-3.2029	0.02284
K05966	3.30264	0.01226
K05979	5.52063	0.00232
K05982	3.46262	0.01332
K05989	2.86951	0.02761
K05997	2.63695	0.04291
K06001	-2.7	0.00488
K06006	4.75529	0.0047
K06019	5.73701	0.00272
K06023	2.68253	0.0087
K06024	2.87697	0.00644
K06039	3.16334	0.03493
K06048	4.59218	0.00775
K06073	3.59683	0.02853
K06074	2.93381	0.02283
K06075	3.03147	0.02966
K06077	4.39796	0.0064
K06078	5.10315	0.00552
K06080	3.71499	0.00767
K06122	5.68572	0.00232
K06131	2.73929	0.00897
K06133	3.27975	0.02264
K06140	4.91492	0.0042
K06144	2.74386	0.03988
K06145	3.29909	0.0188
K06149	3.50331	0.00899
K06155	2.98098	0.02612
K06157	3.77697	0.01262
K06162	4.14212	0.00799
K06167	-4.708	0.00586
K06175	4.87987	0.00531

K06176	3.61374	0.01434
K06177	3.75598	0.00999
K06179	2.12078	0.03036
K06182	6.05813	0.00232
K06186	3.51739	0.01336
K06188	3.50086	0.01557
K06189	3.36075	0.01737
K06190	3.0346	0.02892
K06191	3.14718	0.0179
K06194	3.03583	0.01764
K06195	3.49515	0.03065
K06199	-1.113	0.03601
K06200	3.98262	0.00488
K06202	4.6472	0.00586
K06203	4.0745	0.00986
K06205	3.25363	0.03823
K06206	4.76761	0.00272
K06209	2.67271	0.00777
K06211	4.86581	0.00467
K06214	4.06643	0.00865
K06216	2.90077	0.03823
K06222	3.93514	0.00985
K06223	-1.9909	0.02332
K06281	2.8024	0.02077
K06282	4.0674	0.0049
K06283	-1.923	0.04144
K06297	3.70401	0.01464
K06298	-4.5885	0.00488
K06346	2.50127	0.01409
K06381	2.86705	0.00984
K06382	3.31751	0.00649
K06383	3.99543	0.00488
K06384	5.75356	0.00232
K06387	1.97992	0.02316
K06390	2.28618	0.02892
K06391	3.95244	0.01251
K06392	-1.6301	0.04812
K06393	3.84063	0.00531
K06394	2.79378	0.02287
K06396	2.57181	0.03722
K06400	5.35242	0.00265
K06409	5.14586	0.00232
K06410	2.36108	0.03062
K06415	5.66527	0.00232
K06416	-3.1587	0.01262
K06438	5.20082	0.00272
K06518	2.22221	0.02852
K06726	2.63858	0.01364

K06859	2.73124	0.04302
K06861	-1.7546	0.01645
K06866	3.08189	0.03916
K06867	2.52406	0.04631
K06878	3.15459	0.00751
K06879	4.39136	0.00543
K06881	2.47063	0.02818
K06890	2.50407	0.0218
K06891	3.20074	0.01653
K06896	2.60292	0.01454
K06897	3.37716	0.00857
K06899	3.06931	0.01922
K06909	-4.1971	0.0061
K06910	-2.4728	0.00531
K06911	4.03066	0.00392
K06916	3.61798	0.01341
K06919	-3.2695	0.00579
K06921	-3.0301	0.00531
K06923	3.05636	0.00854
K06925	2.10611	0.0274
K06926	-3.655	0.00353
K06956	4.29185	0.00531
K06957	2.77701	0.04302
K06958	2.44103	0.00986
K06966	3.15232	0.01404
K06970	3.19649	0.02702
K06972	5.33988	0.00263
K06975	2.66647	0.03211
K06980	5.08701	0.00455
K06997	2.94536	0.00531
K07000	4.34602	0.00531
K07014	2.74678	0.0192
K07019	2.99547	0.01613
K07026	4.37572	0.00649
K07030	3.53154	0.00455
K07034	3.59729	0.01106
K07038	4.51647	0.00488
K07039	2.65553	0.03377
K07040	-2.0909	0.02576
K07043	6.59314	0.00232
K07051	-6.1276	0.00286
K07053	4.4522	0.00293
K07054	2.40921	0.02557
K07058	2.94963	0.01312
K07067	5.69503	0.00232
K07071	4.91507	0.00488
K07080	2.99723	0.01175
K07082	3.51681	0.00854

K07088	1.98118	0.00922
K07091	4.05259	0.00512
K07095	1.96999	0.03582
K07099	2.51894	0.01262
K07101	3.60613	0.01685
K07105	2.60554	0.03941
K07107	-2.0962	0.01106
K07109	2.61777	0.04636
K07112	3.82373	0.01024
K07113	2.34131	0.03955
K07114	-1.4545	0.03739
K07119	4.85432	0.00492
K07121	2.82355	0.02853
K07122	3.6452	0.00586
K07124	-2.0052	0.04215
K07127	2.7234	0.04305
K07132	4.26752	0.00852
K07133	-1.6221	0.0212
K07136	2.54023	0.04631
K07137	-2.291	0.0084
K07141	2.02232	0.03686
K07146	4.25338	0.00762
K07147	3.66922	0.01374
K07149	-2.6659	0.04426
K07156	3.3807	0.02062
K07171	-1.6437	0.01949
K07173	1.75817	0.02957
K07175	3.28171	0.01733
K07180	5.8371	0.00232
K07184	2.99209	0.03549
K07216	3.52075	0.01539
K07229	2.89907	0.02816
K07232	4.33211	0.00762
K07235	4.29796	0.00649
K07236	4.2631	0.00829
K07248	2.81448	0.03041
K07258	2.42219	0.00751
K07259	3.46419	0.01997
K07261	5.27122	0.00376
K07262	3.80037	0.00777
K07264	2.74479	0.0485
K07273	2.58453	0.00854
K07274	4.29536	0.00618
K07275	4.16363	0.00748
K07278	2.85905	0.04372
K07284	3.77271	0.00352
K07285	2.92342	0.02645
K07289	2.73799	0.043

K07300	5.20865	0.00303
K07301	2.34808	0.01918
K07304	3.39108	0.0058
K07305	4.91584	0.0037
K07306	3.36463	0.011
K07307	3.49785	0.01369
K07311	2.45187	0.03288
K07312	4.3032	0.00845
K07313	2.76953	0.0309
K07318	2.7343	0.03549
K07320	2.24557	0.03314
K07323	3.42142	0.00775
K07337	3.94456	0.01277
K07339	-3.0687	0.01318
K07341	-3.0708	0.011
K07347	3.12403	0.0154
K07348	3.64998	0.01763
K07351	2.88009	0.02039
K07354	2.97143	0.02966
K07356	3.33861	0.0194
K07387	2.02245	0.04425
K07391	2.68582	0.02866
K07397	3.32217	0.0107
K07399	2.83742	0.04878
K07400	4.19652	0.00854
K07402	5.00273	0.0033
K07405	-3.2112	0.01816
K07448	-4.1662	0.006
K07455	5.83037	0.00232
K07459	4.09141	0.00634
K07461	3.12403	0.00593
K07462	3.38044	0.00585
K07479	3.37266	0.01438
K07481	-4.0876	0.00454
K07490	4.71301	0.00545
K07533	2.40958	0.01574
K07552	3.88211	0.00531
K07559	4.71092	0.00313
K07560	-1.5502	0.01229
K07566	-1.8453	0.01758
K07568	-1.4527	0.01839
K07571	3.83832	0.00565
K07589	3.6186	0.01468
K07590	6.04329	0.00232
K07592	3.96869	0.01052
K07637	3.36845	0.01879
K07638	4.1425	0.00543
K07643	4.05563	0.00797

K07659	3.82517	0.00838
K07663	4.98377	0.00488
K07666	3.76879	0.00586
K07667	1.89253	0.04427
K07674	3.50789	0.01824
K07687	3.72704	0.01628
K07688	4.4572	0.00854
K07689	3.4471	0.02177
K07690	3.4755	0.01475
K07701	3.70325	0.01149
K07708	3.54429	0.00853
K07711	2.84967	0.02568
K07715	3.36172	0.01907
K07738	-1.9798	0.00748
K07740	3.4649	0.02645
K07749	2.21742	0.03299
K07751	3.90976	0.00992
K07771	4.49878	0.00593
K07772	3.13646	0.02459
K07773	2.85099	0.04812
K07782	3.34273	0.02838
K07783	4.1477	0.01946
K07784	4.44144	0.00634
K07791	3.86712	0.00491
K07793	3.79932	0.00644
K07798	2.17764	0.04913
K07799	4.27196	0.00748
K07803	3.15863	0.0277
K07806	4.35585	0.00684
K07810	3.97256	0.01518
K07812	2.63606	0.04419
K07813	4.63626	0.0033
K08092	4.56289	0.00543
K08137	2.89942	0.02702
K08138	3.09377	0.01955
K08154	3.72731	0.01224
K08156	-2.688	0.00546
K08160	3.98554	0.00871
K08161	2.20073	0.03433
K08162	2.82671	0.03064
K08163	4.3058	0.00916
K08172	3.1642	0.01927
K08177	4.75759	0.00372
K08191	4.71437	0.00579
K08217	-1.5515	0.02803
K08219	3.84715	0.00974
K08221	-2.7755	0.03823
K08222	3.26191	0.02355

K08224	5.12761	0.00455
K08227	2.68822	0.0424
K08281	3.75013	0.00899
K08296	4.36781	0.00634
K08299	4.55437	0.00762
K08301	3.32284	0.00868
K08304	2.42688	0.02635
K08306	3.74937	0.01349
K08307	3.06785	0.00992
K08310	4.09053	0.00608
K08311	3.88364	0.00957
K08314	4.48089	0.00634
K08315	4.80899	0.0061
K08320	2.86696	0.03824
K08326	3.55145	0.01334
K08349	4.07018	0.0087
K08351	3.96895	0.00851
K08368	4.11163	0.00603
K08384	2.52245	0.03263
K08483	4.0597	0.0033
K08485	5.25716	0.0033
K08587	5.18219	0.00362
K08591	2.2951	0.01247
K08602	2.0195	0.0385
K08641	3.14914	0.01349
K08678	-2.6091	0.03959
K08722	2.80584	0.02971
K08723	2.90771	0.02702
K08884	3.79947	0.01342
K08970	3.33228	0.02822
K08972	2.97987	0.04353
K08974	4.62521	0.00379
K08981	5.7735	0.00232
K08984	3.62023	0.01764
K08986	5.85936	0.00232
K08989	4.34322	0.00762
K08990	4.51486	0.0061
K08992	4.08664	0.01409
K08993	4.70138	0.00735
K09001	2.39602	0.03441
K09007	-5.3934	0.00481
K09009	2.64248	0.04372
K09018	2.75483	0.03519
K09020	3.05702	0.02751
K09023	2.79088	0.03263
K09117	2.65318	0.02416
K09118	5.67284	0.00232
K09121	-3.8469	0.00779

K09124	3.22632	0.02493
K09128	3.99444	0.01774
K09131	3.84123	0.00868
K09137	5.67583	0.00232
K09158	3.89087	0.00818
K09159	4.97517	0.00358
K09160	4.44665	0.0087
K09161	3.54866	0.01433
K09167	3.87822	0.01755
K09181	3.46642	0.00845
K09470	4.63945	0.00543
K09471	3.54335	0.01819
K09473	3.07605	0.02636
K09702	-1.7195	0.04291
K09705	4.77506	0.00631
K09712	3.72242	0.01044
K09758	5.11259	0.0033
K09760	2.34285	0.0493
K09762	2.30806	0.0206
K09764	-2.5071	0.04671
K09767	4.2779	0.00845
K09770	-3.7585	0.01428
K09771	5.7502	0.00272
K09773	3.14791	0.00592
K09778	5.1971	0.00313
K09779	-3.0369	0.01428
K09786	5.84329	0.00232
K09787	1.78573	0.03133
K09791	3.94707	0.00992
K09802	2.89609	0.04382
K09803	3.42275	0.02999
K09806	4.14228	0.00725
K09811	2.50636	0.01924
K09812	1.82481	0.03093
K09817	3.4239	0.01574
K09819	-6.3092	0.00293
K09824	3.8446	0.01052
K09858	4.82583	0.00638
K09862	3.80626	0.00779
K09889	3.01536	0.01518
K09890	4.09085	0.01711
K09891	3.43969	0.01105
K09892	5.54032	0.00282
K09893	3.64482	0.008
K09894	3.87228	0.01158
K09896	3.02558	0.02989
K09897	4.67877	0.00775
K09898	5.27871	0.00379

K09899	3.63863	0.01045
K09900	5.12306	0.00467
K09901	3.53996	0.01514
K09902	5.08652	0.0033
K09904	4.23201	0.00723
K09906	3.35391	0.0382
K09908	3.22329	0.03093
K09910	3.26847	0.01711
K09911	3.51982	0.01702
K09913	4.81732	0.00735
K09915	3.15018	0.0273
K09916	2.6992	0.03708
K09917	4.94533	0.00796
K09918	3.4402	0.0393
K09920	4.26154	0.00603
K09921	3.52022	0.00671
K09925	2.97871	0.0393
K09933	2.51847	0.04604
K09935	4.31044	0.0061
K09946	3.36997	0.02122
K09954	3.95186	0.01769
K09969	3.89246	0.00563
K09970	3.86354	0.00631
K09971	3.00332	0.02081
K09973	5.15847	0.00272
K09975	4.01497	0.0087
K09979	3.80404	0.01763
K09996	3.88176	0.01755
K09999	4.56407	0.00586
K10001	3.18556	0.02297
K10004	3.44229	0.01037
K10009	2.5731	0.01883
K10011	2.84196	0.03988
K10012	3.7665	0.00865
K10015	3.81163	0.00776
K10017	4.56225	0.00586
K10036	2.60756	0.03097
K10110	4.87643	0.00491
K10111	3.79459	0.00797
K10439	1.80663	0.02822
K10441	1.64903	0.04671
K10537	3.14691	0.01949
K10543	2.61433	0.03299
K10544	3.59284	0.01035
K10555	3.64874	0.01219
K10558	2.57703	0.04964
K10563	2.09054	0.03184
K10680	4.05905	0.00862

K10709	4.82391	0.0047
K10711	3.63051	0.01975
K10716	1.82781	0.04953
K10763	3.47171	0.0124
K10778	3.82255	0.01353
K10797	2.94642	0.03435
K10804	4.56409	0.00531
K10914	3.61974	0.00845
K10939	3.36961	0.02435
K10973	4.03555	0.00671
K10974	3.81065	0.00905
K11057	6.51881	0.00232
K11065	3.23959	0.00805
K11066	3.29813	0.01767
K11073	3.90187	0.00787
K11076	3.27567	0.02554
K11102	5.47703	0.00232
K11104	2.87481	0.02371
K11106	3.81922	0.00845
K11139	2.99844	0.03143
K11175	2.34198	0.01322
K11178	3.60776	0.011
K11183	3.8304	0.00735
K11191	2.83293	0.03263
K11192	2.83293	0.03263
K11201	3.37853	0.00986
K11202	2.95246	0.01101
K11203	3.45991	0.01224
K11209	4.52719	0.00465
K11264	4.79863	0.0047
K11392	3.04485	0.02816
K11472	4.21211	0.00762
K11473	2.62249	0.0454
K11474	3.92591	0.00986
K11477	3.43988	0.02625
K11534	3.71537	0.00657
K11535	3.96813	0.00845
K11615	2.96357	0.03529
K11685	3.76872	0.0094
K11719	4.49702	0.00531
K11734	3.84963	0.00868
K11735	3.12327	0.02657
K11741	3.14899	0.03424
K11742	2.71306	0.04221
K11745	2.61503	0.04494
K11747	4.18383	0.00929
K11748	4.37036	0.00656
K11750	3.31602	0.01189

K11751	3.1869	0.02154
K11752	2.91343	0.02753
K11921	3.3217	0.02534
K11922	4.16285	0.00779
K11924	3.89015	0.01229
K11926	2.64292	0.04291
K11927	4.09924	0.0061
K11929	3.83486	0.01247
K11932	2.96243	0.03106
K11933	3.47642	0.01404
K11934	2.72029	0.04034
K11938	2.62012	0.04657
K11939	4.59636	0.00593
K12056	2.5965	0.04765
K12132	2.28108	0.03768
K12138	3.80701	0.01374
K12146	3.20454	0.02043
K12147	3.64797	0.0083
K12148	3.24324	0.02154
K12151	2.80957	0.03256
K12152	3.73281	0.01102
K12264	2.77323	0.0278
K12265	3.07309	0.02356
K12266	2.75256	0.03525
K12267	-2.8063	0.01682
K12291	2.85457	0.02459
K12297	2.79623	0.0431
K12299	3.40792	0.011
K12340	4.37281	0.00586
K12369	3.35945	0.01336
K12371	4.06144	0.00793
K12452	-4.2347	0.00379
K12507	3.3618	0.02039
K12524	2.50413	0.03739
K12527	4.12522	0.006
K12529	3.84463	0.00845
K12574	1.92072	0.02671
K12582	3.39701	0.02482
K12684	4.25844	0.01734
K12940	5.23472	0.00293
K12943	3.55827	0.011
K12957	2.7551	0.03162
K12961	5.39375	0.00338
K12963	4.58218	0.00857
K12972	3.7495	0.01785
K12973	2.52702	0.02859
K12974	3.16526	0.02091
K13004	3.12497	0.02635

K13012	4.03095	0.00921
K13014	4.20062	0.00726
K13038	2.59451	0.00901
K13040	3.63454	0.04177
K13043	-2.0848	0.00629
K13069	3.50464	0.01453
K13244	2.9979	0.03493
K13255	5.71394	0.00273
K13256	4.08835	0.00488
K13281	5.39028	0.00272
K13283	4.31128	0.00644
K13292	2.98278	0.00608
K13301	3.95403	0.01208
K13483	3.86897	0.01102
K13497	2.61941	0.04574
K13498	3.88855	0.01251
K13542	3.43677	0.0063
K13566	2.6959	0.03593
K13574	2.5813	0.04372
K13628	4.13778	0.0087
K13631	4.28154	0.00897
K13638	4.45032	0.00745
K13639	5.03991	0.0042
K13641	4.43574	0.00531
K13643	2.75845	0.01878
K13650	4.34023	0.01092
K13686	3.40381	0.02195
K13695	3.21842	0.02377
K13771	4.17494	0.00657
K13788	3.46426	0.00868
K13890	3.51307	0.01349
K13891	3.49423	0.02311
K13919	4.37252	0.00748
K13920	3.50012	0.01369
K13922	4.10639	0.00868
K13953	4.64222	0.00586
K13954	4.74837	0.00522
K13963	2.76064	0.02899
K14056	2.43328	0.04591
K14061	2.86147	0.04804
K14062	4.03687	0.00839
K14064	3.97541	0.01054
K14065	3.69519	0.00649
K14155	3.48007	0.00686
K14170	3.87329	0.00543
K14187	4.08435	0.00893
K14261	2.69646	0.04671
K14287	4.01941	0.0092

K14347	3.86264	0.0084
K14348	2.49889	0.04772
K14414	4.74304	0.00379
K14441	-1.5293	0.02853
K14445	-3.8419	0.00332
K14540	2.36094	0.03287
K14623	-2.8484	0.02799
K14682	3.2023	0.0168
K14744	3.21157	0.02264
K14762	3.23092	0.03424
K15256	4.2534	0.00762
K15461	3.50647	0.00796
K15520	3.09279	0.02916
K15524	2.79658	0.03654
K15540	4.5603	0.00586
K15547	3.88576	0.01028
K15553	4.01533	0.00992
K15554	4.14042	0.00656
K15555	2.52591	0.04796
K15580	2.39569	0.03683
K15581	-2.0124	0.0274
K15583	2.03659	0.02666
K15586	2.27757	0.0331
K15633	-1.3239	0.01607
K15634	2.89444	0.02803
K15722	2.5533	0.03838
K15724	3.39369	0.01159
K15737	3.64535	0.01022
K15773	3.51408	0.02272
K15827	3.80901	0.01998
K15828	2.75543	0.02803
K15831	4.83856	0.00531
K15832	4.23103	0.00809
K15833	3.33404	0.01438
K15834	3.36063	0.01042
K15836	3.75991	0.01021
K15866	3.62735	0.01149
K15977	-2.4308	0.00686
K15986	2.82139	0.0084
K15987	-4.4261	0.00352
K16013	2.27232	0.0312
K16074	3.67825	0.01436
K16088	2.98857	0.0277
K16090	2.8419	0.03997
K16092	3.7296	0.01374
K16138	3.71982	0.00765
K16203	2.25591	0.04677
K16212	-2.1403	0.04459

K16322	2.69971	0.02267
K16328	3.66706	0.00686
K16329	2.30906	0.04629
K16345	2.58135	0.04174
K16346	3.89294	0.00971
K16370	3.40232	0.01262
K16650	3.10017	0.02412
K16693	3.37832	0.01231
K16711	3.53389	0.02559
K16789	3.37749	0.00543
K16881	4.12534	0.00829
K16898	2.30373	0.01628
K16899	2.57826	0.011
K16906	2.93602	0.04372
K16923	5.49961	0.00235
K16924	2.05126	0.03415
K16925	3.72786	0.01727
K16950	5.56714	0.00263
K17234	-3.7714	0.01127
K17236	-4.2961	0.00854
K17247	4.17339	0.00765
K17319	-2.0857	0.03891
K17675	-2.6836	0.01971
K17680	3.02261	0.03263
K17686	4.50497	0.00543
K17713	2.68145	0.02205
K17733	3.43572	0.01819
K17734	-3.0195	0.04682
K17837	3.86047	0.01301
K17865	2.67183	0.02114
K17899	4.65198	0.00649
K17948	3.29985	0.0277
K18012	2.61901	0.02803
K18013	2.86529	0.01364
K18118	4.24652	0.00767
K18122	4.08061	0.00801
K18123	4.16645	0.00671
K18138	3.58739	0.02318
K18139	2.88141	0.0436
K18140	4.27132	0.00824
K18220	-1.8074	0.00634
K18344	-4.3598	0.00986
K18345	-3.8019	0.01475
K18350	3.27236	0.01374
K18478	3.81791	0.01051
K18581	-3.1276	0.02534
K18657	3.33866	0.01237
K18692	3.21405	0.0277

K18702	3.20205	0.01275
K18765	3.40844	0.01789
K18778	2.83792	0.01497
K18815	-2.4786	0.03634
K18828	4.32935	0.00762
K18829	3.34242	0.02999
K18840	4.6638	0.00751
K18856	3.08714	0.03117
K18862	4.77772	0.0084
K18866	2.60361	0.04115
K18888	-3.0282	0.01906
K18889	-2.8343	0.01922
K18898	2.92758	0.03117
K18919	6.64565	0.00371
K18921	4.77157	0.0274
K18922	6.46813	0.00382
K18928	3.45514	0.0274
K18979	4.95508	0.00352
K19000	3.17512	0.01369
K19055	5.12135	0.00379
K19075	3.305	0.03637
K19155	4.89245	0.0047
K19159	2.54763	0.03292
K19162	3.46401	0.02616
K19165	-5.0037	0.00754
K19168	5.23921	0.00392
K19169	-5.5833	0.00394
K19170	-6.3155	0.00232
K19171	-3.9213	0.0087
K19172	-6.4384	0.00232
K19221	3.91189	0.01403
K19222	4.0639	0.01059
K19228	4.33264	0.00631
K19230	5.12621	0.00423
K19236	3.2343	0.02303
K19265	4.7233	0.00543
K19267	3.9583	0.00805
K19270	3.38172	0.01324
K19294	2.18383	0.04838
K19303	4.18024	0.00875
K19334	4.02424	0.01052
K19335	3.60679	0.01667
K19336	4.53367	0.00592
K19350	2.25501	0.04454
K19354	4.03158	0.00644
K19405	5.58596	0.0025
K19411	4.30785	0.00613
K19419	2.70234	0.03925

K19431	3.07907	0.04197
K19577	2.66691	0.04282
K19591	2.85385	0.03133
K19611	4.38467	0.00602
K19688	3.5129	0.01428
K19776	3.5672	0.00868
K19777	4.97641	0.00616
K19778	4.21029	0.00992
K19784	2.55838	0.04305
K19789	4.02553	0.00854
K19802	2.62595	0.03332
K19804	3.84649	0.00586
K19955	2.58252	0.01369
K19956	-2.6634	0.01997
K20107	4.52814	0.00531
K20108	4.52814	0.00531
K20265	4.18627	0.00488
K20542	2.60903	0.02108
K20881	2.76858	0.02469
K20885	3.54744	0.01675
K20904	2.8936	0.01658
K21029	4.34691	0.00488
K21065	3.47491	0.01322
K21085	2.71741	0.04139
K21086	2.77148	0.0309
K21088	4.07718	0.00702
K21394	4.03344	0.00697
K21395	4.63152	0.00531
K21399	4.68309	0.01054
K21405	4.01785	0.01079
K21469	3.50458	0.02402
K21514	-2.9198	0.01658
K21637	4.51505	0.00883
K21638	4.18434	0.01037
K21695	6.39739	0.00232
K21742	2.59021	0.02635
K21759	4.10842	0.00854
K21901	2.53164	0.03916
K21908	3.6571	0.0158
K21929	-1.9189	0.02986
K21965	3.22131	0.01464
K21975	3.73672	0.01879
K21976	4.40226	0.00868
K21977	-5.9858	0.00313
K21990	2.81885	0.03925
K21993	2.30911	0.03447
K22015	4.64896	0.00634
K22041	3.75417	0.01105

K22044	3.91077	0.00406
K22110	3.52202	0.00986
K22111	4.01073	0.0084
K22130	4.39616	0.0061
K22132	2.35344	0.02966
K22214	2.59607	0.03891
K22227	2.74176	0.03755
K22304	4.98221	0.00649
K22373	2.59257	0.03916
K22443	2.55178	0.04372
K22444	3.10062	0.02663
K22468	3.14738	0.03762
K22718	5.52892	0.00762
K22719	2.91726	0.02317
K23007	3.22471	0.01454
K23015	3.06317	0.0325

Annex 3. Statistically significant KOs mapped to KEGG pathways. Pathways are shown in decreasing order of mapped KOs. Only pathways containing between 50-20 KOs were considered for subsequent analysis to exclude the most general and the least abundant ones. KO numbers and symbols have been included for each gene.

KEGG pathways	Number of mapped KOs	Mapped KOs
Biosynthesis of aminoacids	47	K00030 IDH3,K00053 ilvC,K00265 gltB,K00266 gltD,K00290 LYS1,K00548 metH,K00620 argJ,K00640 cysE,K00641 metX, K00674 dapD,K00789 metK,K00817 hisC,K00832 tyrB,K00930 argB,K00931 proB,K01609 trpC,K01682 acnB,K01687 ilvD, K01693 hisB,K01695 trpA,K01703 leuC,K01738 cysK,K01760 metC,K01783 rpe,K01958 PC,K02500 hisF,K03785 aroD,K03786 aroQ,K03856 AROA2,K04516 AROA1,K04517 tyrA2,K05822 dapH,K05942 E2.3.3.3,K06001 trpB,K06209 pheB,K07173 luxS,K09758 asdA,K12524 thrA,K13497 trpGD,K13498 trpCF,K14155 patB,K14170 pheA,K14187 tyrA,K14682 argAB,K15633 gpmI,K15634 gpmB,K16370 pfkB
Pyruvate metabolism	35	K00101 lldD,K00116 mqo,K00121 frmA,K00138 aldB,K00161 PDHA,K00170 porB,K00175 korB,K00244 frdA,K00245 frdB,K00247 frdD,K00382 DLD,K00625 pta,K00626 ACAT,K00627 DLAT,K00656 E2.3.1.54,K01512 acyP,K01571 oadA,K01595 ppc,K01679 E4.2.1.2B,K01958 PC,K01962 accA,K01963 accD,K02160 accB,K03737 por,K03777 dld,K04021 eutE,K04073 mhpF,K07248 aldA,K12957 ahr,K12972 ghrA,K13788 pta,K13953 adhP,K13954 yiaY,K18118 aarC,K22373 larA
Purine metabolism	29	K00073 allD,K00087 ygeS,K00526 E1.17.4.1B,K00769 gpt,K00926 arcC,K00957 cysD,K01119 cpdB,K01139 spoT,K01466 allB,K01486 ade,K01488 add,K01525 apaH,K01923 purC,K02083 allC,K02566 nagD,K03651 cpdA,K03783 punA,K03784 deoD,K05810 LACC1,K05873 cyaB,K06966 ppnN,K07127 uraH,K08722 yfbR,K09913 ppnP,K11175 purN,K11178 yagS,K11751 ushA,K13483 yagT,K20881 yrfG
Quorum sensing	27	K01497 ribA,K01897 ACSL,K01999 livK,K02032 ddpF,K02034 ABC.PE.P1,K02035 ABC.PE.S,K02055 ABC.SP.S,K02402 flhC,K03071 secB,K03076 secY,K03666 hfq,K07173 luxS,K07666 qseB,K07667 kdpE,K07711 glrK,K07715 glrR,K07782 sdiA,K07813 agrB,K10555 lsrB,K10558 lsrA,K10914 crp,K11752 ribD,K15580 oppA,K15581 oppB,K15583 oppD,K18139 oprM,K20265 gadC
Butanoate metabolism	24	K00170 porB,K00175 korB,K00242 sdhD,K00244 frdA,K00245 frdB,K00247 frdD,K00248 ACADS,K00626 ACAT,K00634 ptb,K00656 E2.3.1.54,K00823 puuE,K01028 scoA,K01034 atoD,K01035 atoA,K01040 gctB,K01640 HMGCL,K01641 HMGCS

		,K01715 crt,K01782 fadJ,K03737 por,K04073 mhpF,K17865 croR,K18118 aarC,K18122 cat2
Amino sugar and nucleotide metabolism	24	K00075 murB,K00844 HK,K00847 E2.7.1.4,K00884 NAGK,K00885 nanK,K00978 rfbF,K01443 nagA,K01639 E4.1.3.3,K01709 rfbG,K01787 RENBP,K02472 wecC,K02777 crr,K02796 manZ,K04042 glmU,K06859 pgi1,K07806 arnB,K08678 UXS1,K09001 anmK,K10011 arnA,K10012 arnC,K11192 murP,K12452 ascC,K13014 arnD,K16881 EC:2.7.7.13 5.4.2.8
Nucleotide metabolism	23	K00087 ygeS,K00526 E1.17.4.1B,K00757 udp,K00769 gpt,K01250 rihA,K01486 ade,K01488 add,K01494 dcd,K02566 nagD,K03465 thyX,K03783 punA,K03784 deoD,K05810 LACC1,K06966 ppnN,K07043 upp,K08320 nudG,K08722 yfbR,K08723 yjjG,K09913 ppnP,K11178 yagS,K11751 ushA,K13483 yagT,K20881 yrfG
Propanoate metabolism	23	K00005 gldA,K00170 porB,K00248 ACADS,K00382 DLD,K00625 pta,K00656 E2.3.1.54,K00823 puuE,K00932 tdcD,K01659 prpC,K01682 acnB,K01720 prpD,K01782 fadJ,K01903 sucC,K01908 ACSS3,K01962 accA,K01963 accD,K02160 accB,K11264 scpB,K13788 pta,K13919 pduD,K13920 pduE,K13922 pduP,K22214 scpC
Glyoxylate and dicarboxylate metabolism	22	K00042 garR,K00104 glcD,K00123 fdoG,K00124 fdoH,K00127 fdoI,K00281 GLDC,K00282 gcvPA,K00382 DLD,K00626 ACAT,K00865 glxK,K01577 oxc,K01682 acnB,K01816 hyi,K03779 ttdA,K03781 katE,K04835 mal,K07248 aldA,K11472 glcE,K11473 glcF,K12972 ghrA,K17865 croR,K18123 HOGA1
Glycolysis / gluconeogenesis	22	K00121 frmA,K00131 gapN,K00138 aldB,K00161 PDHA,K00170 porB,K00175 korB,K00382 DLD,K00627 DLAT,K00844 HK,K01085 agp,K01792 E5.1.3.15,K02446 glpX,K02777 crr,K03737 por,K03841 FBP,K06859 pgi1,K12957 ahr,K13953 adhP,K13954 yiaY,K15633 gpmI,K15634 gpmB,K16370 pfkB
Pyrimidine metabolism	21	K00254 DHODH,K00526 E1.17.4.1B,K00757 udp,K01119 cpdB,K01250 rihA,K01494 dcd,K02566 nagD,K02823 pyrDII,K03465 thyX,K06966 ppnN,K07043 upp,K08320 nudG,K08722 yfbR,K08723 yjjG,K09018 rutA,K09020 rutB,K09023 rutD,K09913 ppnP,K11751 ushA,K16328 psuK,K16329 psuG
Ribosome	21	K02867 RP-L11,K02874 RP-L14,K02876 RP-L15,K02878 RP-L16,K02879 RP-L17,K02887 RP-L20,K02890 RP-L22,K02892 RP-L23,K02897 RP-L25,K02899 RP-L27,K02919 RP-L36,K02933 RP-L6,K02946 RP-S10,K02948 RP-S11,K02952 RP-S13,K02959 RP-S16,K02965 RP-S19,K02970 RP-S21,K02982 RP-S3,K02992 RP-S7,K07590 RP-L7A
Carbon fixation	21	K00170 porB,K00175 korB,K00198 cooS,K00242 sdhD,K00244 frdA,K00245 frdB,K00247 frdD,K00625 pta,K00626 ACAT,K01491 folD,K01595 ppc,K01679 E4.2.1.2B,K01682 acnB,K0

pathways in prokaryotes		1903 sucC,K01958 PC,K01962 accA,K01963 accD,K02160 accB,K03737 por,K13788 pta,K22015 fdhF
Sulphur metabolism	21	K00380 cysJ,K00381 cysI,K00385 asrC,K00394 aprA,K00640 cysE,K00641 metX,K00957 cysD,K01082 cysQ,K01738 cysK,K02045 cysA,K02046 cysU,K02047 cysW,K02439 glpE,K03119 tauD,K06881 nrnA,K07306 dmsA,K07307 dmsB,K15553 ssuA,K15554 ssuC,K15555 ssuB,K16950 asrA
Oxidative phosphorylation	21	K00242 sdhD,K00244 frdA,K00245 frdB,K00247 frdD,K00331 nuoB,K00333 nuoD,K00334 nuoE,K00338 nuoI,K00340 nuoK,K00425 cydA,K00937 ppk1,K02107 ATPVG,K02110 ATPF0C,K02122 ATPVF,K02257 COX10,K02297 cyoA,K02299 cyoC,K02300 cyoD,K06019 ppaX,K15986 ppaC,K22468 ppk2

8. REFERENCES

1. Chifman J, Laubenbacher R, Torti SV. A systems biology approach to iron metabolism. *Adv Exp Med Biol*. 2014;844:201-225.

2. Besarab A, Hörl WH, Silverberg D. Iron metabolism, iron deficiency, thrombocytosis, and the cardiorenal anemia syndrome. *Oncologist*. 2009;1:22-33.

3. Paul BT, Manz DH, Torti FM, Torti SV. Mitochondria and iron: current questions. *Expert Rev Hematol*. 2017;10(1):65-79.

4. Lopez A, Cacoub P, Macdougall IC, Peyrin-Biroulet L. Iron deficiency anaemia. *Lancet*. 2016;387(10021):907-916.

5. Hunt JR. Dietary and physiological factors that affect the absorption and bioavailability of iron. *Int J Vitam Nutr Res*. 2005;75(6):375-384.

6. Gulec S, Anderson GJ, Collins JF. Mechanistic and regulatory aspects of intestinal iron absorption. *Am J Physiol Gastrointest Liver Physiol*. 2014;307(4):3.

7. Fisher AL, Nemeth E. Iron homeostasis during pregnancy. *Am J Clin Nutr*. 2017;106(Suppl 6):25.

8. Zheng L, Kelly CJ, Colgan SP. Physiologic hypoxia and oxygen homeostasis in the healthy intestine. A review in the theme: cellular responses to hypoxia. *Am J Physiol Cell Physiol*. 2015;309(6):C350-C360.

9. Agnieszka L, Alicja J, Jozef D. HIF-1 and HIF-2 transcription factors - similar but not identical. *Mol Cells*. 2010;29(5):435-442.

10. Duarte TL, Talbot NP, Drakesmith H. NRF2 and hypoxia-inducible factors: key players in the redox control of systemic iron homeostasis. *Antioxid Redox Signal*. 2020;35(6):433-452.

11. Mastrogiannaki M, Matak P, Keith B, Simon MC, Vaulont S, Peyssonnaux C. HIF-2alpha, but not HIF-1alpha, promotes iron absorption in mice. *J Clin Invest*. 2009;119(5):1159-1166.

12. Slobodkin A, Slobodkina G, Allioux M, Alain K, Jebbar M, Shadrin V, et al. Genomic insights into the carbon and energy metabolism of a thermophilic deep-sea bacterium Deferribacter Autotrophicus revealed new metabolic traits in the phylum Deferribacteres. *Genes*. 2019;10(11):849.

13. Krautkramer KA, Fan J, Bäckhed F. Gut microbial metabolites as multi-kingdom intermediates. *Nat Rev Microbiol*. 2021;19(2):77-94.

14. Zhao N, Enns CA. *Iron transport machinery of human cells: Players and their interactions*. In: Argüello JM, Lutsenko S, editors. Current topics in membranes. 69: Academic Press; 2012. p. 67-93.

15. Silvestri L, Nai A, Pagani A, Camaschella C. The extrahepatic role of TfR2 in iron homeostasis. *Front Pharmacol*. 2014;5(93):1-6.

16. Zhang AS, Enns CA. Molecular mechanisms of normal iron homeostasis. *Hematology Am Soc Hematol Educ Program*. 2009:207-214.

17. Hoehn RS, Jernigan PL, Chang AL, Edwards MJ, Pritts TA. Molecular mechanisms of erythrocyte aging. *Biol Chem*. 2015;396(6-7):621-631.

18. Ganz T. Macrophages and iron metabolism. *Microbiol Spectr*. 2016;4(5).

19. Sukhbaatar N, Weichhart T. Iron regulation: macrophages in control. *Pharmaceuticals*. 2018;11(4):137.

20. Recalcati S, Cairo G. Macrophages and iron: a special relationship. *Biomedicines*. 2021;9(11):1585.

21. Consul N, Javed-Tayyab S, Morani AC, Menias CO, Lubner MG, Elsayes KM. Iron-containing pathologies of the spleen: Magnetic resonance imaging features with pathologic correlation. *Abdom Radiol*. 2021;46(3):1016-1026.

22. Manabe E, Ito S, Ohno Y, Tanaka T, Naito Y, Sasaki N, et al. Reduced lifespan of erythrocytes in dahl/salt sensitive rats is the cause of the renal proximal tubule damage. *Sci Rep*. 2020;10(1):22023.

23. Akyuz E, Doganyigit Z, Eroglu E, Moscovicz F, Merelli A, Lazarowski A, et al. Myocardial iron overload in an experimental model of sudden unexpected death in epilepsy. *Front Neurol*. 2021;12:609236.

24. Li Y, Huang X, Wang J, Huang R, Wan D. Regulation of iron homeostasis and related diseases. *Mediators Inflamm*. 2020;2:6062094.

25. Wilkinson N, Pantopoulos K. The IRP/IRE system in vivo: insights from mouse models. *Front Pharmacol*. 2014;5:176.

26. Anderson CP, Shen M, Eisenstein RS, Leibold EA. Mammalian iron metabolism and its control by iron regulatory proteins. *Biochim Biophys Acta*. 2012;9(83):17.

27. Pérez Arellano JL. *Fisiopatología de la serie roja: Síndrome anémico y síndrome policitémico*. Sisinio de Castro: Manual de patología general: Elsevier; 2019.

28. Nemeth E, Ganz T. Hepcidin-ferroportin interaction controls systemic iron homeostasis. *Int J Mol Sci*. 2021;22(12):6493.

29. Madu AJ, Ughasoro MD. Anaemia of chronic disease: an in-depth review. *Med Princ Pract*. 2017;26(1):1-9.

30. Newhall DA, Oliver R, Lugthart S. Anaemia: a disease or symptom. *Neth J Med*. 2020;78(3):104-110.

31. Cappellini MD, Musallam KM, Taher AT. Iron deficiency anaemia revisited. *J Intern Med*. 2020;287(2):153-170.

32. Balarajan Y, Ramakrishnan U, Ozaltin E, Shankar AH, Subramanian SV. Anaemia in low-income and middle-income countries. *Lancet*. 2011;378(9809):2123-2135.

33. DeLoughery TG. Iron deficiency anaemia. *Med Clin North Am*. 2017;101(2):319-332.

34. Marcus H, Schauer C, Zlotkin S. Effect of anemia on work productivity in both labor- and nonlabor-intensive occupations: a systematic narrative synthesis. *Food Nutr Bull*. 2021;42(2):289-308.

35. Stevens GA, Finucane MM, De-Regil LM, Paciorek CJ, Flaxman SR, Branca F, et al. Global, regional, and national trends in haemoglobin concentration and prevalence of total and severe anaemia in children and pregnant and non-pregnant women for 1995-2011: a systematic analysis of population-representative data. *Lancet Glob Health*. 2013;1(1):70001-70009.

36. Tsuboi I, Yamashita T, Nagano M, Kimura K, To'a Salazar G, Ohneda O. Impaired expression of HIF-2α induces compensatory expression of HIF-1α for the recovery from anemia. *J Cell Physiol* 2015;230(7):1534-1548.

37. Koury MJ, Ponka P. New insights into erythropoiesis: the roles of folate, vitamin B12, and iron. *Annu Rev Nutr*. 2004;24:105-131.

38. Maio N, Zhang DL, Ghosh MC, Jain A, SantaMaria AM, Rouault TA. Mechanisms of cellular iron sensing, regulation of erythropoiesis and mitochondrial iron utilization. *Semin Hematol*. 2021;58(3):161-174.

39. Fang S, Zhuo Z, Yu X, Wang H, Feng J. Oral administration of liquid iron preparation containing excess iron induces intestine and liver injury, impairs intestinal barrier function and alters the gut microbiota in rats. *J Trace Elem Med Biol*. 2018;47:12-20.

40. Qi X, Zhang Y, Guo H, Hai Y, Luo Y, Yue T. Mechanism and intervention measures of iron side effects on the intestine. *Crit Rev Food Sci Nutr*. 2020;60(12):2113-2125.

41. Paganini D, Zimmermann MB. The effects of iron fortification and supplementation on the gut microbiome and diarrhea in infants and children: a review. *Am J Clin Nutr*. 2017;106(Suppl 6):1688S-1693S.

42. Mahalhal A, Frau A, Burkitt MD, Ijaz UZ, Lamb CA, Mansfield JC, et al. Oral ferric maltol does not adversely affect the intestinal microbiome of patients or mice, but ferrous sulphate does. *Nutrients*. 2021;13(7):2269.

43. Gómez-Ramírez S, Brilli E, Tarantino G, Muñoz M. Sucrosomial(®) iron: a new generation iron for improving oral supplementation. *Pharmaceuticals*. 2018;11(4):97.

44. Zakrzewski M, Wilkins SJ, Helman SL, Brilli E, Tarantino G, Anderson GJ, et al. Supplementation with sucrosomial® iron leads to favourable changes in the intestinal microbiome when compared to ferrous sulfate in mice. *Biometals*. 2022;35(1):27-38.

45. Mu Q, Kirby J, Reilly CM, Luo XM. Leaky gut as a danger signal for autoimmune diseases. *Front Immunol*. 2017;8:598.

46. Fachi JL, Felipe JdS, Pral LP, da Silva BK, Corrêa RO, de Andrade MCP, et al. Butyrate protects mice from clostridium difficile-induced colitis through an HIF-1-dependent mechanism. *Cell Reports*. 2019;27(3):750-761.

47. Selvamani S, Dailin DJ, Gupta VK, Wahid M, Keat HC, Natasya KH, et al. An insight into probiotics bio-route: translocation from the mother's gut to the mammary gland. *Appl Sci*. 2021;11:7247.

48. Lewis CV, Taylor WR. Intestinal barrier dysfunction as a therapeutic target for cardiovascular disease. *Am J Physiol Heart Circ Physiol*. 2020;319(6):H1227-H1233.

49. Li XY, He C, Zhu Y, Lu NH. Role of gut microbiota on intestinal barrier function in acute pancreatitis. *World J Gastroenterol*. 2020;26(18):2187-2193.

50. Fine RL, Manfredo Vieira S, Gilmore MS, Kriegel MA. Mechanisms and consequences of gut commensal translocation in chronic diseases. *Gut Microbes*. 2020;11(2):217-230.

51. Manfredo Vieira S, Hiltensperger M, Kumar V, Zegarra-Ruiz D, Dehner C, Khan N, et al. Translocation of a gut pathobiont drives autoimmunity in mice and humans. *Science*. 2018;359(6380):1156-1161.

52. Li Y, Hansen SL, Borst LB, Spears JW, Moeser AJ. Dietary iron deficiency and oversupplementation increase intestinal permeability, ion transport, and inflammation in pigs. *J Nutr*. 2016;146(8):1499-1505.

53. Din H., Yu X, Chen L, Han J, Zhao Y, Feng J. Tolerable upper intake levels of iron damage the intestine and alter the intestinal flora in weaned piglets. *J Anim Sci*. 2020;12(9):1356-1369.

54. Das NK, Schwartz AJ, Barthel G, Inohara N, Liu Q, Sankar A, et al. Microbial metabolite signaling is required for systemic iron homeostasis. *Cell Metab*. 2020;31(1):115-130.

55. Lloyd-Price J, Abu-Ali G, Huttenhower C. The healthy human microbiome. *Genome Med*. 2016;8(1):51.

56. Turnbaugh PJ, Ley RE, Hamady M, Fraser-Liggett CM, Knight R, Gordon JI. The human microbiome project. *Nature*. 2007;449(7164):804-810.

57. Perez-Carrasco V, Soriano-Lerma A, Soriano M, Gutiérrez-Fernández J, Garcia-Salcedo JA. Urinary microbiome: yin and yang of the urinary tract. *Front Cell Infect Microbiol*. 2021;11:617002.

58. Malla MA, Dubey A, Kumar A, Yadav S, Hashem A, Abd Allah EF. Exploring the human microbiome: The potential future role of next-generation sequencing in disease diagnosis and treatment. *Front Immunol*. 2019;9:2868.

59. Huttenhower C, Gevers D, Knight R, Abubucker S, Badger JH, Chinwalla AT, et al. Structure, function and diversity of the healthy human microbiome. *Nature*. 2012;486(7402):207-214.

60. Lloyd-Price J, Mahurkar A, Rahnavard G, Crabtree J, Orvis J, Hall AB, et al. Strains, functions and dynamics in the expanded human microbiome project. *Nature*. 2017;550(7674):61-66.

61. Del Chierico F, Ancora M, Marcacci M, Cammà C, Putignani L, Conti S. Choice of next-generation sequencing pipelines. *Methods Mol Biol*. 2015;1231:31-47.

62. Amrane S, Raoult D, Lagier J-C. Metagenomics, culturomics, and the human gut microbiota. *Expert Review of Anti-infective Therapy*. 2018;16(5):373-375.

63. Ranjan R, Rani A, Metwally A, McGee HS, Perkins DL. Analysis of the microbiome: advantages of whole genome shotgun versus 16S amplicon sequencing. *Biochem Biophys Res Commun*. 2016;469(4):967-977.

64. Heintz-Buschart A, Wilmes P. Human gut microbiome: function matters. *Trends Microbiol*. 2018;26(7):563-574.

65. Lagier JC, Hugon P, Khelaifia S, Fournier PE, La Scola B, Raoult D. The rebirth of culture in microbiology through the example of culturomics to study human gut microbiota. *Clin Microbiol Rev*. 2015;28(1):237-264.

66. Gloor GB, Macklaim JM, Pawlowsky-Glahn V, Egozcue JJ. Microbiome datasets are compositional, and this is not optional. *Front Microbiol*. 2017;8:2224.

67. Gomaa EZ. Human gut microbiota/microbiome in health and diseases: a review. *Antonie Van Leeuwenhoek*. 2020;113(12):2019-2040.

68. Thursby E, Juge N. Introduction to the human gut microbiota. *Biochem J*. 2017;474(11):1823-1836.

69. Li J, Jia H, Cai X, Zhong H, Feng Q, Sunagawa S, et al. An integrated catalog of reference genes in the human gut microbiome. *Nat Biotechnol*. 2014;32(8):834-841.

70. Yang X, Xie L, Li Y, Wei C. More than 9,000,000 unique genes in human gut bacterial community: estimating gene numbers inside a human body. *PLoS One*. 2009;4(6):0006074.

71. Hollister EB, Gao C, Versalovic J. Compositional and functional features of the gastrointestinal microbiome and their effects on human health. *Gastroenterology*. 2014;146(6):1449-1458.

72. Rowland I, Gibson G, Heinken A, Scott K, Swann J, Thiele I, et al. Gut microbiota functions: metabolism of nutrients and other food components. *Eur J Nutr*. 2018;57(1):1-24.

73. Koh A, De Vadder F, Kovatcheva-Datchary P, Bäckhed F. From dietary fiber to host physiology: short-chain fatty acids as key bacterial metabolites. *Cell*. 2016;165(6):1332-1345.

74. Chun C, Zheng L, Colgan SP. Tissue metabolism and host-microbial interactions in the intestinal mucosa. *Free Radic Biol Med*. 2017;105:86-92.

75. Kelly CJ, Zheng L, Campbell EL, Saeedi B, Scholz CC, Bayless AJ, et al. Crosstalk between microbiota-derived short-chain fatty acids and intestinal epithelial hif augments tissue barrier function. *Cell Host Microbe*. 2015;17(5):662-671.

76. Liu P, Wang Y, Yang G, Zhang Q, Meng L, Xin Y, et al. The role of short-chain fatty acids in intestinal barrier function, inflammation, oxidative stress, and colonic carcinogenesis. *Pharmacol Res*. 2021;165(105420):9.

77. Beisner J, Filipe Rosa L, Kaden-Volynets V, Stolzer I, Günther C, Bischoff SC. Prebiotic inulin and sodium butyrate attenuate obesity-induced intestinal barrier dysfunction by induction of antimicrobial peptides. *Front Immunol*. 2021;12:678360.

78. Arpaia N, Campbell C, Fan X, Dikiy S, van der Veeken J, deRoos P, et al. Metabolites produced by commensal bacteria promote peripheral regulatory t-cell generation. *Nature*. 2013;504(7480):451-455.

79. Zhao L, Zhang F, Ding X, Wu G, Lam YY, Wang X, et al. Gut bacteria selectively promoted by dietary fibers alleviate type 2 diabetes. *Science*. 2018;359(6380):1151-1156.

80. Vicentini FA, Keenan CM, Wallace LE, Woods C, Cavin J-B, Flockton AR, et al. Intestinal microbiota shapes gut physiology and regulates enteric neurons and glia. *Microbiome*. 2021;9(1):210.

81. Martin-Gallausiaux C, Marinelli L, Blottière HM, Larraufie P, Lapaque N. Scfa: Mechanisms and functional importance in the gut. *Proc Nutr Soc*. 2021;80(1):37-49.

82. Margolis KG, Cryan JF, Mayer EA. The microbiota-gut-brain axis: from motility to mood. *Gastroenterology*. 2021;160(5):1486-1501.

83. Ulluwishewa D, Anderson RC, McNabb WC, Moughan PJ, Wells JM, Roy NC. Regulation of tight junction permeability by intestinal bacteria and dietary components. *J Nutr*. 2011;141(5):769-776.

84. Li D, Chen H, Zhao J, Zhang H, Chen W. Potential functions of the gastrointestinal microbiome inhabiting the length of the rat digest tract. *Int J Mol Sci*. 2019;20(5):1232.

85. Dongyao L, Haiqin C, Bingyong M, Qin Y, Jianxin Z, Zhennan G, et al. Microbial biogeography and core microbiota of the rat digestive tract. *Sci Rep*. 2017;7(1):45840.

86. Coelho LP, Kultima JR, Costea PI, Fournier C, Pan Y, Czarnecki-Maulden G, et al. Similarity of the dog and human gut microbiomes in gene content and response to diet. *Microbiome*. 2018;6(1):72.

87. Douglas AE. Simple animal models for microbiome research. *Nat Rev Microbiol*. 2019;17(12):764-775.

88. Maifeld A, Bartolomaeus H, Löber U, Avery EG, Steckhan N, Markó L, et al. Fasting alters the gut microbiome reducing blood pressure and body weight in metabolic syndrome patients. *Nat Commun*. 2021;12(1):1970.

89. Jie Z, Xia H, Zhong SL, Feng Q, Li S, Liang S, et al. The gut microbiome in atherosclerotic cardiovascular disease. *Nat Commun*. 2017;8(1):845.

90. Singer-Englar T, Barlow G, Mathur R. Obesity, diabetes, and the gut microbiome: an updated review. *Expert Rev Gastroenterol Hepatol*. 2019;13(1):3-15.

91. Zhang L, Qing P, Yang H, Wu Y, Liu Y, Luo Y. Gut microbiome and metabolites in systemic lupus erythematosus: link, mechanisms and intervention. *Front Immunol*. 2021;12:686501.

92. Cryan JF, O'Riordan KJ, Sandhu K, Peterson V, Dinan TG. The gut microbiome in neurological disorders. *Lancet Neurol*. 2020;19(2):179-194.

93. Coe GL, Pinkham NV, Celis AI, Johnson C, DuBois JL, Walk ST. Dynamic gut microbiome changes in response to low-iron challenge. *Appl Environ Microbiol*. 2021;87(3):02307-02320.

94. Dostal A, Chassard C, Hilty FM, Zimmermann MB, Jaeggi T, Rossi S, et al. Iron depletion and repletion with ferrous sulfate or electrolytic iron modifies the composition and metabolic activity of the gut microbiota in rats. *J Nutr*. 2012;142(2):271-277.

95. McClorry S, Zavaleta N, Llanos A, Casapía M, Lönnerdal B, Slupsky CM. Anemia in infancy is associated with alterations in systemic metabolism and microbial structure and function in a sex-specific manner: An observational study. *Am J Clin Nutr*. 2018;108(6):1238-1248.

96. Ho TTB, Kumar A, Louis-Jacques AF, Dishaw LJ, Yee AL, Groer MW. The development of intestinal dysbiosis in anemic preterm infants. *J Perinatol*. 2020; 40(7):1066-1074

97. González A, Gálvez N, Martín J, Reyes F, Pérez-Victoria I, Dominguez-Vera JM. Identification of the key excreted molecule by lactobacillus fermentum related to host iron absorption. *Food Chem*. 2017;228:374-380.

98. Zhang D, Gao X, Li H, Borger DK, Wei Q, Yang E, et al. The microbiota regulates hematopoietic stem cell fate decisions by controlling iron availability in bone marrow. *Cell Stem Cell*. 2022;29(2):232-247.

99. Seyoum Y, Baye K, Humblot C. Iron homeostasis in host and gut bacteria - a complex interrelationship. *Gut Microbes*. 2021;13(1):1-19.

100. Paganini D, Uyoga MA, Kortman GAM, Cercamondi CI, Moretti D, Barth-Jaeggi T, et al. Prebiotic galacto-oligosaccharides mitigate the adverse effects of iron fortification on the gut microbiome: A randomised controlled study in kenyan infants. *Gut*. 2017;66(11):1956-1967.

101. Kortman GA, Dutilh BE, Maathuis AJ, Engelke UF, Boekhorst J, Keegan KP, et al. Microbial metabolism shifts towards an adverse profile with supplementary iron in the TIM-2 in vitro model of the human colon. *Front Microbiol*. 2016;6:1481.

102. Dekker Nitert M, Gomez-Arango LF, Barrett HL, McIntyre HD, Anderson GJ, Frazer DM, et al. Iron supplementation has minor effects on gut microbiota composition in overweight and obese women in early pregnancy. *Br J Nutr*. 2018;120(3):283-289.

103. Dostal A, Baumgartner J, Riesen N, Chassard C, Smuts CM, Zimmermann MB, et al. Effects of iron supplementation on dominant bacterial groups in the gut, faecal SCFA and

gut inflammation: a randomised, placebo-controlled intervention trial in south african children. *Br J Nutr*. 2014;112(4):547-556.

104. Ippolito JR, Piccolo BD, Robeson MS, Barney DE, Jr., Ali J, Singh P, et al. Iron deficient diets modify the gut microbiome and reduce the severity of enteric infection in a mouse model of S. Typhimurium-induced enterocolitis. *J Nutr Biochem*. 2022;107(109065):21.

105. Suez J, Zmora N, Zilberman-Schapira G, Mor U, Dori-Bachash M, Bashiardes S, et al. Post-antibiotic gut mucosal microbiome reconstitution is impaired by probiotics and improved by autologous FMT. *Cell*. 2018;174(6):1406-1423.

106. David LA, Maurice CF, Carmody RN, Gootenberg DB, Button JE, Wolfe BE, et al. Diet rapidly and reproducibly alters the human gut microbiome. *Nature*. 2014;505(7484):559-563.

107. Fragiadakis GK, Wastyk HC, Robinson JL, Sonnenburg ED, Sonnenburg JL, Gardner CD. Long-term dietary intervention reveals resilience of the gut microbiota despite changes in diet and weight. *Am J Clin Nutr*. 2020;111(6):1127-1136.

108. Kok CR, Hutkins R. Yogurt and other fermented foods as sources of health-promoting bacteria. *Nutr Rev*. 2018;76(Suppl 1):4-15.

109. García-Burgos M, Moreno-Fernández J, Alférez MJ, Díaz-Castro J, López-Aliaga I. New perspectives in fermented dairy products and their health relevance. *J Funct Foods*. 2020;72:104059.

110. Bessman NJ, Mathieu JRR, Renassia C, Zhou L, Fung TC, Fernandez KC, et al. Dendritic cell-derived hepcidin sequesters iron from the microbiota to promote mucosal healing. *Science*. 2020;368(6487):186-189.

111. Qi B, Han M. Microbial siderophore enterobactin promotes mitochondrial iron uptake and development of the host via interaction with ATP synthase. *Cell*. 2018;175(2):571-582.

112. Agyei D, Owusu-Kwarteng J, Akabanda F, Akomea-Frempong S. Indigenous african fermented dairy products: processing technology, microbiology and health benefits. *Crit Rev Food Sci Nutr*. 2020;60(6):991-1006.

113. Aryana KJ, Olson DW. A 100-year review: yogurt and other cultured dairy products. *J Dairy Sci*. 2017;100(12):9987-10013.

114. Rasika DMD, Munasinghe M, Vidanarachchi JK, da Cruz AG, Ajlouni S, Ranadheera CS. Probiotics and prebiotics in non-bovine milk. *Adv Food Nutr Res*. 2020;94:339-384.

115. Statista., 2022. Ministerio de Agricultura, Pesca y Alimentos de España. Leche de cabra: producción por Comunidades Autónomas en España 2020. Available from: https://es.statista.com/estadisticas/557331/volumen-de-leche-de-cabra-producida-en-espana-por-comunidad-autonoma/).

116. Moreno-Fernández J, Díaz-Castro J, Alférez MJ, Hijano S, Nestares T, López-Aliaga I. Production and chemical composition of two dehydrated fermented dairy products based on cow or goat milk. *J Dairy Res*. 2016;83(1):81-88.

117. Haenlein GFW. Goat milk in human nutrition. *Small Lumin Res*. 2004;51(2):155-163.

118. Silvani V., Dantas A., Swinden-Prudencio E. Functionality of the components from goat's milk, recent advances for functional dairy products development and its implications on human health. *J Funct Foods*. 2019;52:243-257.

119. Dallas D, Nielsen SD. Milk peptidomics to identify functional peptides and for quality control of dairy products. *Methods Mol Biol*. 2018;1719:223-240.

120. Quigley L, O'Sullivan O, Stanton C, Beresford TP, Ross RP, Fitzgerald GF, et al. The complex microbiota of raw milk. *FEMS Microbiol Rev*. 2013;37(5):664-698.

121. van Leeuwen SS, te Poele EM, Chatziioannou AC, Benjamins E, Haandrikman A, Dijkhuizen L. Goat milk oligosaccharides: their diversity, quantity, and functional properties

in comparison to human milk oligosaccharides. *J Agric Food Chem*. 2020;68(47):13469-13485.

122. Barnett AM, Roy NC, McNabb WC, Cookson AL. Effect of a semi-purified oligosaccharide-enriched fraction from caprine milk on barrier integrity and mucin production of co-culture models of the small and large intestinal epithelium. *Nutrients*. 2016;8(5):267.

123. Kao HF, Wang YC, Tseng HY, Wu LS, Tsai HJ, Hsieh MH, et al. Goat milk consumption enhances innate and adaptive immunities and alleviates allergen-induced airway inflammation in offspring mice. *Front Immunol*. 2020;11:184.

124. Nayik GA, Jagdale YD, Gaikwad SA, Devkatte AN, Dar AH, Dezmirean DS, et al. Recent insights into processing approaches and potential health benefits of goat milk and its products: a review. *Front Nutr*. 2021;8:789117.

125. Alférez M.J.M., López-Aliaga I., Nestares T., Díaz-Castro J., Barrionuevo M, Ros P.B., et al. Dietary goat milk improves iron bioavailability in rats with induced ferropenic anaemia in comparison with cow milk. *Int Dairy J*. 2006;16(7):813-821.

126. Muñoz Alférez MJ, Muñoz-García A, Moreno-Fernández J, López-Aliaga I, Díaz-Castro J. Fermented goat milk consumption improves cardiovascular health during anemia recovery. *J Sci Food Agric*. 2019;99(1):473-481.

127. Muñoz Alférez MJ, Robles Rebollo M, Moreno-Fernández J, Díaz Castro J, López Aliaga MI. Effect of fermented goat milk on body composition, basal metabolism, and food intake control in rats. *Nutr Hosp*. 2020;37(1):123-128.

128. Moreno-Fernandez J, Diaz-Castro J, Alférez MJ, Boesch C, Nestares T, López-Aliaga I. Fermented goat milk improves antioxidant status and protects from oxidative damage to biomolecules during anemia recovery. *J Sci Food Agric*. 2017;97(5):1433-1442.

129. Barnett AM, Roy NC, Cookson AL, McNabb WC. Metabolism of caprine milk carbohydrates by probiotic bacteria and Caco-2:HT29^{-}MTX epithelial co-cultures and their impact on intestinal barrier integrity. *Nutrients*. 2018;10(7):949.

130. Thum C, Roy NC, McNabb WC, Otter DE, Cookson AL. In vitro fermentation of caprine milk oligosaccharides by bifidobacteria isolated from breast-fed infants. *Gut Microbes*. 2015;6(6):352-363.

131. Leong A, Liu Z, Almshawit H, Zisu B, Pillidge C, Rochfort S, et al. Oligosaccharides in goats' milk-based infant formula and their prebiotic and anti-infection properties. *Br J Nutr*. 2019;122(4):441-449.

132. Thum C, McNabb WC, Young W, Cookson AL, Roy NC. Prenatal caprine milk oligosaccharide consumption affects the development of mice offspring. *Mol Nutr Food Res*. 2016;60(9):2076-2085.

133. Li N, Xie Q, Chen Q, Evivie SE, Liu D, Dong J, et al. Cow, goat, and mare milk diets differentially modulated the immune system and gut microbiota of mice colonized by healthy infant feces. *J Agric Food Chem*. 2020;68(51):15345-15357.

134. Ma H, Yu Z, Zhao Y, Li L, Liu Y. Goat milk fermented with combined lactic acid bacterium alter microbial community structures and levels of the targeted short-chain fatty acids in the large intestine of mice. *Food Res Int*. 2022;157:111352.

135. Neves Casarotti A., Borgonovi T.F., de Mello-Tieghi T., Sivieri K., Barretto-Penna A.L. Probiotic low-fat fermented goat milk with passion fruit by-product: In vitro effect on obese individuals' microbiota and on metabolites production. *Food Res Int*. 2020;136:109453.

136. Reeves PG, Nielsen FH, Fahey GC, Jr. AIN-93 purified diets for laboratory rodents: Final report of the american institute of nutrition ad hoc writing committee on the reformulation of the AIN-76A rodent diet. *J Nutr*. 1993;123(11):1939-1951.

137. Pallarés I, Lisbona F, Aliaga IL, Barrionuevo M, Alférez MJM, Campos MS. Effect of iron deficiency on the digestive utilization of iron, phosphorus, calcium and magnesium in rats. *Br J Nutr*. 1993;70(2):609-620.

138. Soriano-Lerma A, Pérez-Carrasco V, Sánchez-Marañón M, Ortiz-González M, Sánchez-Martín V, Gijón J, et al. Influence of 16S rRNA target region on the outcome of microbiome studies in soil and saliva samples. *Sci Rep*. 2020;10(1):13637.

139. Soriano-Lerma A, Magán-Fernández A, Gijón J, Sánchez-Fernández E, Soriano M, García-Salcedo JA, et al. Short-term effects of hyaluronic acid on the subgingival microbiome in peri-implantitis: A randomized controlled clinical trial. *J Periodontol*. 2020;91(6):734-745.

140. Douglas GM, Beiko RG, Langille MGI. *Predicting the functional potential of the microbiome from marker genes using picrust*. In: Beiko RG, Hsiao W, Parkinson J, editors. Microbiome analysis: Methods and protocols. New York, NY: Springer New York; 2018. p. 169-177.

141. Díaz-Faes L, Soriano-Lerma A, Magan-Fernandez A, López M, Gijon J, García-Salcedo JA, et al. Structural and functional microbial patterns in cohabitating family members with history of periodontitis. *Oral Dis*. 2021;28(3):824-828.

142. Beghini F, McIver LJ, Blanco-Míguez A, Dubois L, Asnicar F, Maharjan S, et al. Integrating taxonomic, functional, and strain-level profiling of diverse microbial communities with biobakery 3. *eLife*. 2021;10:e65088.

143. Yang S, Lin S, Kelen GD, Quinn TC, Dick JD, Gaydos CA, et al. Quantitative multiprobe PCR assay for simultaneous detection and identification to species level of bacterial pathogens. *J Clin Microbiol*. 2002;40(9):3449-3454.

144. Supek F, Bošnjak M, Škunca N, Šmuc T. REVIGO summarizes and visualizes long lists of gene ontology terms. *PLoS One*. 2011;6(7):18.

145. Walter W, Sánchez-Cabo F, Ricote M. Goplot: An R package for visually combining expression data with functional analysis. *Bioinformatics*. 2015;31(17):2912-2914.

146. Zeng MY, Cisalpino D, Varadarajan S, Hellman J, Warren HS, Cascalho M, et al. Gut microbiota-induced Immunoglobulin G controls systemic infection by symbiotic bacteria and pathogens. *Immunity*. 2016;44(3):647-658.

147. Hammer Ø, Harper DAT, Ryan PD. Past: Paleontological statistics software package for education and data analysis. *Palaeontologia Electronica*. 2001;4(1):1-9.

148. Kumar S, Stecher G, Tamura K. Mega7: molecular evolutionary genetics analysis version 7.0 for bigger datasets. *Mol Biol Evol*. 2016;33(7):1870-1874.

149. Segata N, Izard J, Waldron L, Gevers D, Miropolsky L, Garrett WS, et al. Metagenomic biomarker discovery and explanation. *Genome Biol*. 2011;12(6):2011-2012.

150. Mohammadi SA, Prasanna BM. Analysis of genetic diversity in crop plants—salient statistical tools and considerations. *Crop Sci*. 2003;43(4):1235-1248.

151. Sankaran K, Holmes SP. Multitable methods for microbiome data integration. *Front Genet*. 2019;10:627.

152. Bray JR, Curtis JT. An ordination of the upland forest communities of southern wisconsin. *Ecol Monogr*. 1957;27(4):325-349.

153. Rivera-Chávez F, Zhang Lillian F, Faber F, Lopez Christopher A, Byndloss Mariana X, Olsan Erin E, et al. Depletion of butyrate-producing clostridia from the gut microbiota drives an aerobic luminal expansion of salmonella. *Cell Host Microbe*. 2016;19(4):443-454.

154. Semenza GL. Hif-1, o(2), and the 3 phds: How animal cells signal hypoxia to the nucleus. *Cell*. 2001;107(1):1-3.

155. Dilly AK, Lee YJ, Zeh HJ, Guo ZS, Bartlett DL, Choudry HA. Targeting hypoxia-mediated mucin 2 production as a therapeutic strategy for mucinous tumors. *Transl Res*. 2016;169:19-30.

156. Vasapolli R, Schütte K, Schulz C, Vital M, Schomburg D, Pieper DH, et al. Analysis of transcriptionally active bacteria throughout the gastrointestinal tract of healthy individuals. *Gastroenterology*. 2019;157(4):1081-1092.

157. Kotrba P, Inui M, Yukawa H. Bacterial phosphotransferase system (PTS) in carbohydrate uptake and control of carbon metabolism. *J Biosci Bioeng*. 2001;92(6):502-517.

158. Teufel R, Kung JW, Kockelkorn D, Alber BE, Fuchs G. 3-hydroxypropionyl-coenzyme A dehydratase and acryloyl-coenzyme A reductase, enzymes of the autotrophic 3-hydroxypropionate/4-hydroxybutyrate cycle in the sulfolobales. *J Bacteriol*. 2009;191(14):4572-4581.

159. Seravalli J, Kumar M, Ragsdale SW. Rapid kinetic studies of acetyl-coA synthesis: evidence supporting the catalytic intermediacy of a paramagnetic nifec species in the autotrophic wood–ljungdahl pathway. *Biochemistry*. 2002;41(6):1807-1819.

160. Louis P, Flint HJ. Formation of propionate and butyrate by the human colonic microbiota. *Environ Microbiol*. 2017;19(1):29-41.

161. Theocharis AD, Manou D, Karamanos NK. The extracellular matrix as a multitasking player in disease. *FEBS J*. 2019;286(15):2830-2869.

162. Tao S, Xiong Y, Han D, Pi Y, Zhang H, Wang J. N-(3-oxododecanoyl)-l-homoserine lactone disrupts intestinal epithelial barrier through triggering apoptosis and collapsing extracellular matrix and tight junction. *J Cell Physiol*. 2021;236(8):5771-5784.

163. Stronati L, Palone F, Negroni A, Colantoni E, Mancuso AB, Cucchiara S, et al. Dipotassium glycyrrhizate improves intestinal mucosal healing by modulating extracellular matrix remodeling genes and restoring epithelial barrier functions. *Front Immunol*. 2019;10:939.

164. Wright JA, Richards T, Srai SK. The role of iron in the skin and cutaneous wound healing. *Front Pharmacol*. 2014;5:156.

165. Bouri S, Martin J. Investigation of iron deficiency anaemia. *Clin Med*. 2018;18(3):242-244.

166. Axling U, Önning G, Combs MA, Bogale A, Högström M, Svensson M. The effect of Lactobacillus Plantarum 299v on iron status and physical performance in female iron-deficient athletes: A randomized controlled trial. *Nutrients*. 2020;12(5):1279.

167. Wang JW, Kuo CH, Kuo FC, Wang YK, Hsu WH, Yu FJ, et al. Fecal microbiota transplantation: review and update. *J Formos Med Assoc*. 2019;118(1):S23-S31.

168. Navarro-Tapia E, Sebastiani G, Sailer S, Toledano LA, Serra-Delgado M, García-Algar Ó, et al. Probiotic supplementation during the perinatal and infant period: effects on gut dysbiosis and disease. *Nutrients*. 2020;12(8):2243.

169. Butts CA, Paturi G, Hedderley DI, Martell S, Dinnan H, Stoklosinski H, et al. Goat and cow milk differ in altering microbiota composition and fermentation products in rats with gut dysbiosis induced by amoxicillin. *Food Funct*. 2021;12(7):3104-3119.

170. Turpin W, Bedrani L, Espin-Garcia O, Xu W, Silverberg MS, Smith MI, et al. Associations of NOD2 polymorphisms with erysipelotrichaceae in stool of in healthy first degree relatives of Crohn's disease subjects. *BMC Med Genet*. 2020;21(1):204.

171. Forbes JD, Chen CY, Knox NC, Marrie RA, El-Gabalawy H, de Kievit T, et al. A comparative study of the gut microbiota in immune-mediated inflammatory diseases-does a common dysbiosis exist?. *Microbiome*. 2018;6(1):221.

9. PUBLICATIONS

Soriano-Lerma A, García-Burgos M, Alférez MJM, Pérez-Carrasco V, Sanchez-Martin V, Linde-Rodríguez Á, et al. Gut microbiome-short-chain fatty acids interplay in the context of iron deficiency anaemia. Eur J Nutr. 2022;61(1):399-412.

ORIGINAL CONTRIBUTION

Check for updates

Gut microbiome–short-chain fatty acids interplay in the context of iron deficiency anaemia

Ana Soriano-Lerma[1,2] · María García-Burgos[1] · María J.M. Alférez[1] · Virginia Pérez-Carrasco[2,3] · Victoria Sanchez-Martin[2,3] · Ángel Linde-Rodríguez[2,3] · Matilde Ortiz-González[4] · Miguel Soriano[4] · José Antonio García-Salcedo[2,3] · Inmaculada López-Aliaga[1]

Other publications I significantly contributed to during my PhD:

Ruiz-Linares M, Monroy-Rojas JF, Solana C, Baca P, Aguado B, **Soriano- Lerma A**, et al. Antimicrobial potential of new diclofenac hydrogels for disinfection in regenerative endodontics: An in vitro and ex vivo study. Int Endod J. 2023;56(1):103-117.

Ortiz-Gonzalez M, Pérez-Victoria I, Ramirez-Macias I, de Pedro N, Linde-Rodriguez A, González-Menéndez V, et al. Curvicollide D isolated from the fungus Amesia sp. kills african trypanosomes by inhibiting transcription. Int J Mol Sci. 2022;23(11):6107.

Sanchez-Martin V, Plaza-Calonge MDC, **Soriano-Lerma A**, Ortiz-Gonzalez M, Linde-Rodriguez A, Perez-Carrasco V, et al. Gallic acid: A natural phenolic compound exerting antitumoral activities in colorectal cancer via interaction with g-quadruplexes. Cancers. 2022;14(11):2648.

Sanchez-Martin V, Schneider DA, Ortiz-Gonzalez M, **Soriano-Lerma A**, Linde-Rodriguez A, Perez-Carrasco V, et al. Targeting ribosomal g-quadruplexes with naphthalene-diimides as RNA polymerase inhibitors for colorectal cancer treatment. Cell Chem Biol. 2021;28(11):1590-1601.

Perez-Carrasco V, **Soriano-Lerma A**, Soriano M, Gutiérrez-Fernández J, Garcia-Salcedo JA. Urinary microbiome: Yin and yang of the urinary tract. Front Cell Infect Microbiol. 2021;11:617002.

Díaz-Faes L & **Soriano-Lerma A**, Magan-Fernandez A, López M, Gijon J, García-Salcedo JA, et al. Structural and functional microbial patterns in cohabitating family members with history of periodontitis. Oral Dis. 2021;28(3):824-828

Soriano-Lerma A, Magán-Fernández A, Gijón J, Sánchez-Fernández E, Soriano M, García-Salcedo JA, et al. Short-term effects of hyaluronic acid on the subgingival microbiome in peri-implantitis: A randomized controlled clinical trial. J Periodontol. 2020;91(6):734-745.

Soriano-Lerma A, Pérez-Carrasco V, Sánchez-Marañón M, Ortiz-González M, Sánchez-Martín V, Gijón J, et al. Influence of 16S rRNA target region on the outcome of microbiome studies in soil and saliva samples. Sci Rep. 2020;10(1):13637.